

Improving the management of drained agricultural areas to optimize the retention of iron-associated phosphorus

Verbetering van het beheer van kunstmatig gedraineerde
landbouwgebieden om de retentie van ijzer-gebonden
fosfor te optimaliseren

(met een samenvatting in het Nederlands)

Proefschrift

ter verkrijging van de graad van doctor aan de Universiteit Utrecht op
gezag van de rector magnificus, prof.dr H. Kummeling, ingevolge het besluit
van het college voor promoties in het openbaar te verdedigen op 26 mei
2023 des morgens te 10.15 uur

door Maria Victoria Barcala Paolillo
geboren op 29 juli 1991 te Montevideo, Uruguay

Promotor:

Prof. dr. Jack Middelburg

Copromotors:

Dr. Thilo Behrends, Dr.ir. Leonard A. Osté

Beoordelingscommissie:

Prof.dr.ir. A.F. Bouwman

Dr.ir. G.F. Koopmans

Prof.dr. S. Peiffer

Prof.dr.ir. C.P. Slomp

Prof.dr. E. Smolders

The research in this thesis has received funding from the European Union's Horizon 2020 research and innovation program under the Marie Skłodowska Curie grant agreement No 813438.

Thesis cover is by Juan Manuel Blanes (1875-1878). *Los dos caminos*, oil on canvas, Museo Blanes, Montevideo, Uruguay.

DOI: <https://doi.org/10.33540/1798>

Table of Contents

1	Chapter 1 Introduction	5
2	Chapter 2	31
	Processes controlling the flux of legacy phosphorus to surface waters at the farm scale. <i>Barcala, V.; Rozemeijer, J.; Osté, L.; Van der Grift, B; Gerner, L.; and Behrends, T. Environ. Res. Lett. 16 (2021) 015003</i> https://doi.org/10.1088/1748-9326/abcdd4	
3	Chapter 3	69
	Value and limitations of Machine Learning in high-frequency nutrient data for gap-filling, forecasting, and transport process interpretation <i>Barcala, V., Rozemeijer, J., Ouwerkerk, K., Gerner, L., Osté, L. Under Review, Journal of Environmental Monitoring and Assessment</i> https://doi.org/10.21203/rs.3.rs-2201325/v1 (Preprint)	
4	Chapter 4	109
	Phosphorus adsorption on iron-coated sand under reducing conditions <i>Barcala, V., Jansen, S., Gerritse, J., Mangold, S., Voegelin, A., and Behrends, T. Journal of Environmental Quality.</i> https://doi.org/10.1002/jeq2.20432	
5	Chapter 5	157
	Transport limited kinetics of phosphate retention on iron-coated sand and practical implications <i>Barcala, V., Zech, A., Osté, L., and Behrends, T. Journal of Contaminant Hydrology.</i> https://doi.org/10.1016/j.jconhyd.2023.104160	
6	Chapter 6 Synthesis	213
7	Acknowledgements	229
8	List of Publications	230
9	Summary	231
10	Samenvatting	234
11	Curriculum Vitae	237



Chapter

1

1 Chapter 1: Introduction

This thesis investigates how to improve the management of drained agricultural areas to optimize the retention of iron-associated phosphorus. **Chapter 1** introduces the motivation behind the need for this specific research. More specifically, it covers: What is phosphorus? Why can high phosphorus concentrations cause water quality issues? Why is phosphorus monitoring and management important in agricultural areas? Why and how can iron be used to retain phosphorus? Then, the state of art in phosphorous research is described, followed by the scope and objectives of the P-TRAP project, and finally, the thesis objectives and outline.

1.1 Motivation

Phosphorous (P) is an essential macronutrient for crop growth. Through sorption, desorption, precipitation and dissolution processes, and microbially mediated processes, nature makes P in the soil available for crops to grow. However, the P availability for crops is limited by the low solubility of P-containing phases, and often the P present naturally in the soil is insufficient to sustain agricultural production. This has led to P application to the soil in the form of fertilizers or animal manure to sustain intensive agriculture. A high food production is needed. The world population is growing, in 2022 the world is home to 8 billion people and is projected to reach 9.8 billion by 2050 (Roser & Rodés-Guirao, 2022). Therefore, agricultural production needs to meet the growing demand if we want to reach the Sustainable Development Goals to eradicate extreme poverty and hunger. Intensive agricultural practices cause nutrient losses which conflict with other Sustainable Development Goals such as having clean water and sustaining life on land and below water. A balance is needed between intensifying food production and making a sustainable use of the resources in the planet. Therefore, research on nutrient retention measures that support the growth of agriculture in a sustainable way are of great importance.

Although P application is needed to maintain a high agricultural production, the availability of P-resources are limited. Nitrogen-based fertilizers can be produced with the Haber-Bosch process where nitrogen gas reacts with methane (natural gas) to obtain ammonia. Air consists to 80% out of nitrogen gas, therefore the supply for nitrogen-based fertilizers is almost

unlimited (ignoring energy limitations). Unlike nitrogen-based fertilizers, the majority of P for fertilizers is produced by mining, and fertilizer production is also the main consumer of mined P. Economically relevant ores of P are concentrated in just a few countries. According to the USGS, 70% of the world's reserves are sedimentary rock found in Morocco and Western Sahara (Jasinski, 2021). It is estimated that globally there is enough P for the next 300 years (Dawson & Hilton, 2011). The biggest economic powers have their own P reserves, the USA reserves may last for the next 40 years (Jasinski, 2021), and the Chinese for about 35 years (Li et al., 2015). Europe does not own P reserves and is dependent on imported P. About 30% of the fertilizers imported by the EU in 2021 came from Russia and costed about one billion euros (ESPP, 2022). Fertilizers are commodities and the price of grains (wheat, soy, corn, barley, etc.) and energy affect their cost as well as conflicts between countries that may compromise the amount of raw material available. Figure 1-1 shows the price of fertilizers in the last 30 years until March 2022. The price of fertilizers hit the highest prices during the 2008 economic crisis and the prices have recently risen again with the increase in corn, soybean, and wheat prices and the increase in gas and energy prices which are linked to the Russian invasion of Ukraine. By the end of September 2022 the price of the DAP (diammonium phosphate) is 947 dollars per ton (Schnitkey et al., 2023).

Humans have modified the P-cycle by accelerating the weathering and transfer of P into oceans (Ruttenberg, 2003). The formation of phosphorites (sedimentary phosphate-containing rock) at the bottom of lakes and oceans takes place at geological time-scales while the extraction of P rock and P use in agriculture happens at a very fast rate. After P is extracted, it is placed in the fields, and a fraction ends up in the rivers through soil erosion, leaching, or after wastewater treatment once humans ate the food. It is estimated that of the P applied 50% and 15% is lost in soil erosion by water globally and in Europe, respectively (Alewell et al., 2020). Once in the water, the P is transported further downstream until it finally reaches the oceans. After P reaches the oceans it is "lost" as P recovery from the ocean bed is economically not feasible (Desmidt et al., 2015). There are very few P recovery streams, mainly in the wastewater treatment; nevertheless, P recovery in waste water treatment plants is estimated to be only about 6.5% of the P mined each year (Wilfert et al., 2015). There is a need for more rational and balanced management of the P cycle to sustain food production and biodiversity in a future with population growth.

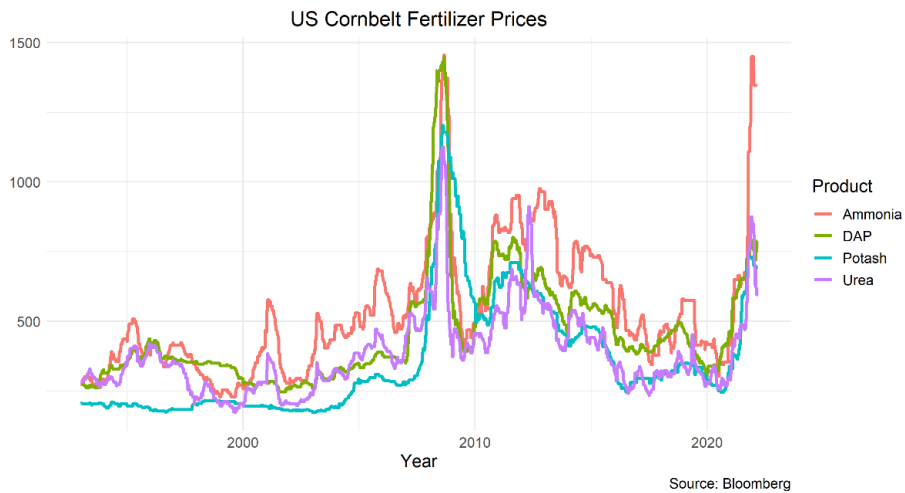


Figure 1-1 Price of fertilizers in US dollars per ton in the last 30 years until March 2022, Ammonia, DAP (di-ammonium phosphate), Potash (potassium based fertilizer), and Urea. From (Davids, 2022).

Apart from the limited availability on the long term, P can also cause harmful effects to aquatic and terrestrial ecosystems on the short term. Eutrophication occurs when surface waters, such as a sea, lake, or river, accumulates an excess of nutrients, particularly of P and nitrogen (N) (Farley, 2012). When nutrients are high, the primary production increases and only some phytoplankton groups grow excessively. As a result, biodiversity declines (Mahroofa et al., 2022). Eutrophication makes the treatment of fresh water for drinking technically more complicated and expensive. Eutrophication causes the appearance of dead zones in lakes and oceans, killing fish due to lack of oxygen (Farley, 2012). The export of P and N to surface waters increased worldwide during the 20th century (Vilmin et al., 2018). Diffuse pollution is the main source of P for the Baltic Sea (50%) and accounts for 46% of the anthropogenic sources for the North Sea (Cordell & Neset, 2014). Livestock farming contributes to 24% of the P in the rivers in Europe (Leip et al., 2015). In the Netherlands, 60% of the P input to regional surface waters is linked to agriculture (Groenenberg et al., 2013), Figure 1-2 shows plankton blooms, excessive macrophyte growth, and duck weed covers in agricultural ditches and small lakes in the Netherlands. It is important to reduce the diffuse P contamination coming from agriculture to improve the quality, biodiversity and ecosystem services of water bodies.

Preserving biodiversity for future generations is important and governments around the world implement directives and plans to preserve water quality. In the US, the Clean Water Act regulates the pollution to surface waters. In Europe, the Water Framework Directive (Directive 2000/60/EC, WFD) sets the legislation to reach a good ecological status in the water bodies of its member states. For this, each state has to set specific targets, the nutrient concentrations are used as supporting elements to determine the ecological status of the water bodies together with other criteria such as the hydromorphology and concentration of toxic substances like trace elements and pesticides. Preserving water quality is still a challenge. It is estimated that only one-third of the water bodies in Europe has a good ecological status (Grizzetti et al., 2017). Most water bodies in Europe fail to have a good ecological status with North-West Europe being the region with poorer results (Figure 1-3). At the same time, North-West Europe is one of the regions with the highest N and P surpluses in the soil (Figure 1-4). The nutrient surplus is defined as the sum of all nutrient inputs such as fertilizers, manure and biosolids, atmospheric deposition, biological fixation and net mineralization minus nutrients removed via crop harvest (and NH_3 volatilization in the case of N) (Schröder & Neeteson, 2008). P surplus is main driver for excessive nutrient transfer into adjacent surface waters.



Figure 1-2 Pictures algae blooms, excessive macrophyte growth, and duck weed covers in the Netherlands in agricultural ditches and small lakes in the summer of 2021 and 2022.

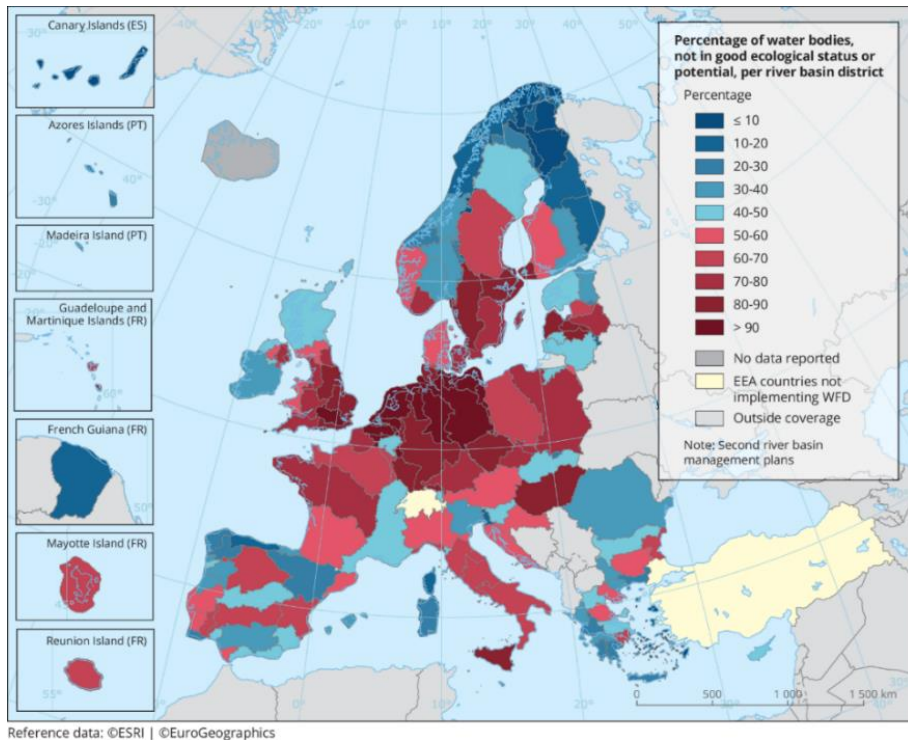


Figure 1-3 Percentage of waterbodies (rivers, lakes, transitional and coastal waters) in Europe that fail to reach a good ecological status as established by the Water Framework Directive. From (EEA, 2021).

In North-West Europe, agriculture intensified after the second world war, in the late 80s environmental legislation was introduced to prevent eutrophication, and in recent years the P surplus of soils is close to zero (Bol et al. 2018; McDonald et al. 2019, Figure 2-1). The manure applied historically produced an accumulation of P beyond the crop requirements in the soil called legacy P (Sharpley et al., 2013). Manure and compost have a N:P ratio between 2 and 4 while the crop uptake ratio is between 5 and 9, which results in an accumulation of P in the soil (Schoumans et al., 2014). In an ideal world, the P in the soil should be enough to sustain crop production but should not cause environmental issues downstream. However, when the soils have a high P content, even if no more P is added to the soil, the existing P desorbs from the soil particles and leaches downstream (Schoumans et al., 2015, Figure 1-5). This is a slow process and the legacy P in the soil can continue leaching for decades after P

application stops before reaching levels that are no longer a threat to the environment (Melland et al., 2018; Schoumans & Chardon, 2014). Therefore, measures are needed to reduce P losses from agricultural areas in the short- to middle-term.

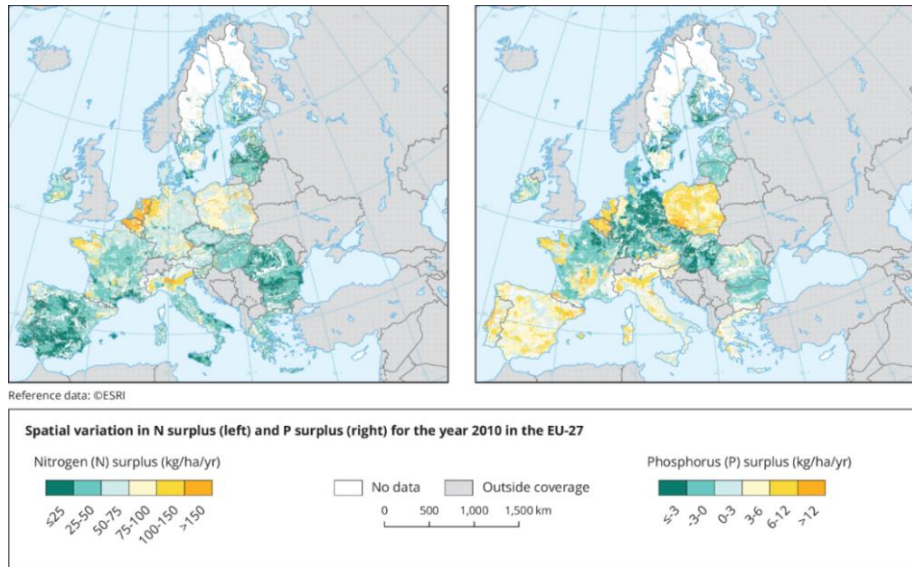


Figure 1-4 The surplus for N (left map) and P (right map). From (EEA, 2022). The nutrient surplus is defined as the sum of all nutrient inputs such as fertilizers, manure and biosolids, atmospheric deposition, biological fixation and net mineralization minus nutrients removed via crop harvest.

Nutrient inputs to water bodies can be divided into point and non-point (diffuse) sources. Point sources concentrate the discharge in a single pipe; examples of point sources are the effluent from industrial and municipal wastewater treatment plants. With the incorporation of tertiary treatment, such as biological P removal and P precipitation with iron (Fe), aluminum (Al), calcium (Ca), or magnesium (Mg), P pollution coming from point sources has been significantly reduced. P precipitation is very advanced, and P can be recovered as struvite, vivianite, or calcium phosphates (Henze et al., 2011; Wilfert et al., 2015, 2018). The most obvious use for the recovered P would be to apply it directly on the agricultural soil. Nevertheless, because of concerns regarding toxic substances and organic contaminants, this practice is banned in many countries (Donatello & Cheeseman, 2013; Kelessidis & Stasinakis,

2012; Smith, 2009). Non-point (or diffuse) sources of nutrients towards surface water occur as precipitation water is transported through the soil and groundwater, through subsurface drainage systems or via surface runoff to local streams. Especially these non-point sources remain a major challenge to reducing P pollution in rivers and lakes in Europe and other parts of the world (Bol et al., 2018; Hart et al., 2004; Withers & Haygarth, 2007).

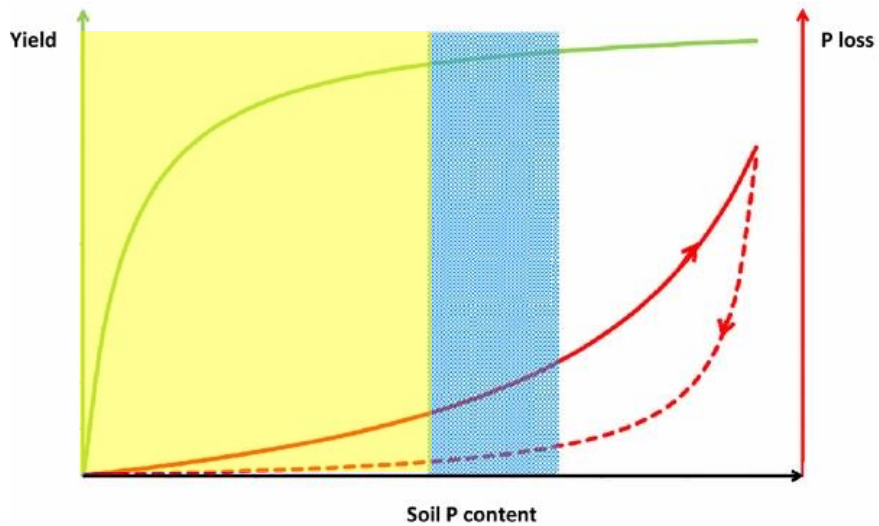


Figure 1-5 Conceptual representation of gains in crop yield and P losses to surface waters (green and red solid lines) when increasing soil P content and the expected P loss or leaching at decreasing soil P content (dotted red line) (caused by phytomining or by a decrease in the P input). Target zone to optimize crop yield (blue area), target zone to minimize P losses (yellow area). Modified from Schoumans et al. (2015)

P retention measures together with a thoughtful addition of P as fertilizer and manure can help reducing the legacy P effect and offer a solution for the short- and middle-term transition period. Keeping the nutrients in the agricultural land as much as possible is beneficial for farming. There are many measures that can be applied to reduce P losses from agriculture to surface waters to reach the WFD targets and allow to continue with agricultural production. Examples of measures to reduce P losses are listed in the categories proposed by Schoumans et al. (2014):

1. Nutrient management: make use of the P already present in the soil, do not add fertilizer or manure at hot spots, use fertilizers and manure combined to get optimal N:P ratios for crops, phase the nutrient application over the year (do not apply manure or fertilizers outside the growing season).
2. Crop management: have grassland instead of arable crops, use catch crops, phytomining (use crops that can take/mine the excess P present in the soil (Svanbäck et al., 2015)).
3. Livestock management: reduce P content in animal feed, treat and transport animal manure.
4. Soil management: no tillage/direct drilling, contour ploughing, add chemical compounds to the soil to bind soluble P (examples include chalk or iron oxides).
5. Water management within agricultural land: add ponding systems and sediment traps to capture particulate P, optimize the drainage systems to minimize P losses through leaching.
6. Land use change and landscape management: buffer strips to intercept nutrient losses, prevent contact of livestock with surface waters, avoid certain crops in hilly areas, afforest or set aside agricultural land.
7. Surface water management: re-meander rivers, restore flood plains and reconnect inundation areas, apply chemicals to bind P in lake sediments, create wetlands in riparian areas.

After the implementation of the Nitrate Directive (91/676/EEC) the livelihood of the farmers and their production has been a sensitive issue. From the farmer's perspective, it is important that the P retention measures do not take up large amounts of arable land. Some measures such as wetlands and riparian buffers result in extensive use of a part of the arable land, making their implementation costly to farmers in areas with high land prices. The effects of other measures, involving crop and nutrient management, may only be noticeable in the long term. This thesis focused on water management measures within the agricultural land and on adding iron-based filters in drainage systems. This type of measures offers the advantage of acting close to the nutrient source instead of effect-oriented measures in the receiving lakes or coastal areas where the problem is already visible. Water management measures within the agricultural land such as water retention may increase productivity but could also change the soil moisture and chemical conditions, reducing P sorption and accelerating P

transport (Chardon and Schoumans 2007; Schoumans and Chardon 2014). Furthermore, adding chemical compounds to the soil or drainage system may interact with other soil processes. Therefore, the design and implementation of effective mitigation measures requires detailed insight into chemical and hydrological P transport routes and mechanisms in drainage systems.

Drainage systems in farms are a good place to implement P retention measures as they concentrate most of the agricultural drainage. It is estimated that 30 million hectares are artificially drained in Europe, both with open ditches and drain pipes (Döll & Siebert, 2005). In Nord-West Europe the proportion of the arable land that is artificially drained with open ditches or pipes is even higher, it accounts for 66% of the arable land in the UK, 40% in the Scandinavian countries, and 87% in the Netherlands (Brown & Van Beinum, 2009). Measurements have shown that the outflow of drains in the Netherlands can contribute up to 80% of the total P reaching surface waters (Rozemeijer et al., 2010; Rozemeijer & Broers, 2007). Drain system outlets open the possibility to intercept the P flux from agricultural soils at well-defined spots.



Figure 1-6 Fe-rich sediment in the agricultural ditches in the Netherlands

The interaction of P with Fe in natural and agricultural areas determine if P is found in dissolved or particulate form as well as its bioavailability to be used by microorganisms as algae to grow. The formation of fresh Fe precipitates can be an effective sink for dissolved P at the interface between drainage pipes and ditches or at the interface between groundwater and drainage pipes. When the groundwater flowing through the drainage system is rich in dissolved Fe (II), the contact of the water with atmospheric oxygen can result in the formation of P-enriched Fe(III) (hydr)oxides (Baken et al., 2016; Van der Grift et al., 2014). These newly formed particles settle at the bottom of ditches and streams (Figure 1-6), and the high Fe affinity makes the P less bioavailable for algae growth than the dissolved phosphate (Baken et al., 2014).

When the groundwater in the drainage system does not contain sufficiently high natural concentrations of Fe (II), Fe-rich sorbents can be used in drains to retain the dissolved P. For example, natural Fe-rich sands have been added to streams to reduce dissolved P concentrations (Van Dael et al., 2021; Xia et al., 2021). To scale up P retention measures, low-cost sorbents based on Fe (III) oxides are needed. It is not hard to find such Fe (III) oxides as Fe is an abundant element, the 4th in the earth's crust. Large amounts of Fe (III) oxides can be obtained as by-products from drinking water production. In the Netherlands drinking water needs to have low Fe values, below 0.05 mg/l and even 0.02 mg/l, while the principal source for drinking water is groundwater which usually has high Fe concentrations. During drinking water treatment, Fe is usually removed by aeration and sand filtration, transforming dissolved Fe (II) into hydrous ferric oxides (Sharma et al., 2002; Van Beek et al., 2020, 2021). The resulting products are called iron sludge and iron-coated sand (ICS) which are commercialized by AquaMinerals (<https://aquaminerals.com/en/>). Fe materials have proven to be more effective than other sorbent materials using Ca for large-scale measures to remove dissolved P (Penn et al., 2017; Penn & Bowen, 2017).

1.2 Relevant previous research on iron-associated phosphorus retention and on nutrient management in drained agricultural areas

Previous studies by Van der Grift et al. (2014, 2016, 2018), Baken et al. (2015, 2016a, 2016b), and Smolders et al. (2017) provide a solid base to look into the P-Fe interactions in lowland catchments. Fe is a redox-sensitive element, it is found dissolved in anoxic groundwater in its reduced form as Fe (II), and forms Fe (III) (hydr)oxides in the presence of oxygen which can co-precipitate or adsorb dissolved P. When groundwater exfiltrates to the surface water, redox gradients can often be found. Redox gradients are often relevant in the sediment of ditches and other surface waters. Once the P-containing Fe (hydr)oxides settle, the P may become available again if the conditions are Fe-reducing, for example during periods with oxygen depletion in the summer. Moreover, the P availability depends on the P/Fe ratio. A large data analysis by Smolders et al. (2017) showed that river sediments with high P/Fe molar ratios (>0.4) mobilize P at low dissolved oxygen concentrations while this effect was not observed for lower P/Fe molar ratios. To implement measures in agricultural areas to reduce downstream eutrophication it is paramount to understand P-Fe interactions and redox dynamics. P-Fe interactions are complex. P can be adsorbed to the Fe and Al present in the soil. However, adsorption has a limit and the high fertilization of agricultural lands in the Netherlands has made soils reach a P saturation degree close to their maximum (Schoumans & Chardon, 2014). To think of interventions such as P retention measures in farms it is important to take all relevant processes into account. Therefore, scientific studies at the farm scale are needed. Nevertheless, many of the available studies are limited to the laboratory or plot scale (Van der Salm et al. 2011; Van der Grift et al. 2014), or in large-scale catchment (De Klein and Koelmans, 2011; Baken et al. 2015; Van der Salm et al. 2011; Van der Grift et al. 2014; Van der Grift et al. 2016).

High-frequency water quality monitoring is a relevant tool to study water quality in small catchments as the detailed data obtained can show the processes involved in nutrient transport (Rode et al., 2016; Rozemeijer et al., 2010). Continuous measurements are especially important for understanding P transport, quantifying P loads, and evaluating the effectiveness of measures. Large loads of P can be transported during short peak flow

conditions and grab samples can miss concentration peaks causing underestimations of P sources. Nevertheless, when sensors and autoanalyzers are used in high-frequency monitoring they create the challenge that large volumes of data are retrieved and the post-processing is often not so straightforward (Zhang et al., 2019). The most time-consuming post-processing tasks include the identification of errors and the filling of missing values. Moreover, standardization of post-processing high-frequency data is also challenging as currently, the final result depends largely on the person who did the data analysis (Jones et al., 2021). To observe the bigger picture in nutrient transport and to evaluate trends related to rain variability and climate change, more long-term high-quality continuous water quality data series are needed.

Relevant research on P retention measures using iron sludge and ICS has been carried out at pilot and full-scale (Chardon et al., 2021; Groenenberg et al., 2013; Lambert et al., 2020; Vandermoere et al., 2018). ICS has been placed around tile drains or in edge-of-field filters at the outlet of drainage pipes to remove P from agricultural drainage. These ICS filters are placed in areas with a high P/Fe ratio in the groundwater and therefore high proportions of P in its dissolved form (PO_4) and take advantage of the ICS capacity to bind P. These ICS filters are likely to be adopted by farmers as the measures are buried and there is no need to take up arable land as is the case with buffer areas or wetlands. In some areas, the traditional method of constructing tile drains includes placing sea shells around them to improve the hydraulic conductivity, replacing the sea shells with ICS implies almost no changes in the constructive methods and can reduce the load of P moving downstream. Figure 1-7 shows the construction of full-scale experiments that used ICS around drains in the Netherlands.

Although using ICS in drainage systems to remove P has shown very good results, there are still issues to be addressed before they can be scaled to a national or regional level. One of the discussions about the use of ICS filters in drainage systems is where to place them, i.e., around the drains or after the drains. Each option has its pros and cons. Placing the ICS around the drains allows applying larger amounts of ICS and therefore a longer life-span while the filters outside the drain are smaller and need to be replaced every 1 or 2 years. In addition, the flow velocity around the drain is slower than out of the drain. However, placing the filter out of the drain allows more flexibility as the material is not buried and it is easier to replace or do maintenance, and the contact with the air can make redox conditions less reducing.

One major issue is that when the ICS is placed below the groundwater level the oxygen availability is limited and the organic matter present in the soil or added as a soil amendment may favor anaerobic microbiological reactions, in which nitrate (NO_3), manganese (Mn) and Fe (hydr)oxides, sulfate (SO_4), and/or carbon dioxide (CO_2) are used as terminal electron acceptors. The dissolution of Fe could eventually release the previously removed P (Schroth et al., 2015; Thamdrup, 2000; Young & Ross, 2001) or alter the Fe oxides in the coating. Previous research has looked into the effect of reducing conditions in the field (Chardon et al., 2021; Groenenberg et al., 2013). But because of difficulties in sampling, the transformations in the ICS material are still unknown and the effect on P retention was indirectly concluded.

Another issue that needs to be addressed for the design of effective measures is the P retention capacity of the ICS. The ICS grains consist of a sand core covered by a porous Fe coating. The outside of the ICS is in contact with the P-containing water, however not all adsorption sites are on the outside, many are inside the coating and are only reachable by diffusion through the micropores. Slow adsorption kinetics are controlled by intra-particle diffusion through the pores inside the iron-coating and are often neglected in studies on the adsorption capacity of iron materials (Ajmal et al., 2018; Koopmans et al., 2004; Willett et al., 1988). The research by Chardon et al. (2012) and Lambert et al. (2020) showed that slow kinetic processes were also relevant in ICS. But the slow kinetics could not be parametrized with the available data. Therefore, a tool for the design of P retention measures that use ICS efficiently considering slow kinetics is still missing.



Figure 1-7 Construction of drains covered with ICS

1.3 The P-TRAP project

This thesis is part of the P-TRAP project. P-TRAP is a European Horizon 2020 Marie Skłodowska Curie Innovative Network. The P-TRAP consortium is composed of 16 international institutions and hosts 11 Ph.D. students also called Early-Stage Researchers (ESR). The scientific problems that P-TRAP aims to address are two. The first is that the flux of P from agricultural areas to surface waters is wasting a resource that is becoming scarce and the second is that the excessive load of P to surface waters coming from agricultural areas is the main cause of eutrophication. P-TRAP stands for P trapping and involves the use of Fe biogeochemical cycles to remove and recycle P in the environment, most specifically it involves the application of Fe-containing by-products from drinking water treatment to capture P in lakes and drained agricultural areas. The project is divided into three scientific work packages. The first package works on closing the cycle of P application in agriculture, the second on novel methods for long-term P binding in lake sediments, and the third on mechanistic studies on P dynamics during Fe phase transformation. This thesis is related to the first work package and aims to develop technologies to retain P leaking from agricultural

soils within drained systems. This study is expected to contribute, in collaboration with other ESRs, to the development of guidelines and recommendations for retaining and recovering Fe-bound P in drainage systems, kinetic models for the transformation of P containing Fe phases, and insights on the fate of P during Fe phase transformations.

1.4 Objectives and outline

The general objective of this thesis is to contribute to improving the management of drained agricultural areas and to optimize the retention of Fe-associated P. The specific objectives are to:

- investigate the Fe coupled P export from a drained agricultural farm,
- develop strategies for the optimization of monitoring of drainage systems,
- investigate how redox dynamics influence P retention in drainage systems that use measures with iron-by products such as ICS,
- contribute to a coupled geochemical/hydrological model for predicting long-term P adsorption into ICS.

The specific objectives were addressed by using different methodologies and a combination of laboratory experiments, field monitoring, and process- and data-based modeling. The transport of P is different when it moves through iron-poor sands in the west or in the iron-rich sands in the east of the Netherlands and call for different P retention strategies. Figure 1-8 shows the location of the investigated field sites in the Netherlands. **Chapters 2 and 3** focus on quantifying the P loading at a drained farm with exfiltration of iron-rich sandy soils in the east of the Netherlands. In this area the iron present acts as a sink for P. In contrast, **chapter 4** investigates two fields in the west of the Netherlands, a region characterized by soils having high P concentrations and not enough iron to bind the P. In the field investigated in **chapter 4** pilot filters with ICS around the drains were implemented as a P retention measure. **Chapters 4 and 5** focus on understanding the redox and kinetic mechanisms of P retention onto ICS to improve the design, operation, and maintenance of ICS filters.

In **chapter 2**, “Processes controlling the flux of legacy phosphorus to surface waters at the farm scale”, high-frequency sensors and auto-analyzers were used to understand the farm

scale transport pathways of P and N from the soil to the surface water. With a mass balance, it is explained how P transport is linked to the Fe content in the sediment and subsoil. In **chapter 3**, “Value and limitations of Machine Learning in high-frequency nutrient data for gap-filling, forecasting, and transport process interpretation”, four years of high-frequency monitoring data were used. High-frequency data offers the challenge of dealing with large amounts of data, especially for post-processing and dealing with missing values. The performance of different Machine Learning techniques for gap-filling was evaluated and it was assessed to what extent these data-based models are valid for making predictions.

In **chapter 4**, “Phosphorus adsorption on iron-coated sand under reducing conditions”, one of the main concerns when applying iron-coated sand filters in the field was investigated. Fieldwork monitoring of two pilot ICS filters in the flower growing area of the Netherlands was combined with microcosm laboratory experiments to investigate the effect of variable redox conditions on P retention by ICS. In **chapter 5**, the focus is on the “Transport limited kinetics of phosphate retention on iron-coated sand and practical implications”. Although ICS filters are used in full-scale measures, there were still doubts about the sorption capacity that may be achieved and which are the best operation and maintenance practices. A reactive transport model was parameterized. This model considers the long-term P retention and allows the calculation of the ICS filter’s efficiency under different flow velocities and stop-flow regimes.

The research questions of **chapters 4 and 5** were discussed together with the engineering company Arcadis to be of use for practical applications. For the last 6 months of the project, the ESR worked for one day a week at Arcadis, one of beneficiaries of the P-TRAP project, to facilitate knowledge transfer. **Chapter 6** synthesizes how the main findings of this thesis can help the monitoring and diagnosis of diffuse P pollution from agricultural areas and provide tools for designing and optimizing Fe-based P-retention measures and includes practical examples of full-scale P retention measures with ICS managed by Water Boards *Brabantse Delta* and *Delfland*.

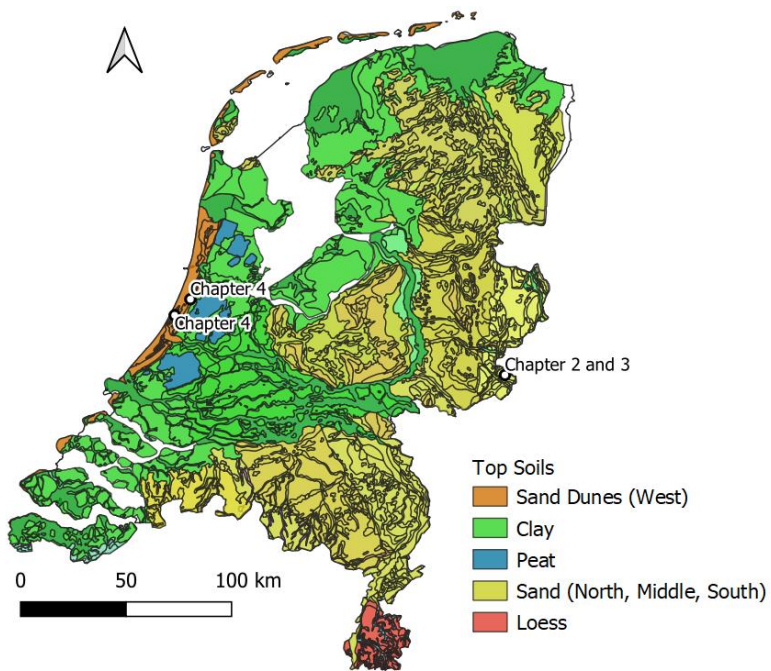


Figure 1-8 Location of the drained farms investigated in chapters 2, 3 and 4 in a map containing the major top soil groups of the Netherlands.

1.5 References

- Ajmal, Z., Muhmood, A., Usman, M., Kizito, S., Lu, J., Dong, R., & Wu, S. (2018). Phosphate removal from aqueous solution using iron oxides : adsorption , desorption and regeneration characteristics. *Journal of Colloid And Interface Science*. <https://doi.org/10.1016/j.jcis.2018.05.084>
- Alewell, C., Ringeval, B., Ballabio, C., Robinson, D. A., Panagos, P., & Borrelli, P. (2020). Global phosphorus shortage will be aggravated by soil erosion. *Nature Communications*, *11*(1). <https://doi.org/10.1038/s41467-020-18326-7>
- Baken, S., Moens, C., Van der Grift, B., & Smolders, E. (2016). Phosphate binding by natural iron-rich colloids in streams. *Water Research*, *98*, 326–333. <https://doi.org/10.1016/j.watres.2016.04.032>
- Baken, S., Nawara, S., Van Moorleghem, C., & Smolders, E. (2014). Iron colloids reduce the bioavailability of phosphorus to the green alga *Raphidocelis subcapitata*. *Water Research*, *59*, 198–206. <https://doi.org/10.1016/j.watres.2014.04.010>
- Baken, S., Regelink, I. C., Comans, R. N. J., Smolders, E., & Koopmans, G. F. (2016). Iron-rich colloids as carriers of phosphorus in streams: A field-flow fractionation study. *Water Research*, *99*, 83–90. <https://doi.org/10.1016/j.watres.2016.04.060>
- Baken, S., Verbeeck, M., Verheyen, D., Diels, J., & Smolders, E. (2015). Phosphorus losses from agricultural land to natural waters are reduced by immobilization in iron-rich sediments of drainage ditches. *Water Research*, *71*, 160–170. <https://doi.org/10.1016/j.watres.2015.01.008>
- Bol, R., Gruau, G., Mellander, P. E., Dupas, R., Bechmann, M., Skarbøvik, E., Bieroza, M., Djodjic, F., Glendell, M., Jordan, P., Van der Grift, B., Rode, M., Smolders, E., Verbeeck, M., Gu, S., Klumpp, E., Pohle, I., Fresne, M., & Gascuel-Oudou, C. (2018). Challenges of reducing phosphorus based water eutrophication in the agricultural landscapes of Northwest Europe. *Frontiers in Marine Science*, *5*(AUG), 1–16. <https://doi.org/10.3389/fmars.2018.00276>
- Brown, C. D., & Van Beinum, W. (2009). Pesticide transport via sub-surface drains in Europe. *Environmental Pollution*, *157*(12), 3314–3324. <https://doi.org/10.1016/j.envpol.2009.06.029>
- Chardon, W., Groenenberg, J. E., Vink, J. P. M., Voegelin, A., & Koopmans, G. F. (2021). Use of iron-coated sand for removing soluble phosphorus from drainage water. *Science of The Total Environment*, *815*, 152738. <https://doi.org/10.1016/j.scitotenv.2021.152738>
- Chardon, W. J., & Schoumans, O. F. (2007). Soil texture effects on the transport of phosphorus from agricultural land in river deltas of Northern Belgium, the Netherlands and North-West Germany. *Soil Use and Management*, *23*(SUPPL. 1), 16–24. <https://doi.org/10.1111/j.1475-2743.2007.00108.x>
- Chardon, W.J., Groenenberg, J. E., Temminghoff, E. J. M., & Koopmans, G. F. (2012). Use of Reactive Materials to Bind Phosphorus. *Journal of Environmental Quality*, *41*(3), 636–646. <https://doi.org/10.2134/jeq2011.0055>
- Cordell, D., & Neset, T. S. S. (2014). Phosphorus vulnerability: A qualitative framework for assessing the

- vulnerability of national and regional food systems to the multi-dimensional stressors of phosphorus scarcity. *Global Environmental Change*, 24(1), 108–122.
<https://doi.org/10.1016/j.gloenvcha.2013.11.005>
- Davids, U. (2022). *The Story of Rising Fertilizer Prices*. <https://asmith.ucdavis.edu/news/story-rising-fertilizer-prices>
- Dawson, C. J., & Hilton, J. (2011). Fertiliser availability in a resource-limited world: Production and recycling of nitrogen and phosphorus. *Food Policy*, 36(SUPPL. 1), S14–S22.
<https://doi.org/10.1016/j.foodpol.2010.11.012>
- De Klein, J. J. M., & Koelmans, A. A. (2011). Quantifying seasonal export and retention of nutrients in West European lowland rivers at catchment scale. *Hydrological Processes*, 25(13), 2102–2111.
<https://doi.org/10.1002/hyp.7964>
- Desmidt, E., Ghyselbrecht, K., Zhang, Y., Pinoy, L., Van Der Bruggen, B., Verstraete, W., Rabaey, K., & Meesschaert, B. (2015). Global phosphorus scarcity and full-scale P-recovery techniques: A review. *Critical Reviews in Environmental Science and Technology*, 45(4), 336–384.
<https://doi.org/10.1080/10643389.2013.866531>
- Döll, P., & Siebert, S. (2005). A digital global map of artificially drained agricultural areas. In *Frankfurt Hydrology Paper 04, Institute of physical geography, Frankfurt University* (Issue 01).
<https://doi.org/10.13140/2.1.3971.3923>
- Donatello, S., & Cheeseman, C. R. (2013). Recycling and recovery routes for incinerated sewage sludge ash (ISSA): A review. *Waste Management*, 33(11), 2328–2340.
<https://doi.org/10.1016/j.wasman.2013.05.024>
- EEA. (2021). *Percentage of water bodies not in good ecological status or potential, per river basic district*.
<https://www.eea.europa.eu/data-and-maps/figures/proportion-of-classified-surface-water-7>
- EEA. (2022). *Spatial variation in N surplus (left) and P surplus (right) for the year 2010 in the EU-27*.
<https://www.eea.europa.eu/data-and-maps/figures/spatial-variation-in-n-surplus>
- ESPP. (2022). *ESPP eNews no. 64 - March 2022*. https://www.phosphorusplatform.eu/scope-in-print/enews/2163-esp-eneews-no-64-march-2022#_Toc97139680
- Farley, M. (2012). Eutrophication in Fresh Waters: An International Review. In *Encyclopedia of Lakes and Reservoirs. Encyclopedia of Earth Sciences Series*. Springer Netherlands.
https://doi.org/https://doi.org/10.1007/978-1-4020-4410-6_79
- Grizzetti, B., Pistocchi, A., Liqueste, C., Udias, A., Bouraoui, F., & Van De Bund, W. (2017). Human pressures and ecological status of European rivers. In *Scientific Reports* (Vol. 7, Issue 1).
<https://doi.org/10.1038/s41598-017-00324-3>
- Groenenberg, J. E., Chardon, W. J., & Koopmans, G. F. (2013). Reducing Phosphorus Loading of Surface Water Using Iron-Coated Sand. *Journal of Environmental Quality*, 42(1), 250–259.
<https://doi.org/10.2134/jeq2012.0344>

- Hart, M. R., Quin, B. F., & Nguyen, M. L. (2004). Phosphorus runoff from agricultural land and direct fertilizer effects: A review. *Journal of Environmental Quality*, 33(6), 1954–1972. <https://doi.org/10.2134/jeq2004.1954>
- Henze, M. ., Van Loosdrecht, M. ., Ekama, G. ., & Brdjanovic, D. (2011). *Biological wastewater treatment, treatment modelling and design*. IWA Publishing.
- Jasinski, S. M. (2021). Phosphate rock. In *U.S. Geological Survey, Mineral Commodity Summaries*.
- Jones, A. S., Jones, T. L., Logan, N., & Horsburgh, J. S. (2021). *Toward automating post processing of aquatic sensor data*. 435, 1–63.
- Kelessidis, A., & Stasinakis, A. S. (2012). Comparative study of the methods used for treatment and final disposal of sewage sludge in European countries. *Waste Management*, 32(6), 1186–1195. <https://doi.org/10.1016/j.wasman.2012.01.012>
- Koopmans, G. F., Chardon, W. J., de Willigen, P., & Van Riemsdijk, W. H. (2004). Phosphorus Desorption Dynamics in Soil and the Link to a Dynamic Concept of Bioavailability. *Journal of Environment Quality*, 33(33), 1393–1402.
- Lambert, N., Van Aken, P., Van den Broeck, R., & Dewil, R. (2020). Adsorption of phosphate on iron-coated sand granules as a robust end-of-pipe purification strategy in the horticulture sector. *Chemosphere*, 267, 129276. <https://doi.org/10.1016/j.chemosphere.2020.129276>
- Leip, A., Billen, G., Garnier, J., Grizzetti, B., Lassaletta, L., Reis, S., Simpson, D., Sutton, M. A., De Vries, W., Weiss, F., & Westhoek, H. (2015). Impacts of European livestock production: Nitrogen, sulphur, phosphorus and greenhouse gas emissions, land-use, water eutrophication and biodiversity. *Environmental Research Letters*, 10(11). <https://doi.org/10.1088/1748-9326/10/11/115004>
- Li, B., Boiakina, I., Young, B., & Yu, W. (2015). Substance Flow Analysis of Phosphorous in China. *International Journal of Environmental Science and Development*, Vol., 6(1), 9–13. <https://doi.org/10.7763/IJESD.2015.V6.552>
- Mahroofa, J., Sumaya, H., & Ara, A. (2022). Freshwater Biodiversity: Indicators of Eutrophication and Pollution. In *Biodiversity of freshwater ecosystems* (p. 22).
- McDonald, N. T., Wall, D. P., Mellander, P. E., Buckley, C., Shore, M., Shortle, G., Leach, S., Burgess, E., O’Connell, T., & Jordan, P. (2019). Field scale phosphorus balances and legacy soil pressures in mixed-land use catchments. *Agriculture, Ecosystems and Environment*, 274(December 2018), 14–23. <https://doi.org/10.1016/j.agee.2018.12.014>
- Melland, A. R., Fenton, O., & Jordan, P. (2018). Effects of agricultural land management changes on surface water quality: A review of meso-scale catchment research. *Environmental Science and Policy*, 84(September 2017), 19–25. <https://doi.org/10.1016/j.envsci.2018.02.011>
- Penn, C., & Bowen, J. M. (2017). Design and construction of phosphorus removal structures for improving water quality. In *Design and Construction of Phosphorus Removal Structures for Improving Water Quality*. <https://doi.org/10.1007/978-3-319-58658-8>

- Penn, C., Chagas, I., Klimeski, A., & Lyngsie, G. (2017). A review of phosphorus removal structures: How to assess and compare their performance. *Water (Switzerland)*, 9(8), 1–22. <https://doi.org/10.3390/w9080583>
- Rode, M., Wade, A. J., Cohen, M. J., Hensley, R. T., Bowes, M. J., Kirchner, J. W., Arhonditsis, G. B., Jordan, P., Kronvang, B., Halliday, S. J., Skeffington, R. A., Rozemeijer, J. C., Aubert, A. H., Rinke, K., & Jomaa, S. (2016). Sensors in the Stream: The High-Frequency Wave of the Present. *Environmental Science and Technology*, 50(19), 10297–10307. <https://doi.org/10.1021/acs.est.6b02155>
- Roser, M., & Rodés-Guirao, L. (2022). *Future Population Growth*. Our World in Data. <https://ourworldindata.org/future-population-growth#:~:text=on fertility rates-,How accurate have past population projections been%3F,at 10.4 billion in 2100>.
- Rozemeijer, J. C., & Broers, H. P. (2007). The groundwater contribution to surface water contamination in a region with intensive agricultural land use (Noord-Brabant, The Netherlands). *Environmental Pollution*, 148(3), 695–706. <https://doi.org/10.1016/j.envpol.2007.01.028>
- Rozemeijer, J. C., Van der Velde, Y., Van Geer, F. C., Bierkens, M. F. P., & Broers, H. P. (2010). Direct measurements of the tile drain and groundwater flow route contributions to surface water contamination: From field-scale concentration patterns in groundwater to catchment-scale surface water quality. *Environmental Pollution*, 158(12), 3571–3579. <https://doi.org/10.1016/j.envpol.2010.08.014>
- Rozemeijer, J., Van der Velde, Y., De Jonge, H., Van Geer, F., Broers, H. P., & Bierkens, M. (2010). Application and evaluation of a new passive sampler for measuring average solute concentrations in a catchment scale water quality monitoring study. *Environmental Science and Technology*, 44(4), 1353–1359. <https://doi.org/10.1021/es903068h>
- Ruttenberg, K. C. (2003). The Global Phosphorus Cycle. *Treatise on Geochemistry*, 8, 585–643. https://doi.org/10.1007/978-94-017-8944-8_20
- Schnitkey, G., Paulson, N., Swanson, K., Baltz, J., & Zulauf, C. (2023). *Weekly Farm Economics: Fertilizer Prices, Rates, and Costs for 2023*. University of Illinois. <https://farmdocdaily.illinois.edu/2022/09/fertilizer-prices-rates-and-costs-for-2023.html>
- Schoumans, O. F., & Chardon, W. J. (2014). Phosphate saturation degree and accumulation of phosphate in various soil types in The Netherlands. *Geoderma*, 237, 325–335. <https://doi.org/10.1016/j.geoderma.2014.08.015>
- Schoumans, O. F., Chardon, W. J., Bechmann, M. E., Gascuel-Oudou, C., Hofman, G., Kronvang, B., Rubæk, G. H., Ulén, B., & Dorioz, J. M. (2014). Mitigation options to reduce phosphorus losses from the agricultural sector and improve surface water quality: A review. *Science of the Total Environment*, 468–469, 1255–1266. <https://doi.org/10.1016/j.scitotenv.2013.08.061>
- Schoumans, Oscar F., Bouraoui, F., Kabbe, C., Oenema, O., & Van Dijk, K. C. (2015). Phosphorus management in Europe in a changing world. *Ambio*, 44(2), 180–192.

<https://doi.org/10.1007/s13280-014-0613-9>

- Schröder, J. J., & Neeteson, J. J. (2008). Nutrient management regulations in The Netherlands. *Geoderma*, 144(3–4), 418–425. <https://doi.org/10.1016/j.geoderma.2007.12.012>
- Schroth, A. W., Giles, C. D., Isles, P. D. F., Xu, Y., Perzan, Z., & Druschel, G. K. (2015). Dynamic Coupling of Iron, Manganese, and Phosphorus Behavior in Water and Sediment of Shallow Ice-Covered Eutrophic Lakes. *Environ. Sci. Technol.*, 49, 9758–9767. <https://doi.org/10.1021/acs.est.5b02057>
- Sharma, S., Petrusevski, B., & Schippers, J. C. (2002). Characterisation of coated sand from iron removal plant. *Water Science and Technology*, 2(2), 247–257. <https://doi.org/10.2166/ws.2002.0070>
- Sharpley, A., Jarvie, H. P., Buda, A., May, L., Spears, B., & Kleinman, P. (2013). Phosphorus Legacy: Overcoming the Effects of Past Management Practices to Mitigate Future Water Quality Impairment. *Journal of Environmental Quality*, 42(5), 1308–1326. <https://doi.org/10.2134/jeq2013.03.0098>
- Smith, S. R. (2009). Organic contaminants in sewage sludge (biosolids) and their significance for agricultural recycling. *Philosophical Transactions of the Royal Society A: Mathematical, Physical and Engineering Sciences*, 367(1904), 4005–4041. <https://doi.org/10.1098/rsta.2009.0154>
- Smolders, E., Baetens, E., Verbeeck, M., Nawara, S., Diels, J., Verdriev, M., Peeters, B., De Cooman, W., & Baken, S. (2017). Internal Loading and Redox Cycling of Sediment Iron Explain Reactive Phosphorus Concentrations in Lowland Rivers. *Environmental Science and Technology*, 51(5), 2584–2592. <https://doi.org/10.1021/acs.est.6b04337>
- Svanbäck, A., Ulén, B., Bergström, L., & Kleinman, P. J. A. (2015). Long-term trends in phosphorus leaching and changes in soil phosphorus with phytomining. *Journal of Soil and Water Conservation*, 70(2), 121–132. <https://doi.org/10.2489/jswc.70.2.121>
- Thamdrup, B. (2000). Bacterial Manganese and Iron Reduction. *Advances in Microbial Ecology*.
- Van Beek, C. G. E. M., Cirkel, D. G., de Jonge, M. J., & Hartog, N. (2021). Concentration of Iron(II) in Fresh Groundwater Controlled by Siderite, Field Evidence. *Aquatic Geochemistry*, 27(1), 49–61. <https://doi.org/10.1007/s10498-020-09390-y>
- Van Beek, C. G. E. M., Hofman-Caris, C. H. M., & Zweere, G. J. (2020). Drinking water treatment and chemical well clogging by iron(II) oxidation and hydrous ferric oxide (HFO) precipitation. *Journal of Water Supply: Research and Technology - AQUA*, 69(5), 427–437. <https://doi.org/10.2166/aqua.2020.140>
- Van Dael, T., Xia, L., Van Dijk, K., Potemans, S., & Smolders, E. (2021). Internal loading of phosphate in rivers reduces at higher flow velocity and is reduced by iron rich sand application: an experimental study in flumes. *Water Research*, 198, 117160. <https://doi.org/10.1016/j.watres.2021.117160>
- Van der Grift, B., Behrends, T., Osté, L. A., Schot, P. P., Wassen, M. J., & Griffioen, J. (2016). Fe hydroxyphosphate precipitation and Fe(II) oxidation kinetics upon aeration of Fe(II) and phosphate-containing synthetic and natural solutions. *Geochimica et Cosmochimica Acta*, 186,

71–90. <https://doi.org/10.1016/j.gca.2016.04.035>

- Van der Grift, B., Broers, H. P., Berendrecht, W. L., Rozemeijer, J. C., Osté, L. A., & Griffioen, J. (2016). High-frequency monitoring reveals nutrient sources and transport processes in an agriculture-dominated lowland water system. *Hydrology and Earth System Sciences Discussions*, *12*(8), 8337–8380. <https://doi.org/10.5194/hessd-12-8337-2015>
- Van der Grift, B., Osté, L., Schot, P., Kratz, A., Van Popta, E., Wassen, M., & Griffioen, J. (2018). Forms of phosphorus in suspended particulate matter in agriculture-dominated lowland catchments: Iron as phosphorus carrier. *Science of the Total Environment*, *631–632*, 115–129. <https://doi.org/10.1016/j.scitotenv.2018.02.266>
- Van der Grift, B., Rozemeijer, J. C., Griffioen, J., & Van der Velde, Y. (2014). Iron oxidation kinetics and phosphate immobilization along the flow-path from groundwater into surface water. *Hydrology and Earth System Sciences*, *18*(11), 4687–4702. <https://doi.org/10.5194/hess-18-4687-2014>
- Van der Salm, C., Dupas, R., Grant, R., Heckrath, G., Iversen, B. V., Kronvang, B., Levi, C., Rubaek, G. H., & Schoumans, O. F. (2011). Predicting phosphorus losses with the PLEASE model on a local scale in Denmark and the Netherlands. *Journal of Environmental Quality*, *40*(5), 1617–1626. <https://doi.org/10.2134/jeq2010.0548>
- Vandermoere, S., Ralaizafisoloarivony, N. A., Van Ranst, E., & De Neve, S. (2018a). Reducing phosphorus (P) losses from drained agricultural fields with iron coated sand (- glauconite) filters. *Water Research*, *141*, 329–339. <https://doi.org/10.1016/j.watres.2018.05.022>
- Vandermoere, S., Ralaizafisoloarivony, N. A., Van Ranst, E., & De Neve, S. (2018b). Reducing phosphorus (P) losses from drained agricultural fields with iron coated sand (- glauconite) filters. *Water Research*, *141*, 329–339. <https://doi.org/10.1016/j.watres.2018.05.022>
- Vilmin, L., Mogollón, J. M., Beusen, A. H. W., & Bouwman, A. F. (2018). Forms and subannual variability of nitrogen and phosphorus loading to global river networks over the 20th century. *Global and Planetary Change*, *163*(February), 67–85. <https://doi.org/10.1016/j.gloplacha.2018.02.007>
- Wilfert, P., Dugulan, A. I., Goubitz, K., Korving, L., Witkamp, G. J., & Van Loosdrecht, M. C. M. (2018). Vivianite as the main phosphate mineral in digested sewage sludge and its role for phosphate recovery. *Water Research*, *144*, 312–321. <https://doi.org/10.1016/j.watres.2018.07.020>
- Wilfert, P., Kumar, P. S., Korving, L., Witkamp, G. J., & Van Loosdrecht, M. C. M. (2015). The Relevance of Phosphorus and Iron Chemistry to the Recovery of Phosphorus from Wastewater: A Review. *Environmental Science and Technology*, *49*(16), 9400–9414. <https://doi.org/10.1021/acs.est.5b00150>
- Willett, I. R., Chertres, C. J., & Nguyen, T. T. (1988). Migration of phosphate into aggregated particles of ferrihydrite. *Journal of Soil Science*, *39*(2), 275–282. <https://doi.org/10.1111/j.1365-2389.1988.tb01214.x>
- Withers, P. J. A., & Haygarth, P. M. (2007). Agriculture, phosphorus and eutrophication: A European

perspective. *Soil Use and Management*, 23(SUPPL. 1), 1–4. <https://doi.org/10.1111/j.1475-2743.2007.00116.x>

Xia, L., David, T., Verbeeck, M., Bruneel, Y., & Smolders, E. (2021). Iron rich glauconite sand as an efficient phosphate immobilising agent in river sediments. *Science of The Total Environment*, 811, 152483. <https://doi.org/10.1016/j.scitotenv.2021.152483>

Young, E. O., & Ross, D. S. (2001). *Landscape and Watershed Processes Phosphate Release from Seasonally Flooded Soils : A Laboratory Microcosm Study*. 91–101.

Zhang, Y. F., Thorburn, P. J., Xiang, W., & Fitch, P. (2019). SSIM - A Deep Learning Approach for Recovering Missing Time Series Sensor Data. *IEEE Internet of Things Journal*, 6(4), 6618–6628. <https://doi.org/10.1109/JIOT.2019.2909038>



Chapter

2

2 Chapter 2: Processes controlling the flux of legacy phosphorus to surface waters at the farm scale

Victoria Barcala¹, Joachim Rozemeijer¹, Leonard Osté¹, Bas Van der Grift², Laurens Gerner³, Thilo Behrends⁴

1 Inland Water Systems, Deltares, Utrecht, the Netherlands

2 KWR Water Research Institute, Nieuwegein, the Netherlands

3 Water Board Rijn and IJssel, Doetinchem, the Netherlands

4 Department of Earth Sciences, Faculty of Geosciences, Utrecht University, the Netherlands

Published in Environmental Research Letters 16 (2021) 015003

<https://doi.org/10.1088/1748-9326/abcdd4>

2.1 Abstract

Phosphorus (P) leaching from agriculture is a major driver of water eutrophication in downstream rivers and lakes. In drained lowland areas with intensive agriculture, a reduction in the fertilizer applications may be insufficient to improve the water quality in the short term as the P accumulated in the soil during decades of high fertilization may continue leaching for many years. A complementary approach to reduce P exports from agriculture is to implement edge-of-field mitigation measures at the farm scale. The selection of effective measures requires a detailed insight into the chemical and hydrological transport mechanisms. Here, we determined the main P sources, processes, and transport routes at the farm scale to support the selection of appropriate mitigation measures. We quantified the legacy P, the different P pools stored in the upper soil, and related it to the yearly P export downstream. To do this, we combined high-resolution monitoring data from the soil, groundwater, surface water, and ditch sediments. The legacy P in the topsoil was high, about 2,500 kg/ha. The predominant subsurface flow and the subsoils' P sorption capacity retained the P mobilized from the topsoil and explained the relative moderate flux of P to surface waters (0.04 kg/ha

during the 2018-2019 drainage season). The dissolved P entering the drainage ditch via groundwater discharge was bound to iron-containing particles formed due to the oxidation of dissolved ferrous iron. Once leached from the soil to the drainage ditch, resuspension of P-rich sediment particles during flow peaks were the most important P transport mechanism (78%). Therefore, we expect that hydraulic constructions that reduce flow velocities and promote sedimentation of P-containing particles could reduce the export of P further downstream.

Keywords: legacy phosphorus, leaching, diffuse sources, mitigation measures, groundwater-surface water interactions, agriculture, eutrophication

2.2 Introduction

Eutrophication of streams and lakes is a global environmental problem; it is triggered by nutrient surplus and causes excessive growth of primary producers such as algae and macrophytes. The European Water Framework Directive obliges member states to achieve a good environmental quality status in streams and lakes. In many inland ecosystems, phosphorus (P) is the nutrient limiting growth (Dodds and Smith 2016; Lee 1973). P can originate from point sources, such as wastewater treatment plants (WWTP), or diffuse sources, such as runoff or leaching from agriculture. Point source pollution has been drastically reduced in the last decades with the implementation of P removal in WWTP. Although measures have been taken to restrict P fertilizer applications, agricultural soils maintain a legacy of accumulated P built up after decades of manure and fertilizer application beyond crop requirements. Up to 20 years are needed to confidently detect the water quality improvements caused by changes in agricultural practices (Melland *et al.* 2018).

In Europe and other parts of the world, diffuse P is still the most important P source in rivers and lakes (Hart *et al.* 2004; Withers and Haygarth 2007). In NW Europe, agriculture intensified in the decades after the second world war and in recent years P surplus is close to zero (Bol *et al.* 2018; McDonald *et al.* 2019). The general size and operations of farms in the Netherlands are similar to the ones in other NW European countries (Eurostat 2015). The average farm size in the Netherlands is 29 ha, agriculture is highly intensive, predominantly arable and dairy farming, over flat and artificially drained lands. Around a quarter of the Dutch

agricultural land is used in dairy farming, farmers grow grass and maize to feed the cows. Figure 2-1 shows the P surplus in the Netherlands from 1970 to 2018 (CBS 2020). The livestock production is mainly located in the central, eastern, and southern non-calcareous sandy soils. Historically, most of the manure was applied close to where it was produced (Schoumans 2015). Some of the P surplus remains in the soil as legacy P and can occur structurally bound in minerals, adsorbed to mineral surfaces, or associated with the organic matter present in soil particles. Later, the accumulated P can leach out of the soil with infiltrating rainwater. Therefore, reducing fertilizer or manure applications might not be enough to reduce downstream eutrophication in the short term.

In lowland areas, drainage occurs largely via subsurface flow (groundwater and tube drains) to surface waters (ditches and streams)(Chardon and Schoumans 2007). In Europe, 30 million hectares of agricultural land are artificially drained (Döll and Siebert 2005). Figure 2-2 shows the share of the arable land that is drained in NW Europe (Brown and Van Beinum 2009), in the Netherlands 60% of the agricultural land is artificially drained. Rozemeijer and Broers (2007) showed that the outflow of drains can contribute up to 80% of the total groundwater-born P flux into surface waters.

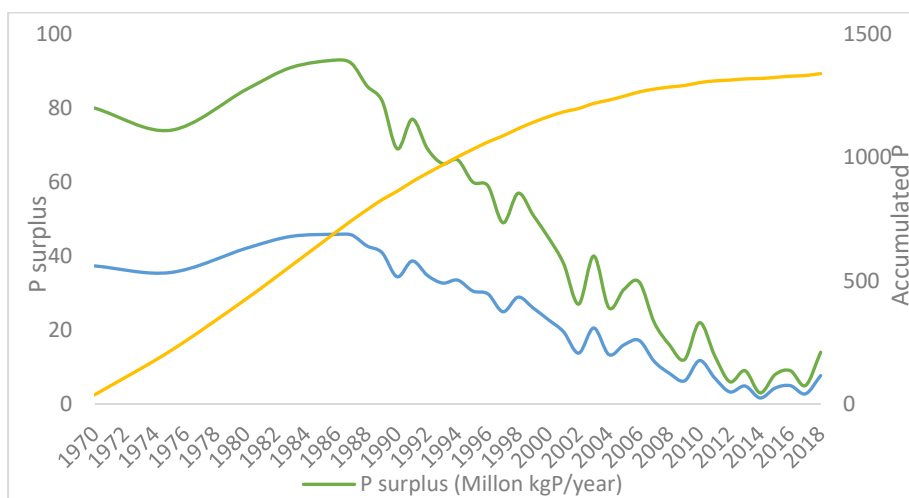


Figure 2-1 P surplus in the Netherlands from 1970 to 2018. (CBS 2020).

Mitigation measures retain P before it is transported downstream and reaches lentic water bodies, which are more prone to become eutrophic. The selection of appropriate measures is not trivial, some make extensive use of arable land, i.e. wetlands and riparian buffers, making their implementation unlikely in areas with high land prices. Other such as water retention measures can increase productivity but may also change the soil moisture and chemical conditions, reducing P sorption and accelerating P transport (Chardon and Schoumans 2007; Schoumans and Chardon 2014). Selecting effective mitigation measures requires detailed insight into chemical and hydrological P transport mechanisms.

In regions with iron-rich groundwater, iron (Fe) is usually reduced and oxidizes as it seeps into the drains or surface waters. During this process, phosphate can be absorbed in iron-rich colloids or co-precipitate with iron (hydr)oxides, becoming particulate phosphorus (PP) (Van der Grift *et al.* 2014). Fe-bound P can be a significant fraction (38%-95%) of the P in suspended solids in ditches and streams (Van der Grift *et al.* 2018). Fe-bound P is less readily available for uptake by algae and less mobile than dissolved phosphate (Baken *et al.* 2014). However, once the PP has settled in the sediment, it can be eroded and remobilized during flow peaks, or dissolved under Fe-reducing conditions (Baken *et al.* 2015; Mellander *et al.* 2016).

Studies on P transport in agricultural landscapes are usually limited to either laboratory or plot scale (Van der Salm *et al.* 2011; Van der Grift *et al.* 2014), or large catchment scale (De Klein and Koelmans, 2011; Baken *et al.* 2015; Van der Grift *et al.* 2016). To propose effective mitigation measures there is a need to assess how the known P transport mechanisms aggregate at the farm and small catchment scales, where management interventions are most effective (Bol *et al.* 2018). Therefore, the objectives of this study were (1) to identify the main phosphorus sources, processes, and transport routes at a farm-scale to support the selection of appropriate P retention measures; and (2) to quantify the farm-scale legacy P storage and assess the risk of mobilization and leaching into surface waters.

The study was performed at a farm chosen because of its size and type of production to be representative of drained lowland farms on sandy soils with seasonal manure application in the Netherlands and parts of NW Europe. All the farm water discharges via a single ditch where we placed a high-frequency monitoring station from April 2018 to April 2019. To

quantify the P transport routes from the soil to surface water, a water and nutrient balance is presented. Finally, based on these insights, we recommend mitigation measures.

2.3 Methods

The research site is located in Huppel, the Netherlands, coordinates 52.00131 N, 6.76112 E, one kilometer from the Dutch-German border (Figure 2-2). The farm has cows for dairy production and has a size of 24 hectares, of which 16 hectares are grassland and 8 hectares are used for crop farming alternating between corn, beets, and potatoes. A map of the farm is shown in Figure 2-3. Dairy farming has been practiced on the farm since 1930. It can be assumed that the historic agricultural practices on this farm followed the general trend in the Netherlands, where manure application had been intensive until 1989 when a new agricultural policy on fertilizers was introduced. In recent years, the farmer applies an amount of P that will likely be in balance with the crop P uptake, P is added to the soil as manure with injection machinery. The manure is applied early in the season; therefore, the P balance will be known after the crops are harvested. The P surplus considers the actual mass harvested and the P content in the manure for this farm. Thus, the P surplus value fluctuates and some years the balance is positive, and some is negative, but always close to zero in recent years. According to Dutch regulations, manure can be applied after 1 February on grasslands and from 15 February on arable land, until 1 September. Table 2-1 presents the P surplus on the farm from 2013 to 2018.

Table 2-1 P surplus in the farm, as KgP/ha the years before the research, 2013 to 2018

2013	2014	2015	2016	2017	2018
2 kg/ha	-2 kg/ha	-6 kg/ha	-2 kg/ha	1 kg/ha	2 kg/ha

The farm is partly drained with tile drains. The drain tubes are installed at approximately 1 m depth and with 10 m horizontal distance between drains. The altitude is between 35 m and 33.5 m above mean sea level, with a marginal slope directing from east to west. The farm drains to a main ditch that runs from east to west parallel to the front road. The land on the eastern side of the ditch is not connected to the ditch via tile drains and there has been no observations of surface flow into the ditch originating from land at the eastern side. As infiltrating water in this area discharges into deeper ground water, it is assumed that the investigated farm is the exclusive catchment area for this ditch. The receiving stream is the

Groenlose Slinge, which in summer shows excessive plant growth in front of weirs and blue-green algae blooms in receiving urban canals. The local water authority is considering the implementation of P retention measures in the area.

The farm is located on top of a glacial tunnel valley, which is filled with a fluvioglacial iron-rich sand layer between 10 and 20 m deep that lies over a marine clay. The combination of sandy soil with the shallow impermeable clay layer makes the system respond relatively quickly to precipitation. More details on the hydrogeology are provided in the supplementary information. The non-calcareous sandy soil present in the farm is characterized by having low levels of P in groundwater (Schoumans and Chardon 2014).

A high-frequency monitoring station (Van der Grift *et al.* 2015) was installed at the westernmost point of the main ditch (Figure 2-3). Just upstream of a V-notch weir, water was pumped to a flow-through vessel where total phosphorus (TP), total reactive phosphorus (TRP), turbidity, and nitrate (NO_3^-), were registered every 15 minutes, from 5 April 2018 to 18 April 2019. The discharge was measured by recording water levels upstream of the calibrated V-notch. Table 2-2 shows an overview of the equipment; more details are provided in the supplementary information.

Soil samples were collected from 24 spots at 0-10 cm and 40-50 cm depth; additionally, 4 points (4, 10, 14, and 19) were analyzed further at 70-80 cm depth. Sediment samples were also retrieved from the main ditch and a secondary contributing ditch. The soil and ditch sediment samples were taken on 16 April and 15 May 2018, respectively. Soil and sediment samples were stored at 4 °C before being analyzed for soluble P (Pw), labile P (PAL), and TP. Furthermore, P, Fe, and aluminum (Al) were extracted from soil and sediment samples with ammonium oxalate (Schwertmann 1964). The Fe plus Al obtained from this extraction represents the soil's P sorption capacity, and the molar relation between P and Fe plus Al is the soil's phosphate saturation degree (PSD). The PSD quantifies the P leaching potential (Schoumans and Chardon 2014). In the sediment, the P/Fe ratio from the oxalate extraction quantifies the risk of P mobilization (Smolders *et al.* 2017; Van Dael *et al.* 2020). Table 2-3 contains an overview of the soil extraction methods.



Figure 2-2 Location of the farm selected for the study, in Huppel, the Netherlands. At the top left there is a map of the region indicating the drained land as a percentage of the total agricultural land (Brown and Van Beinum 2009). UK: United Kingdom, DK: Denmark, NL: the Netherlands, BE: Belgium, FR: France, DE: Germany. Map created using the Free and Open Source QGIS

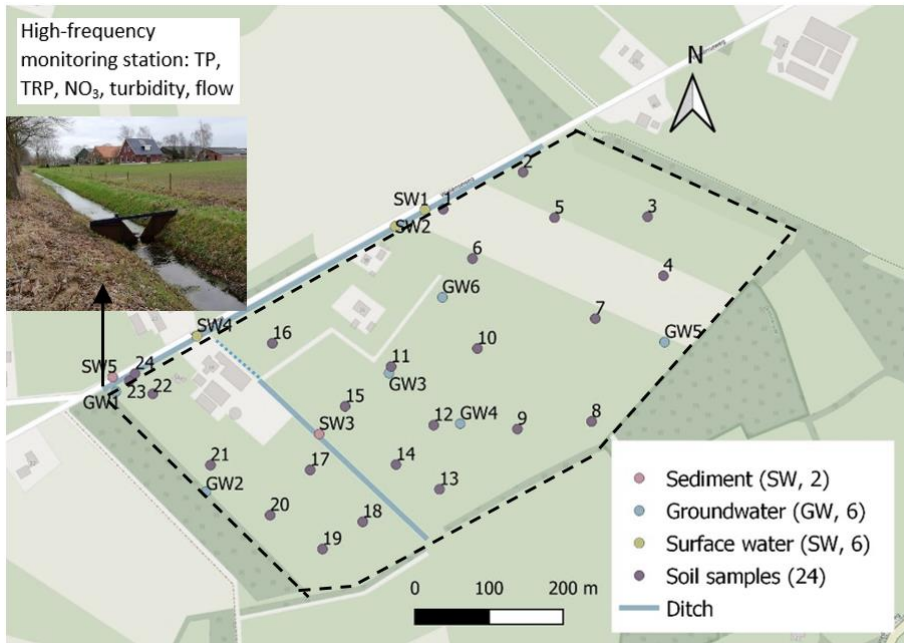


Figure 2-3 Map of the farm: buildings are colored in gray, crops are in beige, grasslands are in light green, and forests in dark green. The main ditch runs from East to West, parallel to the front road. The map shows the location of the high-frequency monitoring station, and the identification number of the soil, sediment, surface water, and groundwater samples. A volumetric pump upstream of the weir takes water into a flow-through tank where the monitoring station registers measures every 15 minutes. TP: total phosphorus, TRP: total reactive phosphorus, NO₃⁻: nitrate. A pressure gauge was installed before the weir for discharge estimations. Map created using the Free and Open Source QGIS

Groundwater samples were taken from six monitoring wells at 1.5-2.5 m depth on 15 May 2018 and 18 October 2018. Five surface water samples were taken on 16 April 2018. The water samples were filtered with a 0.45 µm pore size nylon filter and acidified with 1% HNO₃ on-site and analyzed with ICP-OES. In the period between 20 January to 25 February 2019, the Phosphax autoanalyzer was not working and no TP was measured. To close the gap in the time series TP was estimated using the correlation with NO₃⁻. The precipitation and evaporation time-series from the Hupsel meteorological station, at 12 km distance, were downloaded from the Dutch Royal Meteorological Institute. Additionally, groundwater levels at the farm were continuously monitored with a pressure gauge installed in one well.

Table 2-2 Overview of the equipment used in the high-frequency station equipment.

Parameter	Equipment*	Method	Detection range	Accuracy**
Turbidity	Solitax sensor	Optical (infrared duo scattered light photometer)	0 to 4,000 NTU	1%
NO₃⁻	Nitratax sensor	Double wavelength spectrophotometric UV sensor	0.1 to 50.0 mg/L	3%
TRP	Phosphax and Sigma auto-analyser	Titration and photometric measurement	0.01 to 5.00 mg/L	2%
TP	Phosphax and Sigma auto-analyser	Digestion with H ₂ SO ₄ , titration and photometric measurement (includes mixing and heating/cooling step)	0.01 to 5.00 mg/L	2%

*Hach Lange GmbH, Düsseldorf, Germany. **According to the manufacturer

Table 2-3 Overview of soil extraction methods used.

Method	Extracting solution	Solution pH	Soil-to-solution ratio	Extraction time	Method of measurement	Elements measured
Pw	Distilled H ₂ O	unbuffered	1:60	1 hour	MBM*	P
PAL	ammonium lactate-acetic acid	3.5	1:20	4 hours	MBM*	P
Oxalate	oxalic acid and ammonium oxalate	3	1:50	4 hours	ICP-OES**	P, Fe, Al
Total***	Aqua regia	<1	3:1	48 hours	ICP-OES**	P, Fe

* molybdenum blue method (MBM) (Murphy and Riley 1962) **inductively coupled plasma atomic emission spectroscopy (ICP-OES). *** More details about the extraction methods are found on the supplement information

2.4 Results

Soil, groundwater, and sediment P content

The topsoil consisted of a layer of organic material and roots with high TP and high labile and soluble P and critical PSD. Followed by a layer of brown-red-orange-color caused by iron oxides with no roots and higher P sorption capacity. The underlying sandy layer had a gray-yellow to red-orange color, with little organic matter, and low TP. Figure 2-4 illustrates how the soil composition, presented in Table 2-4, corresponds to visual appearance. More details

on extraction results and pictures from all soil samples are found in the supplementary information.



Figure 2-4 On-site picture of soil sample number 19 (0-100 cm). The topsoil was rich in organic matter followed by a horizon which was brown-red-orange colored due to the presence of iron oxides underlain by a gray-yellow to red-orange sand layer

The average TP content of the soils was 600 mg/kg, this is high considering previously reported TP contents for non-calcareous sandy soils in the Netherlands which in the range 280-500 mg/kg (Koopmans *et al.* 2006). The average TP concentration in the upper 30 cm of the soil on the farm was 60,200 kg or 2,500 kg/ha, which is higher than the average P in agricultural soils in The Netherlands, 2,050 kg P/ha (Schoumans and Chardon 2014). The total P in the soil accounts for the legacy P plus P in the pre-agricultural soil. The large observed differences between the TP results in the topsoil and subsoil suggested that most of the TP in the topsoil originated from manure and fertilizer application.

In the topsoil, the Pw and PAL values were high, on average 12.2 mg/kg \pm 5.1 mg/kg and 165.1 mg/kg \pm 68.0 mg/kg respectively. According to the Dutch Fertilization Grassland and Plants Committee's advice for sandy soils Pw values above 9.8 mg/kg and PAL values above 109 mg/kg are high (Commissie Bemesting Grasland en Voedergewassen 2018). Schoumans and Groenendijk (2000) calculated it would take about 30 years for topsoils with Pw of 10 mg/kg to reach low values (below 4.4 mg/kg). The Pw results were higher in the arable part of the

farm (the northeast side) compared to the grassland part (southwest); PAL and TP show a similar spatial distribution (Figure 2-5). Pw, PAL, and TP notably decrease at 40-50 cm (Table 2-4). Samples 24 and 23 are from both sides of the ditch bank and were not added for the averages in Table 2-4 as they are not representative of the farm's soil. Sample 24 was taken from the between the road and the ditch, which is typically where sediment is laid after dredging the ditch and may explain the high TP concentrations.

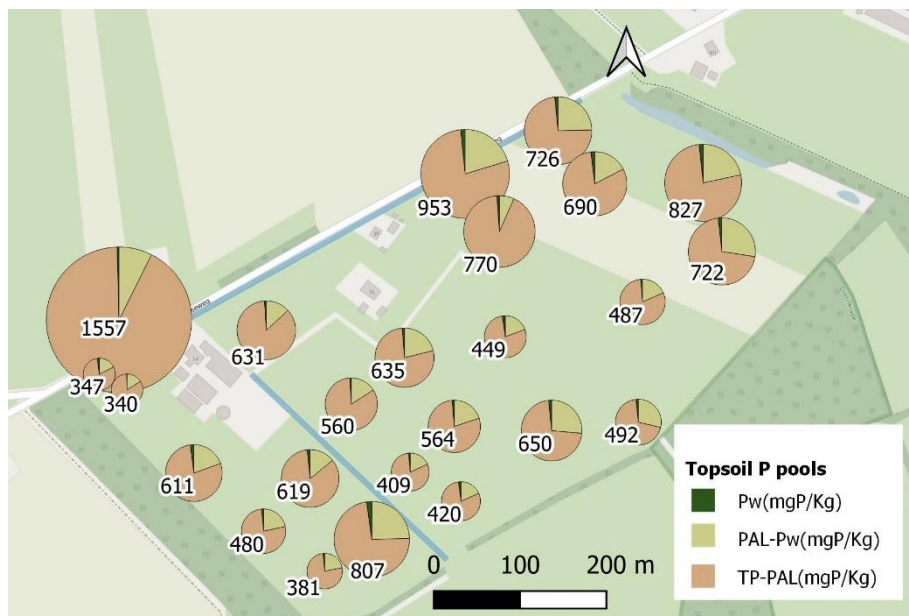


Figure 2-5 Map showing the total phosphorus contents in the topsoil (0-10cm) and its distribution over the different sequential extractions at the different sampling locations. The size of the pie charts is proportional to the TP value displayed. Map created using the Free and Open Source QGIS

In the topsoil, the PSD was 0.26 (Table 2-4). The higher the PSD value, the higher the P saturation in the soil, and the higher the risk of P leaching. The critical PSD value for non-calcareous sandy soils is 0.25 (Schoumans and Chardon 2014). In the sediment, the P/Fe ratio was 0.22; critical values for P release from the sediments during summer anoxia are 0.12 for lakes and 0.4 for lowland rivers (Jensen *et al.* 1992; Smolders *et al.* 2017).

In groundwater the P/Fe molar ratio was calculated for the samples taken on 18 October 2018 (Table 2-5). Some of the P results bear greater uncertainty as they fell below the limit of quantification. Nonetheless, the results show low P concentrations in the groundwater. The Fe concentrations were similar to the average surface water concentrations, 0.21 mg/L \pm 0.05 mg/L.

Table 2-4 Soil and sediment results: number of samples, averages of Pw, PAL, TP, and oxalate extractions

Soil samples	n	Pw mg/kg \pm SDV mg/kg (as % of TP)	PAL mg/kg \pm SDV mg/kg (as % of TP)	TP mg/kg \pm SDV mg/kg (as % of TP)	P _{ox} (mmol/L)	Fe _{ox} +Al _{ox} (mmol/L)	PSD
Depth 0-10 cm	24	12.2 \pm 5.1 (2%)	155.1 \pm 68.0 (26%)	601 \pm 157 (100%)	0.14 \pm 0.04	0.50 \pm 0.16	0.26 \pm 0.07
Depth 40-50 cm	24	1.4 \pm 3.53 (1%)	29.5 \pm 20.9 (18%)	165 \pm 68.3 (100%)	0.03 \pm 0.02	0.63 \pm 0.38	0.06 \pm 0.05
Depth 70-80	4	0.1 \pm 0.1 (0.1%)	12.2 \pm 6.13 (10%)	113 \pm 20.1 (100%)	0.01 \pm 0.01	0.30 \pm 0.18	0.03 \pm 0.02
Sediment	n	Pw mg/kg \pm SDV mg/kg (as % of TP)	PAL mg/kg \pm SDV mg/kg (as % of TP)	TP mg/kg \pm SDV mg/kg	P _{ox} (mmol/L)	Fe _{ox} (mmol/L)	P/Fe
Main ditch	2	10.1 \pm 0.84 (4%)	41.3 \pm 3.2 (17%)	307 \pm 92 (100%)	0.04 \pm 0.01	0.17 \pm 0.01	0.23 \pm 0.01
Secondary ditch	1	32 (13%)	108.8 (45%)	241 (100%)	0.08	0.36	0.22

Table 2-5 Groundwater results of dissolved Fe and P concentrations and molar P/Fe

Groundwater well**	15 May 2018	18 October 2018		
	Fe(mg/L)	Fe (mg/L)	P (mg/L) *	Molar P/Fe ratio
GW 1	0.767	0.390	0.034	0.16
GW 2	0.011	-	-	-
GW 3	0.011	0.018	0.017	1.8
GW 4	0.107	0.139	0.026	0.29
GW 5	0.302	0.182	0.019	0.19
GW 6	0.033	0.024	0.019	1.4

*P limit of quantification was 0.026 mg/L **GW 2 was not sampled on October 18

Water and solute fluxes

Water and solute fluxes were measured during a very dry year. The precipitation deficit was the highest since the first records in 1957, the accumulated precipitation from April 2018 to

April 2019 was 543 mm, while the yearly country average is 800 mm. The groundwater levels varied between 0.42 m and 1.96 m below surface, with an average of 1.42 m \pm 0.42 m. The ditch dried up when groundwater levels fell below 1.20 m; this occurred between 11 May and 22 December 2018. The water quality parameters measured with the high-frequency sensors showed a distinct behavior depending on the hydrological conditions. To illustrate these different behaviors two periods are shown in detail, a 12-day rainy period and a 4-day dry period. The full-time series from the monitoring station can be found in the supplementary information.

The rain period between 7 and 18 January 2019 in Figure 2-6 includes hydrological data and data from the high-frequency monitoring station. There were seven subsequent events, with rain intensities between 1 and 2 mm/hour, the discharge in the ditch varied from 2 L/s to about 4 L/s and the groundwater level fluctuated between 1.1 m and 0.7 m below surface. Turbidity, TP, and TRP peaks occurred simultaneously with a drop in NO_3^- concentration. These responses occurred approximately 2 hours after the rain peaks. Discharge peaks remobilized P-rich sediment in the ditch as is shown in Figure 2-6 by the simultaneity in the discharge, TP, and turbidity peaks and also by the Fe and P content in the sediment (Table 2-4).

Figure 2-7 shows the different high-frequency monitored parameters for the selected window with no rain events, from 28 March to 1 April 2019. Especially the TP and TRP and turbidity showed a diurnal fluctuation. This pattern was also detected through the spring of 2018 and 2019, starting in March and continuing until the ditch dried up in April. The highest values for TP, TRP, and turbidity were always measured between 5:00 pm and 7:00 pm and the lowest values around 5:00 am. The groundwater level decreased from 0.88 m up to 0.96 m. The NO_3^- concentration fluctuated around 10.5 mg/L for the first days and dropped to 9.5 mg/L.

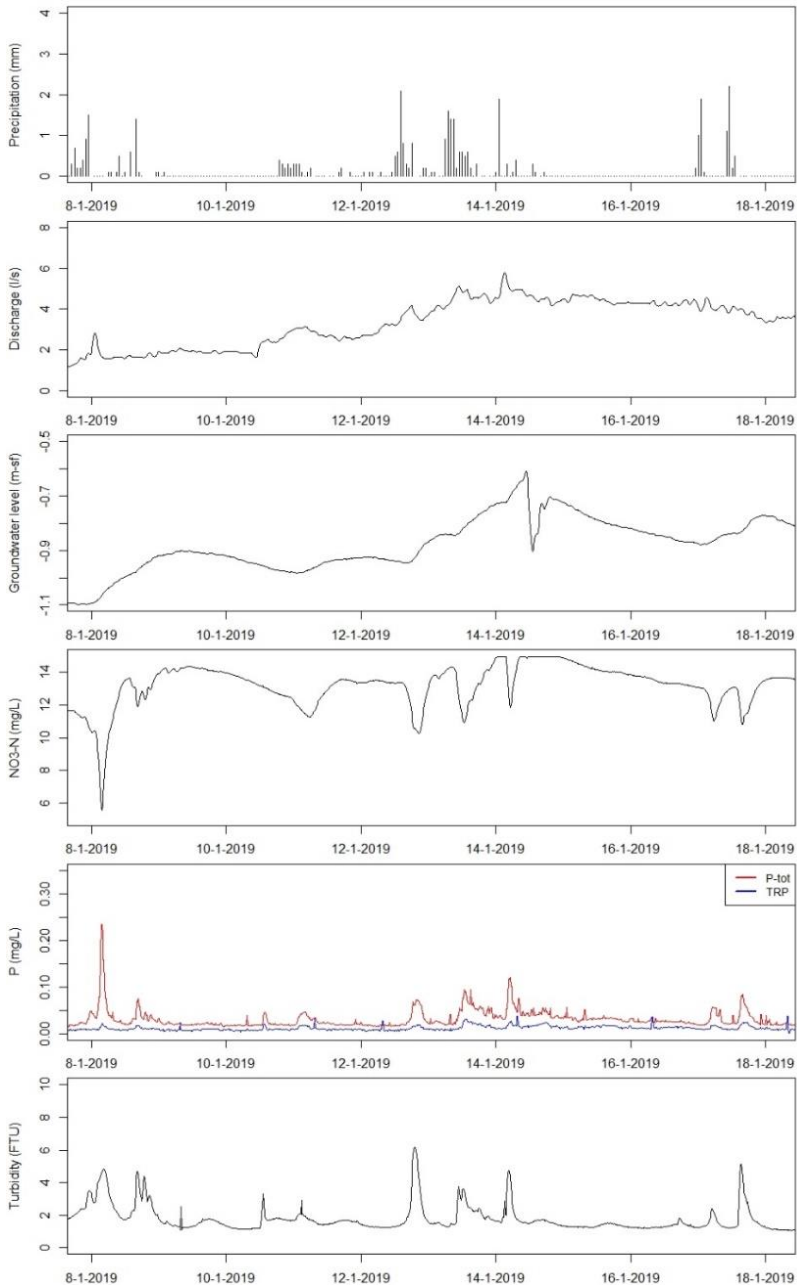


Figure 2-6 Time series of the Precipitation(mm), ditch discharge (L/s), groundwater level (meters below ground surface), NO3- (mg/L), TRP (mg/L),TP (mg/L) and turbidity (NTU), from 7 January to 18 January 2019

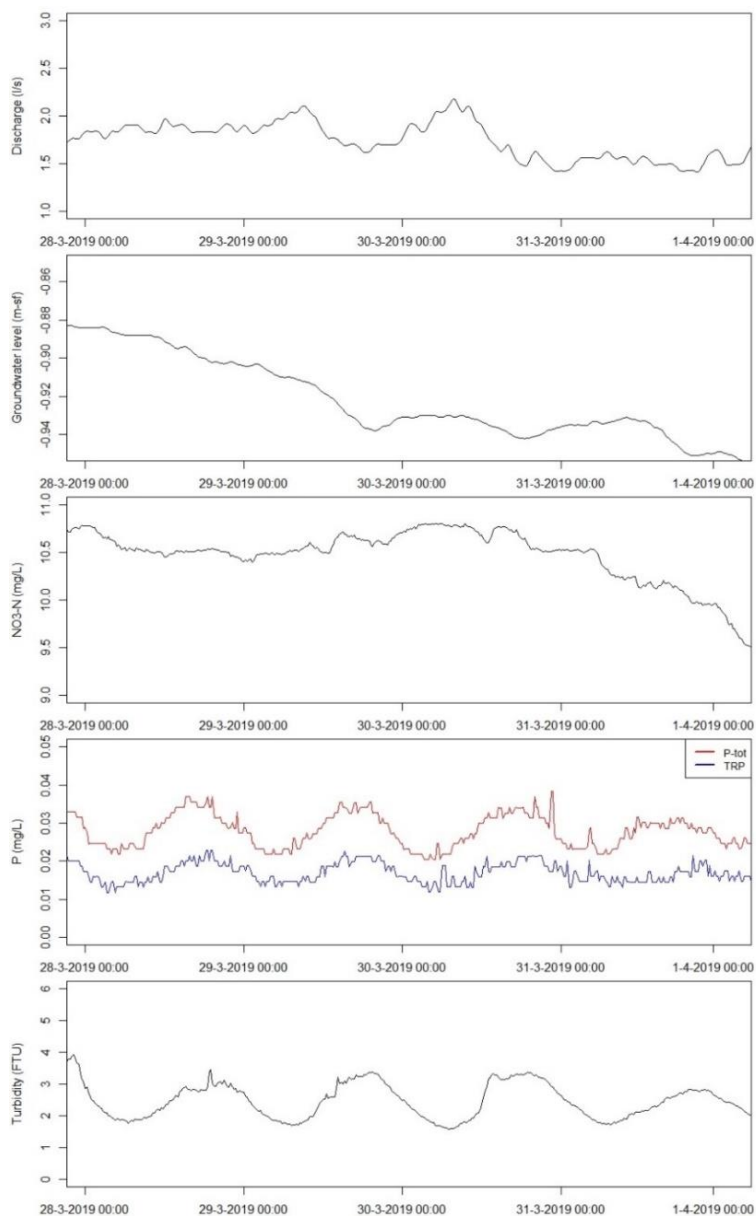


Figure 2-7 Time series of the ditch discharge (L/s), groundwater level (meters below ground surface), concentrations of NO_3^- (mg/L), TRP (mg/L) and TP (mg/L), and turbidity (NTU), from 28 March to 1 April 2019.

Integrated results

Figure 2-8 shows the cumulative loads for TP and NO_3^- during the relatively short drainage season 2018-2019. The total nutrient export for the whole farm over this period was 0.9 kg for P and 282 kg for N. The average TRP was 0.021 mg/L.

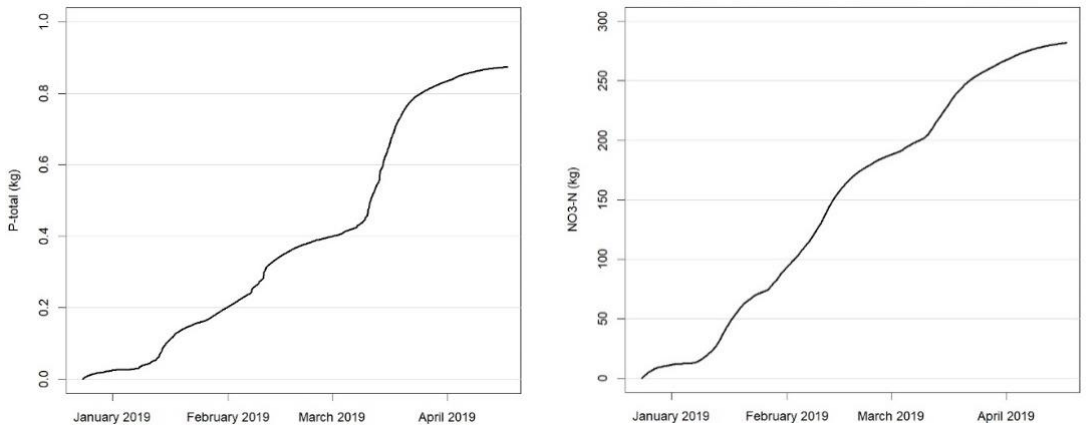


Figure 2-8 Cumulative nutrient exports from the farm from 24 December 2018 to 16 April 2019.

2.5 Discussion

Transport of P to the ditch by groundwater flow

A conceptual model of the P fluxes and the water balance for the 2018-2019 drainage season is shown in Figure 2-9. The model includes the main P sources, manure application, and legacy P; the transport processes through the topsoil and subsoil; and finally, the transport and accumulation of P in the ditch. The P concentrations in the soil water from the upper layers were estimated with the correlation between the PSD and the orthophosphate in equilibrium with the soil solution for non-calcareous sand soils found by Schoumans and Groenendijk (2000). When the groundwater levels are high, the water transport through the topsoil carries higher P concentrations. When the water moves through the subsoil layer, the P is adsorbed by the amorphous iron oxides that have available adsorption sites. This also explains the low dissolved phosphate present in the groundwater below 150 cm (Table 2-5). The contrast

between the TP results in the topsoil and subsoil suggest that most of the TP in the topsoil originated from manure and fertilizer application (Table 2-4).

During the studied drainage period, the water entered the ditch after passing the upper organic-rich layer and the underlying sandy layers of the soil. The dominance of this pathway can be concluded from the similarity of the composition of groundwater and surface water (Table S8); the coupled groundwater level and discharge time-series (Figures 2-6 and 2-7); and no visual observations of overland flow during the 2018-2019 drainage season. This implies that the groundwater level determines the export of dissolved P, which is higher when the infiltrating water does not reach the subsoil with low PSD and unoccupied adsorption capacity and directly discharges into the ditch. At the low groundwater level, there is a net flux from the topsoil into the subsoil and retention of P which reduces the export of dissolved P into the ditch.

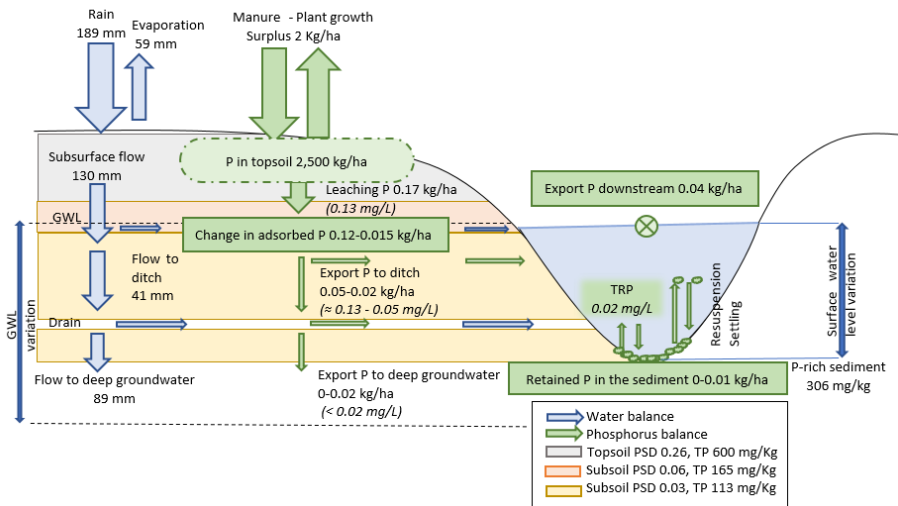


Figure 2-9 Water and phosphorus balance for the period from 24 December to 16 April 2019.

In the model the infiltration to deep groundwater was calculated as the difference between the measured precipitation, corrected evapotranspiration, and measured discharge in the ditch; we assume no groundwater storage. The evapotranspiration was obtained using an average crop factor of 0.6 (0.9 for grass and 0.0 for arable land). The infiltration for the period

was 89 mm, 2/3 of the precipitation surplus. The presence of the glacial tunnel makes the groundwater flow an important component in the water balance.



Figure 2-10 Picture from the main ditch, fluffy orange-red sediments are visible in the bottom

Transport of P in the ditch by remobilization of sediment

The ditch sediment had a different composition of P- and Fe-pools compared to that of the topsoil (Table 2-4), suggesting the sediment consisted of autogenic particles and is not formed by eroded topsoil. The sediment's P/Fe ratio and high P_w suggest that P is adsorbed in Fe (oxy)hydroxide colloids, which are important P carriers (Baken *et al.* 2016; Van der Grift *et al.* 2014; Gu *et al.* 2020). The soluble P in the sediment was 0.02 mg/L (Table S6) which closely matched the TRP baseline in the ditch water (average 0.021 mg/L), and the soluble P in the sediment (Table S6), suggesting the P in the sediment is in equilibrium with the P in the surface water. This implies that during the drainage season the exported TP load consists of 0.20 kg in the form of dissolved P and 0.70 kg in the form of PP, the share of PP in the discharge was 78% of TP, based on the high frequency monitoring. Nonetheless, the PP fraction of the TP may be even higher, as some Fe-bound P particles are smaller than 0.45 μm and may be accounted for in the measurements (Van der Grift *et al.* 2016). TP peaks occurred simultaneously with turbidity after rain events (Figure 2-6). The increase in turbidity is most

likely caused by the resuspension of sediments which have freshly deposited in between rain events (Figure 2-10). For the whole period monitored, 76% of TP was exported in 19% of the time when the discharge was above its median, implying that resuspension of PP during high flow events is the major pathway of TP export.

House and Warwick, (1998) already reported the importance of particle transport as P carriers during rain events. At a close-by site, Rozemeijer and Van der Velde (2014) recently determined that 60% to 90% of the annual P transport was caused by a few rainfall events. De Klein and Koelmans (2011) also found that P transport depended greatly on the seasonal rainfall in the Netherlands.

The TP export per hectare observed in this study was not high, 0.04 kg/ha, which can be explained by the vacant sorption capacity of the subsoil. Ulén and Jakobsson (2005) reported a P export of 0.57 kg/ha/year for a similar catchment in Sweden, a drained agricultural sandy soil with a balanced manure application, but the sand's sorption capacity was low. Gelbrecht *et al.* (2005) reported TP exports between 0.04 and 0.25 kg/ha for sandy catchments with subsurface flow in NE Germany, however, the sorption capacity of the sand was not reported.

The fact that this was a particularly dry year is one of the main uncertainties to this study, we cannot determine to what extent P retention by subsoil will be as effective in wetter years with higher groundwater levels and even if runoff or soil erosion could occur. Wetter years may result in higher discharge and even higher PP transport downstream. Leaving aside these uncertainties, our results show that PP retention would reduce P losses downstream.

Phosphorus retention measures

P retention measures, such as sediment traps can reduce the P losses in the short term (Barber and Quinn 2012). This measure can be implemented alongside water conservation strategies, which may increase the farmers' willingness to implement them, as water retention offers benefits for the farm during droughts. The measure should buffer the discharge peaks after rain events. This farm has the advantage of having a ditch that catches all the water drained from the farm. The most cost-effective measure should consider this asset, for example by widening the ditch before the weir. Water retention measures were classified as having a very positive impact on PP retention in Swedish sandy lowland areas in

the short term (Ulén and Jakobsson 2005). However, not all water retention measures will reduce the yearly P load. First, the outlet should minimize flow peaks and sediment remobilization. For example, some retention water measures widely used in the area include placing inflatable balloons to block culverts. This system only allows open or closed positions causing pronounced transport of P-rich sediment when removed. More suitable outlets are adjustable weirs or small diameter pipes. Second, the water retention measure should use the soil's sorption capacity maintaining the groundwater level 40-50 cm below the surface. If the groundwater level was only 20-30 cm below the surface, much more P would reach the ditch as the dissolved P concentrations in the topsoil are higher than in the subsoil due to the saturation of the sorption capacity. Finally, maintenance needs to be considered, removing periodically the sediment from the ditch bottom. From a P recycling perspective, the sediment had a high P_w , which makes it attractive for reuse. Moreover, if the sediments are not removed there is a risk of remobilizing the phosphate present in the sediment once anaerobic conditions are reached.

Diurnal pattern in phosphorus and turbidity in the spring

Finally, we want to make some remarks on the daily pattern in P concentrations presented in Figure 2-7. The timing of the highest and lowest TP values suggests that the fluctuations are light sensitive, implying that photosynthesis might exert influence on TP concentrations. At the end of March, the solar irradiance goes up at 5 am and reaches zero again around 7 pm. The concentration day vs. night differences are significant ($p < 0.05$), yet the concentration levels are low compared to the water quality target of 0,15 mg/L. It is relevant that processes other than Fe-P dynamics control the P concentration in surface waters during some part of the year. One hypothesis is that these fluctuations are caused by organisms that sink during nighttime and move to the surface during daytime. This was not the first time these daily TP variations are detected. House and Warwick (1998) detected a 30-hour variation in TP in April in the River Swale; as levels of dissolved silica also dropped with TP, diatoms were thought to explain the TP variations. Later, Bowes *et al.* (2016) detected daily TP variations in the river Thames during the springs of 2009 to 2013; they observed that most TP fluctuations went in hand with a Chlorophyll-a increase and phytoplankton growth was associated with the phenomenon. In the same study, another daily TP variation event showed no increase in Chlorophyll-a but a drop in dissolved silica and diatoms were believed to cause the TP

fluctuations. To the best of our knowledge, this daily process has not been thoroughly explained yet. The exact processes and the type of microorganisms that play a role are unknown. In our study area, the TP concentrations during these events are low and do not imply an important P transport year wise.

2.6 Conclusions

The present study thoroughly followed P from its application until it left the farm through surface water. We investigated the principal P routes in a lowland drained farm on sandy soils, and the findings have implications for similar areas with intensive agriculture. The results show that the topsoil accumulated high amounts of TP with high soluble P concentrations and a critical PSD suggesting a high risk of P leaching. P concentrations in groundwater were low, which could be explained by the dominant subsurface flow and the unoccupied sorption capacity of the iron-rich subsoil. In the ditch, most of the exported P was associated to PP resuspension during discharge peaks.

Based on the high proportion of PP and the experiences with trapping P-rich suspended matter (Ulén and Jakobsson 2005; Barber and Quinn 2012), we expect that PP retention could reduce significantly the amount of P leaving the catchment, having a positive impact on downstream eutrophication. Sedimentation traps designed to prevent high discharge peaks are recommended as a suitable P retention measure. We recommend that this approach is used in other areas to identify the main P routes and support the selection of appropriate mitigation measures.

The highlight results of this research are:

- The P in the topsoil, accounted in total 60,200 kg, or 2,500 kg/ha, although nowadays the P input surplus is close to zero, the legacy P is an important component of the P leaving the farm.
- The sorption capacity of the iron-rich subsoil together with a dominant subsurface flow retained the P and reduced the P losses to surface waters or deeper groundwaters.

- The P export was estimated in total 0.90 kg or 0.04 kg/ha, for the 2018-2019 drainage season.
- PP transport accounted for 78% of the TP transported downstream, for the 2018-2019 drainage season. Preventing peak flows is important to reduce P-discharge, but also for water retention. We recommend building sediment traps, widening the ditch or incorporating weirs along the ditch to retain PP.
- The water retention measures implemented should allow the flow to go through the iron-rich sandy soil.
- In spring TP, TRP, and turbidity showed diurnal fluctuations. This process has been only reported a few times before and might be related to light-sensitive processes as photosynthesis, however, the phenomenon is not yet thoroughly understood.

2.7 Acknowledgments

This study was funded by the Province of Gelderland, Water Board Rijn and IJssel, Deltares, and P-TRAP (EU grant number 813438, Marie Skłodowska-Curie Actions). We would like to thank farmer Arjan Tolkamp for his cooperation. We would like to acknowledge Edith Eder for her work on this project.

2.8 References

- Baken, S., Nawara, S., Van Moorleghem, C., & Smolders, E. (2014). Iron colloids reduce the bioavailability of phosphorus to the green alga *Raphidocelis subcapitata*. *Water Research*, *59*, 198–206. <https://doi.org/10.1016/j.watres.2014.04.010>
- Baken, S., Regelink, I. C., Comans, R. N. J., Smolders, E., & Koopmans, G. F. (2016). Iron-rich colloids as carriers of phosphorus in streams: A field-flow fractionation study. *Water Research*, *99*, 83–90. <https://doi.org/10.1016/j.watres.2016.04.060>
- Baken, S., Verbeeck, M., Verheyen, D., Diels, J., & Smolders, E. (2015). Phosphorus losses from agricultural land to natural waters are reduced by immobilization in iron-rich sediments of drainage ditches. *Water Research*, *71*, 160–170. <https://doi.org/10.1016/j.watres.2015.01.008>

- Barber, N. J., & Quinn, P. F. (2012). Mitigating diffuse water pollution from agriculture using soft-engineered runoff attenuation features. *Area*, 44(4), 454–462. <https://doi.org/10.1111/j.1475-4762.2012.01118.x>
- Bol, R., Gruau, G., Mellander, P. E., Dupas, R., Bechmann, M., Skarbøvik, E., Bieroza, M., Djodjic, F., Glendell, M., Jordan, P., Van der Griff, B., Rode, M., Smolders, E., Verbeeck, M., Gu, S., Klumpp, E., Pohle, I., Fresne, M., & Gascuel-Oudou, C. (2018). Challenges of reducing phosphorus based water eutrophication in the agricultural landscapes of Northwest Europe. *Frontiers in Marine Science*, 5(AUG), 1–16. <https://doi.org/10.3389/fmars.2018.00276>
- Bowes, M. J., Loewenthal, M., Read, D. S., Hutchins, M. G., Prudhomme, C., Armstrong, L. K., Harman, S. A., Wickham, H. D., Gozzard, E., & Carvalho, L. (2016). Identifying multiple stressor controls on phytoplankton dynamics in the River Thames (UK) using high-frequency water quality data. *Science of the Total Environment*, 569–570, 1489–1499. <https://doi.org/10.1016/j.scitotenv.2016.06.239>
- Brown, C. D., & Van Beinum, W. (2009). Pesticide transport via sub-surface drains in Europe. *Environmental Pollution*, 157(12), 3314–3324. <https://doi.org/10.1016/j.envpol.2009.06.029>
- CBS. (2020). *Mineral balance agriculture*. 6 January 2020. opendata.cbs.nl/statline/#/CBS/nl/dataset/83475NED/table?*=1601641484793
- Chardon, W. J., & Schoumans, O. F. (2007). Soil texture effects on the transport of phosphorus from agricultural land in river deltas of Northern Belgium, the Netherlands and North-West Germany. *Soil Use and Management*, 23(SUPPL. 1), 16–24. <https://doi.org/10.1111/j.1475-2743.2007.00108.x>
- Commissie Bemesting Grasland en Voedergewassen. (2018). *Bemestingsadvies*. <https://edepot.wur.nl/413891>
- De Klein, J. J. M., & Koelmans, A. A. (2011). Quantifying seasonal export and retention of nutrients in West European lowland rivers at catchment scale. *Hydrological Processes*, 25(13), 2102–2111. <https://doi.org/10.1002/hyp.7964>
- Dodds, W. K., & Smith, V. H. (2016). Nitrogen, phosphorus, and eutrophication in streams. *Inland Waters*, 6(2), 155–164. <https://doi.org/10.5268/IW-6.2.909>
- Döll, P., & Siebert, S. (2005). A digital global map of artificially drained agricultural areas. In *Frankfurt Hydrology Paper 04, Institute of physical geography, Frankfurt University* (Issue 01). <https://doi.org/10.13140/2.1.3971.3923>
- Eurostat. (2015). *Farm Structure Survey* (Issue December 2015). <https://ec.europa.eu/eurostat/statisticsexplained/>
- Gelbrecht, J., Lengsfeld, H., Pöthig, R., & Opitz, D. (2005). Temporal and spatial variation of phosphorus input, retention and loss in a small catchment of NE Germany. *Journal of Hydrology*, 304(1–4), 151–165. <https://doi.org/10.1016/j.jhydrol.2004.07.028>

- Gu, S., Gruau, G., Dupas, R., & Jeanneau, L. (2020). Evidence of colloids as important phosphorus carriers in natural soil/stream waters in an agricultural catchment. *Journal of Environmental Quality*, February, 1–12. <https://doi.org/10.1002/jeq2.20090>
- Hart, M. R., Quin, B. F., & Nguyen, M. L. (2004). Phosphorus runoff from agricultural land and direct fertilizer effects: A review. *Journal of Environmental Quality*, 33(6), 1954–1972. <https://doi.org/10.2134/jeq2004.1954>
- House, W. A., & Warwick, M. S. (1998). Intense measurement of nutrient dynamics in River Swale. In *The Science of the Total Environment: Vol. 210/211* (Issues 1–6, pp. 111–137).
- Jensen, H., Kristensen, P., Jeppensen, E., & Skytthe, A. (1992). Iron:phosphorus ratio in surface sediment as an indicator of phosphate release from aerobic sediments in shallow lakes. *Hydrobiologia*, 253/254, 731–743.
- Koopmans, G. F., Chardon, W. J., Dekker, P. H. M., Römkens, P. F. A. M., & Schoumans, O. F. (2006). Comparing different extraction methods for estimating phosphorus solubility in various soil types. *Soil Science*, 171(2), 103–116. <https://doi.org/10.1097/01.ss.0000187361.00600.d6>
- Lee, G. F. (1973). Role of phosphorus in eutrophication and diffuse source control. *Water Research*, 7(1–2), 111–128. [https://doi.org/10.1016/0043-1354\(73\)90156-5](https://doi.org/10.1016/0043-1354(73)90156-5)
- McDonald, N. T., Wall, D. P., Mellander, P. E., Buckley, C., Shore, M., Shortle, G., Leach, S., Burgess, E., O’Connell, T., & Jordan, P. (2019). Field scale phosphorus balances and legacy soil pressures in mixed-land use catchments. *Agriculture, Ecosystems and Environment*, 274(December 2018), 14–23. <https://doi.org/10.1016/j.agee.2018.12.014>
- Melland, A. R., Fenton, O., & Jordan, P. (2018). Effects of agricultural land management changes on surface water quality: A review of meso-scale catchment research. *Environmental Science and Policy*, 84(September 2017), 19–25. <https://doi.org/10.1016/j.envsci.2018.02.011>
- Mellander, P. E., Jordan, P., Shore, M., McDonald, N. T., Wall, D. P., Shortle, G., & Daly, K. (2016). Identifying contrasting influences and surface water signals for specific groundwater phosphorus vulnerability. *Science of the Total Environment*, 541, 292–302. <https://doi.org/10.1016/j.scitotenv.2015.09.082>
- Murphy, J., & Riley, J. P. (1962). A modified single solution method for the determination of phosphate in natural waters. *Analytica Chimica Acta*, 27(C), 31–36. [https://doi.org/10.1016/S0003-2670\(00\)88444-5](https://doi.org/10.1016/S0003-2670(00)88444-5)
- Rozemeijer, J. C., & Broers, H. P. (2007). The groundwater contribution to surface water contamination in a region with intensive agricultural land use (Noord-Brabant, The Netherlands). *Environmental Pollution*, 148(3), 695–706. <https://doi.org/10.1016/j.envpol.2007.01.028>
- Rozemeijer, J. C., & Van der Velde, Y. (2014). Temporal variability in groundwater and surface water quality in humid agricultural catchments; Driving processes and consequences for regional water

- quality monitoring. *Fundamental and Applied Limnology*, 184(3), 195–209. <https://doi.org/10.1127/1863-9135/2014/0565>
- Schoumans, O. F. (2015). *Phosphorus leaching from soils: process description, risk assessment and mitigation*. Wageningen.
- Schoumans, O. F., & Chardon, W. J. (2014). Phosphate saturation degree and accumulation of phosphate in various soil types in The Netherlands. *Geoderma*, 237, 325–335. <https://doi.org/10.1016/j.geoderma.2014.08.015>
- Schoumans, O. F., Chardon, W. J., Bechmann, M. E., Gascuel-Oudou, C., Hofman, G., Kronvang, B., Rubæk, G. H., Ulén, B., & Dorioz, J. M. (2014). Mitigation options to reduce phosphorus losses from the agricultural sector and improve surface water quality: A review. *Science of the Total Environment*, 468–469, 1255–1266. <https://doi.org/10.1016/j.scitotenv.2013.08.061>
- Schoumans, O. F., & Groenendijk, P. (2000). Modeling Soil Phosphorus Levels and Phosphorus Leaching from Agricultural Land in the Netherlands. *Journal of Environmental Quality*, 29(1), 111–116. <https://doi.org/10.2134/jeq2000.00472425002900010014x>
- Schwertmann, U. (1964). Differentiation of the iron oxides of the soil by extraction with ammonium oxalate solution. *Journal for Plant Nutrition, Fertilization, Soil Science*, 105, 194–202.
- Smolders, E., Baetens, E., Verbeeck, M., Nawara, S., Diels, J., Verdievel, M., Peeters, B., De Cooman, W., & Baken, S. (2017). Internal Loading and Redox Cycling of Sediment Iron Explain Reactive Phosphorus Concentrations in Lowland Rivers. *Environmental Science and Technology*, 51(5), 2584–2592. <https://doi.org/10.1021/acs.est.6b04337>
- Ulén, B., & Jakobsson, C. (2005). Critical evaluation of measures to mitigate phosphorus losses from agricultural land to surface waters in Sweden. *Science of the Total Environment*, 344(1-3 SPEC. ISS.), 37–50. <https://doi.org/10.1016/j.scitotenv.2005.02.004>
- Van Dael, T., De Cooman, T., Verbeeck, M., & Smolders, E. (2020). Sediment respiration contributes to phosphate release in lowland surface waters. *Water Research*, 168, 115168. <https://doi.org/10.1016/j.watres.2019.115168>
- Van der Grift, B., Behrends, T., Osté, L. A., Schot, P. P., Wassen, M. J., & Griffioen, J. (2016). Fe hydroxyphosphate precipitation and Fe(II) oxidation kinetics upon aeration of Fe(II) and phosphate-containing synthetic and natural solutions. *Geochimica et Cosmochimica Acta*, 186, 71–90. <https://doi.org/10.1016/j.gca.2016.04.035>
- Van der Grift, B., Broers, H. P., Berendrecht, W. L., Rozemeijer, J. C., Osté, L. A., & Griffioen, J. (2016). High-frequency monitoring reveals nutrient sources and transport processes in an agriculture-dominated lowland water system. *Hydrology and Earth System Sciences Discussions*, 12(8), 8337–8380. <https://doi.org/10.5194/hessd-12-8337-2015>

- Van der Grift, B., Rozemeijer, J. C., Griffioen, J., & Van der Velde, Y. (2014). Iron oxidation kinetics and phosphate immobilization along the flow-path from groundwater into surface water. *Hydrology and Earth System Sciences*, 18(11), 4687–4702. <https://doi.org/10.5194/hess-18-4687-2014>
- Van der Grift, Bas, Osté, L., Schot, P., Kratz, A., Van Popta, E., Wassen, M., & Griffioen, J. (2018). Forms of phosphorus in suspended particulate matter in agriculture-dominated lowland catchments: Iron as phosphorus carrier. *Science of the Total Environment*, 631–632, 115–129. <https://doi.org/10.1016/j.scitotenv.2018.02.266>
- Van der Salm, C., Dupas, R., Grant, R., Heckrath, G., Iversen, B. V., Kronvang, B., Levi, C., Rubaek, G. H., & Schoumans, O. F. (2011). Predicting phosphorus losses with the PLEASE model on a local scale in Denmark and the Netherlands. *Journal of Environmental Quality*, 40(5), 1617–1626. <https://doi.org/10.2134/jeq2010.0548>
- Withers, P. J. A., & Haygarth, P. M. (2007). Agriculture, phosphorus and eutrophication: A European perspective. *Soil Use and Management*, 23(SUPPL. 1), 1–4. <https://doi.org/10.1111/j.1475-2743.2007.00116.x>

2.9 Supplementary material to Chapter 2: Processes controlling the flux of legacy phosphorus to surface waters at the farm scale

Victoria Barcala¹, Joachim Rozemeijer¹, Leonard Osté¹, Bas Van der Grift², Laurens Gerner³, Thilo Behrends⁴

1 Inland Water Systems, Deltares, Utrecht, the Netherlands

2 KWR Water Research Institute, Nieuwegein, the Netherlands

3 Water Board Rijn and IJssel, Doetinchem, the Netherlands

4 Department of Earth Sciences, Faculty of Geosciences, Utrecht University, the Netherlands

The supplementary material includes extra information on materials and methods, geological information of the subsurface, pictures and results of soil samples, and the complete time series used.

Extra information on materials and methods

The P_w determines P in the soil solution, i.e. dissolved or readily soluble forms of P. It was determined by extracting phosphate from the soil with water at 1:60 (w/w) soil-to-liquid ratio for 1 hour. The PAL is one of the many methods used to determine the labile P in the soil, it is normally used in Dutch grasslands. It was determined by extracting phosphate from the soil with a mixture of ammonium lactate and acetic acid at pH 3.75 for 4 hours, with a 1:20 (w/w) solid-to-liquid ratio. P was determined with the molybdenum blue method (Murphy and Riley 1962) for the P_w , and PAL extractions.

The oxalate extraction method can be used to determine the P sorption capacity of the soil. Fe and Al amorphous hydroxides are dominant in P adsorption in neutral to acidic soils, the $P_{ox}/(Fe_{ox}+Al_{ox})$ molar ratio, also called P saturation degree (PSD), assesses the risk of P leaching to groundwater. The pools of Al and Fe extracted are, the water-soluble, exchangeable and a fraction of the organically bound Fe and Al. The extraction was done with

oxalic acid and ammonium oxalate with a 1:50 solid-to-volume ratio at pH 3 for 4 hours. P, Fe, and Al were determined with inductively coupled plasma atomic emission spectroscopy (ICP-OES).

For TP and TFe, the sample was treated with a mix of concentrated HNO₃ and HClO₄ in a 2:3 volume ratio and HF. The sample was placed in a Teflon vessel, the closed vessel was left overnight on a hot plate at 90°C and then condensed at 140°C for 4 hours, HNO₃ was added and the closed vessel was left another night at 90°C. P and Fe were determined with ICP-OES.

Turbidity and NO₃⁻ concentrations in the flow-through tank were continuously measured with Solitax and Nitratax sensors (Hach Lange GmbH, Düsseldorf, Germany). The Solitax is an optical, color independent turbidity sensor with an infrared duo scattered light photometer, the detection range goes from 0 to 4,000 NTU and 1% accuracy. The Nitratax measures the NO₃ concentrations based on a double wavelength spectrophotometric UV sensor. The Nitratax sensor has a detection range of 0.1 to 50.0 mg/L with 3% accuracy.

TP and TRP concentrations were measured with Phosphax Sigma auto-analyzer (Hach Lange GmbH, Düsseldorf, Germany). TRP is an unfiltered phosphorus fraction, it includes organic and inorganic acid-labile phosphorus compounds. The auto-analyzer is based on titration and photometric measurements. It includes a mixing and heating/cooling step that guarantees all measurements are made at the same temperature, the reagents are automatically added, for TP sulfuric acid and persulfate are used for digestion, finally the samples are measured at 880 nm using a LED photometer. The detection range is from 0.01 to 5.00 mg/L for TP and TRP with a 2% accuracy.

The sensors are suitable for fixed locations and were calibrated upon installation. The equipment requires relatively little maintenance, recommended every 3 or 6 months. The maintenance tasks include changing reagent bottles and checking for error messages on the equipment. High-frequency monitoring is especially useful in quantifying nutrient transformation and retention mechanisms lotic systems (Rode *et al.* 2016), and offer many advantages in comparison to low-frequency monitoring. The variations in grab samples values are greatly influenced by meteorological conditions and do not necessarily describe water


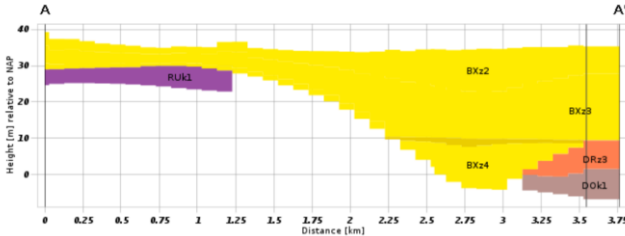

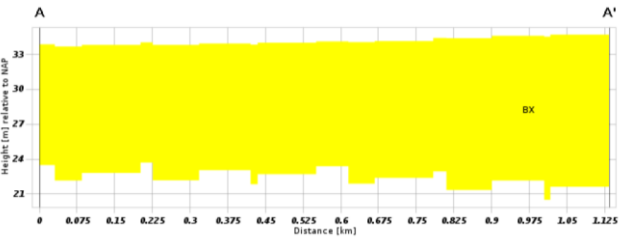
quality trends which creates great uncertainty in understanding the nutrient exports (Rozemeijer and Van der Velde 2014).



Figure S11 The flow through vessel (open) with, from left to right: Phosphax's auto analyzer intake, and Solitax and Nitratex sensors. The equipment is placed in the hut behind.

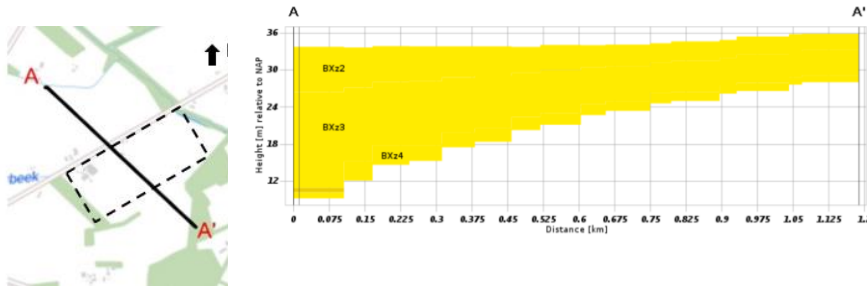
Subsurface Geology of the location

Table S6 Cross sections of the glacial valley formation below the farm

location of cross section	A-A' Cross-section BRO DGM v2.2 (https://www.dinoloket.nl/ondergrondmodellen)	Description
		<p>The farm is less than 1 km away from the U-shaped glacial tunnel valley. The valley is incised into the marine clay and it is filled up with glaciofluvial sands. The high hydraulic conductivity of the sand allows for relatively large proportion of the precipitation surplus to flow into deeper groundwater. Also, this permeable sand layer allows groundwater extractions for irrigation.</p>
		<p>Along the SW-NE direction, parallel to the road and the main ditch the depth of the sandy subsoil is constant.</p>

The sand's hydraulic conductivity is between 5 m/d and 10 m/d horizontally and between 5×10^{-4} m/d and 1×10^{-3} vertically.

The clay formation below is from the early Oligocene (Rupelian).



The glacial tunnel valley increases its depth perpendicular to the road and main ditch (SE-NW). The sand layer is about 10 m deep at the back of the farm and 20 m deep close to the ditch. The sand depositions are aged in the middle Pleistocene - Holocene.

Table S7 On site pictures of all soil samples



Table S8 Topsoil (0-10 cm) extractions results

Soil samples 0 cm-10 cm	Pw (mg/kg)	Pw (mg/L)	PAL (mg/kg)	P oxalate (mg/kg)	TP (mg/kg)	Fe oxalate (mg/kg)	Al oxalate (mg/kg)	P/(Fe+Al) molar ratio
1	19.5	0.21	247.6	133.7	952.9	318.6	116.9	0.4
2	15.3	0.18	242.1	116.8	725.7	201.7	224.3	0.3
3	18.1	0.17	234.1	138.1	827.4	207.0	314.7	0.3
4	17.9	0.18	280.3	121.3	722.4	176.8	332.7	0.3
5	16.7	0.17	148.4	93.4	690.0	299.2	154.6	0.3
6	9.4	0.09	55.5	78.1	769.8	564.1	167.5	0.2
7	8.2	0.10	111.2	76.1	487.0	186.1	183.5	0.2
8	11.8	0.15	202.1	74.6	491.9	136.7	100.9	0.4
9	14.5	0.15	238.5	100.0	650.0	109.9	266.8	0.3
10	13.6	0.11	110.8	59.5	448.8	137.4	90.2	0.3
11	10.3	0.11	172.7	84.6	635.3	208.7	171.3	0.3
12	9.9	0.10	142.8	78.5	564.1	143.4	230.5	0.2
13	10.6	0.12	96.7	66.1	420.4	116.0	135.7	0.3
14	6.9	0.08	92.2	56.4	408.5	154.6	118.0	0.3
15	6.1	0.06	106.8	69.2	559.6	194.6	300.8	0.2
16	7.6	0.10	96.7	85.8	631.1	199.8	213.4	0.2
17	12.3	0.15	103.8	80.1	619.4	169.4	216.6	0.2
18	24.5	0.26	271.5	118.2	807.1	163.9	270.7	0.3
19	7.5	0.08	108.2	52.2	380.8	88.6	148.1	0.2
20	8.9	0.10	135.1	65.6	479.7	147.9	183.4	0.2
21	15.7	0.17	151.5	76.8	611.1	188.5	182.6	0.2
22	2.1	0.02	64.7	43.9	340.3	207.4	334.9	0.1
23	9.0	0.11	74.9	40.4	346.7	334.9	77.3	0.1
24	6.7	0.06	124.3	225.4	1557.2	4023.4	305.9	0.1

Table S9 Subsoil (40-50 cm) extraction results

Soil Samples 40 cm - 50 cm	Pw (mg/kg)	Pw (mg/L)	PAL (mg/kg)	P oxalate (mg/kg)	TP (mg/kg)	Fe oxalate (mg/kg)	Al oxalate (mg/kg)	P/(Fe+AL) molar ratio
1	16.7	0.1694	82.9	40.7	353.6	185.3	66.8	0.2
2	0.1	0.0009	30.1	15.1	117.8	40.0	238.7	0.1
3	0.6	0.0070	36.0	32.5	204.1	361.4	336.7	0.1
4	0.1	0.0009	54.9	23.2	158.1	29.2	294.6	0.1

5	5.4	0.0591	62.6	45.6	358.7	225.8	129.2	0.2
6	0.0	-	9.0	11.6	178.5	244.1	25.8	0.1
7	0.0	-	9.9	9.5	125.1	562.9	193.2	0.0
8	1.6	0.0224	20.4	11.3	130.8	205.2	51.1	0.1
9	1.9	0.0193	71.5	32.6	213.6	70.9	253.3	0.1
10	0.4	0.0040	29.1	21.6	195.6	337.9	199.5	0.1
11	0.0	-	7.3	9.5	137.9	732.6	210.8	0.0
12	0.0	-	19.1	11.8	104.3	18.5	280.1	0.0
13	1.7	0.0224	43.9	19.4	182.2	82.5	140.6	0.1
14	1.5	0.0224	25.1	10.0	117.2	128.7	40.4	0.1
15	0.0	-	9.0	8.1	125.9	178.5	275.8	0.0
16	0.0	-	20.8	9.4	107.3	18.5	233.4	0.0
17	0.0	-	22.0	11.6	131.1	205.9	527.6	0.0
18	0.1	0.0009	21.3	15.2	128.9	199.2	484.2	0.0
19	0.5	0.0070	37.3	12.9	139.2	39.8	130.0	0.1
20	0.5	0.0070	14.1	9.0	110.5	45.7	199.1	0.0
21	0.7	0.0101	9.9	12.3	132.6	1114.8	414.6	0.0
22	0.1	0.0009	13.7	10.2	189.0	361.2	343.6	0.0
23	0.1	0.0009	13.6	10.9	210.6	403.7	44.8	0.0
24	3.1	0.0285	23.3	15.8	205.6	225.0	66.2	0.1

Table S10 Subsoil (70-80 cm) extraction results

Soil Samples 70 cm-80 cm	Pw (mg/kg)	Pw (mg/L)	PAL (mg/kg)	P oxalate (mg/kg)	TP (mg/kg)	Fe oxalate (mg/kg)	Al oxalate (mg/kg)	P/(Fe+AL) Molar ratio
4	0.0	-	16.2	9.7	93.4	22.8	211.3	0.04
10	0.0	-	9.0	9.1	146.9	161.7	49.0	0.06
14	0.3	0.004	19.5	6.6	106.3	103.7	44.5	0.06
19	0.0	-	4.0	5.1	107.0	215.0	105.4	0.02

Table S11 Extraction results of sediment samples

Sediment samples	Pw (mg/kg)	Pw (mg/L)	P PAL (mg/kg)	P oxalate (mg/kg)	TP (mg/kg)	Fe oxalate (mg/kg)	P/(Fe+AL) Mass ratio
3 - secondary ditch	32.0	0.04	108.8	50.9	241.0	398.7	0.11
5 (1) - main ditch	11.0	0.02	38.1	21.7	214.6	195.7	0.08
5 (2) - main ditch	9.3	0.02	44.5	21.6	398.7	179.2	0.09

Table S12 Average of Fe extraction results in the soil and sediment

Fractions	n samples	Fe ox mg/kg ± SDV mg/kg	TFe mg/kg ± SDV mg/kg	Feox/TFe
Soil 0-10 cm	24	361 ± 770	5583 ± 6356	0.06
Soil 40-50 cm	24	250 ± 251.1	7745 ± 5644	0.03
Soil 70-80	4	125 ± 71.3	8643 ± 4835	0.01
Sediment	3	258 ± 100	8062 ± 2184	0.03

Table S13 Groundwater and surface water cation results

Samples	Date	Ca(mg/L)	Fe(mg/L)	Mg(mg/L)	Mn(mg/L)
Limit of quantification		(0.015)	(0.011)	(0.004)	(0.001)
SW 1	16-4-2018	122.835	0.229	8.294	0.196
SW 2	16-4-2018	104.622	0.166	9.544	0.098
SW 3	16-4-2018	66.102	0.161	8.16	0.012
SW 4	16-4-2018	105.813	0.347	8.639	0.11
SW 5	16-4-2018	104.689	0.205	8.78	0.12
GW 1	15-5-2018	101.212	0.767	12.099	0.450
GW 2	15-5-2018	108.873	0.011	15.570	0.563
GW 3	15-5-2018	66.821	<0.011	13.625	0.104
GW 4	15-5-2018	26.780	0.107	8.823	0.089
GW 5	15-5-2018	24.522	0.302	6.417	0.025
GW 6	15-5-2018	81.005	0.033	9.657	0.222

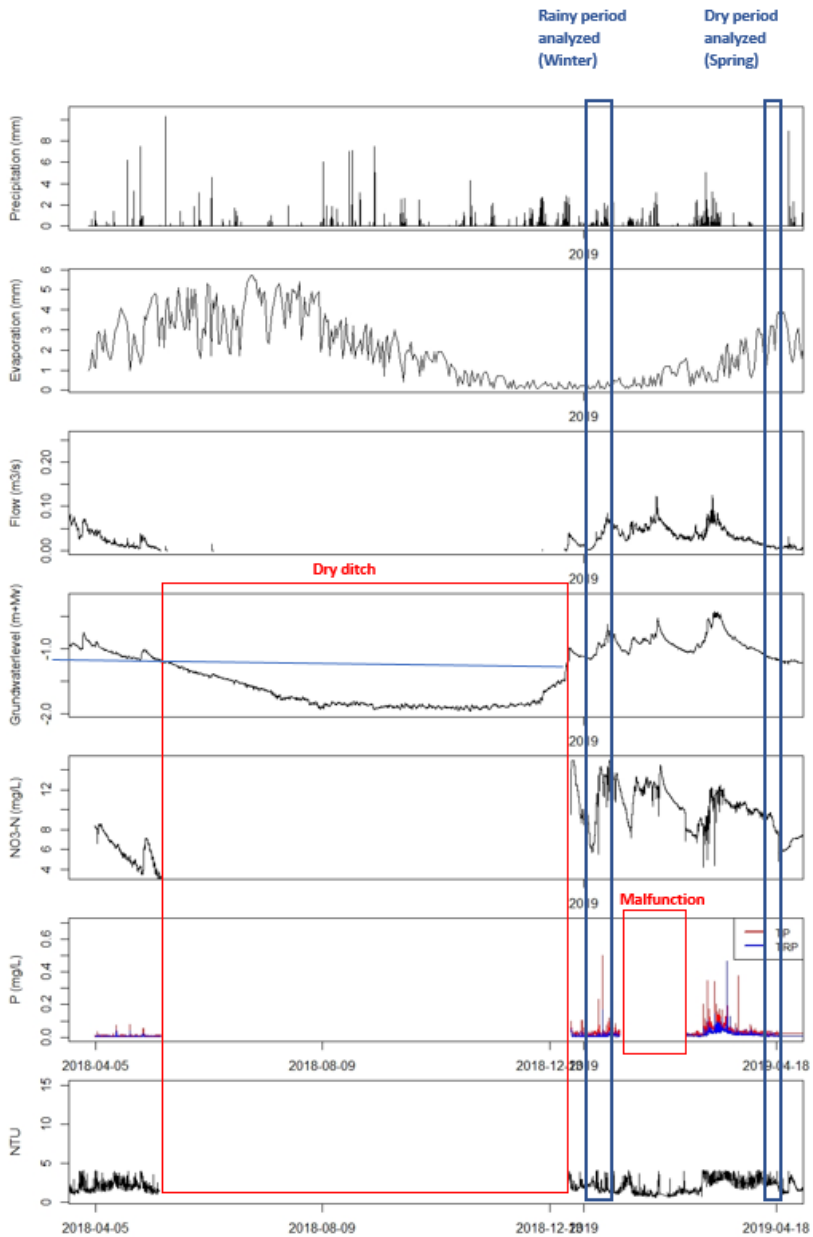


Figure S12 Complete time series of the high-frequency monitoring station from 5 April 2018 to 18 April 2019



Chapter

3

3 Chapter 3: Value and limitations of Machine Learning in high-frequency nutrient data for gap-filling, forecasting, and transport process interpretation

Victoria Barcala^{1,4}, Joachim Rozemeijer², Leonard Osté¹, Kevin Ouwerkerk², Laurens Gerner³

1 Inland Water Systems, Deltares, Utrecht, The Netherlands

2 Subsurface and Groundwater Systems, Deltares, Utrecht, The Netherlands

3 Water Board Rijn and IJssel, Doetinchem, the Netherlands

4 Department of Earth Sciences, Faculty of Geosciences, Utrecht University, the Netherlands

Journal of Environmental Monitoring and Assessment, in review (preprint)

<https://doi.org/10.21203/rs.3.rs-2201325/v1>

3.1 Abstract

High-frequency monitoring of water quality in catchments brings along the challenge of post-processing large amounts of data. Moreover, monitoring stations are often remote and technical issues resulting in data gaps are common. Machine Learning algorithms can be applied to fill these gaps, and to a certain extent, for predictions and interpretation. The objectives of this study were (1) to evaluate six different Machine Learning models for gap-filling in a high-frequency nitrate and total-phosphorus concentration time series, (2) to showcase the potential added value (and limitations) of Machine Learning to interpret underlying processes, and (3) to study the limits of Machine Learning algorithms for predictions outside the training period. We used a four-year high-frequency dataset from a ditch draining one intensive dairy farm in the east of The Netherlands. Continuous time series of precipitation, evaporation, groundwater levels, discharge, turbidity, and nitrate or total-phosphorus were used as predictors for total-phosphorus and nitrate concentrations respectively. Our results showed that the Random Forest algorithm had the best performance to fill in data-gaps, with

R^2 higher than 0.92 and short computation times. The feature importance helped understanding the changes in transport processes linked to water conservation measures and rain variability. Applying the Machine Learning model outside the training period resulted in a low performance, largely due to system changes (manure surplus and water conservation) which were not included as predictors. This study offers a valuable and novel example of how to use and interpret Machine Learning models for post-processing high-frequency water quality data.

Abbreviations: ANN, artificial neural network; kNN, K-nearest neighbor, M5R, M5-Rules, MAE, mean average error; MLR, multivariable linear regression; N, nitrogen; NO_3 , nitrate; P, phosphorous; R^2 , coefficient of determination; RF, Random Forest; RMSE, root mean square error; SMO, sequential minimal optimization; TP, total phosphorous; ZR, zero rules.

Key words: water management, missing data, data-based models, Random Forest, groundwater surface water interactions

3.2 Introduction

Intensive agriculture is an important source of nutrients in surface waters (Bol et al., 2018; Van der Grift et al., 2016; Van der Salm et al., 2012; Withers et al., 2014). High total phosphorus (TP) or high nitrate (NO_3) concentrations are two of the parameters that can lead to a poor ecological quality status in surface waters. High NO_3 and TP concentrations are being pointed out as one of the main causes of biodiversity loss (Dise et al., 2011; Porter et al., 2013) and algae blooms (Withers & Haygarth, 2007). In many cases, the nutrients lost to surface water do not just originate from the freshly applied manure or fertilizer, but from the nutrient legacy accumulated in the soil which is transported into surface waters through natural or artificial drainage systems (Bierozza et al., 2019; Lucas et al., 2021; Sharpley et al., 2013). Realistic goals and appropriate mitigation measures are needed (Schoumans et al., 2014). Therefore, it is central for the water authorities to monitor the water quality of surface waters and quantify the effect that nutrient sources and system changes have in the transport processes of nutrients into larger water systems.

High-frequency monitoring of water quality data offers a detailed understanding of the processes involved in nutrient transport (Rode et al., 2016; Rozemeijer et al., 2010). However,

technicians often face the challenge to deal with large data volumes and missing data (Zhang et al., 2019). It is often the case that sensors and autoanalyzers have technical problems which can result in a significant number of gaps in the data. The post processing of the data, including identification of errors and filling missing values can be time consuming and the final result depends on the individual who does the post processing (Jones et al., 2021). Furthermore, the amount of data collected by high-frequency sensors can easily exceed the amount of data that can be treated manually (Dupas et al., 2015; Kirchner & Neal, 2013). Nevertheless, without complete data series it is not possible to accurately calculate total annual loads and the value of high-frequency monitoring is reduced to the observation of specific events that might not be representative of the overall system's response.

Machine Learning algorithms build models based on sample (training) data in order to make numerical predictions (regression models) or decisions (classification models). Machine Learning algorithms, such as Trees, Rules, Support Vector Machines, and Artificial Neural Networks, offer an advantage to linear methods when treating non-linear problems such as concentration-discharge relationships. Although Machine Learning algorithms are powerful tools to post-process high-frequency water quality data, their use is still below their potential in many fields of environmental sciences (Liu et al., 2022). The relative low acceptance of Machine Learning in some environmental sciences may lie in reluctance to shift from a process-based approach to a data-based approach and the tradeoff between interpretability, performance, and complexity (Liu et al., 2022b; Visser et al., 2022). Gap-filling of continuous water quality datasets is a so far unexplored, yet potentially powerful application of Machine Learning. Machine Learning algorithms have been successfully applied for gap-filling in medical datasets (Shah et al., 2014), eddy-covariance evaporation and CO₂ flux data sets (Kang et al., 2019), soil moisture (Mao et al., 2019) and more recently also for daily streamflow time series (Arriagada et al., 2021). Most water quality applications of Machine Learning focus on predicting nutrient concentrations from catchment characteristics (e.g. Castrillo & García, 2020; Chen et al., 2020; Olson & Hawkins, 2012) or from other chemical parameters measured in conventional monitoring networks (e.g. Ha et al., 2020; Visser et al., 2022). Nevertheless, most of these studies focus on the forecasting performance and do not explore the limitations of using predictive data-based models (Tyrallis & Papacharalampous, 2019).

The objectives of this study were to: (i) to evaluate six different Machine Learning models for gap-filling in a high-frequency NO₃ and TP concentration time series, (ii) to showcase the potential added value and limitations of Machine Learning to interpret underlying nutrient transport processes, and (iii) to study the limits of Machine Learning algorithms for making predictions outside the training period. As case study, we used four years of high-frequency data from a ditch draining one dairy farm in the east of The Netherlands where the nutrient transport from the soil to the surface water were previously investigated (Barcala et al., 2020). We applied open source and popular data-science software such as WEKA (Frank et al., 2017) and R (R Core Team, 2020) for the data post-processing and model implementation. This study offers a valuable and novel example of how to use and interpret Machine Learning models for post-processing high-frequency water quality data.

3.3 Materials and Methods

Field site and time series description

The data was collected from a dairy farm near Winterswijk, the Netherlands (52.00131 N, 6.76112 E). The nutrient routes from the soil to the surface water were previously studied by Barcala *et al.* (2020). Manure is applied in the fields for fertilization between March and August. After measuring the crop productivity, the annual nutrient surpluses are calculated by the farmer. The topsoil is high in organic matter and has a 0.26 phosphorus saturation degree, meaning it can no longer retain more P. The water extractable P content (P_w) was on average 11.2 mg/kg in the topsoil, 1.5 mg/l just below the tillage zone (40-50 cm depth), and 0.1 mg/kg at 70-80 cm depth (Barcala et al., 2020). The average P in the topsoil is 2.630 kg/ha and the N in the topsoil is 565 kg/ha (Barcala et al., 2020). Below the topsoil, there is a Fe- and Al-rich sand layer. The farm is artificially drained by a main ditch that collects the water of the whole farm and runs parallel to the road in front of the farm. A secondary ditch runs perpendicular to the main ditch into the fields behind the farmyard. The northeast part of the fields has subsurface drainpipes draining into the most upstream part of the main ditch. The terrain is flat and surface runoff only occasionally contributed to the ditch discharge. Therefore, nutrients are transported mainly from the soil to the main ditch via lateral groundwater flow and the tile drains. During the summer months, the groundwater level falls below the ditch level and the main ditch falls dry. During this study, farmers were particularly affected by the

extreme drought of 2018. Water shortage is a stress factor for crop growth and climate change is causing greater rainfall variability (Greve et al., 2021; Masson-Delmotte et al., 2021). To adapt against droughts, the farmer implemented different water conservation measures to control the groundwater level in the field before the start of the last drainage season. An adjustable weir was placed in the main ditch in front of the farm, and an adjustable pipe was installed in the side ditch behind the farmyard (Figure 3-1).

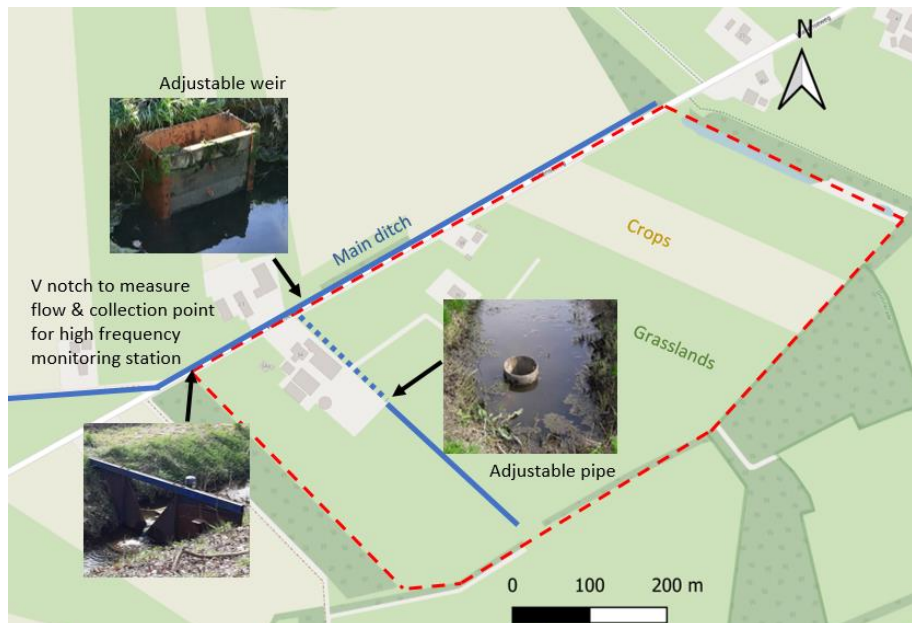


Figure 3-1 Farm layout (dashed red line) with water conservation measures implemented for the 2020-2121 season

At the end of the main ditch, we installed a v-notch weir and a high-frequency monitoring station was operative from 17 February 2018 to 7 June 2021. Every 15 minutes TP (Phosphax Sigma autoanalyzer, Hach), NO_3 (Nitratax Sensor, Hach), and turbidity (Solitax Sensor, Hach) were measured. Also, every 15 minutes, the discharge from the v-notch weir was calculated using a pressure gauge upstream from the weir and groundwater levels at the farm were monitored with a pressure gauge installed in a groundwater piezometer. As meteorological data may contribute to the prediction of the missing values, hourly rainfall and daily evapotranspiration data were downloaded from a meteorological station 12 km from the farm

that belongs to the Dutch Royal Meteorological Institute Network (<https://www.knmi.nl/nederland-nu/klimatologie>, station 283). The hourly rain, and daily evaporation, were linearly interpolated to have one value every 15 minutes using the *approxfun* function in R. All the times were taken to Dutch wintertime (GMT+1). All the time series were quality checked, discharge measurements were checked based on manual measurements and concentrations measurements were controlled based on laboratory measurements taken on routine visits every approximately four weeks. More detailed information about the field site characteristics and the high-frequency monitoring station can be found in Barcala *et al.* (2020).

Using the 2017-2018 values as a reference, the groundwater levels were on average 25 cm higher in 2020-2021 when the farmer implemented water retention measures (Table S1). In the year 2018 (2017-2018 season), TP correlated with turbidity (0.70) and NO₃ correlated strongly with discharge and groundwater level (0.91, 0.86) as was already discussed in Barcala *et al.* (2020). However, these correlations became weaker in the following years, especially between TP and turbidity (Figure S2). NO₃ concentrations showed a similar temporal pattern to the groundwater levels but were shortly diluted during rain events (Figure 3-3 and S3). Before starting with the selection of the Machine Learning models, we did some basic exploration of the available data available in the supplementary material. The N and P application to the fields are limited by the national Action Plans for the EU Nitrate Directive (Schroder *et al.*, 2007). The manure applied targets at a 0 kg/ha P surplus. However, the crop growth can be limited by the water availability; in years with low rainfall less P was taken up, which resulted in a positive surplus. The average yearly N surplus was 142 kg/ha N, which falls just below the national average (160 kg/ha). Table 1 gives a quantitative summary of the drainage seasons.

Table 3-1 Summary of the nutrient surplus, first and last day of drainage, seasonal rainfall, evaporation, and discharge.

		All seasons	2017-2018	2018-2019	2019-2020	2020-2021
- Nutrient surplus -						
N surplus	(kg/ha)	568	126	209	167	66
P surplus	(kg/ha)	0	2	4	16	-22
- Drainage season characteristics -						
First drainage season	day dd-mm-yy	17/02/18	17/02/18	23/12/18	18/10/19	1/12/20
Last drainage season	day dd-mm-yy	7/06/21	8/05/18	16/04/19	20/04/20	7/06/21
Rain	Total (mm)	1121	105	221	379	416
Evaporation	Total (mm)	380	86	58	94	142
Rain – Evap.	Total (mm)	741	19	163	285	275
Discharge	Total (m ³)	178,768	20,361	31,773	64,727	61,908
- Data gaps -						
Turbidity sensor	% missing	5.9%	24.6%	1.8%	4.8%	1.6%
NO₃ sensor	% missing	5.6%	25.4%	1.5%	3.4%	1.9%
TP autoanalyzer	% missing	33%	57%	34 %	22%	34%
Number of instances	N	54912	7776	11040	17952	18144
Averages * -						
Turbidity	(NTU)	9.40	2.06	14.1	4.89	13.4
Groundwater levels	(m)	-1.28	-0.989	-0.916	-0.858	-0.769
NO₃	(mg/L)	9.52	4.91	9.97	12.7	7.77
TP	(mg/L)	0.050	0.010	0.035	0.045	0.077

* To use as a reference for the average concentration, the Water Framework Directive target for surface waters is 2.3 mg/L for TN and 0.11 mg/L for TP (average summer concentrations).

Data analysis

To calculate and compare accurate annual nutrient loads leaving the catchment we needed to fill the missing NO₃ and TP values of the high-frequency dataset. Table 3-1 shows the duration of each drainage season and the percentage of NO₃ and TP missing data. To fill in missing data we evaluated six Machine Learning algorithms and compared them to filling in the gaps with the mean. The measured data was split and 60% was used for training (calibration) and 40% for testing (validation). The data was randomly split three times to improve the statistical representation and robustness of the results by using three different seeds. Seeds ensure that the results are reproducible, dividing the data in the same way each time. We opted for a wide pre-selection of Machine Learning algorithms because one cannot know beforehand which will perform best for a specific problem. The performance depends on the available dataset and the defined problem, in our case the accuracy in filling missing data in high-frequency nutrient concentration time series. The Waikato Environment for Knowledge Analysis (WEKA) was used to preprocess the data and for evaluation of all Machine Learning models. WEKA is open software widely used for data mining programmed in Java (Frank et al., 2017). If it is not stated otherwise, the default parameter settings in WEKA were used. R studio (R Core Team, 2020) was used for data visualization and pre- and post-processing of the data. Six algorithms were pre-selected following the criteria that they were well documented and accepted, able to predict a numeric class (regression), and capable of handling missing data.

The pre-selected algorithms use different principles in order to build the models. Zero Rules (ZR) predicts the mean of the numeric class, it is used as a benchmark to determine if other algorithms perform better than filling the missing values with the mean. Multivariate Linear Regression (MLR) finds the best fit for a line between multiple independent variables and the output is an explicit equation. Sequential minimal optimization regression (SMO) is similar to a support vector machine but can solve regression problems. SMO solves analytically the smallest possible optimization problem at every step using two Lagrange multipliers that obey a linear equality constraint (Platt, 2008). K-nearest neighbor (kNN), also called instance-based learner, generates a prediction by first finding k instances in the training dataset which are closest to the value that we want to predict (Aha et al., 1991). K was set to 1 and we used the Euclidean distance. M5 Rules (M5R) combines rules with trees, it generates list of rules for regression problems using the “separate-and-conquer” strategy, in each iteration a tree is built,

and the "best" leaf is made into a rule (Leman, 1997). Random Forest (RF) grows an ensemble of trees and takes the average of the trees for the regression problem (Breiman, 2001), 100 trees were grown to maximal depth. Artificial Neural Networks (ANN) are networks of linear classifiers (perceptrons), they implement a weighted decision given two hidden layers, we used 7 nodes or "neurons" in the hidden layer as this was equal to the number of nodes in the input layer (Wolpert, 1992).

To build the TP and NO₃ models, we used time series of precipitation, evaporation, groundwater levels, discharge, turbidity, and NO₃ or TP respectively. Seasonal changes as the manure surplus and the implementation of water retention measures are not included as predictors. To evaluate and select the best model, we used the coefficient of determination (R²), the mean absolute error (MAE), and the root mean square error (RMSE) between the measured and the predicted values of the test subset. The models were done for each drainage season (2017-2018, 2018-2019, 2019-2020, 2020-2021) and for all the seasons together (2017-2021). The seasons are defined as the time during the year when there is water discharge in the ditch. Separate models were preferred to one single model to evaluate the model response to different yearly features that are not considered as predictors, such as year-to-year variations in total rainfall, nutrient surpluses, and the implementation of water conservation measures in the 2020-2021 drainage season.

To study the performance of predicting nutrient concentrations we evaluated two scenarios. First, the 2018-2019 model was used to predict the 2019-2020 measurements and second, 2019-2020 model was used to predict the 2020-2021 measurements. Both predictions used the input variables (rain, evaporation, groundwater, discharge, turbidity, and NO₃ or TP) of the season we wanted to predict. The first scenario represents the prediction with no system changes and the second represents the prediction with changes (water retention measures). This way we evaluate if the model can predict system changes outside the training window. Also, both predictions were done with the all seasons (2017-2021) model to assess if the model could represent system changes inside the training window. Although the retention measures are not incorporated into the model, the groundwater levels measured were and they were higher on the last season.

The feature importance (also called permutation variable importance metrics) allows to weight the influence of each input variable in the prediction, improving the interpretability of the

results. The feature importance is calculated as the percentual increase in predictive error of not including one variable as compared to the out-of-bag rate with all other variables intact (Breiman, 2001). The feature importance was used to interpret which variables are most relevant for the prediction outcomes. An extra random variable was included in the feature importance calculations as a benchmark. If any variable was equally or less important than the random variable, then it would not contribute for the prediction. The importance values are related to the output magnitude of the predicted variable; therefore, the feature importance was normalized to 1 to facilitate the comparison. Without this normalization step, the NO₃ predictors would have a higher feature importance values than those for TP. The 2017-2018 season is only used for gap filling and not for future predictions or for variable feature importance calculations because it is not a full drainage season (it starts in half February). Lastly, after filling the missing data with the best performing model, the total loads of NO₃ and TP were calculated for each season by multiplying the concentrations by the discharge. Total loads were also calculated for the predictive models.

3.4 Results

Filling in missing data

The TP autoanalyzer had a larger amount of missing data, grouped in 2 to 4 large gaps per season. Besides 2018, the amount values missing from the NO₃ sensor were very low and concentrated at the beginning of the season. The summary of the R², RMSE, and MAE for three test subsets for the different NO₃ and TP season models are shown in Figure 3-2 (values and computation times are shown in Tables S2 and S3). For each drainage season, the Random Forest model had the best fit (R² ~ 0.99 for NO₃ and 0.96 for TP) with low computation times and was therefore selected to fill in the missing values. Figure 3-3 shows the complete measured and modeled time series together with the input variables for the 2019-2020 and 2020-2021 seasons (seasons 2017-2018 and 2018-2019 are in Figure S3). Random Forest gave consistently very good results for each seasons' model, while other algorithms showed larger differences in performance from season to season. Following Random Forest, k-Nearest Neighbor and M5 Rules had a good performance for all seasons (R² ~ 0.84 and 0.81 for TP and 0.73 and 0.92 for NO₃ respectively), yet they had poorer results for TP in the 2019-2020 season (R² ~ 0.59 and 0.65 respectively). M5 Rules gave, for little extra computation time, a very good

performance in the all seasons model and has the advantage that the output of the model are explicit rules that could be interpreted. However, as the problem was complex, more than 190 rules were obtained, which makes interpretation very difficult. Artificial Neural Networks came in fourth place with a lower performance in the all seasons model ($R^2 \sim 0.67$ for NO_3 and 0.50 for TP). Sequential Minimal Optimization obtained even lower results than Artificial Neural Networks ($R^2 \sim 0.38$ NO_3 and 0.19 TP) and the longer times needed to build and validate the model are a mayor disadvantage. For example, for the all seasons model, the Sequential Minimal Optimization model took 46 hours computing time to train and test the NO_3 data series while Random Forest took only 2 minutes. Multivariable Linear Regression offers the benefit of having an explicit equation as output, but the trade-off is a lower performance ($R^2 \sim 0.39$ for NO_3 and 0.21 for TP; MAE > mean). Only in 2018 when NO_3 was strongly correlated to discharge and groundwater levels the results for the Multivariable Linear Regression were very good ($R^2 \sim 0.89$). Nevertheless, the correlation was almost the same as doing a simple one variable linear regression with the discharge and this relationship was not maintained through the years (Figure S2).

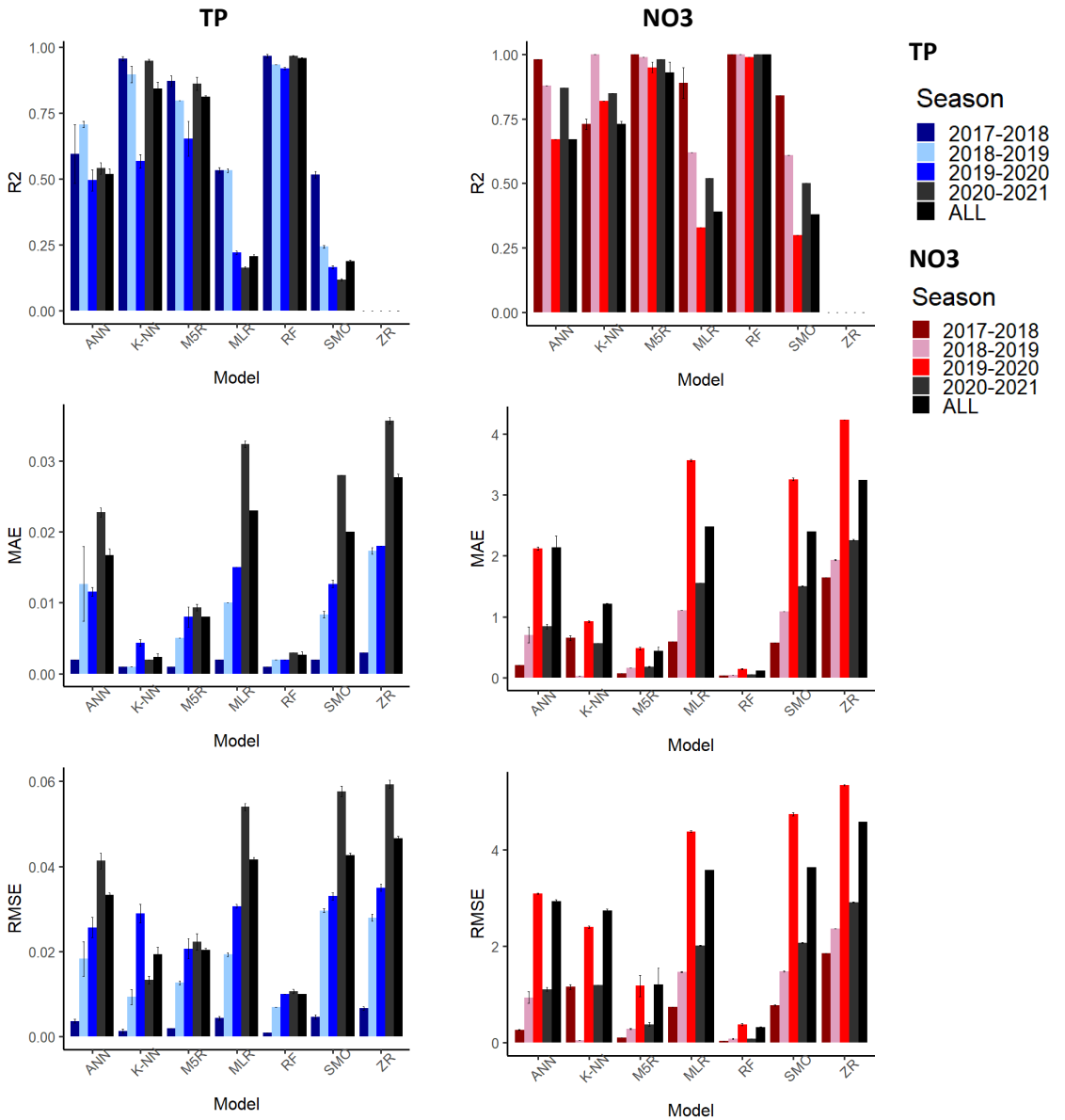


Figure 3-2 Performance of the different Machine Learning models in the test set. Average of R2, MAE, and RMSE for the 3 seeds used. The standard deviation is shown with the error bars. Models: Artificial Neural Networks (ANN), K-Nearest Neighbor (K-NN), M5 Rules (M5R), Random Forest (RF), Sequential Minimal Optimization (SMO), Zero Rules (ZR).

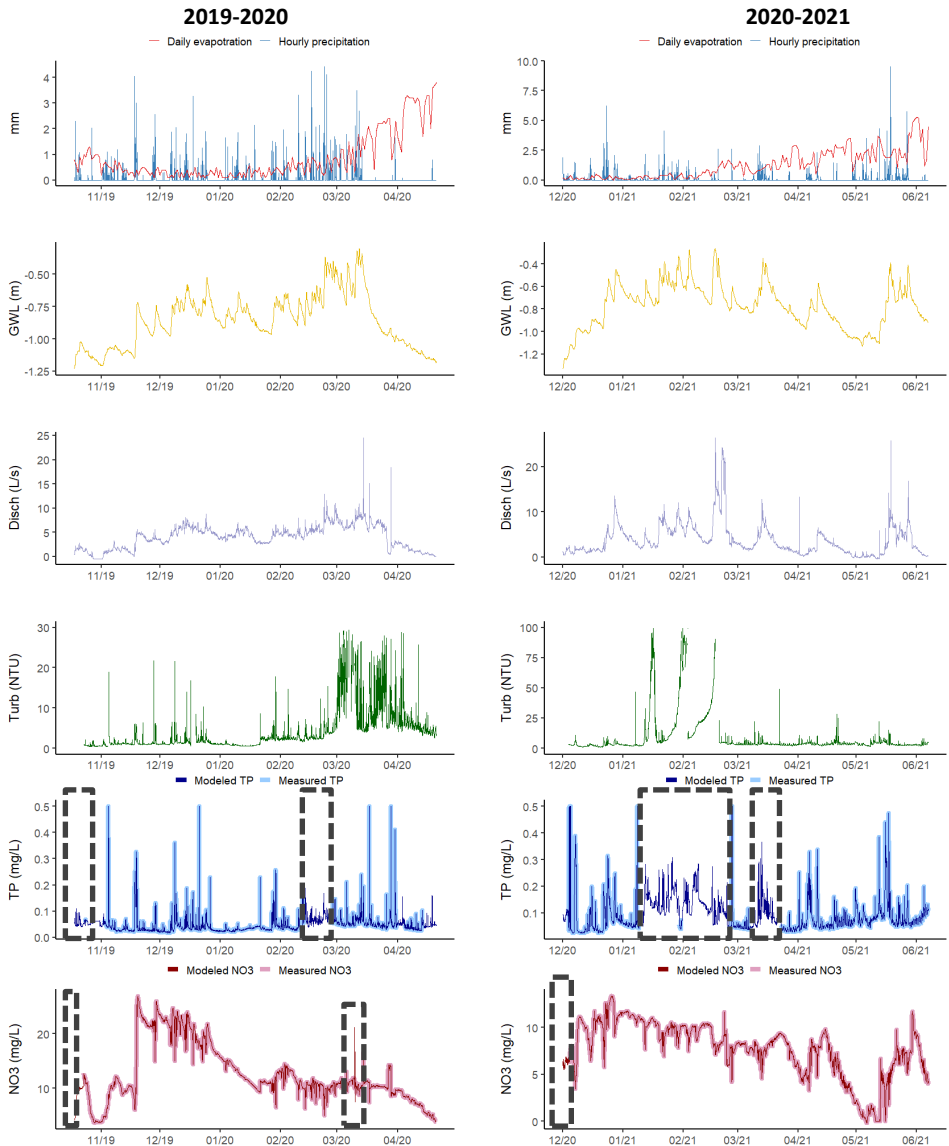


Figure 3-3 Measured and modeled time series for the 2019-2020 and 2020-2021 season. The nutrient measured data was plotted thicker to see it behind the model. Gaps in the data are indicated with a dashed box.

Future predictions

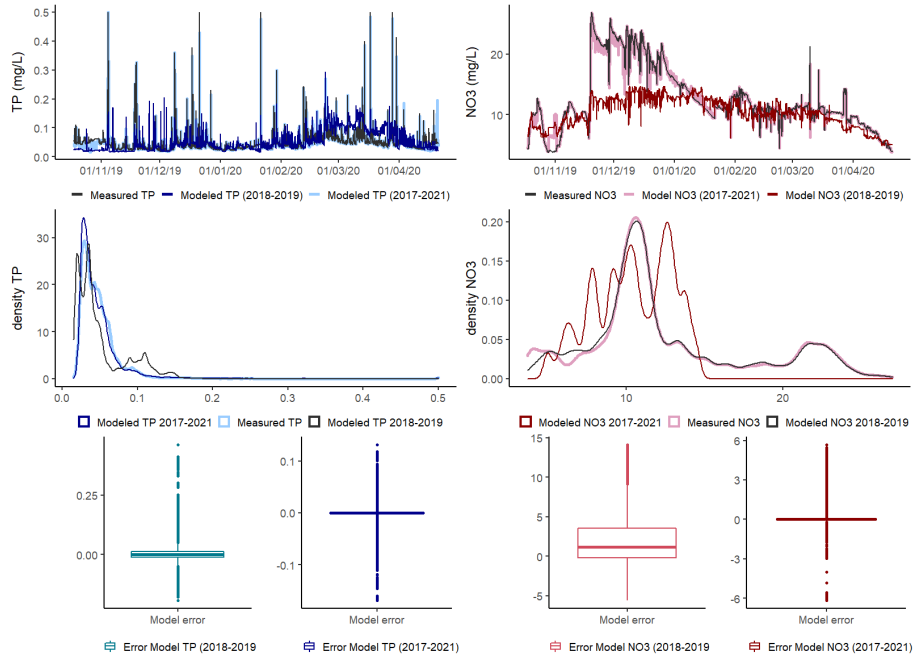


Figure 3-4 Prediction of 2019-2020 measured concentrations using 2018-2019 and 2017-2021 models. Concentrations timeseries (top), density distribution of values (middle), and box plots of the error (measured – modeled) (bottom).

First, we compared the predictive performance between the 2019-2020 measured data and the prediction of the same measured season using the 2018-2019 and the all seasons' Random Forest models (Figure 3-4). This prediction illustrates the Random Forest performance outside the training period without system changes (besides manure surplus). The R^2 using the TP predictive 2018-2019 model was only 0.41 (MAE 0.02 and RMSE 0.04), fewer and lower TP peaks were obtained but the baseline concentrations were reproduced, except for some baseline overestimations in March. For NO_3 the largest difference in concentrations was from the end of November to January, when there is an increase in the measured NO_3 values that were not predicted by the model, still the R^2 was 0.75 (MAE 3.02 and RMSE 4.40), as the model performs well outside this window. The NO_3 load using 2018-2019 model was 723 kg while the measured load was 885 kg. TP exported using 2018-2019 model was 4.1 kg while the measured

load was 3.3 kg. On the other hand the 2017-2021 model prediction follows the measured values closely, the error is centered in zero and the TP peaks and NO₃ increase between November and January are well represented.

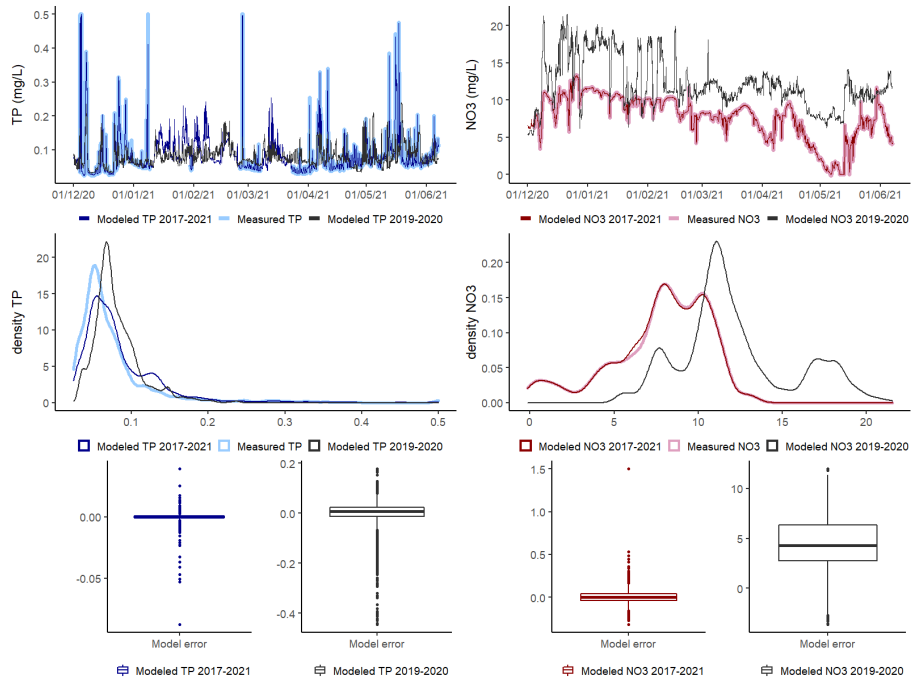


Figure 3-5 Prediction of 2020-2021 concentrations using 2019-2020 and 2017-2021 model. Concentrations timeseries (top), density distribution of values (middle), and box plots of the error (measured – modeled) (bottom).

Second, we compared the predictive performance between the 2020-2021 measurements and the prediction of the same season using the 2019-2020 and the all seasons' Random Forest models (Figure 3-5). The predictions represent how suitable is Random Forest to capture system changes (water conservation). The performance of the 2019-2020 model TP predictions was poor (0.09 R², 0.034 MAE, and 0.057 RMSE) while the all seasons model performed well (0.96 R², 0.001 MAE, and 0.003 RMSE). In the case of NO₃, the R² of the 2019-2020 model with the measured values was 0.44 (4.53 MAE and 5.15 RMSE) while with the all seasons model it was 0.99 (0.050 MAE and 0.070 RMSE). The distribution of the error of the all seasons model was always around zero and the differences with the measurements were mainly in the

outliers. Despite the very good results for gap-filling within the training period, the predictive performance of Random Forest outside the training period was poor. The total TP load using the 2019-2020 model predictions was 5.57 kg while the measured load was 6.55 kg. On the other hand, the 2019-2020 model overestimated the NO₃ load at 760 kg, while the measured load was 534 kg. During the first three seasons the total nutrient loads increased with the increase in rainfall. A change in this trend is observed for the last season after the water conservation measures were implemented. Although the predicted loads differ from the measured loads for 2020-2021, the change in trend is to some extent captured by the model (Figure 3-6). All measured variables had between four and a hundred times the importance of the random variable introduced (Figure 3-7). Turbidity had the highest feature importance in most models (except the 2018-219 and 2020-2021 NO₃ models).

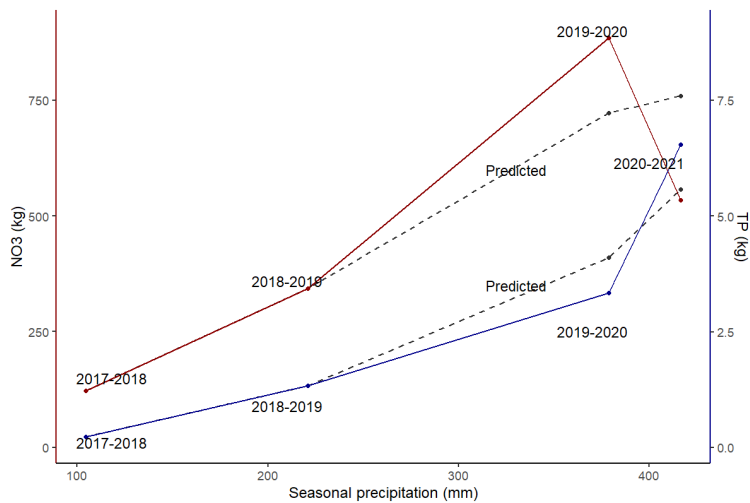


Figure 3-6 Total loads of NO₃ and TP per season against the seasonal precipitation. The predicted loads for the last seasons with the 2018-2018 and 2019-2020 model are included in gray.

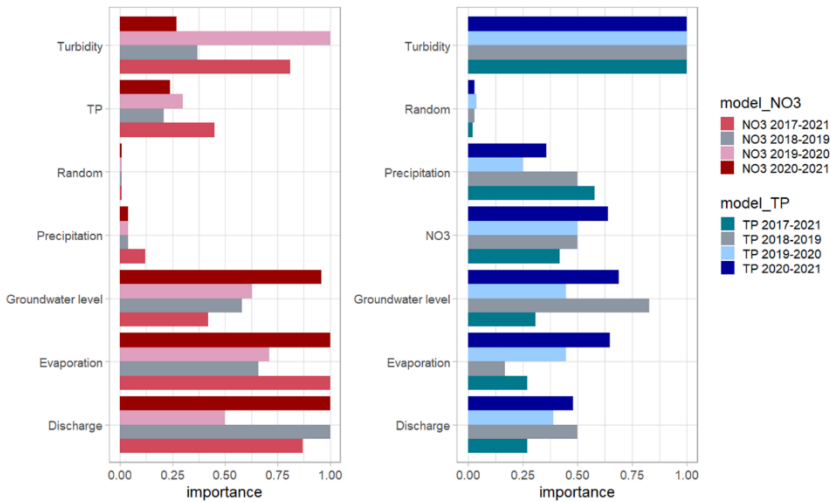


Figure 3-7 Relative feature importance of the variables in the Random Forest models of the 2017-2021, 2018-2019, 2019-2020 and 2020-2021 seasons.

3.5 Discussion

Using Machine Learning models to fill in missing data

The first objective of this study was to evaluate six different Machine Learning models for gap-filling in a high-frequency NO₃ and TP concentration time series. Random Forest had the best performance for both NO₃ and TP with a constantly high R² (> 0.92) and low MAE and RMSE for every randomly selected testing set and application period. The short computing times are another advantage for using Random Forest for gap filling. The Random Forest gap-filling model could reproduce short-term trends in the time series as the TP peaks after rain events, NO₃ dilution after rain events, and NO₃ increase with increase in the groundwater levels. The good results of the 2017-2021 model show that the Random Forest algorithm can also largely incorporate system changes within the training period, such as the introduction of water conservation measures and different soil nutrient surpluses. We observed that the NO₃ models performed systematically slightly better than the TP models. This may be caused by the larger proportion of missing values in our TP time series. Kang et al. (2019) and Zhang & Thorburn (2022) also reported a reduction in model performance when the amount of missing data is

larger as this reduces the size of the training set. Another reason could be the relatively smooth behavior of NO₃ concentration dynamics compared to the spikier TP patterns.

Other comparative studies have also found Random Forest to perform better than Linear Regression and other Machine Learning algorithms in problems related to water quality (Castrillo & García, 2020; Ha et al., 2020; Shen et al., 2020; Visser et al., 2022). Methods such as Artificial Neural Networks that here had a low performance have shown very good results in other studies (Astuti et al., 2020; Chen et al., 2020; Daliakopoulos & Ioannis, 2016; Dastorani et al., 2010; Kim et al., 2020; Najah et al., 2009, 2013). Nevertheless, in other comparative studies they have also underperformed Random Forest (Bedi et al., 2020; Chen et al., 2020; Kim et al., 2020; Qiao et al., 2021; Visser et al., 2022). The low performance of Multivariable Linear Regression can be explained by the non-linear relationships between hydrological variables and concentrations. Multivariable Linear Regression has shown low performance in other non-linear problems such as epidemiological studies (Shah et al., 2014). As there is no one-fits-all model we recommend the used approach of evaluating different algorithms and seasonal performance to select the most robust model.

Conventional approaches for dealing with missing data included not considering the missing data or substituting the missing data with the mean (Tyrallis & Papacharalampous, 2017). Not including the missing data makes calculations of total annual loads uncertain, especially because short, extreme rain events can account for a large portion of the yearly nutrient load export (Rozemeijer & Van der Velde, 2014). Substituting the missing data with the mean was done as a benchmark (Zero Rules model) and it underperformed all other methods having the highest MAE and RMSE. It has been already shown that statistical gap filling methods usually underperform Machine Learning methods (Zhang & Thorburn, 2022). Another gap-filling method includes stepwise linear regression, this approach has exhibited a good treatment of the missing data (Rozemeijer et al. (2010), R² 0.74) but it requires a more a complex and time-consuming analysis of the time series than Machine Learning models as Random Forest. In our previous publication (Barcala et al., 2020), TP was correlated with NO₃ for gap-filling in the 2018-2019 season, this lead to a lower load estimations, 0.96 kg for TP and 282 kg for NO₃ compared with loads obtained with the new method, 1.33 kg for TP and 344 kg for NO₃. Random Forest, and other Machine Learning algorithms, are underused tools in water quality studies. We encourage their application for gap-filling because of the good performance, short

calculation times, and the availability of open source packages in R and user-friendly software like WEKA. Beside gap-filling, algorithms like Random Forest could also be useful for similar applications as real time anomaly detection in sensors and autoanalyzers which could support system maintenance, for example by comparing the incoming data with one-step ahead predictions to detect anomalies and trigger a warning message.

Process interpretation

Our second objective was to show potential added value of Machine Learning to interpret underlying nutrient transport processes. In most cases, the high number of trees in Random Forest models makes their physical interpretation difficult or impossible (Tyralis & Papacharalampous, 2019). The feature importance represents the information gain of including each variable in the model and could be indicative for the influence of variables on physical processes. As a first observation, all predictor variables in our data set contributed to the information gain for all drainage seasons. This was indicated by the higher relative feature importance values compared to the random variable introduced (Breiman, 2001; Doshi-Velez & Kim, 2017). Besides the feature importance, other approaches for process interpretation include to evaluate the variable coefficients obtained by Multivariable Linear Regression for process interpretation together with the results of “less transparent” models as Random Forest (Visser et al., 2022). However, we would not recommend this approach for case studies as this one where results obtained with Multivariate Linear Regression are poor. Instead, a similar sensitivity analysis to the variable feature importance can be done for other Machine Learning algorithms by training the models without one input variable at a time and evaluating the impact on the model’s results.

For NO_3 , the feature importance values were quite different between the 2019-2020 and 2020-2021 seasons. In the 2019-2020 season, turbidity was the most important predictor, although groundwater levels, evaporation and discharge also contributed significantly. In the 2020-2021 season, groundwater levels, evaporation and discharge were the most important variables, but turbidity did not rank high. The connection between groundwater levels, discharge and NO_3 losses was described before by Rozemeijer & Broers (2007) and for this field site by Barcala et al. (2020). With higher groundwater levels, a larger relative contribution of shallow NO_3 -rich groundwater flow routes (including tube drain discharge) towards surface water increases the NO_3 concentrations while rain events dilute the concentrations. The NO_3 concentrations

reached up to 25 mg/l NO₃-N after an increase in the groundwater level in mid-November 2019. During the second part of the drainage season, the mineral N residue in the soil was depleted and the NO₃ concentrations decrease to around 10 mg/L. Turbidity was also high in the second part of the season and splitting the trees by turbidity resulted in a positive information gain. In this case, the predictive power of turbidity does not seem to have a direct process-based explanation.

For TP, turbidity has the highest relative feature importance values in all models. This relation is directly linked to the role of sediment transport in TP concentration dynamics. As described by Barcala et al. (2020) and Baken et al. (2015), iron and phosphorus from groundwater form iron(hydr)oxides which precipitate at the ditch bottom. During steady hydrological conditions, a P-rich sediment layer builds up. This sediment is transported during the next discharge event, causing a peak in both turbidity and TP. The data gaps in 2020-2021 coincided with the highest turbidity peaks and although it is likely, it is not possible to assess if there was an underestimation of TP peaks during this period. Furthermore, almost no high TP peaks were predicted with the 2019-2020 model when compared with the 2020-2021 measured series. Shen et al. (2020) observed that high values were underestimated when using Random Forest to predict N and P concentrations in streams. The high skewness of the data was offered as explanation. Surprisingly, the TP export increased in the last season (2020-2021) despite the negative P surplus. The groundwater level increased in importance in the 2020-2021 model. The risk of mobilization of phosphate (and heavy metals) with the introduction of water conservation has been proposed theoretically before (Rozemeijer & Griffioen, 2004; Schoumans & Groenendijk, 2000), but to the best of our knowledge it has not been directly measured yet. The topsoil had higher P and lower Al and Fe content, therefore watering the topsoil may have increased the risk of P leaching. In a recent data-based model of NO₃ leaching from agricultural soils across the Netherlands comparable trends were found (Spijker et al., 2021), the TP concentrations were inversely correlated with NO₃ emissions and TP was important for the prediction of NO₃ concentrations. They hypothesized that the high TP concentrations were a proxy for high groundwater levels (which were not included in that model), and that areas with high groundwater levels had higher denitrification rates and therefore lower NO₃ concentrations. In addition, Skidmore et al. (2022) has recently shown that extreme rain events increase the TP loads from agriculture.

Overall, Machine Learning can support process interpretation but justification of findings by other methods is needed, as the feature importance can be related to indirect links. Finally, turbidity was the variable that represented the largest information gain. Arriagada et al. (2021) and Fox et al. (2017) showed that Random Forest performance increased with the number of input variables used. Sensors are cheaper than autoanalyzers, require less maintenance and do not use reagents. The sensor data can then be trained to fill in data gaps in more complex equipment as TP autoanalyzers. This reason largely justify adding sensors (such as for turbidity, conductivity, dissolved oxygen, or temperature) next to autoanalyzers at high-frequency monitoring stations. Moreover, if a TP autoanalyzer is removed, the combination of continued cheap sensor measurements, low-frequency conventional TP sampling, and the previously trained RF model could still produce accurate continuous TP concentration time series for the site.

Using machine models for forecasting

The third objective of this study was to show the limits of Machine Learning algorithms for making predictions outside the training period. As reported by Tyralis & Papacharalampous (2019) the most important limitation to data-based models is that they should not be generalized to predict new processes or changes in unaccounted variables that were not covered by the training data set. Moreover, Kang et al. (2019), observed that interannual variations in nutrient loads are caused by year-to-year system changes for example in manure application, crop rotation, and cultivated area percentage, which were not fully captured by their Random Forest models. One disadvantage of Random Forest is that a small change in the data set, caused for example by different manure surpluses, can lead to a large change in the structure of the optimal decision tree. This effect can be seen in the changes in the variable feature importance between 2018-2019 and 2019-2020 seasons. Therefore, although for each season the all seasons model and the model of the season had similar R^2 , MAE and RMSE, the trees of each model were built splitting by different variables. This is one of the reasons why although the fitting was good for testing sets contained in the training period it did not show such a good predictive performance outside that period.

Despite both predictive models underperform the gap-filling results, the 2018-2019 model does a better job reproducing the 2019-2020 data than the 2020-2019 for the 2020-2021 data. Especially the NO_3 prediction with the 2019-2020 gives quite fair results. The relatively low N

surplus in 2020-2021 may explain the differences in NO₃ loads obtained with the predictive model. In the last season water retention measures were introduced and the nutrient N and P surpluses were lower, both changes were not directly introduced in the model as predictors but indirectly through the groundwater levels and the water quality data. Therefore, the groundwater level measurements were not enough to explain the system changes outside the training window. Nevertheless, the all seasons model performed very well for each of the individual seasons, including the 2020-2021 season. Random Forest can cover the system changes as long as they occur within the training period. The presented example shows that historical trends are no guarantee for future performance and that emerging processes may not be accurately predicted by the model. This highlights the need for cautious interpretations of Machine Learning model predictions and for keeping the models up to date using longer data sets to improve the robustness of the models.

It is important to notice that the issue regarding the uncertainty of predictions outside the training period is not likely to be caused by overfitting. Overfitting occurs when the performance of the model is good in the training set but not in the testing set. The training set was 60% of the data and it was randomly divided three times. The resulting Random Forest models were robust, with good results on all different validation sets and application periods. Moreover, we used a high-quality dataset with seven variables and about 18,000 instances in the last two seasons. For further studies we recommend evaluating ways to include low-frequency annual system changes in data-based models and quantifying the impact of the amount of missing data for the model performance.

3.6 Conclusions

- Random Forest was the best out of six Machine Learning algorithms to fill in missing data, with an R^2 higher than 0.92 for all test sets. Random Forest could effectively reproduce non-linear processes as concentration-discharge relationships and represent system changes that were considered in the training set.
- Machine Learning may support process interpretation, but justification of findings by other methods is needed. Accounting for changes in the groundwater levels was not enough to accurately predict system changes as the water conservation caused changes in the nutrient processes. After water conservation, higher groundwater levels resulted in more TP leaving the farm despite the negative P surplus and was represented by an increase of the relative feature importance of the groundwater level variable. This effect was likely related to higher desorption from the topsoil layers. For NO_3 , the variable feature importance values were caused by indirect links and were not directly related to processes.
- The incorporation of subsidiary sensors can pay-off in monitoring stations with more sensitive autoanalyzers. Here the turbidity showed the largest information gain in predictions.
- Random Forest predictions outside their training period can be uncertain. Keeping the Machine Learning models up to date with newly retrieved data increases the reliability of the predictions.
- Similar to gap-filling, Random Forest can be used for anomaly detection in monitoring stations.

3.7 Acknowledgments

We would like to acknowledge, the Farmer, Rhine and IJssel Water Board waterboard, Thilo Behrends and the P-TRAP group for the discussions. This project has received funding from the European Union's Horizon 2020 research and innovation program under the Marie Skłodowska-Curie grant agreement No 813438. The project is closely related to the activities of Vruchtbare Kringloop Achterhoek and Liemers (VKA), a partnership between LTO Noord, Water Board Rijn en IJssel, ForFarmers, Vitens, FrieslandCampina, Rabobank and the Province of Gelderland that focuses on circular agriculture and sustainable water and soil management.

3.8 Supplementary Material

The supplementary material includes the full data series, basic statistical exportation of the data series, model results including time calculations, plots of the modeled and measured data for 2017-2018 and 2018-2019 seasons, plots of the cumulative load for each season, scatter plots of measured vs modeled data with Random Forest for every season. The data series are available on <https://github.com/victoriabarcala/Huppel> .

3.9 References

- Aha, D., Kilbert, D., & Albert, M. (1991). Instance-based learning algorithms. *Machine Learning*, 6, 37–66.
- Arriagada, P., Karelavic, B., & Link, O. (2021). Automatic gap-filling of daily streamflow time series in data-scarce regions using a machine learning algorithm. *Journal of Hydrology*, 598(May), 126454. <https://doi.org/10.1016/j.jhydrol.2021.126454>
- Astuti, A. D., Aris, A., Salim, M. R., Azman, S., Salmiati, & Said, M. I. M. (2020). Artificial intelligence approach to predicting river water quality: A review. *Journal of Environmental Treatment Techniques*, 8(3), 1093–1100.
- Baken, S., Verbeeck, M., Verheyen, D., Diels, J., & Smolders, E. (2015). Phosphorus losses from agricultural land to natural waters are reduced by immobilization in iron-rich sediments of drainage ditches. *Water Research*, 71, 160–170. <https://doi.org/10.1016/j.watres.2015.01.008>
- Barcala, V., Rozemeijer, J., Osté, L., Van Der Grift, B., Gerner, L., & Behrends, T. (2020). Processes controlling the flux of legacy phosphorus to surface waters at the farm scale. *Environmental Research Letters*, 16(1). <https://doi.org/10.1088/1748-9326/abccd4>
- Bedi, S., Samal, A., Ray, C., & Snow, D. (2020). Comparative evaluation of machine learning models for groundwater quality assessment. In *Environmental Monitoring and Assessment* (Vol. 192, Issue 12). <https://doi.org/10.1007/s10661-020-08695-3>
- Bieroza, M., Bergström, L., Ulén, B., Djodjic, F., Tonderski, K., Heeb, A., Svensson, J., & Malgeryd, J. (2019). Hydrologic Extremes and Legacy Sources Can Override Efforts to Mitigate Nutrient and Sediment Losses at the Catchment Scale. *Journal of Environmental Quality*, 48(5), 1314–1324. <https://doi.org/10.2134/jeq2019.02.0063>
- Bol, R., Gruau, G., Mellander, P. E., Dupas, R., Bechmann, M., Skarbøvik, E., Bieroza, M., Djodjic, F., Glendell, M., Jordan, P., Van der Grift, B., Rode, M., Smolders, E., Verbeeck, M., Gu, S., Klumpp, E., Pohle, I., Fresne, M., & Gascuel-Oudou, C. (2018). Challenges of reducing phosphorus based water eutrophication in the agricultural landscapes of Northwest Europe. *Frontiers in Marine Science*, 5(AUG), 1–16. <https://doi.org/10.3389/fmars.2018.00276>
- Breiman, L. (2001). Random forests. *Machine Learning*, 45(1), 5–32. <https://doi.org/10.1023/A:1010933404324>
- Castrillo, M., & García, Á. L. (2020). Estimation of high frequency nutrient concentrations from water quality surrogates using machine learning methods. *Water Research*, 172. <https://doi.org/10.1016/j.watres.2020.115490>
- Chen, K., Chen, H., Zhou, C., Huang, Y., Qi, X., Shen, R., Liu, F., Zuo, M., Zou, X., Wang, J., Zhang, Y., Chen, D., Chen, X., Deng, Y., & Ren, H. (2020). Comparative analysis of surface water quality prediction performance and identification of key water parameters using different machine learning models based on big data. *Water Research*, 171, 115454. <https://doi.org/10.1016/j.watres.2019.115454>
- Daliakopoulos, I. N., & Ioannis, K. T. (2016). Comparison of an artificial neural network and a conceptual

- rainfall–runoff model in the simulation. *Hydrological Sciece Journal*, *61*, 2763–2774. <https://doi.org/https://doi.org/10.1080/02626667.2016.1154151>
- Dastorani, M., Moghadamnia, A., Piri, J., & Rico-Ramirez, M. (2010). Application of ANN and ANFIS models for reconstrcuting missing flow data. *Environmental Monitoring and Assessment*, *166*, 421–434.
- Dise, N. B., Ashmore, M., Belyazid, S., Bleeker, A., Bobbink, R., Vries, W. De, Erisman, J. W., Spranger, T., Stevens, C. J., & Berg, L. Van Den. (2011). Nitrogen deposition as a threat to European Terrestrial Biodiversity. In *The European Nitrogen Assessment* (Issue 2011). Cambridge University Press.
- Doshi-Velez, F., & Kim, B. (2017). Towards A Rigorous Science of Interpretable Machine Learning. *ArXiv Preprint ArXiv:1702.08608*, *ML*, 1–13.
- Dupas, R., Tavenard, R., Fovet, O., Gilliet, N., Grimaldi, C. and, & Gascuel-Odoux, C. (2015). Identifying seasonal patterns of phosphorus storm dynamics with dynamic time warping. *Water Resources Research*, *51*, 8868–8882. <https://doi.org/10.1002/2015WR017338>. Received
- Fox, E. W., Hill, R. A., Leibowitz, S. ., & Weber, M. H. (2017). Assessing the accuracy and stability of variable selection methods for random forest modeling in ecology. *Environ Monit Assess*, *316*(189). <https://doi.org/https://doi.org/10.1007/s10661-017-6025-0>
- Frank, E., Hall, M. A., & Witten, I. H. (2017). The WEKA workbench. *Data Mining*, 553–571. <https://doi.org/10.1016/b978-0-12-804291-5.00024-6>
- Greve, P., Brunner, L., Weiland, F. C. S., Visser, R. D., Greve, P., & Bisselink, B. (2021). *Estimating Regionalized Hydrological Impacts of Climate Change Over Europe by Performance-Based Weighting of CORDEX Projections*. *Estimating Regionalized Hydrological Impacts of Climate Change Over Europe by Performance-Based Weighting of CORDEX Projections*. November. <https://doi.org/10.3389/frwa.2021.713537>
- Ha, N. T., Nguyen, H. Q., Truong, N. C. Q., Le, T. L., Thai, V. N., & Pham, T. L. (2020). Estimation of nitrogen and phosphorus concentrations from water quality surrogates using machine learning in the Tri An Reservoir, Vietnam. In *Environmental Monitoring and Assessment* (Vol. 192, Issue 12). <https://doi.org/10.1007/s10661-020-08731-2>
- Jones, A. S., Jones, T. L., Logan, N., & Horsburgh, J. S. (2021). *Toward automating post processing of aquatic sensor data*. *435*, 1–63.
- Kang, M., Ichii, K., Kim, J., Indrawati, Y. M., Park, J., Moon, M., Lim, J. H., & Chun, J. H. (2019). New gap-filling strategies for long-period flux data gaps using a data-driven approach. *Atmosphere*, *10*(10), 1–18. <https://doi.org/10.3390/atmos10100568>
- Kim, Y., Johnson, M. S., Knox, S. H., Black, T. A., Dalmagro, H. J., Kang, M., Kim, J., & Baldocchi, D. (2020). Gap-filling approaches for eddy covariance methane fluxes: A comparison of three machine learning algorithms and a traditional method with principal component analysis. *Global Change Biology*, *26*(3), 1499–1518. <https://doi.org/10.1111/gcb.14845>
- Kirchner, J. W., & Neal, C. (2013). Universal fractal scaling in stream chemistry and its implications for solute transport and water quality trend detection. *PNAS*, *110*(30).

<https://doi.org/10.1073/pnas.1304328110>

- Leman, M. (1997). Lecture notes in artificial intelligence. In *Lecture Notes in Computer Science (including subseries Lecture Notes in Artificial Intelligence and Lecture Notes in Bioinformatics)* (Vol. 1317).
- Liu, X., Lu, D., Zhang, A., Liu, Q., & Jiang, G. (2022a). Data-Driven Machine Learning in Environmental Pollution: Gains and Problems. *Environmental Science & Technology*. <https://doi.org/10.1021/acs.est.1c06157>
- Liu, X., Lu, D., Zhang, A., Liu, Q., & Jiang, G. (2022b). Data-Driven Machine Learning in Environmental Pollution: Gains and Problems. *Environmental Science & Technology*, *56*(4), 2124–2133. <https://doi.org/10.1021/acs.est.1c06157>
- Lucas, E. R., Toor, G. S., & Mcgrath, J. M. (2021). Agronomic and environmental phosphorus decline in coastal plain soils after cessation of manure application. *Agriculture, Ecosystems and Environment*, *311*(January), 107337. <https://doi.org/10.1016/j.agee.2021.107337>
- Mao, H., Kathuria, D., Duffield, N., & Mohanty, B. P. (2019). Gap Filling of High-Resolution Soil Moisture for SMAP / Sentinel-1 : A Two-Layer Machine Learning-Based Framework. *Water Resources Research*, *1*, 6986–7009. <https://doi.org/10.1029/2019WR024902>
- Masson-Delmotte, V., Zhai, P., Pirani, A., Connors, S. L., Péan, C., Berger, S., Caud, N., Chen, Y., Goldfarb, L., Gomis, M. I., Huang, M., Leitzell, K., Lonnoy, E., Matthews, J. B. R., Maycock, T. K., Waterfield, T., Yelekçi, O., Yu, R. A., & Zhou, B. (2021). *IPCC, 2021: Climate Change 2021: The Physical Science Basis. Contribution of Working Group I to the Sixth Assessment Report of the Intergovernmental Panel on Climate Change*. <https://www.ipcc.ch/report/ar6/wg1/>
- Najah, A., El-Shafie, A., Karim, O. A., & El-Shafie, A. H. (2013). Application of artificial neural networks for water quality prediction. *Neural Comput Applic*, *22*(1), 187–201. <https://doi.org/10.1007/s00521-012-0940-3>
- Najah, A., Elshafie, A., Karim, O. A., & Jaffar, O. (2009). Prediction of Johor River Water Quality Parameters Using Artificial Neural Networks. *European Journal of Scientific Research*, *28*(3), 422–435.
- Olson, J. R., & Hawkins, C. P. (2012). Predicting natural base-flow stream water chemistry in the western United States. *Water Resources Research*, *48*(2), 1–19. <https://doi.org/10.1029/2011WR011088>
- Platt, J. . (2008). Fast training Support Vector Machines using parallel Sequential Minimal Optimization. *Proceedings of 2008 3rd International Conference on Intelligent System and Knowledge Engineering, ISKE 2008*, 997–1001. <https://doi.org/10.1109/ISKE.2008.4731075>
- Porter, E. M., Bowman, W. D., Clark, C. M., Compton, J. E., Pardo, L. H., & Soong, J. L. (2013). Interactive effects of anthropogenic nitrogen enrichment and climate change on terrestrial and aquatic biodiversity. *Biogeochemistry*, 93–120. <https://doi.org/10.1007/s10533-012-9803-3>
- Qiao, Z., Sun, S., Jiang, Q., Xiao, L., Wang, Y., & Yan, H. (2021). Retrieval of total phosphorus concentration in the surface water of miyun reservoir based on remote sensing data and machine learning algorithms. *Remote Sensing*, *13*(22). <https://doi.org/10.3390/rs13224662>
- R Core Team. (2020). *R: A language and environment for statistical computing* (4.0.5). R Foundation for

Statistical Computing.

- Rode, M., Wade, A. J., Cohen, M. J., Hensley, R. T., Bowes, M. J., Kirchner, J. W., Arhonditsis, G. B., Jordan, P., Kronvang, B., Halliday, S. J., Skeffington, R. A., Rozemeijer, J. C., Aubert, A. H., Rinke, K., & Jomaa, S. (2016). Sensors in the Stream: The High-Frequency Wave of the Present. *Environmental Science and Technology*, 50(19), 10297–10307. <https://doi.org/10.1021/acs.est.6b02155>
- Rozemeijer, J. C., & Broers, H. P. (2007). The groundwater contribution to surface water contamination in a region with intensive agricultural land use (Noord-Brabant, The Netherlands). *Environmental Pollution*, 148(3), 695–706. <https://doi.org/10.1016/j.envpol.2007.01.028>
- Rozemeijer, J., & Griffioen, J. (2004). Effecten van waterconservering op de waterkwaliteit in Noord-Brabant en Limburg. *H2O*, 20, 30–33.
- Rozemeijer, J., Van der Velde, Y., De Jonge, H., Van Geer, F., Broers, H. P., & Bierkens, M. (2010). Application and evaluation of a new passive sampler for measuring average solute concentrations in a catchment scale water quality monitoring study. *Environmental Science and Technology*, 44(4), 1353–1359. <https://doi.org/10.1021/es903068h>
- Rozemeijer, J. C., & Van der Velde, Y. (2014). Temporal variability in groundwater and surface water quality in humid agricultural catchments; Driving processes and consequences for regional water quality monitoring. *Fundamental and Applied Limnology*, 184(3), 195–209. <https://doi.org/10.1127/1863-9135/2014/0565>
- Rozemeijer, Joachim C., Van der Velde, Y., Van Geer, F. C., De Rooij, G. H., Torfs, P. J. J. F., & Broers, H. P. (2010). Improving load estimates for NO₃ and P in surface waters by characterizing the concentration response to rainfall events. *Environmental Science and Technology*, 44(16), 6305–6312. <https://doi.org/10.1021/es101252e>
- Schoumans, O. F., Chardon, W. J., Bechmann, M. E., Gascuel-Oudou, C., Hofman, G., Kronvang, B., Rubæk, G. H., Ulén, B., & Dorioz, J. M. (2014). Mitigation options to reduce phosphorus losses from the agricultural sector and improve surface water quality: A review. *Science of the Total Environment*, 468–469, 1255–1266. <https://doi.org/10.1016/j.scitotenv.2013.08.061>
- Schoumans, O. F., & Groenendijk, P. (2000). Modeling Soil Phosphorus Levels and Phosphorus Leaching from Agricultural Land in the Netherlands. *Journal of Environmental Quality*, 29(1), 111–116. <https://doi.org/10.2134/jeq2000.00472425002900010014x>
- Schroder, J. J., Aarts, H. F. M., Middelkoop, J. C. Van, Schils, R. L. M., Velthof, G. L., Fraters, B., & Willems, W. J. (2007). Permissible manure and fertilizer use in dairy farming systems on sandy soils in The Netherlands to comply with the Nitrates Directive target. *European Journal of Agronomy*, 27, 102–114. <https://doi.org/10.1016/j.eja.2007.02.008>
- Shah, A. D., Bartlett, J. W., Carpenter, J., Nicholas, O., & Hemingway, H. (2014). Comparison of random forest and parametric imputation models for imputing missing data using MICE: A CALIBER study. *American Journal of Epidemiology*, 179(6), 764–774. <https://doi.org/10.1093/aje/kwt312>
- Sharpley, A., Jarvie, H. P., Buda, A., May, L., Spears, B., & Kleinman, P. (2013). Phosphorus Legacy:

- Overcoming the Effects of Past Management Practices to Mitigate Future Water Quality Impairment. *Journal of Environmental Quality*, 42(5), 1308–1326. <https://doi.org/10.2134/jeq2013.03.0098>
- Shen, L. Q., Amatulli, G., Sethi, T., Raymond, P., & Domisch, S. (2020). Estimating nitrogen and phosphorus concentrations in streams and rivers, within a machine learning framework. In *Scientific Data* (Vol. 7, Issue 1). <https://doi.org/10.1038/s41597-020-0478-7>
- Skidmore, M., Andarge, T., & Foltz, J. (2022). Climate change and water pollution: the impact of extreme rain on nutrient runoff in Wisconsin. *Agricultural and Applied Economics Association*. <https://doi.org/10.22004/ag.econ.322113>
- Spijker, J., Fraters, D., & Vrijhoef, A. (2021). A machine learning based modelling framework to predict nitrate leaching from agricultural soils across the Netherlands. *Environmental Research Communications*, 3.
- Tyralis, H., & Papacharalampous, G. (2017). Variable selection in time series forecasting using random forests. *Algorithms*, 10(4). <https://doi.org/10.3390/a10040114>
- Tyralis, H., & Papacharalampous, G. (2019). A Brief Review of Random Forests for Water Scientists and Practitioners and Their Recent History. *Water*.
- Van der Grift, B., Broers, H. P., Berendrecht, W. L., Rozemeijer, J. C., Osté, L. A., & Griffioen, J. (2016). High-frequency monitoring reveals nutrient sources and transport processes in an agriculture-dominated lowland water system. *Hydrology and Earth System Sciences Discussions*, 12(8), 8337–8380. <https://doi.org/10.5194/hessd-12-8337-2015>
- Van der Salm, C., Van den Toorn, A., Chardon, W. J., & Koopmans, G. F. (2012). Water and nutrient transport on a heavy clay soil in a fluvial plain in the Netherlands. *Journal of Environment Quality*, 41, 229–241.
- Visser, H., Evers, N., Bontsema, A., Rost, J., Niet, A. De, Vethman, P., Mylius, S., Linden, A. Van Der, Roovaart, J. Van Den, & Gaalen, F. Van. (2022). What drives the ecological quality of surface waters ? A review of 11 predictive modeling tools. *Water Research*, 208, 117851. <https://doi.org/10.1016/j.watres.2021.117851>
- Withers, P. J.A., & Haygarth, P. M. (2007). Agriculture, phosphorus and eutrophication: A European perspective. *Soil Use and Management*, 23(SUPPL. 1), 1–4. <https://doi.org/10.1111/j.1475-2743.2007.00116.x>
- Withers, Paul J.A., Neal, C., Jarvie, H. P., & Doody, D. G. (2014). Agriculture and eutrophication: Where do we go from here? *Sustainability (Switzerland)*, 6(9), 5853–5875. <https://doi.org/10.3390/su6095853>
- Wolpert, D. H. (1992). Stacked generalization. *Neural Networks*, 5(2), 241–259.
- Zhang, Y. F., Thorburn, P. J., Xiang, W., & Fitch, P. (2019). SSIM - A Deep Learning Approach for Recovering Missing Time Series Sensor Data. *IEEE Internet of Things Journal*, 6(4), 6618–6628. <https://doi.org/10.1109/JIOT.2019.2909038>

Zhang, Y., & Thorburn, P. J. (2022). Handling missing data in near real-time environmental monitoring: A system and a review of selected methods. *Future Generation Computer Systems*, 128, 63–72.
<https://doi.org/10.1016/j.future.2021.09.033>

3.10 Supplementary material to Chapter 3: Value and limitations of Machine Learning in high-frequency nutrient data for gap-filling, forecasting, and transport process interpretation

Victoria Barcala^{1,4}, Joachim Rozemeijer², Leonard Osté¹, Kevin Ouwerkerk², Laurens Gerner³

1 Inland Water Systems, Deltares, Daltonlaan 600, 3584 BK, Utrecht, The Netherlands

2 Deltares, Unit Subsurface and Groundwater Systems, Daltonlaan 600, 3584 BK, Utrecht, The Netherlands

3 Water Board Rijn and IJssel, Doetinchem, the Netherlands

4 Department of Earth Sciences, Faculty of Geosciences, Utrecht University, the Netherlands

The supplementary material includes: high-frequency datasets per season with measured TP and NO₃ with data gaps, statistical summary data for all seasons, correlation coefficients of the measured data series in the four drainage seasons, results of the different NO₃ and TP models with values of R², MAE, and RMSE, and computation times, 2017-2018 and 2018-2019 datasets with measured and modeled TP and NO₃, and the cumulative NO₃ and TP in the 2020-2021 drainage season.

Full high-frequency datasets per season with measured TP and NO₃ with data gaps

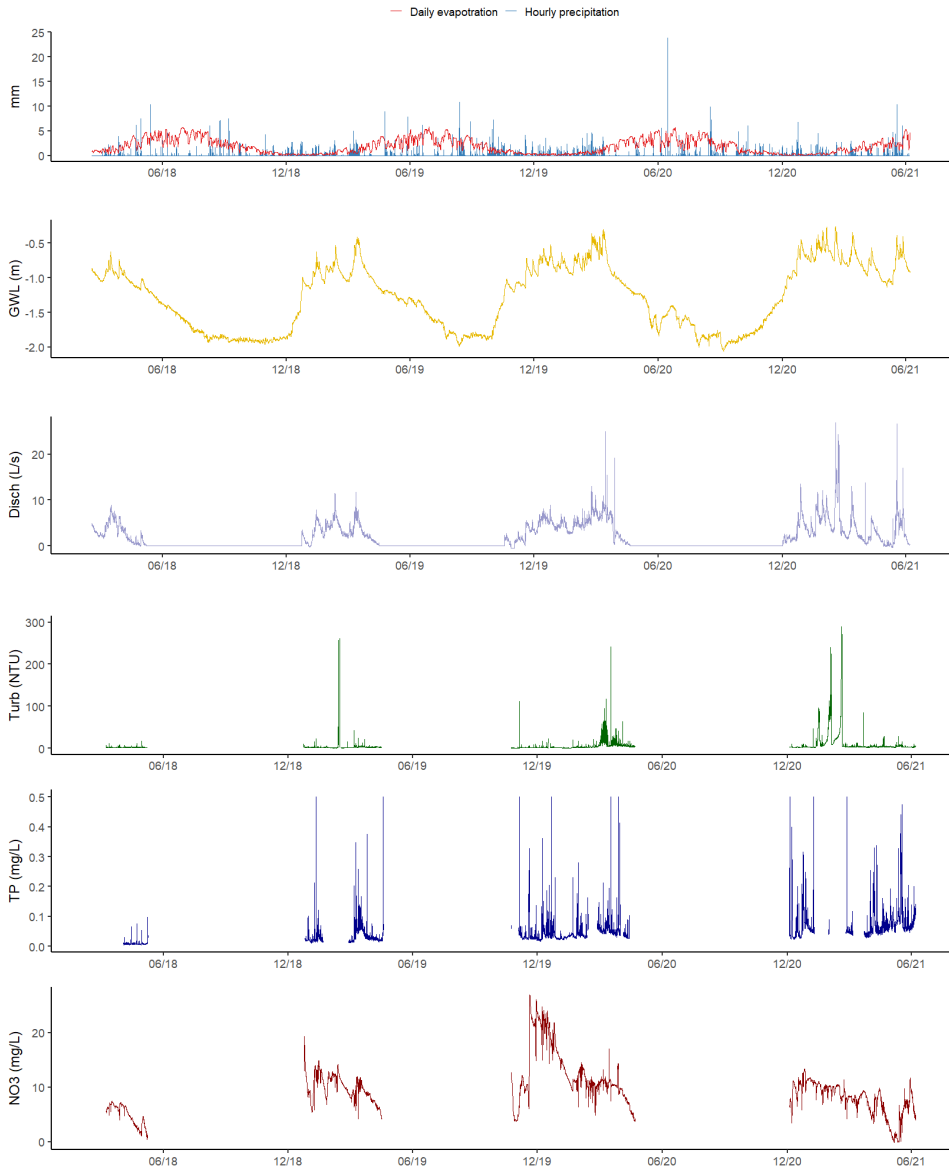


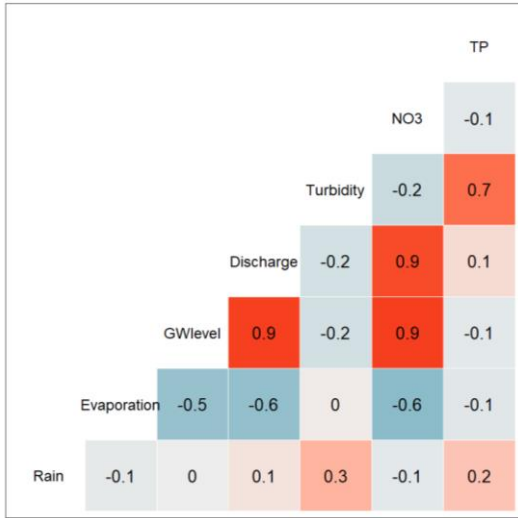
Figure S1 Measured time series with gaps in the data

Table S1 Statistical summary of the groundwater, turbidity, NO₃, and TP data for all seasons

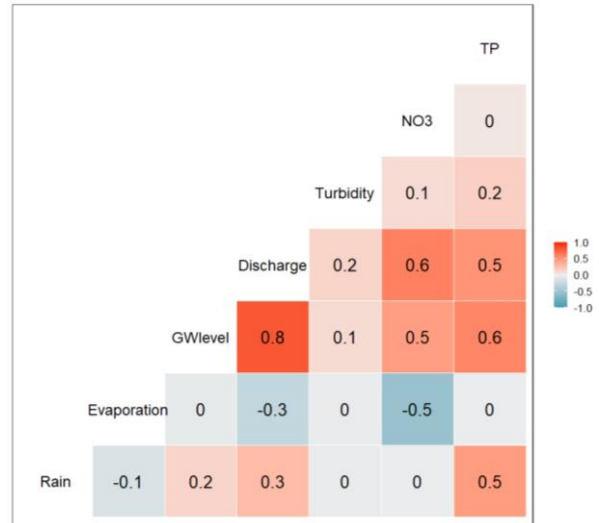
		All seasons	2017-2018	2018-2019	2019-2020	2020-2021
Groundwater level (m)	Min*	-1.34	-1.18	-1.20	-1.24	-1.34
	1Q	-1.18	-1.06	-1.04	-1.04	-0.907
	Median	-1.23	-0.994	-0.935	-0.854	-0.754
	Mean	-1.28	-0.989	-0.916	-0.858	-0.769
	3Q	-0.898	-0.917	-0.838	-0.726	-0.630
	95 perc	-0.261	-0.630	-0.417	-0.301	-0.261
Turbidity (NTU)	Min	0.21	0.93	0.21	0.40	1.04
	1Q	1.51	1.47	1.30	1.04	2.78
	Median	2.59	1.82	2.03	2.19	3.51
	Mean	9.40	2.06	14.1	4.89	13.4
	3Q	4.15	2.29	2.88	4.84	5.50
	95 perc	23.1	7.12	5.26	19.4	52.4
NO₃ (mg/L)	Min	0.10	0.601	3.98	3.73	0.10
	1Q	6.81	3.23	8.46	9.73	6.29
	Median	9.32	5.57	9.78	11.1	8.23
	Mean	9.52	4.91	9.97	12.7	7.77
	3Q	11.18	6.49	11.7	15.0	10.1
	95 perc	20.81	3.46	13.63	23.0	11.37
TP (mg/L)	Min	0.005	0.005	0.007	0.016	0.023
	1Q	0.030	0.008	0.020	0.029	0.047
	Median	0.040	0.005	0.026	0.036	0.059
	Mean	0.050	0.010	0.035	0.045	0.077
	3Q	0.060	0.010	0.038	0.050	0.084
	95 perc	0.120	0.017	0.077	0.091	0.182

***Below this level there was no water flow discharge**

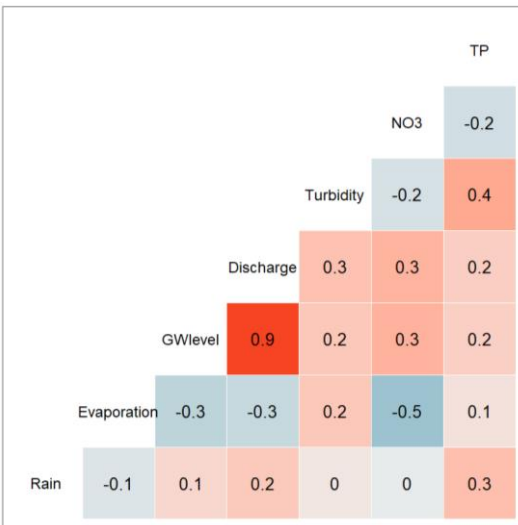
2017-2018 season correlation matrix



2018-2019 season correlation matrix



2019-2020 season correlation matrix



2020-2021 season correlation matrix

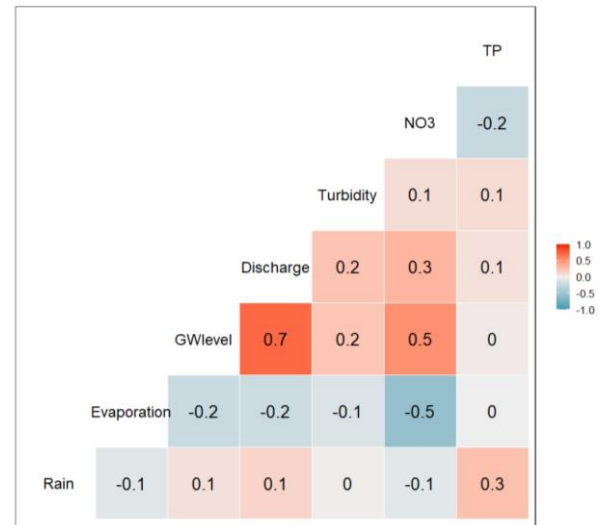


Figure S2 Matrix with the correlation coefficients of the measured data series in the four drainage seasons

Table S2 Results of the different NO₃ models, showing R², MAE, RMSE, and computation times

		All seasons (2017-2021)	2017-2018	2018-2019	2019-2020	2020-2021	
NO ₃	Random Forest*	R ²	0.996/0.995/0.995	0.998/0.998/0.998	0.998/0.998/0.998	0.995/0.994/0.994	0.998/.998/0.998
		MAE	0.112/0.113/0.113	0.027/0.026/0.027	0.043/0.040/0.041	0.134/0.140/0.148	0.046/0.047/0.047
		RMSE	0.311/0.322/0.328	0.039/0.036/0.040	0.086/0.074/0.086	0.375/0.357/0.415	0.077/0.080/0.080
		Time(s)	118/102/100	0.52/0.54/0.48	5.45/6.10/5.66	22/22/22	21/23/22
	K-Nearest Neighbor	R ²	0.735/0.735/0.721	0.737/0.753/0.712	0.998/0.998/0.998	0.821/0.812/0.812	0.846/0.848/0.846
		MAE	1.21/1.20/1.23	0.638/0.615/0.709	0.018/0.017/0.017	0.900/0.925/0.926	0.567/0.565/0.561
		RMSE	2.71/2.72/2.79	1.14/1.11/1.22	0.049/0.046/0.049	2.37/2.42/2.42	1.20/1.199/1.197
		Time(s)	4151/2458/2161	8.38/7.52/8.33	6.69/6.18/6.81	84/73/97	128/103/93
	Multivariable Linear Regression	R ²	0.941/0.877/0.968	0.996/0.996/0.996	0.988/0.984/0.984	0.964/0.964/0.924	0.988/0.982/0.980
		MAE	0.454/0.503/0.368	0.071/0.074/0.070	0.158/0.156/0.156	0.471/0.471/0.503	0.179/0.193/0.166
		RMSE	1.13/1.66/0.826	0.109/0.116/0.104	0.270/0.298/0.298	1.02/1.02/1.49	0.328/0.389/0.418
		Time(s)	1494/1361/2143	12.97/14.09/12.03	34/26/30	137/124/119	282/258/287
	Sequential minimal optimization	R ²	0.389/0.386/0.388	0.974/0.843/0.841	0.612/0.621/0.621	0.322/0.329/0.327	0.522/0.518/0.519
		MAE	2.48/2.49/2.48	0.583/0.585/0.590	1.10/1.11/1.10	3.59/3.55/3.57	1.54/1.55/1.55
		RMSE	3.58/3.58/3.58	0.731/0.736/0.740	1.48/1.46/1.46	4.41/4.36/4.38	2.00/2.02/2.02
		Time(s)	0.3/0.5/0.3	0.04/0.03/0.03	0.03/0.03/0.02	0.06/0.07/0.06	0.06/0.06/0.06
	Zero Rules	R ²	0.386/0.379/0.384	0.838/0.848/0.848	0.604/0.615/0.612	0.293/0.300/0.300	0.497/0.497/0.493
		MAE	2.39/2.40/2.40	0.565/0.572/0.572	1.0885/1.0902/1.0843	3.2899/3.2433/3.253	1.4976/1.4976/1.5094
		RMSE	3.6367/3.6376/3.6362	0.768/0.783/0.783	1.49/1.47/1.48	4.78/4.72/4.73	2.06/2.06/2.08
		Time(s)	154983/166755/173023	1320/1479/1728	1834/2020/1880	15876/19126/20921	18976/14022/18456
Artificial Neural Networks	R ²	0/0/0	0/0/0	0/0/0	0/0/0	0/0/0	
	MAE	3.25/3.24/3.25	1.64/1.65/1.64	1.92/1.94/1.93	4.25/4.24/4.24	2.25/2.27/2.26	
	RMSE	4.58/4.57/4.58	1.85/1.86/1.86	2.37/2.38/2.37	5.36/5.33/5.34	2.89/2.92/2.91	
	Time(s)	0.2/0.3/0.2	0.01/0.01/0.01	0.01/0.01/0.01	0.01/0.01/0.01	0.01/0.01/0.01	
Artificial Neural Networks	R ²	0.663/0.667/0.669	0.978/0.980/0.980	0.880/0.882/0.880	0.672/0.664/0.664	0.870/0.863/0.863	
	MAE	1.87/2.28/2.28	0.205/0.201/0.201	0.603/0.879/0.603	2.16/2.10/2.10	0.896/0.812/0.812	
	RMSE	2.87/2.96/2.96	0.285/0.269/0.269	0.857/1.12/0.857	3.08/3.10/3.10	1.16/1.08/1.08	
	Time (s)	97/103/111	10/11/12	16/12/12	37/32/29	42/37/48	

Table S3 Results of the different TP models, showing R², MAE, RMSE, and computation times

		All seasons (2017-2021)	2017-2018	2018-2019	2019-2020	2020-2021	
TP	Random Forest*	R ²	0.963/0.958/0.958	0.960/0.975/0.969	0.934/0.934/0.934	0.927/0.917/0.917	0.972/0.967/0.967
		MAE	0.002/0.003/0.003	0.001/0.001/0.001	0.002/0.002/0.002	0.002/0.002/0.002	0.003/0.003/0.003
		RMSE	0.010/0.010/0.010	0.001/0.001/0.001	0.007/0.007/0.007	0.010/0.010/0.010	0.010/0.011/0.011
		Time(s)	134/112/131	3.13/3.04/3.05	11.3/7.4/8.9	23/22/25	21/15/15
	K-Nearest Neighbor	R ²	0.836/0.817/0.877	0.946/0.966/0.962	0.874/0.941/0.876	0.589/0.532/0.584	0.945/0.958/0.948
		MAE	0.002/0.003/0.002	0.001/0.001/0.001	0.001/0.001/0.001	0.004/0.005/0.004	0.002/0.002/0.002
		RMSE	0.020/0.021/0.017	0.002/0.001/0.001	0.011/0.007/0.010	0.028/0.032/0.027	0.014/0.012/0.014
		Time(s)	1598/1455/1590	1.92/1.90/1.77	11.3/6.5/6.4	56/51/49	31/32/37
	M5 rules	R ²	0.808/0.815/0.815	0.901/0.858/0.858	0.798/0.798/0.799	0.561/0.701/0.701	0.828/0.880/0.880
		MAE	0.008/0.008/0.008	0.001/0.001/0.001	0.005/0.005/0.005	0.01/0.007/0.007	0.010/0.009/0.009
		RMSE	0.021/0.020/0.020	0.002/0.002/0.002	0.013/0.013/0.012	0.024/0.019/0.019	0.025/0.021/0.021
		Time(s)	1351/1151/1047	22/20/24	62/61/56	125/111/80	171/196/157
	Multivariate Linear Regression	R ²	0.211/0.199/0.213	0.548/0.529/0.524	0.523/0.542/0.534	0.212/0.23/0.219	0.158/0.168/0.163
		MAE	0.023/0.023/0.023	0.002/0.002/0.002	0.010/0.010/0.010	0.015/0.015/0.015	0.032/0.033/0.032
		RMSE	0.041/0.042/0.042	0.004/0.005/0.004	0.020/0.019/0.019	0.031/0.031/0.030	0.053/0.055/0.054
		Time(s)	1.6/0.5/0.5	0.01/0.01/0.01	0.05/0.06/0.06	0.06/0.05/0.06	0.06/0.04/0.04
	Sequential minimal optimization regression	R ²	0.190/0.180/0.193	0.533/0.514/0.503	0.237/0.246/0.246	0.156/0.170/0.171	0.123/0.120/0.112
		MAE	0.020/0.020/0.020	0.002/0.002/0.002	0.009/0.008/0.008	0.013/0.013/0.012	0.028/0.028/0.028
		RMSE	0.042/0.043/0.043	0.005/0.005/0.004	0.030/0.029/0.030	0.033/0.034/0.032	0.056/0.058/0.059
		Time(s)	60008/55637/51993	191/210/207	1098/1019/1018	7193/7126/4746	3559/5722/6457
Zero Rules	R ²	0/0/0	0/0/0	0/0/0	0/0/0	0/0/0	
	MAE	0.027/0.028/0.028	0.003/0.003/0.003	0.018/0.017/0.017	0.018/0.018/0.018	0.035/0.036/0.036	
	RMSE	0.046/0.047/0.047	0.007/0.007/0.006	0.029/0.027/0.028	0.035/0.036/0.034	0.058/0.060/0.060	
	Time(s)	0.8/0.6/1.5	0/0/0	0/0/0	0/0/0	0/0/0	
Artificial Neural Networks	R ²	0.489/0.534/0.534	0.753/0.516/0.516	0.702/0.699/0.724	0.438/0.524/0.524	0.510/0.557/0.557	
	MAE	0.018/0.016/0.016	0.002/0.002/0.002	0.020/0.008/0.010	0.0124/0.0111/0.0111	0.0236/0.022/0.0226	
	RMSE	0.034/0.033/0.033	0.003/0.004/0.004	0.024/0.015/0.016	0.029/0.024/0.024	0.044/0.040/0.040	
	Time(s)	70/68/75	8/7/9	12/12/12	35/28/30	22/23/26	

* the RF times include computing the variable importance

Seasonal loads vs time

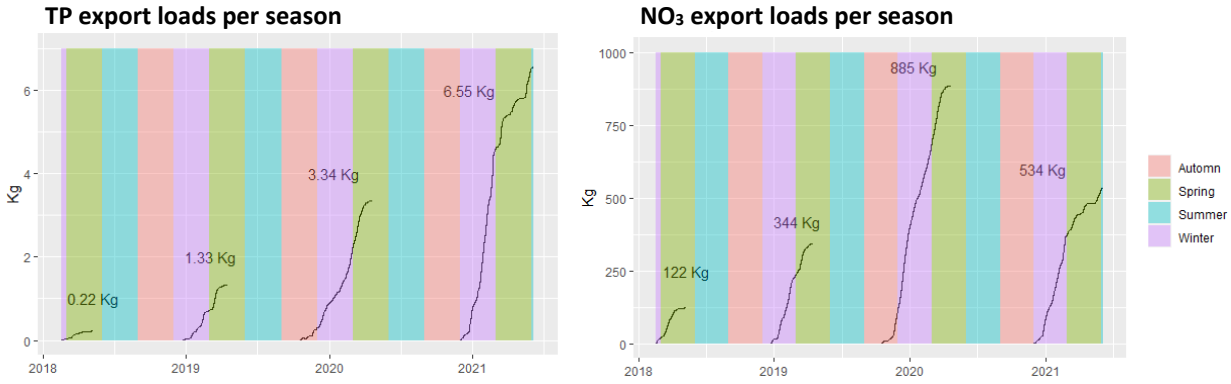


Figure S3 Cumulative NO₃ and TP in the 2020-2021 drainage season: measured and modeled with Random Forest

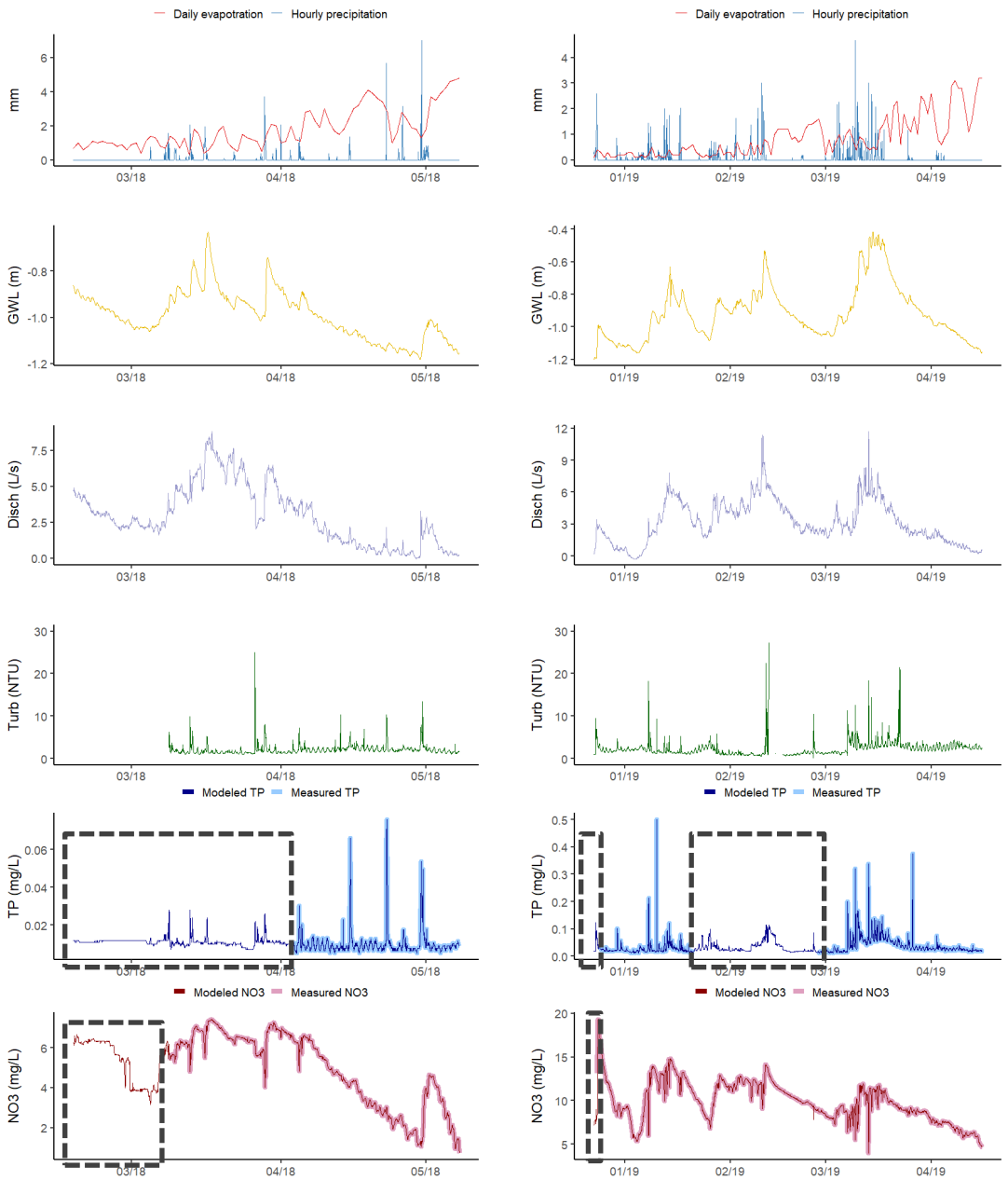


Figure S4 2017-2018 and 2018-2019 datasets with measured and modeled TP and NO3. The dash boxes show data gaps.



Chapter

4

4 Chapter 4: Phosphorus adsorption on iron-coated sand under reducing conditions

Victoria Barcala^{1,2}, Stefan Jansen³, Jan Gerritse³, Stefan Mangold⁴, Andreas Voegelin⁵, and Thilo Behrends²

1 Inland Water Systems, Deltares, Utrecht, The Netherlands

2 Department of Earth Sciences, Faculty of Geosciences, Utrecht University, Utrecht, The Netherlands

3 Subsurface and Groundwater Systems, Deltares, Utrecht, The Netherlands

4 Karlsruhe Institute of Technology, Institute for Photon Science and Synchrotron Radiation, D-76344 Eggenstein-Leopoldshafen, Germany

5 Eawag, Swiss Federal Institute of Aquatic Science and Technology, Ueberlandstrasse 133, CH-8600 Duebendorf, Switzerland

Published in the Journal of Environmental Quality <https://doi.org/10.1002/jeq2.20432>

4.1 Abstract

Mitigation measures are needed to prevent large loads of phosphate originating in agriculture from reaching surface waters. Iron-coated sand (ICS) is a residual product from drinking water production. ICS has a high phosphate adsorption capacity and can be placed around tile drains taking no extra space which increases the farmers' acceptance. The main concern regarding the use of ICS filters below groundwater level is that limited oxygen supply and high organic matter concentrations may lead to the reduction and dissolution of iron (hydr)oxides present and the release of previously adsorbed phosphate. This study aimed to investigate phosphate adsorption on ICS at the onset of iron reduction. First, it was investigated whether simultaneous metal reduction and phosphate adsorption were relevant at two field sites in the Netherlands that use ICS filters around tile drains. Second, the onset of microbially mediated reduction of ICS in drainage water was mimicked in complementary laboratory microcosm experiments by varying the intensity of reduction through controlling the oxygen availability and the concentration of degradable organic matter. After 3 years, ICS filters in the field removed phosphorus under low redox conditions. Over 45 days, the microbial

reduction of manganese and iron oxides did not lead to phosphate release confirming field observations. Electron microscopy and X-ray absorption spectroscopy did not evince systematic structural or compositional changes, only under strongly reducing conditions did iron sulfides formed in small percentages in the outer layer of the iron coating. Our results suggest that detrimental effects only become relevant after long operation periods.

Keywords: phosphorus, iron-coated sand, microbial redox reactions, drainage systems, nutrient retention

Abbreviations: Ca, calcium; CH₄, methane; CO₂, carbon dioxide gas; DOC, dissolved organic carbon; EXAFS, extended X-ray absorption fine structure; Fe, iron; FeS, iron sulfide; IC, ion chromatography; ICP-OES, inductively coupled plasma - optical emission spectrometry; ICS, iron-coated sand; Mn, manganese; N₂, nitrogen gas; NH₄, ammonia; NO₃, nitrate; ORP, oxidation reduction potential (mV); P, phosphorus; PO₄, phosphate; SEM-EDX, scanning electron microscope with energy dispersive x-ray spectroscopy; SO₄, sulfate; TDP, total dissolved phosphorus; XAS, x-ray absorption spectroscopy.

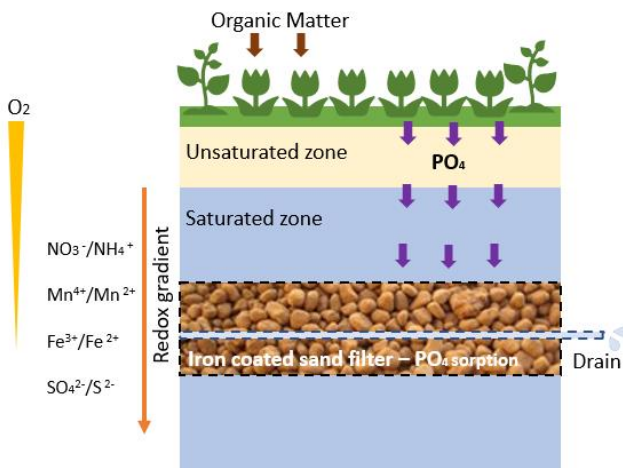


Figure 4-0. Graphical Abstract

4.2 Introduction

Phosphorus (P) is an essential nutrient for plant growth, required to increase the food available for the growing world population. However, P run-off and leaching from agriculture can trigger algae blooms, eutrophication, and water quality problems (Bol et al., 2018; Withers & Haygarth, 2007). Due to the legacy of P in the soil, reducing the fertilizer application may be insufficient to reduce the P load to surface waters in the short- to mid-term (Barcala et al., 2020; Chardon & Schoumans, 2007; Mellander et al., 2016; Sharpley et al., 2013). To achieve a faster decrease in the P levels in surface waters we need mitigation measures that reduce the diffuse P inputs from arable fields (Mendes, 2020; Penn et al., 2017; Schoumans et al., 2014). These mitigation measures should be cost-efficient and make no or little use of valuable arable land to be readily accepted by farmers. Iron-coated sand (ICS) is a phosphate (PO_4) adsorbing material, which is readily available as a by-product of drinking water production (Chardon et al., 2012; Sharma et al., 2002; Van Beek et al., 2020) and can be placed around tile drains or in edge-of-field filters to remove PO_4 taking no extra space (Chardon et al., 2021; Groenenberg et al., 2013; Lambert et al., 2020; Vandermoere et al., 2018). The iron (Fe) in the ICS coating is formed around sand particles at the top of rapid sand filters when they remove the suspended Fe (hydr)oxides that are formed upon the aeration of anoxic Fe (II)-containing groundwater or after the addition of Fe salts to remove organic matter. ICS combines favorable adsorption properties with a high hydraulic conductivity. These properties together with its abundant availability at a low cost make ICS a suitable material for large-scale PO_4 removing filters (Chardon et al., 2012; Vandermoere et al., 2018).

The major concern about the use of ICS filters below groundwater level is that the reductive dissolution or the reductive transformation of Fe (hydr)oxides over time may eventually lead to the release of previously retained PO_4 . When drains are below the groundwater level, the oxygen supply is limited. The absence of oxygen and the presence of dissolved organic matter can enable anaerobic dissimilation, in which microorganisms use nitrate (NO_3), manganese (Mn) and Fe (hydr)oxides, sulfate (SO_4), and/or CO_2 as terminal electron acceptors. The redox sensitivity of Fe has been identified as the primary reason for the mobilization of PO_4 in natural environments under suboxic or anoxic conditions (Schroth et al., 2015; Thamdrup, 2000; Young & Ross, 2001). In addition, previously adsorbed or co-precipitated PO_4 may be released when amorphous Fe (III)-(hydr)oxides continue to polymerize or transform into

more crystalline forms such as goethite, possibly catalyzed by dissolved Fe (II) (Kraal et al., 2019; Pedersen et al., 2005; Senn et al., 2017). On the other hand, at the onset of Fe reduction, PO₄ release may be compensated by re-adsorption onto Fe (hydr)oxides that have not been reduced yet or by uptake into transformation products such as vivianite or mixed-valence Fe (II/III) oxides (Baken et al., 2016; Borch & Fendorf, 2008; Heiberg et al., 2012; Szilas et al., 1998; Van der Grift et al., 2016).

Groenenberg et al. (2013) and Chardon et al. (2021) performed a long-term experiment on the PO₄ removing efficiency of ICS enveloped tile drains in a flower-bulb field in the Netherlands. The flower-bulb area is characterized by intensive agriculture, calcareous sandy soils with low P binding capacity, and P- and Fe (II)-rich seepage (Griffioen, 1994). In Chardon et al. (2021), after 26 months, higher Fe levels were found in the effluent of the ICS enveloped drains than in reference drains which indicated that microbial metal reduction was occurring. During the first 26 months of operation, Mn concentrations were high in the effluent of ICS enveloped drains. Mn (hydr)oxides are energetically more favorable as electron acceptors than Fe (III)-(hydr)oxides. Mn (hydr)oxides reduction may occur by microbial respiration of Mn (IV) or by abiotic reduction of Mn (IV) by Fe (II) (Postma & Appelo, 2000). The Fe (II) may be produced by microbial respiration in the filter or be already present in the groundwater. Mn composed about 0.4 % of the dry weight in most ICS (Groenenberg et al., 2013; Sharma et al., 2002). Despite ongoing Fe reduction and dissolution of Fe (III)-(hydr)oxides, the ICS enveloped tile drains still removed on average 93% of the dissolved P after 54 months of operation. These results suggested that (i) the rates of Fe reduction in the ICS filter depended on the rates of organic matter oxidation and the availability of electron acceptors and (ii) the onset of Fe reduction did not necessarily cause the release of PO₄ or loss of PO₄ removal efficiency.

The objective of this study was to expand earlier field observations with new field sites and well-controlled laboratory tests to better constrain the effect of emerging reducing conditions on the performance of ICS in filter systems used to reduce the PO₄ export from agricultural areas. For this, we (i) investigated two sites in the flower-bulb growing area of the Netherlands where ICS-enveloped drains have been installed since 2018 for PO₄ removal to assess whether simultaneous metal reduction and PO₄ adsorption occurred and (ii) performed microcosm experiments to mimic the onset of microbially-mediated reduction of

ICS in drainage water by varying the intensity of reduction though controlling the oxygen availability and the concentration of degradable organic matter. The findings of this research provide a better understanding of the behavior of ICS under reducing conditions. This is relevant for the implementation of ICS filters previous research mainly focused on the adsorption capacity of the ICS and not on its stability under reducing conditions.

4.3 Materials and Methods

Field sites

Two sites in the flower-bulb growing region of the Netherlands were investigated. The region has poor sandy soils and the farmers add a mix of compost and straw as fertilizer which are sources of PO_4 and organic matter, these conditions combined result in a high risk for P leaching. In the two investigated sites ICS enveloped drains were constructed in 2018 to reduce the PO_4 loads to surface waters. ICS was placed around the drains following the previous experience by Groenenberg et al. (2013) and a pilot study by Buijert et al. (2015) where the ICS around drains performed better than other two end-of-pipe filters. After the construction of the systems used in this study successful end-of-pipe filters were reported by Lambert et al. (2020) and Vandermoere et al. (2018). If there is space and enough hydraulic head available in the ditch, end-of-pipe filters offer the advantage of being easier to replace with new material and the redox conditions may be less extreme. Field A is located in Noordwijkerhout ($52^\circ15'52''\text{N}$; $4^\circ30'25''\text{W}$) and Field B in Vogelenzang ($52^\circ19'44''\text{N}$; $4^\circ34'52''\text{W}$). The total area drained in Field A is 7 ha and in Field B 12 ha. In both fields, about 0.015 m^3 of ICS were added per linear meter of drain ($\sim 26.5\text{ kg ICS/m}$) without mechanical packing. The drains were constructed every 10 m, placed 90 cm below surface, and the groundwater level is kept at around 60 cm. The drains are connected to a main drain that discharges into a pumping station with a floater-activated pump that maintains the groundwater level constant by discharging into a ditch. The average annual rainfall between 2019 and 2021 was about 860 mm (Royal Netherlands Meteorological Institute, 2022). The drains remove excess infiltrating rainwater and upwelling groundwater. The estimated groundwater seepage in field A is between 0.10 and 1.0 mm/day and in field B it is between 0.10 and 0.25 mm/day (Janssen et al., 2020). In the summer, evapotranspiration is higher than precipitation and there is no need to continuously pump water out of the field, instead,

the drains are used for irrigation, the level in the ditch is elevated and oxic water infiltrates from the ditch into the field. Unlike the field studied by Groenenberg et al. (2013) and Chardon et al. (2021) where water flowed freely to the ditch, fields A and B use pumps to keep the groundwater levels constant. A video of the construction of the ICS enveloped drains is included in the supplement.

To investigate the relationship between redox conditions and P retention at the field scale, fields A and B were sampled 4 times, from June 2019 to October 2020. Each time, a piezometer standpipe with a perforated bottom covered with a cloth filter was used to take one groundwater sample in the middle of the field 60 to 100 cm below ground level. A second sample was taken from the outflow of the main drain. Samples were not taken during summer since water was not flowing out of the drains. The samples were filtered (0.45 μm) and total dissolved phosphorus (TDP), Fe, Mn, NO_3 , and ammonium (NH_4) were measured. The oxidation-reduction potential (ORP) and pH were measured on-site with a sensor (GMH3511, Geisinger) in a flow-through system. Dissolved organic carbon (DOC) was measured with the combustion catalytic oxidation method (TOC-V, Shimadzu). Shallow groundwater can be redox stratified and not be representative of the composition of drainage water entering the drains. Therefore, in August 2021 a gas vapor probe (GVP, Kit w/ DeWALT D25600K Hammer Drill, AMS) was used to make a depth-concentration profile in the groundwater below the drains. A GVP has a metal tip with a filter and extensions that are drilled in the soil to take water samples at precise depths. Samples were taken about every 30 cm from 100 cm to 380 cm depth and filtered (0.45 μm) into a pre-acidified tube on-site to measure TDP, Fe, and Mn.

Laboratory experiment

Starting materials

The groundwater used for microcosms experiments was collected from a third field, located in Noordwijkerhout (52°15'38''; 4°28'46''). This field is 1000 m apart from field A and has similar soil and flower production characteristics but does not have ICS filters around the drains. The groundwater composition, before starting the experiment and after being stored for one week in the dark at 4 °C under oxic conditions, was: 19.5 mg/L of DOC, 0 mg/L acetate, 8.3 mg-P/L TDP, 10.6 mg-N/L NH_4 , 0.9 mg-N/L NO_3 , 3.4 mg-S/L SO_4 , 65.2 mg/L Ca, 0.09 mg/L

Mn, and 0.03 mg/L Fe. We used the same analytical methods as for the other groundwater samples.

The ICS used for the microcosms and the field filters is a by-product of groundwater iron removal by aeration during drinking water production. Both ICS were obtained from AquaMinerals BV (<https://aquaminerals.com/en/>), a company that develops sustainable chains for by-products of the water treatment process. Because the material from the batch used in the construction of the ICS enveloped drains was no longer available, the ICS used was from a different batch. The ICS used for the microcosms was air-dried and stored in the dark with no additional washing or pretreatment and characterized by total extraction, scanning electron microscopy with energy dispersive x-ray spectroscopy (SEM-EDX), and x-ray absorption spectroscopy (XAS). It contained on average 127.0 mg/g Fe, 9.4 mg/g Mn, 0.5 mg/g S, 9.6 mg/g Ca, and 0.9 mg/g P (± 0.1 mg/g standard deviation) implying that the molar P/Fe ratio of the fresh ICS was about ~ 0.013 . The grain size distribution of the ICS batch received from Aquaminerals was D_{10} , 0.46 mm and D_{60} , 2.11 mm. The maximum porosity was 0.50 and the minimum was 0.39. The saturated hydraulic conductivity at the lowest porosity was 5.5×10^{-3} cm/s and the bulk density was 1770 kg/m^3 . As for the maximum P adsorption capacity, Chardon et al. (2012) calculated 18.7 mg/g Fe for iron by-products obtained from drinking water treatment plants in the Netherlands, equivalent to a 0.10 P/Fe molar ratio.

Microcosm experiments

In the microcosm experiments, we aimed to capture the onset of weakly, moderately, and strongly reducing conditions and to have similar P concentrations and P loadings as in the field setting. The initial TDP concentration of 8.3 mg-P/L is close to the highest values we have measured in the field. We decided not to pre-load the ICS with P. Chardon et al. (2021) measured with total extractions that the P/Fe molar ratio of the ICS in the field had only marginally increased from 0.030 to 0.033 after 59 months of operation. That is, the dominant P pool of ICS used in the field was still the P inherited from production and the additionally adsorbed P represented only a minor fraction. The P originally present in the ICS is likely on the inside of the coating and the freshly adsorbed P on the outside of the coating. Therefore, we assume that freshly adsorbed P is most prone to be released under reducing conditions.

Consequently, we used groundwater with relatively high TDP concentration to create freshly adsorbed P in our experiments.

The intensity of reduction in the microcosms was modulated by introducing acetate as a carbon and electron source and by varying the availability of dioxygen (O_2). This allowed us to investigate the fate of PO_4 partitioning in the ICS at different rates of microbial respiration in the presence of alternative electron acceptors to Fe (hydr)oxides such as O_2 , NO_3 , Mn (hydr)oxides, and SO_4 . Four different treatments were investigated:

- i. Strongly reducing conditions were introduced by closing the bottles, replacing the headspace with 95% N_2 and 5% CO_2 , and stimulating microbial respiration by adding acetate as an electron donor.
- ii. Moderately reducing conditions were introduced by allowing the resupply of O_2 via diffusion through the headspace that was kept unaltered with atmospheric composition and adding acetate as an electron donor.
- iii. Weakly reducing conditions were introduced by replacing the headspace with 95% N_2 and 5% CO_2 and omitting the addition of acetate. The same amount of deionized anoxic water as from the acetate stock solution was added to maintain an equal dilution as in the other treatments. The DOC present in the groundwater was the only available electron donor.
- iv. Abiotic controls were autoclaved (20 minutes, 121 °C) on day 1 to prevent microbiologically induced electron transfer. The headspace was replaced with 95% N_2 and 5% CO_2 , and acetate was added.

Each treatment was done in triplicate in 250 mL glass bottles with 30 g of ICS and 80 mL of groundwater. The groundwater was flushed with CO_2 containing anoxic gas (95% N_2 and 5% CO_2) to use the carbonate system as a pH buffer. This was done for all treatments, including the one with air in the headspace, to achieve a comparable starting pH. Immediately before sealing the bottles the pH was measured with a semi-microprobe (877 Metrohm Titrimo) and was 6.8 ± 0.3 . After the bottles were sealed the pH was checked by placing one drop on pH paper. Only small pH differences were observed after acetate addition. The bottles were sealed with butyl rubber stoppers and incubated horizontally in the dark for 45 days at $20 \pm 1^\circ C$ with no mechanical shaking beside the movement introduced by sampling. The

temperature chosen was higher than the measured field temperatures and conservative with respect to the extent of microbial reduction in the field.

To represent the onset of the different reducing conditions, enough acetate was added to stoichiometrically reduce one-third of the Fe in the ICS if the entire acetate was respired using Fe (III) as an electron acceptor. The acetate was introduced by injecting 3 mL of a 0.95 mol/L sodium acetate solution, giving a final acetate concentration of 2.27 g/L (2.88 mmol) in the corresponding bottles. On day 10 when the acetate was added, the initially present TDP was largely adsorbed by the ICS (corresponding to a molar P_{ads}/Fe of ~ 0.00035) and residual TDP was below 0.006 ± 0.003 mg-P/L. The P originally present in the ICS was still the most important fraction (P_0/Fe of ~ 0.013).

The bottles were sampled three times per week. Aqueous samples were taken with a needle (0.5x25 mm) and a syringe. Before sampling the syringe was pre-filled with the same gas as in the headspace of the bottles and a volume of 2.5 mL of gas was injected to maintain the pressure in the bottles and avoid O₂ intrusion. The samples were directly filtered (0.45 μm) and 1 mL was placed on a 2 mL tube (Eppendorf) containing 100 μL of nitric acid (14 M) for photometric measurements. On three occasions, an extra 1 mL sample without acid was taken for IC measurements. On day 31, additional P was added to a concentration of 1.00 ± 0.05 mg-P/L to all the bottles to assess the adsorption after the ICS has been subjected to microbial reduction, and microbial activity is expected to have declined.

Analytical techniques

Dissolved Fe (II) and total dissolved Fe were determined photometrically with an acetate buffered phenanthroline solution at 510 nm (Saywell & Cunningham, 1971). For total dissolved Fe, the samples were pre-reduced with hydroxylammonium chloride. Total dissolved Mn was determined photometrically with hydroxylamine, formaldehyde, and ammonium hydroxide, at 450 nm (Brewer & Spencer, 1969). TDP was measured photometrically at 880 nm after 30 minutes of incubation with ammonium heptamolybdate solution acidified with sulfuric acid and freshly added ascorbic acid (Murphy & Riley, 1962). Acetate, NH₄, Ca, NO₃, and SO₄ were measured in non-acidified filtered samples with IC (ICS-6000, Thermo Scientific). The ICS-6000 has two columns to perform anion and cation analysis at 30 and 60 °C, respectively. The equipment has an autosampler and eluent generator that

uses a standard potassium hydroxide solution for cations and a meta-sulfuric acid solution for anions together with freshly produced MiliQ water (Advantage, A10, Merk).

For the total extraction the ICS was ground using an agate mortar, 0.125 g of sample was weighed into a vessel, and 2.5 ml of a mixture of HClO₄ (72%) and HNO₃ (65%) with a 3:2 volume ratio and 2.5 mL HF (48%) were added. After being left overnight at 90 °C, the vessel was heated at 140 °C for 4 hours to evaporate the liquids. Then 25 mL of HNO₃ were added and the samples were left once again overnight at 90 °C. After filtration (0.45 µm) the solution was analyzed with ICP-OES (Avio 500, Perkin-Elmer). The extraction was done in duplicate.

XAS was used to characterize the Fe in the ICS before and after the different treatments. To obtain samples with an edge-step of around unity in transmission spectra, 10 mg of ICS were air-dried, ground, mixed with 40 g of cellulose, and pressed into 7-mm diameter pellets. To prevent oxidation artifacts during sample preparation, all manipulations were performed in a glovebox. For storage and transport, the pellets were placed in sealed aluminum bags under an inert N₂ atmosphere. The fresh ICS was measured at the SuperXAS beamline at the Swiss Light Source (SLS, Paul Scherer Institute, Villingen, Switzerland) at room temperature. The treated samples were measured at the XAS beamline at the KIT Light Source at the Karlsruhe Institute of Technology (KIT; Germany) under vacuum. Based on a preliminary inspection of the sample spectra, the following reference spectra were included (i) silicate-containing ferrihydrite (Fh-Si) formed by the oxidation of Fe(II) in bicarbonate-buffered silicate-containing synthetic groundwater, (ii) 2-line ferrihydrite (2L-Fh) synthesized by the forced hydrolysis of a concentrated ferric iron solution (Schwertmann & Cornell, 2000) (both spectra from (Senn et al., 2017)) and (iii) mackinawite (FeS; spectrum kindly provided by Mingkai Ma, Utrecht University). For data extraction and evaluation by linear combination fitting (LCF), the software code Athena was used (Ravel & Newville, 2005).

SEM-EDX was used to observe the ICS grains before and after the different microcosm treatments. The ICS grains were embedded in resin and polished to investigate cross-sections of the Fe coating. Samples were mounted directly on 1.25 cm aluminum stubs using double-sided carbon adhesive stickers. No platinum coating layer was used as it can interfere with P detection. Secondary electron and backscattered electron images were acquired on a Zeiss EVO 15 SEM, using the SmartSEM user interface (v 6.06). Qualitative (or semi-quantitative)

chemical compositions were obtained using a Bruker XFlash EDS system (Esprit v. 2.1). The electric high tension (EHT), scale, and working distance are indicated on the images.

4.4 Results

Field results

The composition of the shallow groundwater varied considerably between the four sampling campaigns (Table 1). TDP was consistently lower in the drain outflow than in the shallow groundwater at all sampling dates. In contrast, Fe and Mn concentrations were higher in the drain outlet compared to in the shallow groundwater at all sampling dates, except for 14 October 2020. The influence of the deeper groundwater on the drained water can be seen for example in the NH_4 concentrations (Table and Figure 4-1). In the deep groundwater, Fe and Mn concentrations showed the general tendency to increase with depth and were higher than in the shallow groundwater at both field sites (Figure 4-1). The TDP concentrations were higher in the deep groundwater in field A than in B and the TDP removal calculated taking the shallow groundwater as reference was lower in A than in B.

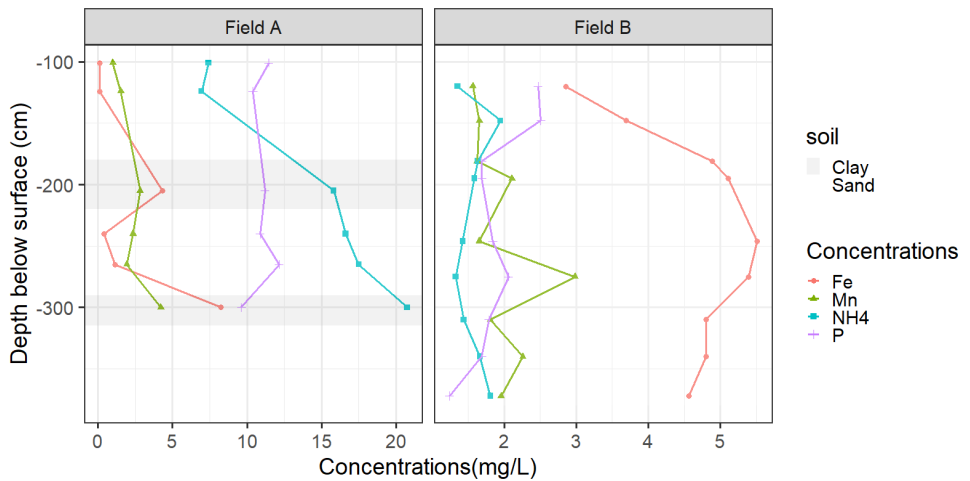


Figure 4-1. Concentration profiles of dissolved (<0.45 μm) Fe, Mn, NH_4 , and TDP in the groundwater below the drains at fields A and B. The groundwater level is at about -60 cm depth, the drains are installed at around -90 cm depth. Notice the different scales on the x-

axis. The clay and sand were classified on site while making the profiles based on the plasticity of the soil.

Table 4-1 Concentrations in the shallow groundwater above ICS enveloped drains, 60 to 100 cm below the surface, and in the drain outflow in Fields A and B of dissolved (0.45 µm) Fe, Mn, TDP, DOC, EC, ORP, NO₃, and NH₄.

Date (d-m-y)	Field A shallow groundwater				Field A drain outflow			
	11-Jun-19	9-Dec-19	7-Feb-20	14-Oct-20	11-Jun-19	9-Dec-19	7-Feb-20	14-Oct-20
Fe (mg/L)	0.03	0.02	0.04	0.95	0.03	0.11	1.1	0.05
Mn (mg/L)	0.8	1.4	1.1	1.6	3.9	2.4	2.6	5.0
TDP (mg-P/L)	0.68	7.1	3.2	2.0	0.34	3.6	1.2	0.4
TDP retention (%)*					50	50	63	80
NO ₃ (mg-N/L)	<0.02	<0.02	<0.02	<0.02	<0.02	<0.02	<0.02	<0.02
NH ₄ (mg-N/L)	0.9	4.0	1.3	2.1	3.2	4.9	4.9	3.9
DOC (mg/L)	15.7	19.1	11.5	24.4	15.4	20.6	15.3	20.1
EC (µS/cm)	1700	1300	1100	1500	1200	1100	1000	1200
Temp (°C)			5	12.7			6	13
pH			7.1	6.9			7	7.2
ORP (mV)			-160	-194			-96	95

Date (d-m-y)	Field B shallow groundwater				Field B drain outflow			
	11-Jun-19	9-Dec-19	7-Feb-20	14-Oct-20	11-Jun-19	9-Dec-19	7-Feb-20	14-Oct-20
Fe (mg/L)	0.05	0.04	0.44	0.06	0.05	0.71	1.3	0.24
Mn (mg/L)	0.1	0.4	0.2	0.6	1.2	1.4	1.1	1.4
TDP (mg-P/L)	2.2	4.0	4.3	3.7	0.34	0.41	0.38	0.32
TDP retention (%)*					85	90	91	91
NO ₃ (mg-N/L)	4.5	0.09	<0.02	2.6	<0.02	<0.02	<0.02	<0.02
NH ₄ (mg-N/L)	<0.04	0.08	0.23	0.08	1.8	1.8	1.6	1.6
DOC (mg/L)	23.2	31.6	26.2	28.9	15.0	20.1	15.7	17.2
EC (μS/cm)	830	850	710	950	950	1000	910	940
Temp (°C)			5	13.5			6	13.4
pH			7	6.8			7	7.2
ORP (mV)			70	176			-105	-114

$$*TDP \text{ retention (\%)} = \frac{TDP_{\text{shallow groundwater}} - TDP_{\text{drain outflow}}}{TDP_{\text{shallow groundwater}}} \cdot 100$$

Dynamics of solution composition in microcosm experiments

Changes in dissolved concentrations in the four different microcosms are shown in Figure 4-2. The addition of acetate induced microbially mediated metal reduction. Mn concentrations peaked 2-4 days after acetate addition increasing from 0.09 mg/L to 24.8 ± 2.0 mg/L and 10.3 ± 1.7 mg/L under strongly (no O₂) and moderately (with O₂ diffusion) reducing conditions, respectively. Only under strongly reducing conditions, Fe concentrations peaked 6 days after acetate addition around 5.50 ± 0.59 mg/L and the color of the ICS changed from orange/brown to black (Figure S2). The presence of DOC alone was not enough to induce an increase in Fe concentrations. Under weakly reducing conditions (only DOC was available as electron donor) the Mn concentration increased slightly to 2.9 ± 0.16 mg/L and the decrease was not as pronounced as in the treatments with acetate addition. In the abiotic control, Mn concentrations increased abruptly on day 2 (after the bottles were autoclaved) to values around 9.7 ± 0.6 mg/L and stayed constant afterward throughout the experiment. The increase in Mn concentration was possibly caused by abiotic, thermally induced reduction of Mn oxides during autoclavation and possibly followed by disproportionation of Mn (III).

In all treatments, after PO₄ adsorption onto the ICS, the SO₄ concentration increased from 3.4 to 9.8 ± 2.0 mg/L S. This was possibly caused by ligand exchange between PO₄ and SO₄ ions on adsorption sites. Under strongly reducing conditions, the SO₄ concentrations eventually decreased to 2.6 ± 0.6 mg/L S after 45 days, indicating microbial SO₄ reduction. No P release was measured in any of the treatments. The P concentrations at the end of the experiment and after 1.00 ± 0.05 mg-P/L were added on day 31 were 0.09 ± 0.03 mg-P/L in strongly reducing conditions, 0.005 ± 0.02 mg-P/L in moderately reducing conditions, and 0.003 ± 0.001 mg-P/L in the weakly reducing conditions and in the autoclaved control.

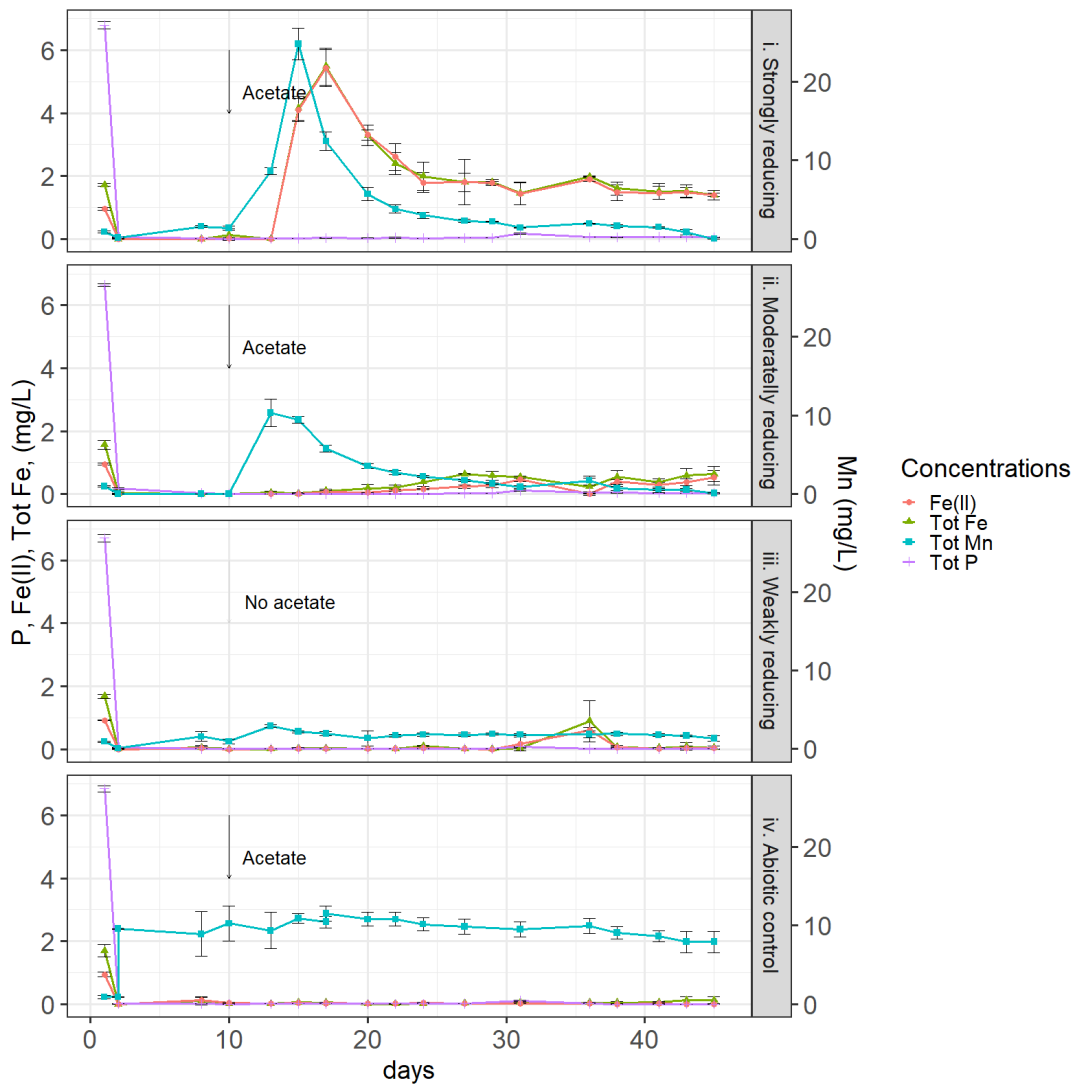


Figure 4-1. Dissolved (<0.45 μm) concentrations of Fe (II), total Fe and Mn, and TDP in the microcosm experiments with ICS in groundwater at varying reducing conditions. In the bottles with acetate, 2.27 g/L was added on day 10. In the abiotic control, the bottles were autoclaved on day 1. The points are the mean and the error bars indicate the standard deviation of three replicates.

Ca, NH₄ and NO₃ concentrations decreased at the end of the experiments, in the microcosms under strongly and moderately reducing conditions. Ca decreased from 65.2 mg/L to 8.50 ± 0.78 mg/L and 8.00 ± 0.28 mg/L, respectively. In both treatments, NH₄ and NO₃ were consumed. Under strongly reducing conditions both dropped to below detection (<0.02 mg-N/L) and under moderately reducing conditions NH₄ decreased to 1.8 ± 0.1 mg-N/L and NO₃ to 0.02 ± 0.01 mg-N/L. In both treatments, all acetate was consumed. Under weakly reducing conditions, the final NH₄ was approximately half of the initial concentration, 5.07 ± 0.08 mg-N/L, and NO₃ was 0.02 ± 0.01 mg-N/L. In the abiotic control, the acetate was not consumed, and NH₄ and NO₃ did not change. Water chemistry data is available in the supplement (Table S2).

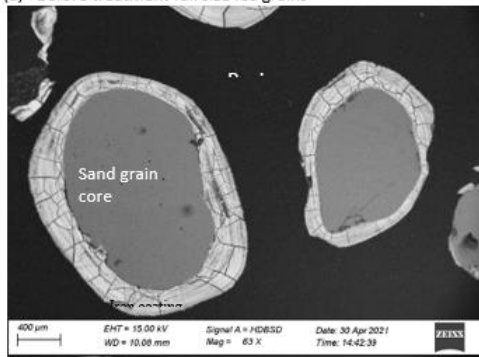
Characterization of solids from the microcosm experiment

Fe K-edge XAS was used to assess the speciation of Fe in the fresh and incubated ICS (see supplement; Figure S1). The Fe in the fresh ICS coatings was mainly contained in silicate-containing ferrihydrite, consistent with its accumulation by oxidation of Fe (II) in silicate-containing aerated groundwater (Senn et al., 2015), and in line with earlier XAS characterization results for Fe-sludge and ICS from drinking water treatment (Chardon et al., 2021; Koopmans et al., 2020). Three of the reacted sample spectra closely matched the spectrum of the unreacted material, but one spectrum showed a spectral difference that was attributed to a contribution of 7% (XANES) to 13% (EXAFS) FeS based on LCF analysis. Although the four incubated samples were misplaced during pellet preparation or sample mounting in the glove box, this LCF result was attributed to the strongly reducing treatment (acetate, anoxic) which in contrast to the others showed clear signs of sulfidation, including a decrease in SO₄ concentration during incubation and a change in color to black. The similarity of the Fe K-edge XAS spectra of the other three incubated samples to the spectrum of the fresh material indicating that silicate-containing ferrihydrite had not detectably transformed during incubation under less reducing conditions in the absence of sulfide formation. This observation was in line with earlier results suggesting that ICS deployed in a field did not detectably transform over 14 to 59 months (Chardon et al., 2021).

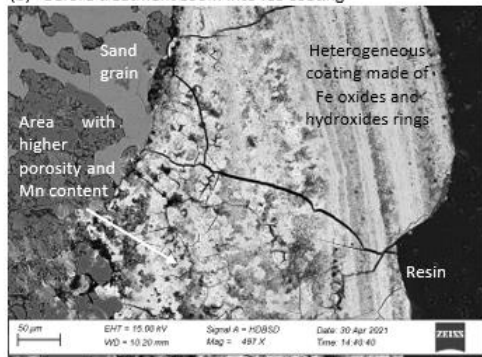
Figure 4-3 shows the SEM images of the ICS. The ICS grains are larger than 1 mm in diameter, have a sand core, and a 100 µm to 500 µm coating composed of iron (hydr)oxides with a 1:3

average Fe:O ratio in a layered structure and regions of higher porosity and Mn contents (Figures 4-3-a and -b). The P:Fe ratio measured with EDX was 0.015 which closely matches the total extraction results of the original ICS. After the strongly reducing treatment, the grain surface transformed into a curved amorphous pattern (Figure 4-3-e). Although S could not be detected with EDX, other researchers detected the same pattern when ferrihydrite was transformed into FeS (Akhtar et al., 2012; Csákberényi-Malasics et al., 2012; Zhang et al., 2021; Zou et al., 2018). In the samples from strongly and moderately reducing microcosms precipitates with similar C:O:Ca:Mn ratios were seen in suspension close to the grains and inside macropores (Figure 4-3-c, 4-3-d, S6, and S7). The average C:O:Ca:Mn molar ratio obtained with EDX point measurements was 20:65:13:2. No major differences in the coating characteristics were detected in the abiotic control and after the weakly reducing treatment. In the abiotic control, the autoclavation could potentially modify the structure of the iron (hydr)oxides, nevertheless, this sample looked similar to the original material under SEM-EDX and XAS suggesting no major structural transformation occurred.

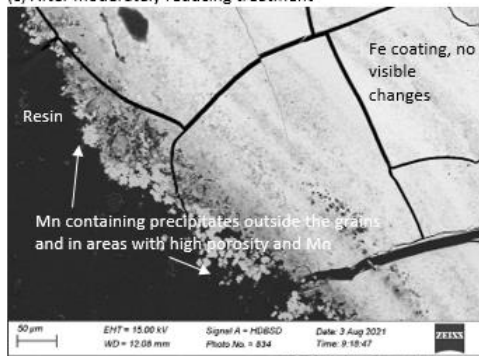
(a) Before treatment full size ICS grains



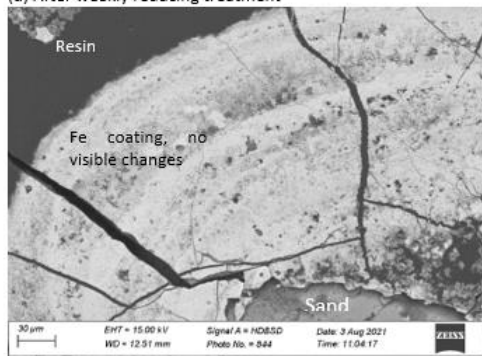
(b) Before treatment zoom into ICS coating



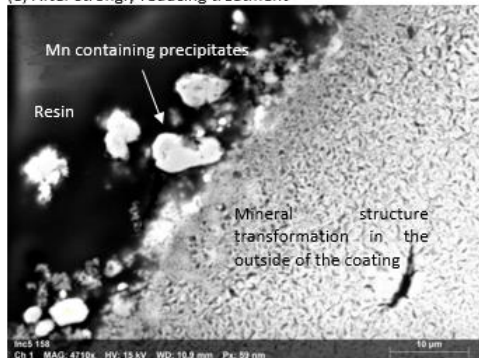
(c) After moderately reducing treatment



(d) After weakly reducing treatment



(e) After strongly reducing treatment



(f) Autoclaved control

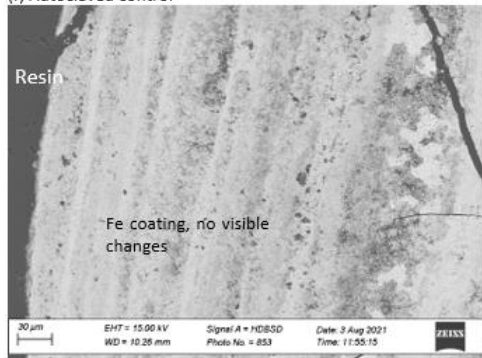


Figure 4-2 SEM images of ICS grains before treatment and after incubation in microcosms under a range of reducing conditions. Scale bars are indicated on each image. Most of the cracks that can be observed were most likely produced during the vacuum step at the SEM-EDX.

4.5 Discussion

Fe and Mn reduction in ICS at the field sites and P retention

Removal of dissolved P from the drainage water by the ICS was indicated by consistently lower TDP concentrations in the drain outflow than in the groundwater at the same sampling event. Taking the concentrations in the shallow groundwater as a reference, the TDP removal efficiency varied between 50-80% and 85-91% in fields A and B, respectively. One of the reasons for the lower removal in field A may be the underestimation of the drainage water concentrations as the deeper groundwater had very high P concentrations. Although the field data suggests a significant TDP removal, it appears to be less effective than the TP removal observed by Chardon et al. (2021) who reported a 93% efficiency. Chardon et al. (2012) and Lambert et al. (2020) observed lower TDP removal efficiencies at higher flow velocities and at higher TDP inflow concentrations in ICS. The flow velocity was 60 cm/d in Chardon et al. (2021) while it was 180 cm/d at our sites. In field A, the lowest outflow TDP concentrations and highest removal efficiency coincided with Mn dissolution, suggesting TDP removal was not affected by metal reduction.

On most occasions, dissolved Fe concentrations were higher in the drain outflow than in the shallow groundwater but not higher than in deeper groundwater. For example, on February 2020, dissolved Fe concentrations were high in the drain outflow. This could be explained either by a larger contribution of deep groundwater in the drained water or by Fe reduction from the ICS. Therefore, without constraining the relative contribution of drainage water with different compositions to the drain outflow it cannot be unambiguously concluded that Fe concentrations increased while flowing through the ICS. Although direct evidence for Fe reduction in the ICS layers at the two field sites is missing, NO_3^- concentrations were consistently below the detection limit in the drain outflow, NH_4^+ concentrations were higher in the outflow than in the shallow groundwater, and there was a constant supply of electron donors in the form of DOC. Hence, in the absence of oxygen and nitrate, it is likely that the abundant Fe and Mn (hydr)oxides were used in the ICS layers as terminal electron acceptors by dissimilatory metal-reducing organisms. The reduction of Fe (hydr)oxides may lead to transformations in the solid phase and does not necessarily lead to an increase in dissolved

Fe concentrations. The reduced Fe (II) can be effectively adsorbed by Fe (hydr)oxides or form secondary minerals such as magnetite (Fe₃O₄), siderite (FeCO₃), or iron sulfides.

Because it was difficult to quantify the importance of the metal reduction from the field data, we made an estimation of the metal reduction based on the stoichiometry of the reaction with DOC. When 12 g (1 mol) of C are oxidized going from C(0) to C(IV) oxidation state, 4 electrons are transferred to reduce 4 mol Fe (III) to Fe (II). As the drains are 10 m apart from each other, each linear meter of pipe drains 10 m². We assumed that 70 % of the precipitation surplus was transported through the drains obtaining an annual flow of 3215 L/m/year ((860-450+36.5) mm x 10 m² x 70 %). Assuming the DOC concentration was 19.5 mg/L, the average TDP concentration in the drained water was 4.0 mg-P/L, 73 % TDP was retained, that there were originally 26.5 kg-Fe per linear meter of drain, and all reduced Fe (II) was removed from the filter. It is possible to estimate the lifespan in years of the ICS filter before a 0.10 P/Fe molar ratio is reached with the following formula:

$$P/Fe_{(n_{year})} = P/Fe_0 + \frac{n_{year} \cdot 0.3 \text{ mol P/year/m}}{474 \text{ mol Fe/m} - \%_{DOC} \cdot n_{year} \cdot 20 \text{ mol Fe/year/m}} < 0.10$$

Where: P/Fe_0 is the original molar ration in the ICS 0.013, n is the filter lifespan in years, $\%_{DOC}$ is the percentage of DOC oxidized in the filter, 0.3 mol P/year/m is the P removal load per year, 474 mol Fe/m is the original amount of Fe, and 20 mol Fe/year/m is how much Fe we assume is lost per year.

We supposed two scenarios: one in which 100 % of the DOC was respired using Fe (III)-(hydr)oxides as electron acceptors (which is not realistic, as part of the DOC is expected to be slowly or not degrading), and a more realistic case in which 10% of the DOC was respired. For these cases, respectively 4 and 0.4 % of the iron would be reduced annually and a 0.10 P/Fe (III) molar ratio would be reached after 20 and 80 years. These results are positive as drainage systems are traditionally designed for a lifespan between 20 and 40 years (Skaggs et al., 1994). The remaining question is whether P release can also be expected at the onset of Fe and Mn reduction. For that reason, microcosm experiments were used to systematically investigate the dependency of P removal on microbially induced redox conditions in ICS.

Phosphate release from ICS in microcosms at different reducing conditions

The metal reduction in the microcosms was microbially mediated as no changes occurred in the abiotic control after acetate addition. Mn dissolved from ICS in the microcosms with moderately and strongly reducing conditions. Fe dissolution only occurred in the microcosm with strongly reducing conditions when oxygen was not available and SO_4 reduction in the water and solid phases occurred. Fe reduction affected the outer layer of the coating, which is likely where P was initially adsorbed, and the risk of P release is highest. However, even under strongly reducing conditions neither the adsorbed P nor the P originally present in the ICS were mobilized into the overlying water in the microcosm experiments. These results are in agreement with the observation that P release upon reduction of P-loaded Fe (hydr)oxides can be effectively prevented if sufficient sorption sites remain available on unaltered Fe (hydr)oxides or secondary Fe minerals (Loeb et al., 2008; Smolders et al., 2017; Young & Ross, 2001). Our results do not allow us to identify a critical P/Fe ratio or, more specifically, a critical P/Fe (III) ratio at which P release cannot be effectively counteracted anymore. Nevertheless, considering the presence of silicate in the drainage water, a 0.1 ratio could be used (Hilbrandt et al., 2019). Our mass balance calculations point towards a potentially long lifespan before a 0.1 P/Fe (III) is reached.

The dynamics of dissolved Fe and Mn concentrations indicate the formation of Fe (II) and Mn (II) containing secondary products in the moderately and strongly reducing microcosms. The decrease in Mn concentration after an initial increase can be attributed to the formation of carbonate precipitates, possibly in the form of rhodochrosite (MnCO_3) or as a solid solution with calcium carbonates. The newly formed carbonates were not part of the coating but formed precipitates in suspension or inside macropores. In contrast to Mn (II), Fe (II) was not enriched in carbonates but formed FeS, which remained associated with the Fe coating. Neither the carbonates nor FeS showed visible P enrichment in the SEM-EDX analyses, implying that the formation of secondary minerals did not significantly contribute to the retention of solid-bound P. Nevertheless, the formation of precipitates and microbial biomass could affect the performance of ICS filters by reducing the hydraulic conductivity and cause clogging. For instance, Vandermoere et al., (2018) observed a slight decrease in the hydraulic conductivity of ICS filters after 10 weeks of use.

A minor FeS fraction formed in the strongly reducing microcosm. Microbial SO_4 reduction can happen before or simultaneously with Fe (III) reduction. Sulfate-reducing bacteria such as *Desulfotomaculum* spp. use acetate as a carbon source and Fe (III) can be reduced by sulfide or by iron-reducing bacteria such as *Geobacter* spp. that also use acetate as a carbon source (Hansel et al., 2015; Islam et al., 2004; Kwon et al., 2016). The acetate added to each bottle was 2.85 mmol which, upon oxidation to CO_2 , should have been enough to reduce one-third of the initial metal (hydr)oxides present (22.8 mmol of Fe (III) to Fe (II), or 11.4 mmol of Mn (IV) to Mn (II)). Only 0.04 % and 1.54 % of the initially added Fe and Mn, respectively, were recovered in reduced form in solution. This suggests that most electrons released by acetate reduction were consumed by SO_4 reduction or by the formation of solid-bound reduced metals. Based on XAS analyses 7 to 13% (corresponding to 4.77 and 8.86 mmol) of the Fe transformed into FeS in these microcosms, which accounts for most of the acetate consumption (0.57 to 1.05 mmol for Fe (III) reduction and 0.91 to 1.68 mmol SO_4 reduction). Although these calculations close the electron balance, XAS might be overestimating the FeS fraction as it is not consistent with the sulfur mass balance based on the change in dissolved SO_4 . Furthermore, nitrogen was consumed, possibly in processes involving oxidation of NH_4 to N_2 , NO_2^- , or NO_3^- by iron-reducing bacteria (Feammox, Zhu et al., 2022), denitrification, and assimilation in biomass. Fe was in excess, if all the NH_4 was transformed to NO_3^- and then denitrified, this could have reduced 0.38 mmol Fe (0.6%) and consumed a maximum of 0.23 mmol (8%) of the acetate. Denitrification, generation of elemental hydrogen, or methane are potentially additional sinks for electrons.

Changes in the material were only noted in the outer layer of the coating with SEM, which suggests that the access to Fe(III) in deeper layers of the coating was restricted by the small micropore sizes and the absence of electron-conducting materials or electron shuttles (Bonneville et al., 2006; Lies et al., 2005). The outer layer is expected to be relevant for fast removal of dissolved PO_4 from the surrounding solution and formation at the ICS surface could, hence, limit further adsorption since FeS has a lower sorption capacity than Fe (III)-(hydr)oxides such as ferrihydrite (Kocar et al., 2010). After PO_4 was re-introduced 91% was adsorbed in the strongly reducing microcosm while 99% was adsorbed in the other microcosms. Therefore, for the moderately and weakly reducing conditions set in this study, the reductive pressure introduced was not enough to decrease the fast PO_4 sorption capacity of Fe (III)-(hydr)oxides. However, after longer exposure to strongly reducing conditions, Fe

(III)-(hydr)oxide reduction and the formation of secondary minerals such as FeS could eventually become a limiting factor in the in the performance of ICS filters for PO₄ retention.

4.6 Conclusion

This research aimed to investigate PO₄ (im)mobility at the onset of ICS reduction. In the two investigated fields, the ICS filters still removed PO₄ after 3 years of use while being subject to metal-reducing conditions. In the microcosm experiment, a range of treatments mimicked the field conditions. For exposure times of 45 days under weakly, moderately, and strongly reducing conditions for ICS with a molar P/Fe ratio of 0.013, P was not released even after Fe and Mn partial reduction. The P sorption capacity of the ICS and its mineral structure remained mostly unchanged after being exposed to moderately and weakly reducing conditions. After moderately and strongly reducing conditions we observed the formation of manganese calcium carbonate precipitates in suspension. Only under strongly reducing conditions, a small percentage of Fe became transformed into iron sulfides in the outer layer of the Fe coatings. These secondary products could be detrimental to filters by causing filter clogging or by reducing their P sorption capacity. However, our results and the results from earlier work suggest that these detrimental effects only become relevant at operation periods substantially longer than periods of up to 5 years tested so far.

4.7 Acknowledgments

This study was funded by P-TRAP (EU Grant No. 813438, Marie Skłodowska- Curie Actions). We would like to thank Delphy and the farmers from the two fields for their participation in this study. We would like to acknowledge Mingkai Ma for XAS sample preparation, Eric Hellebrand for SEM-EDX operation, and Olga Safonova (SLS, PSI) for her help with data acquisition at the SuperXAS beamline, and the SLS is thanked for the allocation of beamtime. Thanks to Menno Tiesma for fieldwork support.

4.8 Supplementary Material

The supplementary material includes a video of the drain construction, XAS spectra, images of the treatment bottles during the experiment, SEM-EDX spectra and images, chemical

equations used for stoichiometric calculations, the mass balance of iron losses in the field, and tables with water quality results.

4.9 References

- Akhtar, M., Abdelhady, A. L., Azad Malik, M., & Obrien, P. (2012). Deposition of iron sulfide thin films by AACVD from single source precursors. *Journal of Crystal Growth*, *346*(1), 106–112. <https://doi.org/10.1016/j.jcrysgro.2012.02.013>
- Baken, S., Moens, C., Van der Grift, B., & Smolders, E. (2016). Phosphate binding by natural iron-rich colloids in streams. *Water Research*, *98*, 326–333. <https://doi.org/10.1016/j.watres.2016.04.032>
- Barcala, V., Rozemeijer, J., Osté, L., Van Der Grift, B., Gerner, L., & Behrends, T. (2020). Processes controlling the flux of legacy phosphorus to surface waters at the farm scale. *Environmental Research Letters*, *16*(1). <https://doi.org/10.1088/1748-9326/abcdd4>
- Bol, R., Gruau, G., Mellander, P. E., Dupas, R., Bechmann, M., Skarbøvik, E., Bierozza, M., Djodjic, F., Glendell, M., Jordan, P., Van der Grift, B., Rode, M., Smolders, E., Verbeeck, M., Gu, S., Klumpp, E., Pohle, I., Fresne, M., & Gascuel-Oudou, C. (2018). Challenges of reducing phosphorus based water eutrophication in the agricultural landscapes of Northwest Europe. *Frontiers in Marine Science*, *5*(AUG), 1–16. <https://doi.org/10.3389/fmars.2018.00276>
- Bonneville, S., Behrends, T., Cappellen, P. Van, Hyacinthe, C., & Röling, W. F. M. (2006). Reduction of Fe(III) colloids by *Shewanella putrefaciens*: A kinetic model. *Geochimica et Cosmochimica Acta*, *70*(23 SPEC. ISS.), 5842–5854. <https://doi.org/10.1016/j.gca.2006.04.029>
- Borch, T., & Fendorf, S. (2008). *Phosphate Interactions with Iron (Hydr) oxides : Mineralization Pathways and Phosphorus Retention upon Bioreduction*. 9197(07). [https://doi.org/10.1016/S1571-9197\(07\)07012-7](https://doi.org/10.1016/S1571-9197(07)07012-7)
- Brewer, P. ., & Spencer, D. W. (1969). Colorimetric determination of manganese in anoxic waters. *Limnology and Oceanography*, *18*(25), 107–110.
- Buijert, A., Talens, R., Chardon, W. J., Groenenberg, J. E., Jansen, S., & Gerritse, J. (2015). *Pilot effectgerichte verwijdering fosfaat bollenstreek*. https://www.rijnland.net/documents/700/Onderzoeksproject_bollensector.pdf
- Chardon, Groenenberg, J. E., Temminghoff, E. J. M., & Koopmans, G. F. (2012). Use of Reactive Materials to Bind Phosphorus. *Journal of Environmental Quality*, *41*(3), 636–646. <https://doi.org/10.2134/jeq2011.0055>
- Chardon, W., Groenenberg, J. E., Vink, J. P. M., Voegelin, A., & Koopmans, G. F. (2021). Use of iron-coated sand for removing soluble phosphorus from drainage water. *Science of The Total Environment*, *815*, 152738. <https://doi.org/10.1016/j.scitotenv.2021.152738>
- Chardon, W. J., & Schoumans, O. F. (2007). Soil texture effects on the transport of phosphorus from agricultural land in river deltas of Northern Belgium, the Netherlands and North-West Germany.

- Soil Use and Management*, 23(SUPPL. 1), 16–24. <https://doi.org/10.1111/j.1475-2743.2007.00108.x>
- Csákberényi-Malasics, D., Rodríguez-Blanco, J. D., Kis, V. K., Rečnik, A., Benning, L. G., & Pósfai, M. (2012). Structural properties and transformations of precipitated FeS. *Chemical Geology*, 294–295, 249–258. <https://doi.org/10.1016/j.chemgeo.2011.12.009>
- Griffioen, J. (1994). Uptake of Phosphate by Iron Hydroxides during Seepage in Relation to Development of Groundwater Composition in Coastal Areas. *Environmental Science and Technology*, 28(4), 675–681. <https://doi.org/10.1021/es00053a022>
- Groenberg, J. E., Chardon, W. J., & Koopmans, G. F. (2013). Reducing Phosphorus Loading of Surface Water Using Iron-Coated Sand. *Journal of Environmental Quality*, 42(1), 250–259. <https://doi.org/10.2134/jeq2012.0344>
- Hansel, C. M., Lentini, C. J., Tang, Y., Johnston, D. T., Wankel, S. D., & Jardine, P. M. (2015). Dominance of sulfur-fueled iron oxide reduction in low-sulfate freshwater sediments. *ISME Journal*, 9(11), 2400–2412. <https://doi.org/10.1038/ismej.2015.50>
- Heiberg, L., Koch, C. B., Kjaergaard, C., Jensen, H. S., & Hansen, H. C. B. (2012). Vivianite precipitation and phosphate sorption following iron reduction in anoxic soils. *Journal of Environmental Quality*, 41(3), 938–949. <https://doi.org/10.2134/jeq2011.0067>
- Hilbrandt, I., Lehmann, V., Zietzschmann, F., Ruhl, A. S., & Jekel, M. (2019). Quantification and isotherm modelling of competitive phosphate and silicate adsorption onto micro-sized granular ferric hydroxide. In *RSC Advances* (Vol. 9, Issue 41, pp. 23642–23651). <https://doi.org/10.1039/c9ra04865k>
- Islam, F. S., Gault, A. G., Boothman, C., Polya, D. A., Chamok, J. M., Chatterjee, D., & Lloyd, J. R. (2004). Role of metal-reducing bacteria in arsenic release from Bengal delta sediments. *Nature*, 430(6995), 68–71. <https://doi.org/10.1038/nature02638>
- Janssen, G. M. C. M., van Walsum, P. E. V., America, I., Pouwels, J. R., Hunink, J. C., Vermeulen, P. T. M., Meshgi, A., Prinsen, G. F., Mulder, N., Visser, M., T. Kroon.Janssen, G.M.C.M., P.E.V. van Walsum, I. America, J.R. Pouwels, J.C. Hunink, P.T.M. Vermeulen, A. Meshgi, G.F. Prinsen, N. Mulder, M. V., & Kroon, T. (2020). *Veranderingsrapportage LHM 4.1: Actualisatie van het lagenmodel, het topsysteem en de bodemplant relaties*. https://nhi.nu/nl/files/5516/1011/9690/11205261-000-BGS-0001_-_Veranderingsrapportage_LHM_4.1_-_definitief_2020.pdf
- Kocar, B. D., Borch, T., & Fendorf, S. (2010). Arsenic repartitioning during biogenic sulfidization and transformation of ferrihydrite. *Geochimica et Cosmochimica Acta*, 74(3), 980–994. <https://doi.org/10.1016/j.gca.2009.10.023>
- Koopmans, G. F., Hiemstra, T., Vaseur, C., Chardon, W. J., Voegelin, A., & Groenberg, J. E. (2020). Use of iron oxide nanoparticles for immobilizing phosphorus in-situ: Increase in soil reactive surface area and effect on soluble phosphorus. *Science of the Total Environment*, 711, 135220.

<https://doi.org/10.1016/j.scitotenv.2019.135220>

- Kraal, P., van Genuchten, C. M., Behrends, T., & Rose, A. L. (2019). Sorption of phosphate and silicate alters dissolution kinetics of poorly crystalline iron (oxyhydr)oxide. *Chemosphere*, *234*(lii), 690–701. <https://doi.org/10.1016/j.chemosphere.2019.06.071>
- Kwon, M. J., O'Loughlin, E. J., Boyanov, M. I., Brulc, J. M., Johnston, E. R., Kemner, K. M., & Antonopoulos, D. A. (2016). Impact of organic carbon electron donors on microbial community development under iron-and sulfate-reducing conditions. In *PLoS ONE* (Vol. 11, Issue 1). <https://doi.org/10.1371/journal.pone.0146689>
- Lambert, N., Van Aken, P., Van den Broeck, R., & Dewil, R. (2020). Adsorption of phosphate on iron-coated sand granules as a robust end-of-pipe purification strategy in the horticulture sector. *Chemosphere*, *267*, 129276. <https://doi.org/10.1016/j.chemosphere.2020.129276>
- Lies, D. P., Hernandez, M. E., Kappler, A., Mielke, R. E., Gralnick, J. A., & Newman, D. K. (2005). *Shewanella oneidensis* MR-1 uses overlapping pathways for iron reduction at a distance and by direct contact under conditions relevant for biofilms. In *Applied and Environmental Microbiology* (Vol. 71, Issue 8, pp. 4414–4426). <https://doi.org/10.1128/AEM.71.8.4414-4426.2005>
- Loeb, R., Lamers, L. P. M., & Roelofs, J. G. M. (2008). Prediction of phosphorus mobilisation in inundated floodplain soils. *Environmental Pollution*, *156*(2), 325–331. <https://doi.org/10.1016/j.envpol.2008.02.006>
- Mellander, P. E., Jordan, P., Shore, M., McDonald, N. T., Wall, D. P., Shortle, G., & Daly, K. (2016). Identifying contrasting influences and surface water signals for specific groundwater phosphorus vulnerability. *Science of the Total Environment*, *541*, 292–302. <https://doi.org/10.1016/j.scitotenv.2015.09.082>
- Mendes, L. R. D. (2020). Edge-of-Field technologies for phosphorus retention from agricultural drainage discharge. *Applied Sciences (Switzerland)*, *10*(2). <https://doi.org/10.3390/app10020634>
- Murphy, J., & Riley, J. P. (1962). A modified single solution method for the determination of phosphate in natural waters. *Analytica Chimica Acta*, *27*(C), 31–36. [https://doi.org/10.1016/S0003-2670\(00\)88444-5](https://doi.org/10.1016/S0003-2670(00)88444-5)
- Pedersen, H. D., Postma, D., Jakobsen, R., & Larsen, O. (2005). Fast transformation of iron oxyhydroxides by the catalytic action of aqueous Fe(II). *Geochimica et Cosmochimica Acta*, *69*(16), 3967–3977. <https://doi.org/10.1016/j.gca.2005.03.016>
- Penn, C., Chagas, I., Klimeski, A., & Lyngsie, G. (2017). A review of phosphorus removal structures: How to assess and compare their performance. *Water (Switzerland)*, *9*(8), 1–22. <https://doi.org/10.3390/w9080583>
- Postma, D., & Appelo, C. A. J. (2000). Reduction of Mn-oxides by ferrous iron in a flow system: Column experiment and reactive transport modeling. *Geochimica et Cosmochimica Acta*, *64*(7), 1237–1247.

- Ravel, B., & Newville, M. (2005). ATHENA, ARTEMIS, HEPHAESTUS: Data analysis for X-ray absorption spectroscopy using IFEFFIT. *Journal of Synchrotron Radiation*, 12(4), 537–541. <https://doi.org/10.1107/S0909049505012719>
- Royal Netherlands Meteorological Institute (KNMI). (2022). *Daily weather data in the Netherlands*. <https://www.knmi.nl/nederland-nu/klimatologie/daggegevens>
- Saywell, L. G., & Cunningham, B. B. (1971). Determination of Iron colorimetric o-phenathroline method. *Limnology and Oceanography*, 67–69.
- Schoumans, O. F., Chardon, W. J., Bechmann, M. E., Gascuel-Oudou, C., Hofman, G., Kronvang, B., Rubæk, G. H., Ulén, B., & Dorioz, J. M. (2014). Mitigation options to reduce phosphorus losses from the agricultural sector and improve surface water quality: A review. *Science of the Total Environment*, 468–469, 1255–1266. <https://doi.org/10.1016/j.scitotenv.2013.08.061>
- Schroth, A. W., Giles, C. D., Isles, P. D. F., Xu, Y., Perzan, Z., & Druschel, G. K. (2015). Dynamic Coupling of Iron, Manganese, and Phosphorus Behavior in Water and Sediment of Shallow Ice-Covered Eutrophic Lakes. *Environ. Sci. Technol.*, 49, 9758–9767. <https://doi.org/10.1021/acs.est.5b02057>
- Schwertmann, U., & Cornell, R. M. (2000). Iron oxides in the laboratory, preparation and characterization. In W.-V. V. GmbH (Ed.), *American Journal of Psychiatry* (Second edi, Vol. 164, Issue 4). WILEY-VCH Verlag GmbH,. <https://doi.org/10.1176/ajp.2007.164.4.566>
- Senn, A. C., Kaegi, R., Hug, S. J., Hering, J. G., Mangold, S., & Voegelin, A. (2015). Composition and structure of Fe(III)-precipitates formed by Fe(II) oxidation in water at near-neutral pH: Interdependent effects of phosphate, silicate and Ca. *Geochimica et Cosmochimica Acta*, 162, 220–246. <https://doi.org/10.1016/j.gca.2015.04.032>
- Senn, A. C., Kaegi, R., Hug, S. J., Hering, J. G., Mangold, S., & Voegelin, A. (2017). Effect of aging on the structure and phosphate retention of Fe(III)-precipitates formed by Fe(II) oxidation in water. *Geochimica et Cosmochimica Acta*, 202, 341–360. <https://doi.org/10.1016/j.gca.2016.12.033>
- Sharma, S., Petrusevski, B., & Schippers, J. C. (2002). Characterisation of coated sand from iron removal plant. *Water Science and Technology*, 2(2), 247–257. <https://doi.org/10.2166/ws.2002.0070>
- Sharpley, A., Jarvie, H. P., Buda, A., May, L., Spears, B., & Kleinman, P. (2013). Phosphorus Legacy: Overcoming the Effects of Past Management Practices to Mitigate Future Water Quality Impairment. *Journal of Environmental Quality*, 42(5), 1308–1326. <https://doi.org/10.2134/jeq2013.03.0098>
- Skaggs, R. W., Brevé, M. A., & Gilliam, J. W. (1994). Hydrologic and water quality impacts of agricultural drainage. *Critical Reviews in Environmental Science and Technology*, 24(1), 1–32. <https://www.tandfonline.com/action/journalInformation?journalCode=best20>
- Smolders, E., Baetens, E., Verbeeck, M., Nawara, S., Diels, J., Verdriev, M., Peeters, B., De Cooman, W., & Baken, S. (2017). Internal Loading and Redox Cycling of Sediment Iron Explain Reactive Phosphorus Concentrations in Lowland Rivers. *Environmental Science and Technology*, 51(5),

2584–2592. <https://doi.org/10.1021/acs.est.6b04337>

- Szilas, C. P., Borggaard, O. K., & Hansen, H. C. B. (1998). Potential iron and phosphate mobilization during flooding of soil material. *Water, Air, and Soil Pollution*, 106, 97–109. <https://doi.org/https://link.springer.com/content/pdf/10.1023/A:1004965631574.pdf>
- Thamdrup, B. (2000). Bacterial Manganese and Iron Reduction. *Advances in Microbial Ecology*.
- Van Beek, C. G. E. M., Hofman-Caris, C. H. M., & Zweere, G. J. (2020). Drinking water treatment and chemical well clogging by iron(II) oxidation and hydrous ferric oxide (HFO) precipitation. *Journal of Water Supply: Research and Technology - AQUA*, 69(5), 427–437. <https://doi.org/10.2166/aqua.2020.140>
- Van der Grift, B., Behrends, T., Osté, L. A., Schot, P. P., Wassen, M. J., & Griffioen, J. (2016). Fe hydroxyphosphate precipitation and Fe(II) oxidation kinetics upon aeration of Fe(II) and phosphate-containing synthetic and natural solutions. *Geochimica et Cosmochimica Acta*, 186, 71–90. <https://doi.org/10.1016/j.gca.2016.04.035>
- Vandermoere, S., Ralaizafisoarivony, N. A., Van Ranst, E., & De Neve, S. (2018). Reducing phosphorus (P) losses from drained agricultural fields with iron coated sand (- glauconite) filters. *Water Research*, 141, 329–339. <https://doi.org/10.1016/j.watres.2018.05.022>
- Withers, P. J. A., & Haygarth, P. M. (2007). Agriculture , phosphorus and eutrophication: a European perspective. *Soil Use and Management*, 23, 1–4.
- Young, E. O., & Ross, D. S. (2001). *Landscape and Watershed Processes Phosphate Release from Seasonally Flooded Soils : A Laboratory Microcosm Study*. 91–101.
- Zhang, Y., Zhu, Z., Liao, Y. G., Dang, Z., & Guo, C. (2021). Effects of Fe(II) source on the formation and reduction rate of biosynthetic mackinawite: Biosynthesis process and removal of Cr(VI). *Chemical Engineering Journal*, 421(P1), 129723. <https://doi.org/10.1016/j.cej.2021.129723>
- Zhu, T., Lai, W., Zhang, Y., & Liu, Y. (2022). Feammox process driven anaerobic ammonium removal of wastewater treatment under supplementing Fe (III) compounds. *Science of the Total Environment*, 804, 149965. <https://doi.org/10.1016/j.scitotenv.2021.149965>
- Zou, X., Wu, Y., Liu, Y., Liu, D., Li, W., Gu, L., Liu, H., Wang, P., Sun, L., & Zhang, Y. (2018). In Situ Generation of Bifunctional, Efficient Fe-Based Catalysts from Mackinawite Iron Sulfide for Water Splitting. *Chem*, 4(5), 1139–1152. <https://doi.org/10.1016/j.chempr.2018.02.023>

4.10 Supplementary material to Chapter 4: Phosphorus adsorption on iron-coated sand under reducing conditions

Victoria Barcala^{1,2}, Stefan Jansen³, Jan Gerritse³, Stefan Mangold⁴, Andreas Voegelin⁵, and Thilo Behrends²

¹ Inland Water Systems, Deltares, Daltonlaan 600, 3584 BK Utrecht, The Netherlands

² Department of Earth Sciences, Faculty of Geosciences, Utrecht University, 8 Princetonlaan, 3584 CB Utrecht, The Netherlands

³ Deltares, Unit Subsurface and Groundwater Systems, Daltonlaan 600, 3584 BK, Utrecht, The Netherlands

⁴ Karlsruhe Institute of Technology, Institute for Photon Science and Synchrotron Radiation, D-76344 Eggenstein-Leopoldshafen, Germany

⁵ Eawag, Swiss Federal Institute of Aquatic Science and Technology, Ueberlandstrasse 133, CH-8600 Duebendorf, Switzerland

The supplementary material includes: video of ICS drain construction, XAS spectra, images of the treatment bottles during the microcosm-experiment, SEM-EDX results, chemical equations used for stociochemical calculations, mass balance of Fe losses in the field, and tables with water quality results.

Video link

<https://www.youtube.com/watch?v=5ycj5CCzfpw>

XAS results

The X-ray absorption near-edge structure (XANES) and the extended X-ray absorption fine structure (EXAFS) spectra of samples and references are shown in Figure S1. The inspection of the sample spectra indicated that three reference spectra were required to describe the sample spectra by LCF: (i) silicate-containing ferrihydrite (Fh-Si) formed by the oxidation of Fe(II) in bicarbonate-buffered silicate-containing synthetic groundwater, (ii) 2-line ferrihydrite (2L-Fh) synthesized by the forced hydrolysis of a concentrated ferric iron solution (Schwertmann and Cornell, 1991) (both spectra from (Senn et al., 2017)), and (iii) mackinawite (FeS; spectrum kindly provided by Mingkai Ma, Utrecht University). Silicate-containing ferrihydrite exhibits a similar degree of edge-sharing linkage of Fe(III)-octahedra but a lower degree of corner-sharing linkage than 2-line ferrihydrite, due to the inhibiting effect of Si on corner-sharing Fe(III)-octahedra linkage. The two ferrihydrite references thus served to describe ferrihydrite with a level of Fe(III)-polymerization slightly varying from the reference materials. Indeed, the spectrum of the fresh unreacted Fe-coated sand closely matched the reference spectrum of silicate-containing ferrihydrite obtained by Fe (II) oxidation in bicarbonate-buffered solution in the presence of silicate (Senn et al., 2015), whereas LCF analysis of both the XANES and EXAFS spectra (Table S1) returned a minor contribution for the 2-line ferrihydrite (2L-Fh). This result was in good agreement with XAS characterization results for Fe in Fe-sludge and ICS derived from drinking water treatment (Chardon et al. 2021; Koopmans et al. 2020) and indicated that Fe in the coatings was contained in ferrihydrite with a slightly higher degree of polymerization than the silicate-containing ferrihydrite (Fh-Si) reference, possibly because of the aging of the coatings over the duration of sand used in water treatment.

Three of the reacted sand samples closely matched the unreacted fresh sand. Nevertheless, minor but systematic differences were observed relative to the fresh sand, most notably a slight increase of the spectral feature at 7.5 \AA^{-1} (see overlay of spectrum of fresh sand in Figure S1). These small differences may point to a slight increase in ferrihydrite polymerization during incubation, but for sure indicated that no substantial formation of a more crystalline Fe(III)-(hydr)oxide had occurred. The spectrum of the reacted sample 4 more distinctly differed from the fresh ICS. LCF analysis of the respective XANES and EXAFS spectra indicated that this difference could be described by a contribution of 7% (XANES) to 13% (EXAFS) FeS.

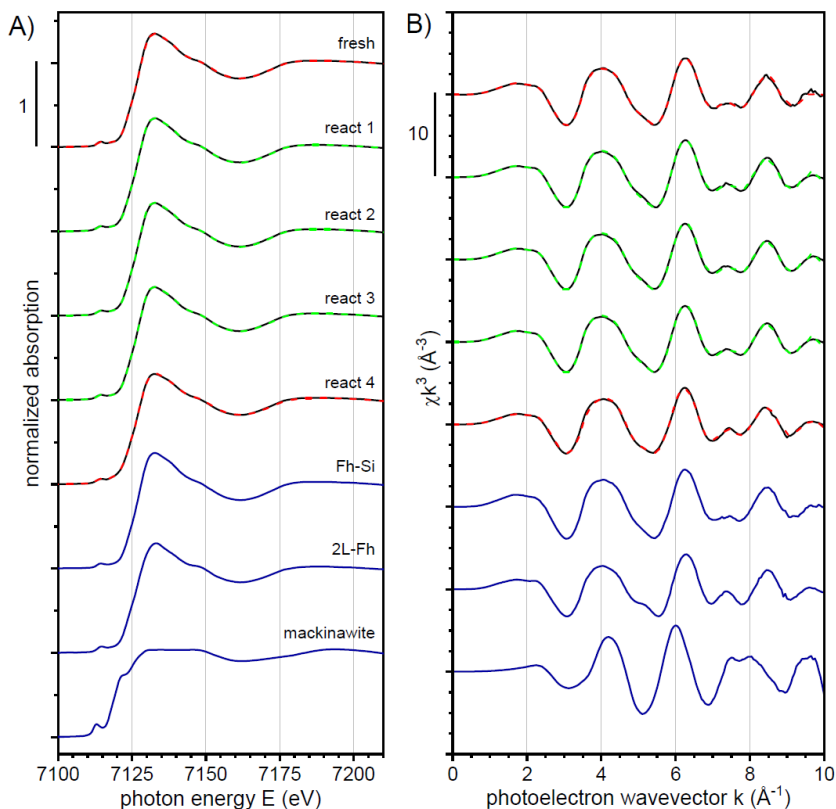


Figure S1. XANES and EXAFS spectra of the fresh unreacted Fe-coated sand and of four reacted samples in comparison to reference spectra of Fe(II)-derived silicate-containing ferrihydrite, of 2-line ferrihydrite and mackinawite (FeS). Red dashed spectra are linear reconstructions based on the LCF results listed in Table S1. Green dashed spectra represent the spectrum of the fresh unreacted sand.

Because of the apparent signs of Fe sulfidization in the non-sterile incubation experiment with added C source (acetate; anoxic), and because the sample label of the reacted sample 4 did not match with this treatment, we noted that the reacted samples must have been misplaced during pellet preparation or sample mounting in the glove box. Nevertheless, it is highly plausible that the spectrum of the reacted sample 4 corresponded to the experiment in which Fe sulfidization was inferred from color changes, solution chemistry and microscopy. We therefore conclude from the XAS results that in the non-sterile experiment with added

acetate, about 10% of the Fe was transformed into FeS during incubation, whereas in the sterile control and the experiment without acetate addition, no such transformation occurred.

Table S1. Linear combination fit results for the spectra of fresh unreacted sand and for the reacted sample 4.

		Fh-Si	2L-Fh	FeS	sum	r-factor
fresh sand	XANES	0.75	0.25	-	1.00	0.0001
	EXAFS	0.85	0.13	-	0.99	0.0024
reacted sample 4	XANES	0.58	0.34	0.07	1.00	0.0001
	EXAFS	0.61	0.26	0.13	1.00	0.0065

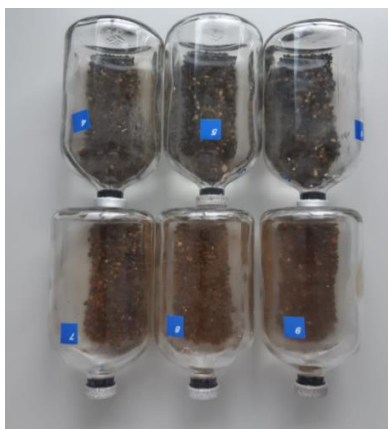


Figure S2. Observable changes in incubation: ICS grains in anoxic treatment with acetate addition turned black (top). Bottles without acetate addition (bottom) used as reference.

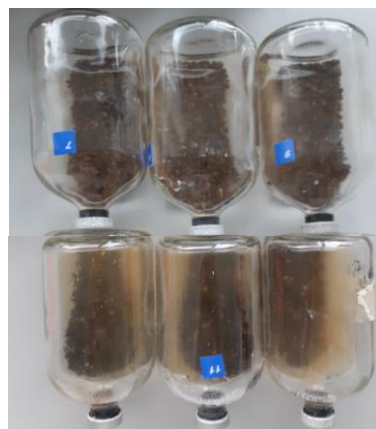
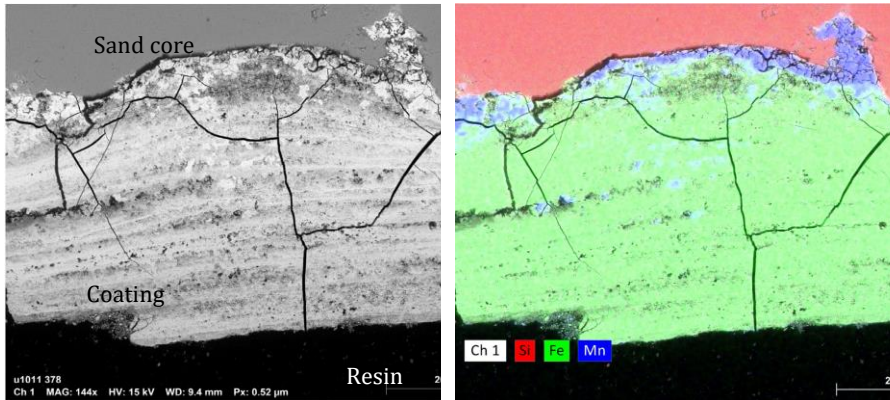


Figure S3. Observable changes in incubation: bottles with Moderately reducing addition were less transparent and had whitish precipitates (bottom). Bottles without acetate addition (top) used as reference

SEM-EDX



Atomic concentration [%]

Spectrum	Carbon	Oxygen	Silicon	Calcium	Iron
V1 1	0.00	64.70	35.30		
V1 2	0.00	64.46	35.54		
V1 3	0.00	69.19	6.50	2.30	22.02
Mean	0.00	66.11	25.78	2.30	22.02
Sigma	0.00	2.66	16.70	0.00	0.00
SigmaMean	0.00	1.54	9.64	0.00	0.00

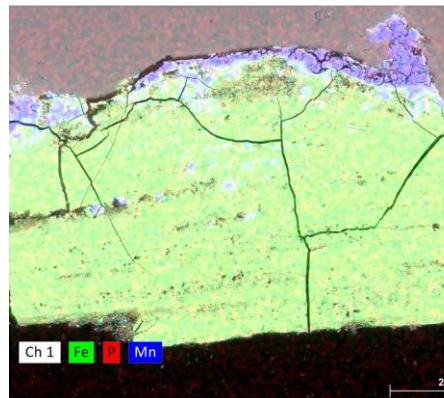
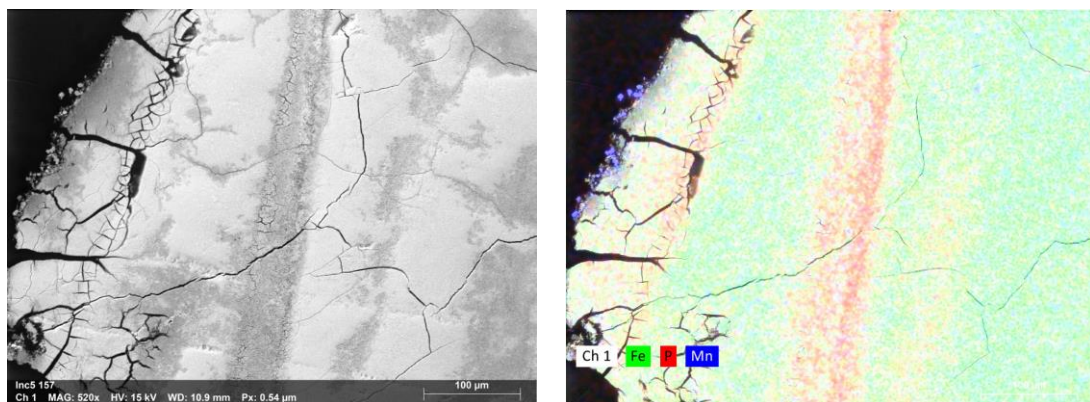
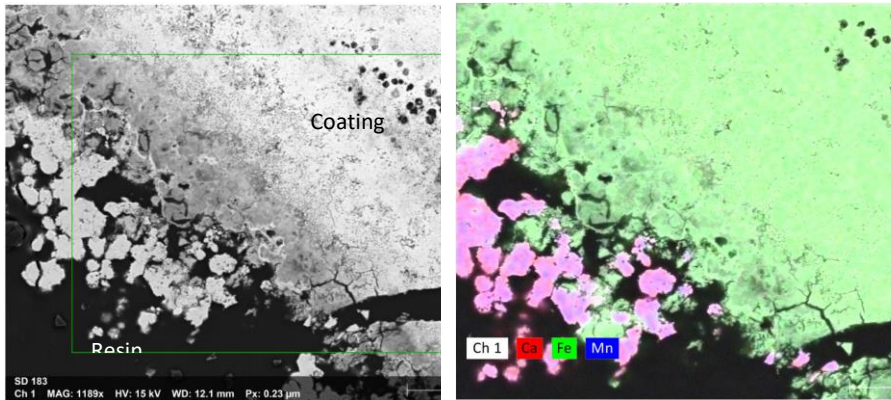


Figure S4. SEM image of ICS grain cross-section before treatment (left), EDX elemental map (right). The sand core is rich in silica, the coating is made of iron (hydr)oxides with manganese (hydr)oxides in separated areas. Points V1 and V2 were taken in the sand core and point V3 on the coating.



Element	At. No.	Netto	Mass [%]	Mass Norm. [%]	Atom [%]	abs. error [%] (1 sigma)	rel. error [%] (1 sigma)
Oxygen	8	236067	28.14	37.87	66.44	3.08	10.94
Iron	26	169628	41.53	55.88	28.09	1.24	2.99
Silicon	14	43802	2.59	3.49	3.49	0.13	5.16
Calcium	20	13757	1.35	1.81	1.27	0.07	5.00
Phosphorus	15	5940	0.35	0.47	0.42	0.04	11.38
Manganese	25	1621	0.30	0.41	0.21	0.04	12.31
Sodium	11	290	0.04	0.05	0.06	0.00	10.38
Aluminium	13	160	0.01	0.01	0.02	0.00	10.78
		Sum	74.31	100.00	100.00		

Figure S5. SEM image of ICS grain coating after adsorption and anoxic treatment with acetate addition (top-left), EDX elemental map of P (top-right), EDX analysis on a point in the high P red zone (bottom). Molar P/Fe ratio of 0.015 is in the range of typical ratios in fresh ICS



Atomic concentration [%]				
Spectrum	Carbon	Oxygen	Calcium	Manganese
SD 761	22.69	61.59	14.32	1.39
SD 762	18.67	67.21	11.82	2.30
SD 763	18.51	66.56	12.62	2.30
SD 764	19.77	65.51	12.74	1.99
Mean	19.91	65.22	12.88	2.00
Sigma	1.94	2.52	1.05	0.43
SigmaMean	0.97	1.26	0.52	0.21

Figure S6. SEM image of ICS grain coating in treatment with Moderately reducing addition (top-left), EDX elemental map of Mn and Ca (top-right), EDX analysis on 4 different points from the Ca-Mn particles (bottom)

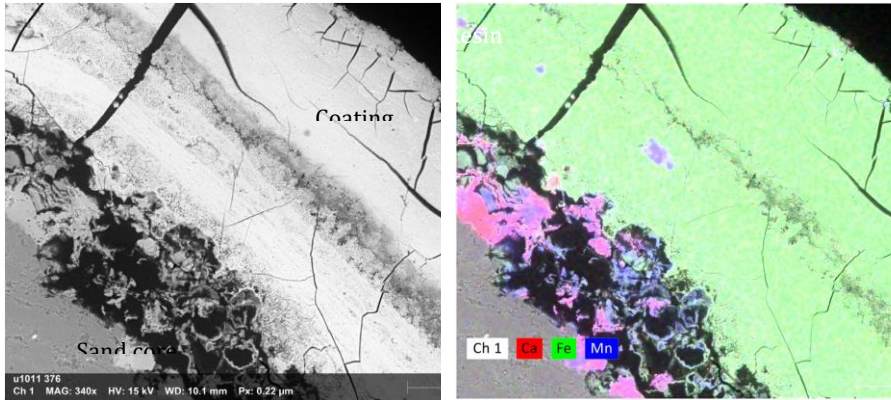


Figure S7. SEM image of ICS grain coating in treatment with Moderately reducing addition (left), EDX elemental map of Fe, Mn and, Ca(right), The Ca-Mn particles formed not only on the outside of the grain but on macropores or inner areas with originally high Mn.

Grain size distribution of the ICS

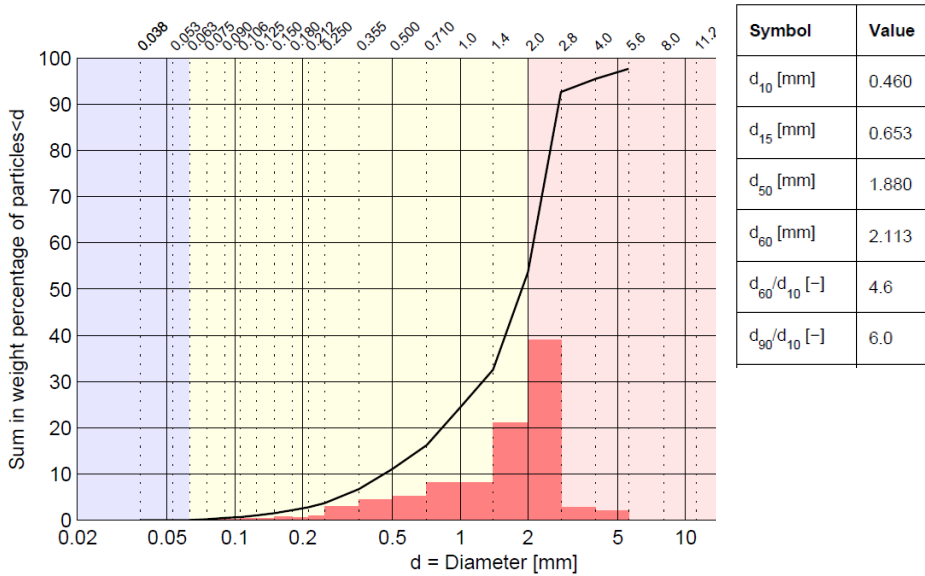
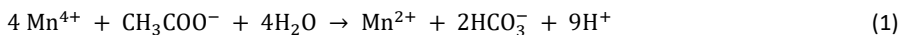
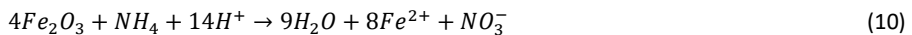
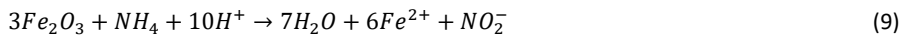
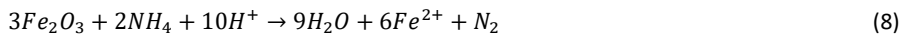
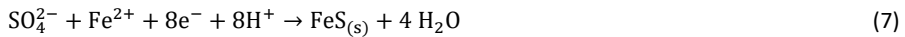
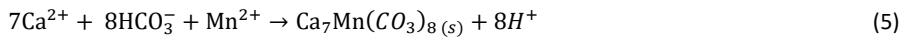
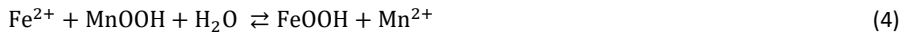
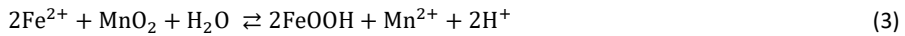
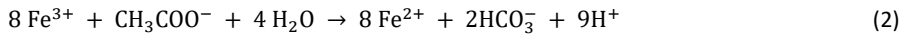


Figure S8 Grain size distribution of the ICS

Chemical equations used for stoichiometrically calculations

Equations 1 and 2 represent the dissolution of Fe and Mn, mediated by microorganisms as *Geobacter* that use acetate as a carbon source and Fe and Mn (hydr)oxides as electron acceptors (Islam et al. 2004; Villinski, Saiers, and Conklin 2003). Equations 3 and 4 represent Fe (II) re-oxidation by Mn (IV) (Postma and Appelo 2000). Equation 5 represents the precipitation of manganese containing calcium carbonates. Equations 6 and 7 represent FeS precipitation as microbes reduced sulfate from the coating and groundwater (Van Beek et al. 2021; Finke, Vandieken, and Jorgensen 2007; Kwon et al. 2016; Zhang et al. 2021). Equation 8, 9, and 10 represents the possible Feammox reactions (Zhu et al. 2022) and equation 11 denitrification.





Mass balance of Iron losses in the field per linear meter of ICS enveloped drain

Mass of Iron: each linear meter of drain, has approximately 0.015 m³ of ICS, with a density of 1770 kg/m³, and an iron content of 0.127 gFe/gICS, we get there are 26.5 kg-Fe/m or 474 mol-Fe/m.

Water balance: drains are 10 m apart from each other, therefore each linear meter drains 10 m², the estimated early rainfall is 860 mm, the yearly evapotranspiration is 450 mm, and the seepage 36.5 mm. Assuming 70 % of the groundwater is transported through the drains and the flow direction is vertical through the ICS layer, we get 3125.5 L/m/year.

Available carbon load: the measured DOC in the groundwater is 19.5 mg/L, not all the carbon will react in the drains, some may be recalcitrant organic matter, and some may not have

enough time to react. If 100 % of DOC is consumed 61 g-C/m/year are available and if 10 % is consumed 6 g-C/m/year.

Balance: When 12 g (1 mol) of C are oxidized going from C(0) to C(IV) oxidation state, 4 electrons are transferred to reduce 4 mol Fe(III) to Fe(II). Therefore, if 100 % DOC is oxidized 20 mol-Fe/m/year are reduced, and if 10 % DOC is oxidized 2 mol-Fe/m/year are reduced. If we express it as a percentage of the original mass of iron per meter of drain, we get: 4 % and 0.4% could be reduced per linear meter per year.

P removal: From the field measurements, it seems reasonable to assume a P inflow concentration of 4.5 mg-P/L and outflow of 1.2 mg-P/L (73 % removal efficiency). If 3125.5 L/m/year are drained and the removal efficiency does not decrease with time, 10.31 g-P/m/year (0.3 mol/m/year) would be removed.

Filter lifespan: It is possible now to estimate when (n_{year}) a 0.10 P/Fe molar ratio would be reached if 100 % or 10 % of the DOC is used for iron reduction and the initial P/Fe₀ is 0.013.

$$P/Fe_{n_{year}} = P/Fe_0 + \frac{n_{year} \cdot 0.3 \text{ mol P/year/m}}{474 \text{ mol Fe/year/m} - \%_{DOC} \cdot n_{year} \cdot 20 \text{ mol Fe/year/m}} < 0.10$$

If 100 % DOC is used in iron reduction a 0.10 P/Fe molar ratio is reached after 20 years and if 10 % DOC is used a 0.10 P/Fe molar ratio is reached after 80 years.

Water quality results

Table S2. Average of triplicate bottles in different treatments in the microcosm experiment

Microcosm	Day	P (mg-P/L)	Fe II (mg/L)	Tot Fe (mg/L)	Mn (mg/L)	Acetate (mg/L)	Ca (mg/L)	SO4 (mg-S/L)
Autoclaved control	1	8.31	0.94	1.70	0.92	0	65.24	3.4
Strongly reducing	1	8.32	0.96	1.72	0.89	0	65.24	3.4
Weakly reducing	1	8.32	0.91	1.68	0.95	0	65.24	3.4
Moderately reducing	1	8.31	0.95	1.57	0.98	0	65.24	3.4
Autoclaved control	2	0.02	0.00	0.00	0.92	24		
Autoclaved control	2	0.02	0.00	0.00	9.58	24		
Strongly reducing	2	0.06	0.00	0.00	0.15	2		
Weakly reducing	2	0.05	0.00	0.00	0.09	1		
Moderately reducing	2	0.17	0.01	0.03	0.02	2		
Autoclaved control	8	0.01	0.13	0.10	8.92	0		
Strongly reducing	8	0.01	0.00	0.00	1.60	0		
Weakly reducing	8	0.02	0.03	0.05	1.58	0		
Moderately reducing	8	0.02	0.00	0.00	0.00	0		
Autoclaved control	10	0.01	0.03	0.00	10.25	2316		
Strongly reducing	10	0.00	0.02	0.13	1.40	2316		
Weakly reducing	10	0.01	0.00	0.00	0.97	0		

Moderately reducing	10	0.00	0.00	0.00	0.00	2316
Autoclaved control	13	0.01	0.02	0.02	9.35	507
Strongly reducing	13	0.01	0.00	0.00	8.63	633
Weakly reducing	13	0.01	0.00	0.00	2.92	11
Moderately reducing	13	0.00	0.01	0.04	10.32	550
Autoclaved control	15	0.02	0.04	0.05	10.90	491
Strongly reducing	15	0.02	4.10	4.15	24.79	536
Weakly reducing	15	0.01	0.00	0.04	2.22	0
Moderately reducing	15	0.01	0.01	0.03	9.45	493
Autoclaved control	17	0.01	0.03	0.05	10.46	467
Strongly reducing	17	0.03	5.43	5.49	12.42	463
Weakly reducing	17	0.01	0.01	0.03	1.96	0
Moderately reducing	17	0.00	0.07	0.10	5.77	421
Autoclaved control	17	0.02	0.03	0.05	11.50	447
Strongly reducing	20	0.03	3.31	3.29	5.69	394
Weakly reducing	20	0.01	0.01	0.02	1.38	0
Moderately reducing	20	0.00	0.05	0.19	3.53	373
Autoclaved control	20	0.01	0.03	0.00	10.79	436
Strongly reducing	22	0.04	2.61	2.40	3.80	353
Weakly reducing	22	0.01	0.01	0.01	1.73	0
Moderately reducing	22	0.00	0.12	0.20	2.73	338
Autoclaved control	22	0.01	0.03	0.00	10.79	436

Strongly reducing	24	0.02	1.80	1.99	3.00	328		
Weakly reducing	24	0.01	0.03	0.09	1.85	0		
Moderately reducing	24	0.01	0.16	0.39	2.23	304		
Autoclaved control	24	0.01	0.04	0.01	10.15	407		
Strongly reducing	27	0.04	1.80	1.80	2.30	315		
Weakly reducing	27	0.01	0.01	0.01	1.83	0		
Moderately reducing	27	0.03	0.24	0.63	1.73	231		
Autoclaved control	27	0.01	0.03	0.03	9.86	383		
Strongly reducing	29	0.03	1.79	1.80	2.21	236		
Weakly reducing	29	0.01	0.00	0.00	1.90	1		
Moderately reducing	29	0.03	0.26	0.58	1.32	176		
Autoclaved control	31	0.11	0.01	0.06	9.52	401	340.1	9.9
Strongly reducing	31	0.18	1.44	1.45	1.43	264	18.4	7.8
Weakly reducing	31	0.07	0.16	0.03	1.82	0	144.2	10.4
Moderately reducing	31	0.11	0.46	0.54	0.90	155	11.3	8.9
Autoclaved control	36	0.02	0.03	0.05	9.97	367		
Strongly reducing	36	0.06	1.90	1.98	1.96	4		
Weakly reducing	36	0.01	0.59	0.89	1.87	0		
Moderately reducing	36	0.06	0.01	0.23	1.70	0		
Autoclaved control	38	0.01	0.01	0.05	9.09	335		
Strongly reducing	38	0.05	1.47	1.60	1.64	0		
Weakly reducing	38	0.01	0.05	0.06	1.94	0		

Moderately reducing	38	0.04	0.39	0.55	0.72	0		
Autoclaved control	41	0.01	0.03	0.06	8.65	0		
Strongly reducing	41	0.06	1.47	1.51	1.50	0		
Weakly reducing	41	0.00	0.01	0.04	1.78	0		
Moderately reducing	41	0.03	0.30	0.38	0.57	0		
Autoclaved control	43	0.01	0.00	0.13	7.93	0	231.3	9.7
Strongly reducing	43	0.06	1.48	1.52	0.86	0	8.50	7.3
Weakly reducing	43	0.00	0.04	0.08	1.71	0	103.1	9.9
Moderately reducing	43	0.03	0.38	0.59	0.56	0	7.73	8.8
Autoclaved control	45	0.01	0.00	0.13	7.93	0	236.0	9.6
Strongly reducing	45	0.05	1.40	1.40	0.02	0	8.56	7.2
Weakly reducing	45	0.00	0.04	0.04	1.37	0	115.0	10.3
Moderately reducing	45	0.03	0.52	0.64	0.10	0	8.02	9.0

Table S4. PH in microcosms. Day 1 was measured with electrode (877, Mtrohm Titrimo) and days 31 and 45 controlled with pH paper (Merk).

PH	Day 1	Day 31	Day 45
Autoclaved control	6.66	6.5-7	6.5-7
Strongly reducing	6.67	7.0	7.0
Moderately reducing	6.68	6.5	6.0
Weakly reducing	6.80	8.0-8.5	8.0

Table S5. Profiles of A and B fields made with GVP. Samples filtered (0.45um)

Field	Depth	pH	ORP (mV)	Tot Fe (mg/L)	Mn (mg/L)	P (mg-P/L)	P/Fe (molar)	Cl /Br ratio	NO3 (mg-N/L)	SO4 (mg-S/L)	NH4 (mg-N/L)
A	-101	7.27	-135	0.1	1.0	11.4	174.0	447.4	0.02	25.9	5.8
A	-124	7.21	-160	0.1	1.5	10.4	157.9	312.7	0.02	18.5	5.4
A	-205	7.2	-150	4.3	2.8	11.2	4.7	191.6	0.02	0.03	12.3
A	-240	6.9	-125	0.4	2.3	10.9	49.7	166.2	0.36	0.03	12.9
A	-265	7	-127	1.2	1.9	12.1	18.9	167.0	0.02	0.03	13.6
A	-300	6.9	-175	8.2	4.2	9.6	2.1	156.8	0.02	0.03	16.1
B	-120	7.76	-55	2.9	1.6	2.5	1.6	367.7	0.0	6.10	1.1
B	-148	7.46	-100	3.7	1.7	2.5	1.2	343.4	0.0	11.3	1.5
B	-181	7.3	-120	4.9	1.6	1.7	0.6	315.0	0.02	12.5	1.2
B	-195	7.4	-75	5.1	2.1	1.7	0.6	312.7	0.0	12.1	1.2
B	-246	7.6	-120	5.5	1.7	1.8	0.6	313.6	0.07	12.3	1.1
B	-275	7.4	-110	5.4	3.0	2.1	0.7	315.6	0.07	12.2	1.0
B	-310	7.3	-120	4.8	1.8	1.8	0.7	311.9	0.02	11.7	1.1
B	-340	7.3	-100	4.8	2.3	1.7	0.6	303.4	0.02	9.9	1.3
B	-372	7.3	-100	4.6	2.0	1.2	0.5	298.2	0.02	9.6	1.4

References

- Van Beek, C. G. E. M., D. G. Cirkel, M. J. de Jonge, and N. Hartog. 2021. "Concentration of Iron(II) in Fresh Groundwater Controlled by Siderite, Field Evidence." *Aquatic Geochemistry* 27(1):49–61.
- Chardon, WJ, Jan E. Groenenberg, Jos P. M. Vink, Andreas Voegelin, and Gerwin F. Koopmans. 2021. "Use of Iron-Coated Sand for Removing Soluble Phosphorus from Drainage Water." *Science of The Total Environment* 815:152738.
- Finke, N., V. Vandieken, and B. Jorgensen. 2007. "Acetate, Lactate, Propionate, and Isobutyrate as Electron Donors for Iron and Sulfate Reduction in Arctic Marine Sediments, Svalbard." *Federation of European Microbiological Societies* (59):10–22.
- Islam, Farhana S., Andrew G. Gault, Christopher Boothman, David A. Polya, John M. Chamok, Debashis Chatterjee, and Jonathan R. Lloyd. 2004. "Role of Metal-Reducing Bacteria in Arsenic Release from Bengal Delta Sediments." *Nature* 430(6995):68–71.
- Koopmans, G. F., T. Hiemstra, C. Vaseur, W. J. Chardon, A. Voegelin, and J. E. Groenenberg. 2020. "Use of Iron Oxide Nanoparticles for Immobilizing Phosphorus In-Situ: Increase in Soil Reactive Surface Area and Effect on Soluble Phosphorus." *Science of the Total Environment* 711:135220.
- Kwon, Man Jae, Edward J. O'Loughlin, Maxim I. Boyanov, Jennifer M. Brulc, Eric R. Johnston, Kenneth M. Kemner, and Dionysios A. Antonopoulos. 2016. "Impact of Organic Carbon Electron Donors on Microbial Community Development under Iron-and Sulfate-Reducing Conditions." *PLoS ONE* 11(1).
- Postma, D., and C. A. J. Appelo. 2000. "Reduction of Mn-Oxides by Ferrous Iron in a Flow System: Column Experiment and Reactive Transport Modeling." *Geochimica et Cosmochimica Acta* 64(7):1237–47.
- Senn, Anna Caterina, Ralf Kaegi, Stephan J. Hug, Janet G. Hering, Stefan Mangold, and Andreas Voegelin. 2015. "Composition and Structure of Fe(III)-Precipitates Formed by Fe(II) Oxidation in Water at near-Neutral PH: Interdependent Effects of Phosphate, Silicate and Ca." *Geochimica et Cosmochimica Acta* 162:220–46.
- Villinski, J., J. Saiers, and M. Conklin. 2003. "The Effects of Reaction-Product Formation on the Reductive Dissolution of MnO₂ by Fe (II)." *Environ. Sci. Technol.* 37(24):5589–96.
- Zhang, Yuyang, Ziyang Zhu, Yan Guang Liao, Zhi Dang, and Chuling Guo. 2021. "Effects of Fe(II) Source on the Formation and Reduction Rate of Biosynthetic Mackinawite: Biosynthesis Process and Removal of Cr(VI)." *Chemical Engineering Journal* 421(P1):129723.
- Zhu, Ting-ting, Wen-xia Lai, Yao-bin Zhang, and Yi-wen Liu. 2022. "Science of the Total Environment Feamox Process Driven Anaerobic Ammonium Removal of Wastewater Treatment under Supplementing Fe (III) Compounds." *Science of the Total Environment* 804:149965.



Chapter

5

5 Chapter 5: Transport limited kinetics of phosphate retention on iron-coated sand and practical implications

Victoria Barcala^{1,2}, Alraune Zech², LeonardOsté¹, and Thilo Behrends²

1 Inland Water Systems, Deltares, Utrecht, The Netherlands

2 Department of Earth Sciences, Faculty of Geosciences, Utrecht University, Utrecht, The Netherlands

Published in Journal of Contaminant Hydrology

<https://doi.org/10.1016/j.jconhyd.2023.104160>

5.1 Abstract

Iron-coated sand (ICS) is a by-product from drinking water treatment made of sand coated with ferric iron (hydr)oxides. It is considered a suitable material for large-scale measures for phosphate removal from natural and agricultural waters to prevent eutrophication. Previous studies demonstrated that the residence time of water must be very long to reach equilibrium partitioning between phosphate and ICS but specifics for application are missing. First, SEM-EDX images were used to support the conceptual assumption that P adsorption inside the coating is a transport-limited process. Second, a conceptual model of phosphate adsorption was proposed considering two types of sites: one type with fast adsorption kinetics and reaching equilibrium with the percolating solution, and another type for which adsorption is also reversible but described by pseudo-first-order kinetics. The latter is conceived to account for transport-limited adsorption in the interior of the coating while the former fraction of sites is assumed to be easily accessible and located close to the grain surface. Third, the kinetics of phosphate adsorption on ICS were quantitatively determined to describe and predict phosphate retention in filters under various flow conditions. The model was calibrated and validated with long-term column experiments, which lasted for 3500 hours to approach equilibrium on the slowly reacting sites. The model reproduced the outflowing

phosphate concentrations: the pronounced increase after a few pore volumes and the slow increase over the remaining part of the experiment. The parameterized model was also able to predict the time evolution of phosphate concentrations in the outflow of column experiments with different flow velocities, flow interruption, and in desorption experiments. The equilibrium partition coefficient for the experimental conditions was identified as 28.1 L/g-Fe at pH 6.8 and a phosphate concentration of 1.7 mg-P / L. The optimized first-order mass transfer coefficient for the slow adsorption process was $1.56 \cdot 10^{-4} \text{ h}^{-1}$, implying that the slow adsorption process has a time scale of several months. However, based on the parameterized model, the slow adsorption process accounted for 95.5 % of the equilibrium adsorption capacity, emphasizing the potential relevance of this process for practical applications. The implications for the design, operation, and lifespan of ICS filters are exemplarily illustrated for different scenarios.

Keywords: water treatment residuals, phosphorous, phosphorus sorbing materials, reactive transport model, mitigation measures, recycled iron oxides

Abbreviations: BET-SSA, Brunauer-Emmet-Teller specific surface area; DDL, diffuse double layer; Fe, iron; IC, ion chromatography; ICP-OES, inductively coupled plasma - optical emission spectrometry; ICS, iron coated sand; Mn, manganese; P, phosphorus; SEM-EDX, scanning electron microscope with energy dispersive x-ray spectroscopy;

Highlights

- The presented model specifically accounts for slow P adsorption kinetics on ICS
- The model is validated by column experiments with different flow scenarios
- Time scale of slow P adsorption is determined and is in the order of months
- Slow P adsorption by ICS accounts for 95 % of adsorption capacity
- Performance of ICS filters can be improved when considering sluggish kinetics

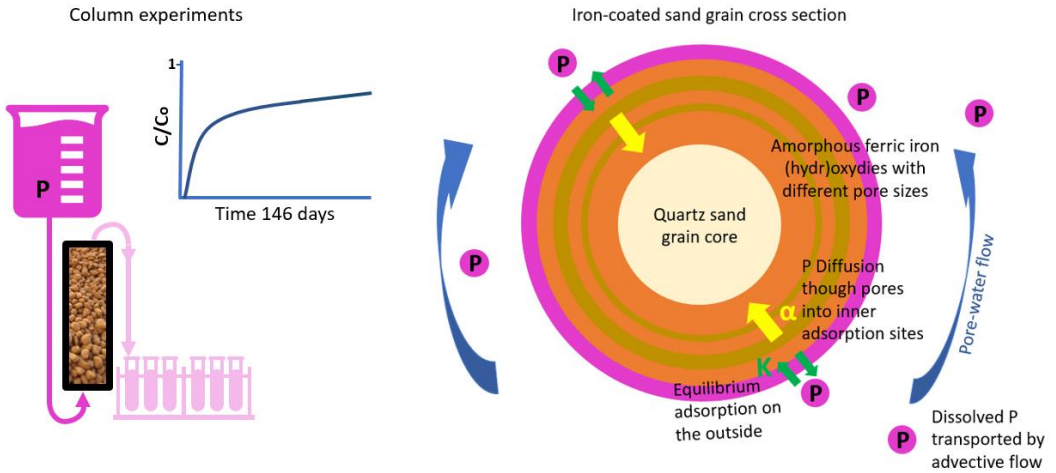


Figure 5-0 Graphical abstract.

5.2 Introduction

Particulate and dissolved phosphorus (P) losses from agriculture are a major threat to surface water quality (Bol et al., 2018; De Klein & Koelmans, 2011; Dupas et al., 2018; Kronvang et al., 2007; Schoumans et al., 2014; Withers et al., 2014). Because of the legacy P stored in the soil, reducing manure and fertilizer application is insufficient to reduce P loads reaching surface waters (Barcala et al., 2020; Bieroza et al., 2019; Gu et al., 2017; Sharpley et al., 2013). Phytoremediation, reducing the P in the soils by plant uptake, can reduce the legacy P but it will take decades before P losses to surface waters are reduced (Fiorellino et al., 2017; Koopmans et al., 2004; Lucas et al., 2021; Stoll et al., 2021). One option for short-term P load reduction is the implementation of permeable reactive barriers filled with iron (Fe)-containing materials. They can remove P from percolating water on its hydrological pathway from groundwater to surface waters (Das Gupta et al., 2012; Nur et al., 2014; Penn et al., 2011, 2017, 2020; Rittmann et al., 2011; Stoner et al., 2012). Particularly well-suited are byproducts from water treatment containing ferric iron (hydr)oxides given their easy availability and high binding affinity for P.

Iron-coated sand (ICS) and Fe sludge are residuals of deferrization of drinking water. A common procedure for deferrization is to oxidize dissolved Fe (II) and remove the produced Fe (hydr)oxides using sand filters. By this, an Fe coating develops around the sand grains resulting in ICS (Ippolito et al., 2011; Sharma et al., 2002; Van Beek et al., 2016, 2020). ICS and Fe sludge have been used to adsorb phosphate in soils, in filters around or at the end of tile drains, and in decentralized water treatment at farms (Boujelben et al., 2008; Chardon et al., 2021; Koopmans et al., 2020; Lambert et al., 2020; Moelants et al., 2011; Vandermoere et al., 2018; Zhang et al., 2022). The adsorption capacity of ICS is often underestimated as slow adsorption kinetics, controlled by intra-particle diffusion, are neglected (Ajmal et al., 2018; Koopmans et al., 2004; Willett et al., 1988). Iron (hydr)oxides in the coating of ICS are usually poorly crystalline or amorphous and exhibit a large specific surface area accounting for a high adsorption capacity (Chardon et al., 2012; Koopmans et al., 2020). However, the coating can be several hundreds of micrometers thick implying that the outer surface only represents a minor part of the total interfacial area. The outer surface of the ICS is in direct contact with the percolating water and the rates of adsorption are only controlled by the kinetics of the reaction. However, adsorption sites located in the interior of the coating can only be accessed via intra-particle diffusion.

The time scale of intra-particle diffusion is generally much longer than that of the surface reactions and, hence, the phosphate adsorption rates in the interior of the coating are transport limited. The long-term adsorption capacity of ICS can be underestimated when neglecting the slow transport limited kinetics. The time scale of the slow adsorption exceeds the duration of typical batch adsorption experiments. Chardon et al. (2012) showed that the experimentally derived adsorption capacity of Fe sludge progressively increased in batch experiments over the duration of 21 days and in column experiments which lasted 238 days even further. The relevance of processes with different time scales was also reflected in the column experiments: P concentrations in the effluent quickly increased without reaching the inflow concentrations; instead, a quasi-steady state was reached at different P concentrations depending on the amount of Fe sludge in the column. This implies that the removal efficiency of Fe-containing filters depends on the contact time of the water in the filter being a function of pore volume and flow rates.

Lambert et al. (2020) and Zhang et al. (2022) investigated phosphate adsorption on ICS in batch and column experiments. Zhang et al. (2022) reported that the P outflow concentrations reached a quasi-steady state while the experimental data in Lambert et al. (2020) only represent fast P adsorption as experiments were stopped before the quasi-steady state was reached. In both studies, the Bohart-Adams model was applied to describe the breakthrough curves of phosphate. The Bohart-Adams model only accounts for the kinetics of one irreversible adsorption reaction and, consequently, its performance is limited when dealing with processes proceeding with different paces. Lambert et al. (2020) parameterized the model for the pronounced increase in dissolved P concentrations until adsorption equilibrium is reached for the fast-reacting sites. However, when changing flow velocities, the contribution of the slow adsorption processes to P retention varied and, consequently, column experiments with different flow velocities required individual optimization of model parameters. In particular, the obtained P adsorption capacity was larger for the column operated at slow flow than that at fast flow, and both were significantly larger than the capacity obtained in a 1-day batch experiment. Furthermore, Lambert et al. (2020) reported that a pilot filter operated with intermittent resting periods performed better than when operated with continuous flow for the same treated volumes. These results demonstrate that slow adsorption kinetics need to be considered for optimizing the operation of ICS filters and the need for a reactive transport model, which accounts for the kinetics of both, fast and slow, adsorption processes. Here and in the following, the term 'kinetics' is used in the broadest sense, encompassing rates and mechanisms of chemical reactions as well as transport processes such as diffusion (Zhang, 2008).

The objective of this study was to develop a quantitative model for phosphate adsorption on ICS that can adequately account for slowly proceeding phosphate adsorption, which can be easily implemented and applied to optimize the operation of ICS containing filters. Electron microscopy in combination with energy-dispersive X-ray spectroscopy was used to illustrate the model consideration that phosphate retention in the interior of the iron coating is transport limited. A process-based physical model, including kinetic adsorption of phosphate on ICS, was parameterized using long-term column measurements. The model represents the slow kinetics dominated by the diffusion of phosphate inside the ICS coating and the fast adsorption on the outer surface of the ICS. It is shown that the model can be a valuable tool

to optimize the design and operation of ICS filters over their whole lifespan with different flow velocities and intermittent flow regimes.

5.3 Materials and methods

Iron Coated Sand

The ICS used in this study was provided by AquaMinerals BV (<https://aquaminerals.com/en/>). The material was obtained from one mixed batch originating from different drinking water production sites. The ICS received no pre-treatment, was obtained air-dried, and stored in the dark at room temperature. The ICS contained on average 127.2 mg/g Fe, 9.4 mg/g Mn, 0.5 mg/g S, 9.6 mg/g Ca, and 0.9 mg/g P (± 0.1 mg/g standard deviation) determined by total destruction. The Brunauer-Emmet-Teller specific surface area (BET-SSA) was 71.2 m²/g and was determined using argon gas with an ASiQwin instrument (Quantachrome Instruments). In addition, the pore size distribution in the ICS was determined with the BET-SSA analysis, nano-pores with a diameter between 0.42 and 2.00 nm were related to 54% of the specific surface and mesopores between 2.00 and 50.0 nm to 46%. Details of the measurement are specified in the *Supplement Material*.

Column Experiments

We performed flow experiments in 3 columns, named I, II, and III. The three columns were made from transparent polyethylene tubes of 30.8 cm height and 4.3 cm internal diameter. The column dimensions were selected accounting for dispersivity and reducing boundary flow effects along the tube walls (Bromly et al., 2007; Lewis & Sjöstrom, 2010). The reactive core of the columns contained 30 g of ICS and 300 g of quartz sand, both with grain diameters between 1.18 mm and 2.00 mm. The ICS was mixed with quartz sand to reduce the breakthrough times by maintaining column dimensions according to recommendations based on previous column experiments (Bromly et al., 2007; Lewis & Sjöstrom, 2010). Quartz sand is commonly used as an inert filling material in column experiments (Chardon et al., 2012; Jerez & Flury, 2006; Mystrioti et al., 2015; Pérez-López et al., 2007) and it is assumed that it does not contribute to phosphate retention in the columns. This implies that equilibrium constants or partition coefficients K_p [L/g] determined for the whole stationary phase can

be normalized to the content of ICS. Two layers of 180 g quartz gravel (> 2 mm) were added at the top and bottom of the columns to improve the flow distribution.

The columns were fed from the bottom via tubes of 0.8 mm internal diameter, which were also used for the outflow. The total volume of the tubing was 14.5 cm³ and taken into consideration in the parametrization of the models. The inflow solution was stored in 10 L glass bottles protected from the light with black plastic bags. The bottles' cups were modified to work as Mariotte bottles (Maroto et al., 2002) to maintain a constant head pressure of approximately 2 cm above the columns assuring full saturation. A peristaltic pump (Masterflex L/S) with its tubing (13 L/S, Masterflex) was used for each column to maintain a constant flow. The pump-tubes system was calibrated before the experiment to know the discharge obtained at a given pump speed. Different flow regimes were used in the three different columns, including constant flow at various velocities, but also variable flow patterns. Furthermore, one column was used for a desorption experiment. The flow rates chosen are in the range of the flow velocities measured in field applications (Barcala et al., 2022; Groenberg et al., 2013). The flow rate in column I was 0.65 ml/min for 3500 hours (over 560 pore volumes).

For the first 1440 hours, column II was running in parallel to column I with a flow rate of 0.65 ml/min. Afterward, the flow rate was reduced to 0.39 ml/min for 600 hours. We also aimed to maintain the flow rate in column III at 0.65 ml/min during the first 1440 hours of the experiment but clogging occurred. The cause of the clogging was the obstruction of the outflow tube by particles. The issue was solved by flushing the tube with water. The tube was cleaned six times during this period. Although unintended, clogging provided the opportunity to study the effect of interrupted flow and the data were included in this study. After the problematic tube had been replaced for a new one, column III was used without interruptions during 720 hours in a desorption experiment at 0.65 ml/min. In addition, a second adsorption experiment with a flow rate of 0.39 ml/min was performed in column III for the last 600 hours. Adsorption experiments were performed with a solution prepared from demineralized water containing 1.70 ± 0.05 mg /L P in the form of monobasic sodium phosphate solution. In order to maintain the ionic strength constant 0.10 M NaCl was also added. The desorption experiment was performed with 0.10 M NaCl without P. The pH was adjusted with NaOH to

6.80 ± 0.05 and controlled weekly in the inflow and outflow. The retention times at 0.65 mL/min were 375 min in column I, 329 min in column II, and 301 min in column III.

Samples were collected every 8 hours with an autosampler (SC-4DXS, Elemental Scientific) in 50 mL PE centrifuge tubes pre-acidified with 1 mL 6M HCl. The volume collected by the autosampler served as a periodic control of the flow rate. P concentrations [mg/L] (equivalent to mg-P/L) in samples were measured photometrically (DR3900, Hach), as samples form a blue complex that follows Beer's law when reacting with an acidified ammonium heptamolybdate solution and freshly added ascorbic acid (Murphy & Riley, 1962). For the first 40 days, one sample per day was analyzed with ICP-OES (Avio 500, Perkin-Elmer) as an independent measurement. Because Stanmod (Simunek et al., 1999; Van Genuchten et al., 2012) can only deal with constant flow velocities, the data series from columns I and II were quality checked and a few points that were affected by flow rate reductions were removed. Preliminary tracer experiments were performed in all columns to determine pore volumes and porosities. For this 0.10 M NaCl solution was used containing additionally 0.10 M NaBr. The flow was 0.65 ml/min. Samples were taken manually every 12 minutes for 9 hours. Electric conductivity (EC) was measured and bromine (Br) concentrations were determined by ion chromatography (ICS6000, Thermo Scientific) to determine the breakthrough of the non-reactive tracer.

ICS Imaging techniques

SEM-EDX images and elemental maps were made for fresh ICS and for ICS after adsorption from column III. The grains were embedded in resin and polished to investigate cross-sections. Secondary electron and backscattered electron images were acquired on a SEM (EVO 15, Zeiss), using the SmartSEM user interface (v 6.06). (Semi-) qualitative chemical compositions were obtained using EDX (Esprit v. 2.1, Bruker XFlash). The images helped to conceptualize the two-site adsorption model. The first type of sites was considered to describe fast adsorption kinetics of the sites close to the grain surface reaching equilibrium with the percolating solution. The second type of sites describe transport-limited kinetic adsorption in the interior of the coating.

Reactive Transport Model

The conceptual model was parametrized into a reactive transport model using the advection-dispersion equation, and including two reactive adsorption terms. In order to account for different adsorption rates, two types of adsorption sites were included: fast-reacting sites for which the reaction progresses in time scales shorter than the hydraulic residence and conceived to reach equilibrium with the P concentrations in the mobile phase, and sites for which the adsorption is kinetically controlled. Adsorption of P to ICS is conceived as a reversible process. The fast adsorption process was characterized by linear adsorption using an equilibrium partition coefficient (K_p). The assumption of linearity is warranted at relatively low P concentrations as the relative occupation of adsorption sites remains low in equilibrium and the concentrations of occupied sites can be neglected in the mass balance for the reactive sites. When the content of vacant sites can be assumed to be constant, the kinetics of P adsorption to ICS simplify to pseudo-first-order rate laws for P adsorption and desorption solely depending on the P concentration in the mobile phase and P adsorbed to slowly reacting sites, respectively. The derivation of the equations is available in the *Supplementary Material*.

Based on this conceptual model, the corresponding mass balance equations for P in the mobile and stationary phase in one-dimension read:

$$\left(1 + \frac{\rho f K_p}{\theta}\right) \frac{\partial c}{\partial t} = D \frac{\partial^2 c}{\partial x^2} - v \frac{\partial c}{\partial x} - \frac{\rho \alpha}{\theta} (s_{eq} - s) \quad (\text{equation 1})$$

$$\frac{\partial s}{\partial t} = \alpha (s_{eq} - s) \quad (\text{equation 2})$$

Where c is the P concentration [mg/L] in the mobile phase, x is the longitudinal coordinate [cm], t is time [h], ρ is the bulk ICS density [g/L], f is the fraction of fast reacting sites, θ is the porosity, K_p is the equilibrium constant or partition coefficient [L/g], D is the dispersion coefficient [cm²/h], v is the pore-water velocity equal to the darcian flow velocity divided by porosity [cm/h], α can be attributed to the rate constant for P desorption but also conceived as the exchange coefficient between the stagnant and mobile phase [1/h] (see *Supplementary Material* for details), and s is the P concentration in the solid phase for which adsorption is kinetically controlled [mg/g]. s_{eq} is not an extra variable but the equilibrium concentration in the solid phase of the slow sites equal to $K_p(1 - f)c$. The concentration of

P bound to the fast-reacting sites, being in equilibrium with the percolating solution, is not a state variable in the model but is calculated based on the product of f , c , and K_p .

Model Solution and Parameter Estimation

At constant flow and constant P concentrations in the inflow, the equation system has an analytical solution that has been implemented in the code Stanmod (Simunek et al., 1999; Van Genuchten et al., 2012). We used the module CXTFIT (Toride et al., 1995) for parameter estimation that minimizes the root mean squared error (RMSE) between the experimental and calculated concentrations.

The hydraulic properties, pore-water velocity v , and the porosity θ , of each column, were determined separately from the tracer experiments. We identified adsorption parameters f , α , and K_p by calibrating the P concentrations in the effluent of column I over the first 690 hours of the experiment. During the first 690 hours, ICP-OES was used to measure P concentrations. Afterward, the photometric method was used, having a higher analytical uncertainty and some irregularities occurred in the flow such as short periods of flow decrease. These points were still included in the data series as the long-term P retention could still be observed. The model was validated by calculating RMSE and the coefficient of determination (R^2) for the effluent concentrations in column I over the whole experiment duration of 3500 hours, the concentrations in column II during the first 1440 hours, and the P concentration of the last 600 hours of column III. In the latter case, the experiment was conceived as an independent P-removal experiment and any possibly remaining P in the column after the preceding adsorption and desorption experiments was neglected.

For variable flow rates, equations 1 and 2 do not have an analytical solution. Therefore, we implemented a numerical solution using the R-packages `ReacTran` and `deSolve` (Soetaert & Herman, 2009; Soetaert & Meysman, 2012; Soetaert & Petzoldt, 2010). The model in R was fed with the calibrated parameters obtained from column I. The dynamic model allows to validate the experiment with intermittent flow velocities (flow interruptions). We calculated the RMSE and R^2 between the parametrized model's results and the effluent of column III during the flow interruptions and for the desorption experiments. The model is available at https://github.com/victoriabarcala/ICS_adsorptionmodel.

The optimized value for K_p is conditional and accounts for the affinity of sorption sites for P at the given conditions plus the total concentration of sites. For example, phosphate adsorption to ferric iron (hydr)oxides depends, among other factors, on pH and ionic strength (Morel & Hering, 1993). To assess the possibility to extrapolate the model to other conditions, we compared the obtained value of K_p with calculated values based on surface complexation models. For this, the generic diffuse double layer (DDL) model parameterized by Dzombak and Morel (1991) for hydrous ferric oxide and implemented in MINEQL(version 5.0) was used to calculate the P partition for the given experimental conditions and calculate the corresponding K_p .

Practical example

We used the numerical R-model to set up a practical example illustrating the implications of considering the kinetics of P adsorption in the application of ICS. The example considers the use of ICS to remove dissolved P from water at the effluent of tile drains installed in an agricultural area. Thus, the chosen setting parameters are close to reality. The average P concentration in the incoming water is assumed to be 1.0 mg/L and the target P concentration should be below 0.15 mg/L after passing the filter. This concentration was chosen as the Dutch implementation of the water framework directive establishes a 0.15 mg/L limit in total phosphorus for open regional waters such as ditches (Fraters et al., 2021). The filter has a porosity of 0.50, 1770 g/L bulk density with a Fe concentration of 0.13 mg-Fe/g-ICS, and the filter dimensions are 40x40x40 cm. The flow rate during operation is 4 L/h. We compare the efficiency of four different filter operations: (i) continuous flow, (ii) resting 3 months a year (during summertime), (iii) resting 1 week, and (iv) 2 weeks per month.

5.4 Results

Microscopy and ICS analysis

The coatings around ICS grains have a thickness between 100 μm and 300 μm and often exhibited an anisotropic structure (Figure 5-1). The Fe-rich coating is traversed by Mn-rich layers typically exhibiting a higher porosity (Figure 5-1-a and 1-b). In the investigated coatings, EDX analyses show a distinct P enrichment in their outer part (Figure 5-1-d, highlight point 1 and 1-f, point 4, EDX spectra are available in the supplementary material). In the outer parts

(Figure 5-1-f point 4), comprising about 20 % of the coating, P/Fe ratios were around 0.040 and about 10 times larger than in the P-poor areas (Figure 5-1-f, point 5) with ratios about 0.004. Additionally, several thin layers with elevated P/Fe ratios were identified close to the core (Figure 5-1-f point 3). No P was detected in the Mn-rich areas (Figure 5-1-f point 6). The coatings were disrupted by several cracks. Some of the cracks exhibited P enrichments at the margins (Figure 5-1-d, point 2). However, most cracks seen on Figures 1-c and 1-d do not show this feature and were possibly created when vacuuming the sample before SEM analysis.

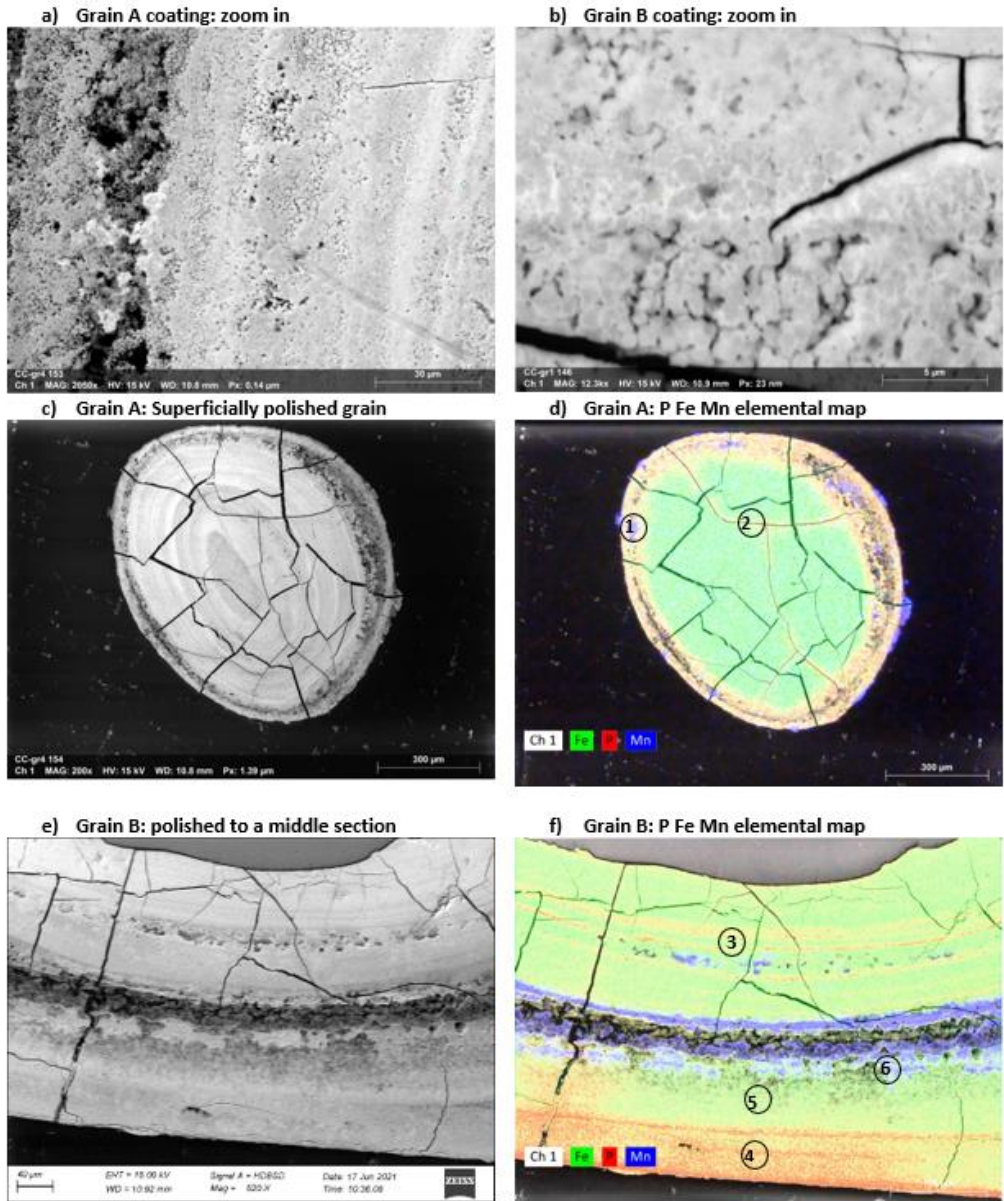


Figure 5-1: SEM-EDX images of ICS grains from column III after adsorption experiments. While grain A (c&e) is superficially polished, grain B (d&f) shows a cross-section. Electric high tension (EHT), scales and working distances are indicated on each image.

Adsorption experiments

The general features of the time evolution of P concentrations in the effluent of column I were representative of the adsorption experiments with all columns. After an initial increase in outflow concentrations, a quasi-steady-state was reached at concentrations lower than in the inflow solution (Figure 5-2-a). Between hours 240 and 960, the outflow concentrations were about 1.05 mg/L for column I representing 62 % of the inflow concentration. The pronounced increase in P concentrations occurred significantly later than the hydraulic retention time, reflecting the retention of P via adsorption also at the beginning of the experiment. A one-site model assuming equilibrium partitioning of P cannot trace the measured effluent P concentrations (Figure 5-2-a). In particular, the model cannot produce a prolonged period of virtually constant concentrations below inflow concentration. In contrast, the two-site model based on equations 1 & 2 was able to reproduce the features of the concentration curve including the pronounced increase after the first days of operation and the plateau concentration reached after about 240 hours (Figure 5-2). The equilibrium constant for the fast sites K_p was identified with 0.155 L/g for the ICS-sand mix and 3.57 L/g for pure ICS with 95% confidence intervals [1.15, 5.98] L/g (Table 5-1). The small value for the fraction of fast adsorption sites f , 0.045, indicates that most adsorption sites were located within the Fe coating. The small value for the mass transfer coefficient α , $1.56 \cdot 10^{-4} \text{ h}^{-1}$ reflects the slow transfer process. Hydraulic parameters have been identified separately through tracer tests, which showed recovery rates of 97%. The dispersion coefficient D was fitted to $30 \text{ cm}^2/\text{h}$, and the Peclet number to 5.05. The tracer test curves and sensitivity analysis of the parameters in Stanmod are available in the *Supplementary Material*.

The model was first validated for column I by modeling the whole duration of the experiment (3500 hours) beyond the first 960 hours for which parameters were determined. The larger deviation between observed and calculated data is associated with an increase in analytical uncertainty due to the switch in the analytical method. Notably, the model accounted for the slow increase in P concentration as the system was approaching equilibrium (Figure 5-2-b and 3-b). The change in outflow concentration due to the slow adsorption process is emphasized when comparing concentrations at an early and a late stage of the experiment in Figure 5-3-b.

By the end of the experiment the effluent concentration in column I reached around 1.35 mg/L, corresponding to a P content in the solid phase of around 2.16 mg/g-ICS or 17.0 mg/g-Fe (0.03 P/Fe molar ratio). At this moment, the effluent concentrations were still below the inflow concentration implying that equilibrium was not reached. With the model we extended the running-time to two years, the projected outflow P concentration was 1.60 mg/L (94 % of the inflow concentration) and the concentration in the solid phase was 6.00 mg/g-ICS or 47.02 mg/g-Fe. This value is close to the expected P loading in equilibrium ($s_{eq_{tot}} = c \cdot K$) of 6.07 mg/g-ICS or 47.57 mg/g-Fe (0.09 P/Fe molar ratio). We thus conclude that when the experiment ended, about 36 % of the equilibrium concentration in the solid was reached.

We obtained more validation results by running the transport model for the other columns with the parameters f , α , and Kp identified for column I and the specific hydraulic parameters for each column. The model reproduced very well the effluent concentrations from column II (Figure 5-2-c, Table 5-1) and column III (Figure 5-2-d, Table 5-1) at different flow velocities. When column III reached quasi-steady-state the effluent concentrations were around 0.75 mg/L and significantly lower than the values reached in columns I and II with higher flow velocities. The flow rate in column II was decreased to 0.39 ml/min to investigate the effect of changing the flow rate on the P concentrations at quasi-steady-state. As expected, P concentrations decreased and stabilized at a new quasi-steady-state about 0.2 mg/L lower than effluent concentrations of column I (Figure 5-3-a) illustrating the increasing effect of the slow adsorption process at increasing contact time.

Stop-flow situations were studied with the early column III data where unintended flow interruptions due to obstructions in the outflow tube. Our conceptual model predicts the transfer of P from fast to slow sites due to diffusion during stopped flow accompanied by decreasing concentrations of dissolved P in the column. Consequently, we expect lower P concentrations in the effluent after resuming the flow, similar to the initial phase of the column experiments. Indeed, at most flow interruptions, the P concentrations in the effluent followed the expected pattern and the previous concentrations were approached with some retardation (Figure 5-4-a).

Table 5-1: Summary of tracer experiment results, as well as results of model calibration and validation for column experiments

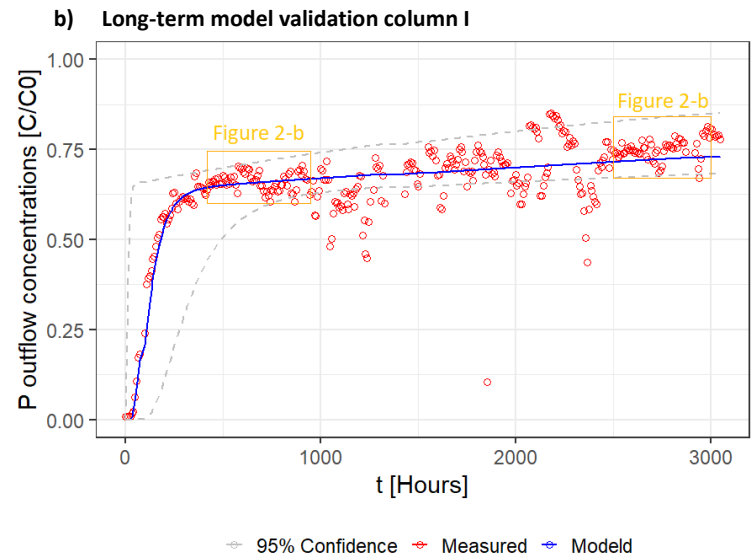
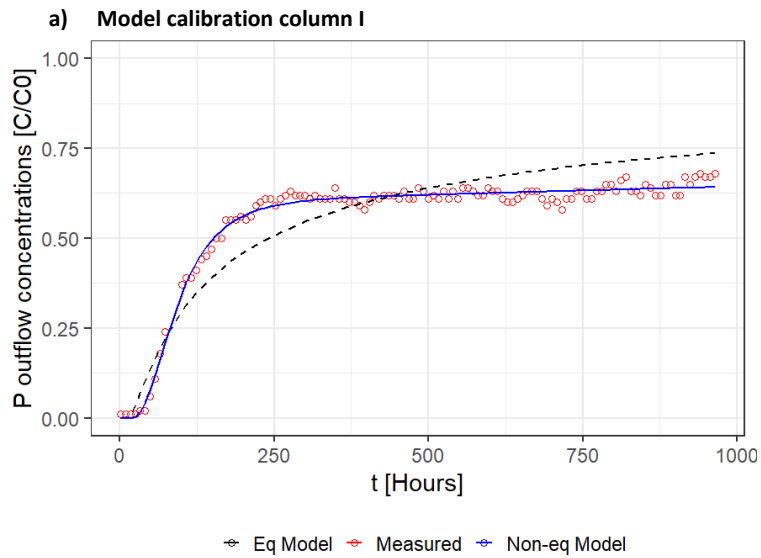
Tracer experiment			
	column I	column II	column III
Hydraulic retention time (min) (at 0.65 mL/min)	375	329	301
Porosity Θ	0.55	0.49	0.44
Pore volume (mL)	243	241	196
Flow velocity v (cm/h) at 0.65 mL/min	4.92	5.55	6.09
Flow velocity v (cm/h) at 0.39 mL/min	-	3.33	3.66
Calibration, figure 5-2-a			
	K_p [L/g]*	α [1/h]	f
Column I, adsorption, 4.92 cm/h, 960 h	0.155	1.56e-4	0.045
Lower 95% confidence interval	0.05	1.47e-4	0.012
Upper 95% confidence interval	0.259	1.65e-4	0.076
R^2	0.988		
RMSE (mg/L)	0.03		
Validation			
		r	RMSE (mg/L)
Column I, adsorption, 5.55 cm/h, figure 5-2-b, 3024 h		0.88	0.138
Column II, adsorption, 5.55 cm/h, figure 5-2-c		0.99	0.058
Column III, adsorption, 3.66 cm/h, figure 5-2-d		0.98	0.059
Column III, stop-flow, 6.09 cm/h, figure 5-4-a		0.91	0.182
Column III, desorption, 6.09 cm/h, figure 5-4-b		0.96	0.074

* K_p is of the ICS-sand mix. The K_p of the ICS is 3.57 L/g, 95% confidence intervals [1.15, 5.98] L/g. For the equilibrium model, parameter fitting yielded unrealistic values in order to approach the quasi steady state concentrations after the initial rise in P concentrations: K_p was 2.2 x1034 L/g with 95% CI [-5.6 x1035, 6.1 x1036] L/g, D was 0.169x1038 cm with 95% CI [-0.434 x1039cm, 0.468 x1039cm], and R^2 was 0.82.

The numerical model was able to reproduce the stop flow regime in column III (R^2 0.91, Table 5-1). Figures 4-c and 4-d show the calculated time evolution of the concentrations in the mobile and stationary phases inside column III. The flow interruptions were reflected in a pronounced decrease in dissolved P concentrations, in particular at the lower part of the

column where the solution was entering. The continuation of P adsorption during stopped flow resulted in increasing contents of adsorbed P (Figure 5-4-d). After 1481 hours but only 693 hours with flow, 1.39 mg/g-ICS of P were adsorbed, being 22% of the equilibrium concentration. Later, 0.57 mg/g (about 40% of the previously adsorbed mass) was recovered in the desorption experiment, in 720 hours.

The transfer of phosphate from fast to slowly reacting sites becomes less efficient when the slow sites approach equilibrium as the distance from equilibrium ($s_{eq} - s$), which drives the transfer, becomes smaller. During the desorption experiment in column III, the effluent concentrations decreased and reached a quasi-state concentration of about 0.4 mg/L (Figure 5-4-b). This can be attributed to the release of P from the slow-reacting sites. The quasi-steady-state behavior was well reproduced by the model while the agreement between the model's results and observation is lower in the transition period as concentrations drop faster than predicted. The desorption process was modeled with the same mass transport rate (α), implying that transport limitations also retard desorption. Consequently, techniques only relying on P desorption may not be efficient for phosphate recovery due to the long time-scale of desorption.



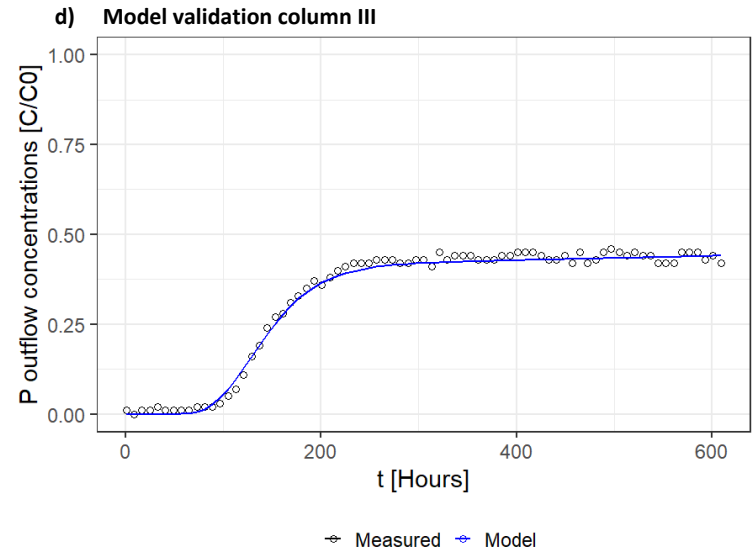
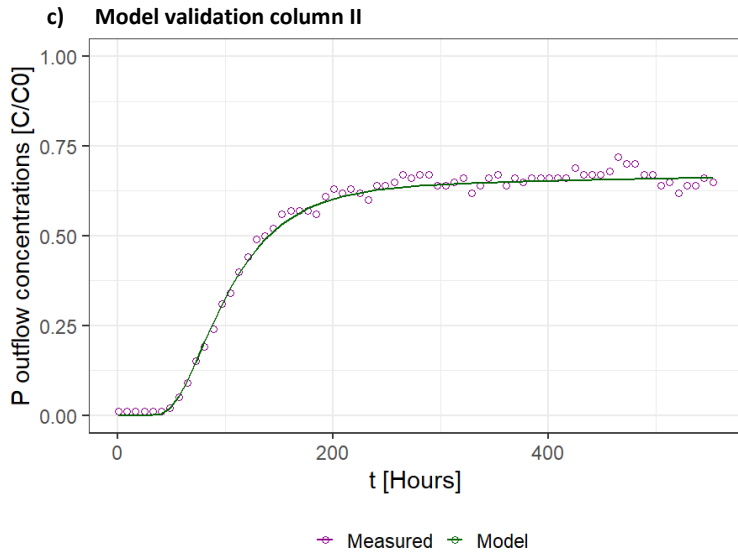


Figure 5-2: Results from continuous flow adsorption experiments and reactive transport model implemented in Stanmod with different pore-water velocities, a) model calibration column I at $v = 4.92$ cm/h the black dashed line in a shows the best fit using a one-site equilibrium adsorption model, b) long-term validation in column I at $v = 4.92$ cm/h, c) validation in column II at $v = 5.55$ cm/h, and d) validation in column III at $v = 3.66$ cm/h. The black dashed line in a shows the best fit using a one-site equilibrium adsorption model. The inflow concentration C_0 is 1.70 mg/L.

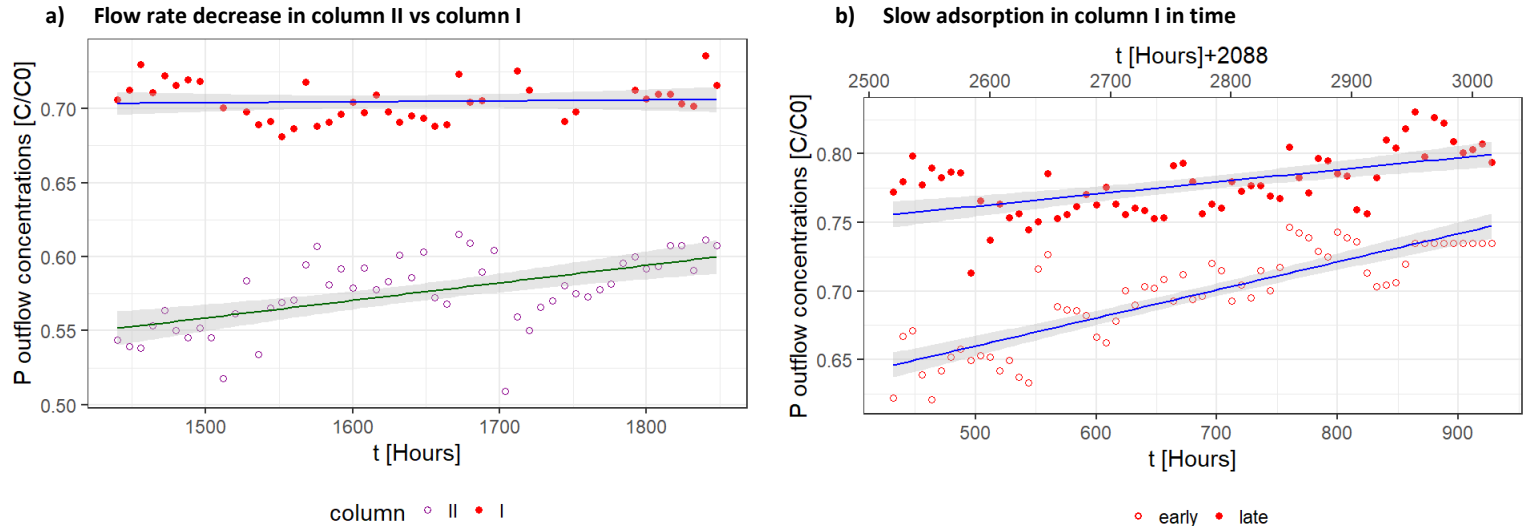
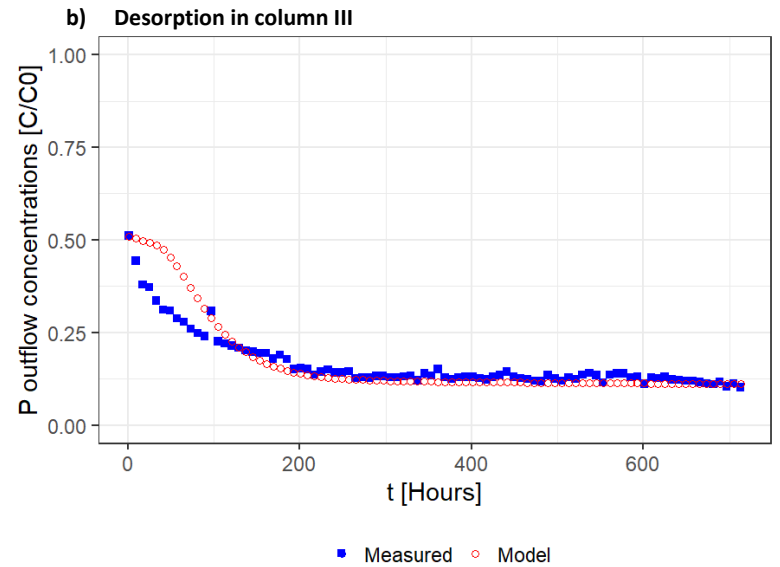
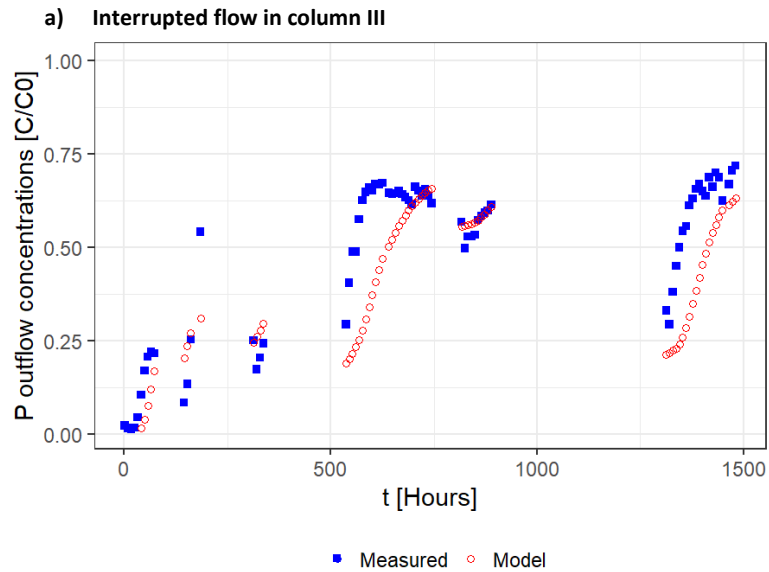


Figure 5-3: Measured concentrations during slow adsorption. a) Effect of flow rate decrease: column II with $v = 3.33$ cm/h and column I with $v = 4.92$ cm/h at a late stage of the experiment. b) Differences in the slow adsorption in column I with time: steeper increase at early times (hour 460 to 930) compared to late time (hours 2520 to 3020). Shaded areas indicate 95% confidence interval of the trend lines. The inflow concentration C_0 is 1.70 mg/L.



**c) Model results for interrupted flow in column III
P in the mobile phase [mg/L]**

**d) Model results for for interrupted flow in column III P adsorbed
[mg/g]**

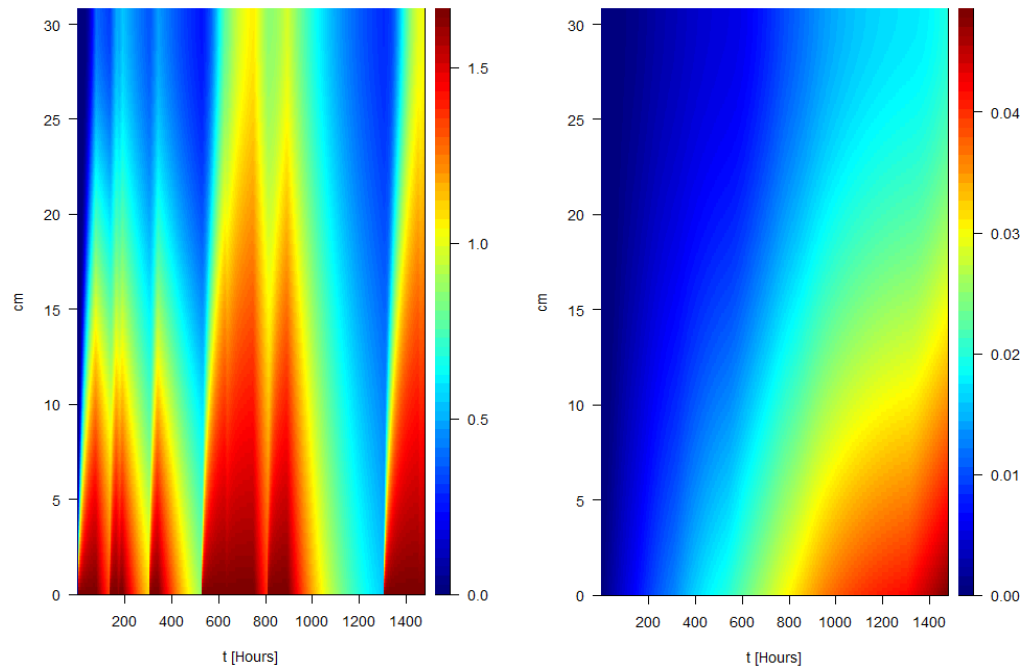


Figure 5-4: Column III results of P concentrations. The inflow concentration C_0 is 1.70 mg/L. a) Measured and numerically modeled P in the outflow during interrupted flow, b) measured and modeled outflow P during desorption, c) P in the mobile phase along the column during the experiment with flow interruptions, d) adsorbed P content along the column during the experiment with flow interruptions.

5.5 Discussion

Expediency of the two-side model

Considering a transport limited kinetic adsorption process in a two-site model was crucial to reproduce P outflow concentrations of long-term column experiments. The two-site adsorption model proved suitable to describe and predict P retention for different operational scenarios, including the variations in constant flow velocities, interrupted flow, and desorption. Although parameterized for one column experiment for a limited duration, it was able to reproduce the features of the observed effluent P concentrations in all other experimental settings.

In particular, quasi-steady-state concentrations, being key in determining the P removal throughout the experiments, were well reproduced at all flow conditions. Only during transient flow periods, when resuming the flow or after abrupt changes in inflow concentrations, the predictive capability of the model was lower. The apparent delay in the predicted P concentrations in the outflow after flow interruptions or in the desorption experiment can be partially attributed to the remaining solution in the inert gravel layer at the top of the column. This layer is not included in the dynamic model and dissolved P concentrations do not change during no-flow concentrations due to the absence of ICS.

The reactive model does not include an explicit description of the intra-coating diffusion process. Instead, the transport limitation is accounted for in the parameter α , which can be interpreted as an exchange coefficient between the stagnant phase (intra-coating porosity) and a mobile phase (see Supplementary Material for details). An equivalent approach was used before to describe phosphate desorption from soil particles (Koopmans et al., 2004). Adsorption was considered to be reversible and to follow a linear isotherm. The desorption experiment demonstrates that adsorption of P to ICS is reversible. Studying P adsorption onto ICS, Lambert et al. (2020) employed Langmuir and Freundlich isotherms for dissolved P concentrations in the range of 0-1200 mg/L. Both isotherms may be approximated by a linear relationship at concentrations lower than 20 mg/L. In our study, dissolved P concentrations remain below levels at which deviation from linearity is typically reported for P adsorption isotherms and solid phase contents remain below the saturation capacity, for example,

reported for ferrihydrites (Wang et al., 2013). The linear approximation is justified in the context of applying ICS for P removal in drainage water in the Netherlands which typically have soluble reactive phosphate concentrations below 2 mg/L P (Rozemeijer et al., 2014).

Model Parameters

Despite the dilution of ICS with non-reactive sand and the long duration of the experiment, equilibrium between dissolved and adsorbed P was not achieved. The correlation of parameters f , Kp and α complicate the unequivocal determination of each parameter. Particularly, the pronounced, initial increase in P concentrations can be reproduced with infinite combinations of f and Kp . Similarly, quasi-steady-state concentrations are controlled by a combination of Kp and α . However, the very slow increase in dissolved P concentrations after the initial increase constrains α , and allows a robust estimation of the partition coefficient Kp and consequently f .

The major part of the adsorption capacity lays inside the coating. The fraction of fast adsorption sites f was only 4.5 % reflecting the small number of sites at the outermost layer of the coating, which is in direct contact with the porewater. SEM-EDX analyses support the conceptual assumption that P adsorption inside the coating is a transport-limited process: P is not homogeneously distributed but enriched in the outer part of the coating and in some narrow layers inside the coating. Although SEM-EDX micrographs indicate the possibility of P transport through macro pores in the coating, transport into the bulk of the coating is likely controlled by diffusion through the intra-porosity of the Fe precipitates, which is supposed to be faster than solid diffusion (Willett et al., 1988). The Fe-(hydr)oxides in the coating are expected to be of low crystallinity comparable to the structure of ferrihydrite. A pore width between 0.42 and 50 nm was obtained from BET analyses being about half of them mesopores (2-50 nm). The range of pore widths indicates that the majority of pores are sufficiently large to allow for diffusion of hydrogen- and dihydrogen phosphate with Stoke's radii of 0.35 and 0.26 nm, respectively (Hong et al., 2009). The relevance of mesopores for P adsorption was demonstrated by Suresh Kumar et al. (2017) who found, at low P concentrations, a linear relationship between the mesopore BET specific surface area and P adsorption in granulated activated carbon coated with Fe oxides. The pore size values for 2-L and 6-L ferrihydrite obtained by Wang et al. (2013) range from 1.6 to 4.4 nm. The relatively

large variability of pore sizes measured for ICS can be explained by changing conditions in the surrounding water during the growth of the coating. The composition of the inflow water in the sand filter can be variable as well as the position of the grains in the filter caused by backflushing. Both types of events might affect the structure of Fe precipitates in the sand filters (Jentsch & Penn, 2006; Van Beek et al., 2020) and hence pore size distribution.

Based on the optimized mass transfer coefficient α of $1.56 \cdot 10^{-4} \text{ h}^{-1}$ the time scale of the slow adsorption process is about 6400 hours. Consequently, the required equilibration times for determining K_p in batch experiments using ICS grains would be much longer than the duration of the column experiments. This implies that column experiments in combination with reactive transport modeling appear to be more efficient for estimating the equilibrium partition coefficient of P for ICS. Furthermore, there are practical limitations for the use of batch experiments to constrain K_p for ICS as the coating can be lost during shaking and reduced to small pieces (Chardon et al., 2012).

The obtained value of K_p compares well to those reported in other studies. We found $K_p = 3.56 \text{ L/g}$ for pure ICS or 28.1 L/g-Fe (deduced from the estimated K_p for the ICS-sand mixture, see Table 5-1) at an equilibrium P concentration of 1.70 mg/L , corresponding to P contents of 6.06 mg/g-ICS or 47.7 mg-P/g-Fe (0.09 P:Fe molar ratio) in the solid phase. Wang et al. (2013) report a value of 52.3 mg/g-Fe for 2-L ferrihydrite powder in equilibrium with 1.0 mg/L dissolved P, while Chardon et al. (2012) obtained 56.83 mg/g-Fe for iron sludge from drinking water treatment in column experiments at 3.95 mg/L after 283 days (6792 hours). Lambert et al. (2020) report a maximum adsorption of 16.3 mg/g-Fe for ICS in a column experiment after 280 days (6720 hours) and a 20 mg/L inflow concentration. Surprisingly, the value is lower than ours, as the inflow concentrations in Lambert et al. (2020) experiment were considerably higher, and the duration of their experiment was longer compared to our experiments. However, the amount of ICS in the column used by Lambert et al. (2020) was 195 g , about seven times larger than in this study at a comparable flow rate of 2.53 cm/h . The experiment only captured the pronounced, initial increase in effluent concentrations and not the prolonged slow increase afterward. In this stage of the experiment, adsorption at the slow sites is of lower relevance leading to lower values when calculating an apparent partition coefficient. According to our results, the equilibrium solid concentration at a dissolved P concentration of 20 mg/L is 120.7 mg/g-Fe . When only considering the fraction with fast rates

(4.5% of total adsorbed), 5.5 mg/g-Fe are reached, which is close to the value obtained by Lambert et al. (2020) in their batch experiments with 24 h equilibration time (5.93 mg/g-Fe). Per surface area, the maximum P adsorption we obtained was 0.084 mg/m² which is very similar to the value of 0.081 mg/m² obtained by Koopmans et al. (2020) for Fe-containing precipitates from drinking water treatment, which was used 14 months for soil amendment.

The optimized partition coefficient K_p is conditional and expected to depend on pH, ionic strength, and the presence of other ions adsorbing to ICS. The model was calibrated and validated for pH 6.80 ± 0.05 , 0.10 M ionic strength, 1.70 ± 0.05 mg/L inflow concentration, and no competing ions. Higher pH reduces P adsorption (R. Zhang et al., 2022) due to competing OH⁻ ions and a decreasing surface charge at higher pH. Differences in ionic strengths can alter P adsorption by mitigating electrostatic effects. The effect of pH and ionic strength could be accounted for when applying surface complexation models including the acid-base chemistry of surface sites and electrostatic corrections such as the generic DDL model parameterized by Dzombak & Morel (1991) for hydrous ferric oxides (HFO). The generic DDL provides a K_p value of 36.10 L/g-Fe for HFO at our experimental conditions. This value is 28% higher than the K_p we obtained for ICS but is in the same order of magnitude. The corresponding surface excess of 0.064 mg/m² is, however, lower than calculated by the DDL model as Dzombak & Morel (1991) consider a theoretical SSA of 600 m²/g for HFO, which is higher than the BET surface area of ICS. Nevertheless, we consider the possibility that based on the DDL model the K_p value could be adjusted to other conditions by determining the relative effect of P distribution when changing pH or ionic strength. Next to pH and ionic strength, the equilibrium distribution coefficient can be affected by the presence of ions such as organic matter, sulfate, carbonates, silicates, and arsenate competing with phosphate for surface sites (Grafe et al., 2002; Hiemstra, 2018; Liu et al., 2018; Mendez & Hiemstra, 2019) and should be taken into consideration when treating natural waters. Also temperature is expected to effect both equilibrium concentrations and rate constants, but the temperature effect is out of the scope of this study.

Implications for practical applications

The contribution of slow sites to P adsorption has practical consequences for the design, operation, and lifespan of ICS filters. Integrating stop-flow periods in the operation of filters

allows the regeneration of fast adsorption sites, but the resting times have to be sufficient for P to be transferred to slow sites. We tested five different operation scenarios: (i) continuous flow, (ii) resting 3 months a year (during summer time), (iii) resting 1 week and (iv) 2 weeks per month, for a 40x40x40 cm filter with 4 L/h flow and 1 mg/L inflow water. The target is to keep concentrations below 0.15 mg/L. The scenarios are not strictly comparable, scenarios (ii) and (iii) treat the same volume, 75% of the total volume in scenario (i). Scenarios (ii) and (iii) demonstrate the contributions of slow kinetics and the effect of different lengths in the resting periods on P retention. To make the treated volume in scenario (iv) comparable to scenario (i), we assumed that 2 filter compartments (of the given dimensions) are used with alternating resting periods every 2 weeks. Figure 5-5 displays the P concentrations in the effluent for all scenarios.

Scenario (ii) exhibits a larger recovery than scenario (iii), this effect is reached because the resting period is longer. Nevertheless, after 24,000 hours (2 years in operation) they both reach a comparable final concentration of about 0.15 mg/L and retain a similar mass of P for the same treated volume, about 0.065 kg P. Comparing scenario (i) and (iv) with the same treated volume, the continuous filter scenario (i) needs to be replaced three times in five years (every 1.65 years) to meet the 0.15 mg/L target. Instead, scenario (ii) can meet target using only two filters and alternating operation every 2 weeks. Making use of two filters scenario (ii) retains 0.342 kg while scenario (i) retains 0.167 kg P using three filters in five years.

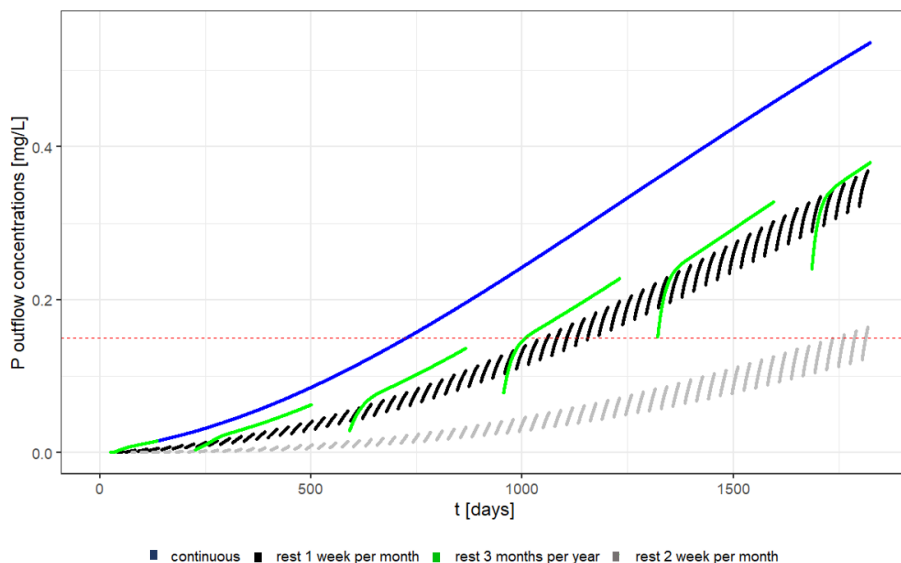


Figure 5-1: P outflow concentrations for practical example of a 5-year ICS filter operation with 4 different operative scenarios: (i) continuous flow, (ii) resting 3 months a year (during summer time), (iii) resting 1 week and (iv) 2 weeks per month. Dashed red line indicates the target outflow concentration, 0.15 mg/L.

5.6 Summary and conclusion

A quantitative model for phosphate adsorption on ICS was developed, which was able to account for slow adsorption reactions, with the intention to provide a tool for optimizing the application of ICS filters. The conceptual two-site model including transport-limited adsorption kinetics was supported by electron microscopic analyses of ICS. Long-term column experiments under several flow conditions were used to calibrate and validate the model. The model reproduced phosphate concentration of continuous and intermittent flow conditions, as well as adsorption and desorption. Adsorption proceeded rapidly on a small number of sites (4.5 %) and is described with a linear equilibrium adsorption model. Adsorption on most sites proceeded slowly on the time scale of months, which we related to intra-particle diffusion. The calculated maximum adsorption capacity under experimental conditions was 47.7 mg/g-Fe, or 0.084 mg/m² at 1.70 mg-P/L inflow implying an equilibrium partition coefficient of 28.1 L/g-Fe. The model was used to test how ICS filter operation can

be optimized to exploit the high capacity of the slow adsorption. An example shows how introducing resting periods improve the phosphate removal and operation duration of ICS filters.

From these results we conclude:

- Phosphate adsorption on ICS takes place at two times scales: fast adsorbing sites at the outside of the grains and slow kinetic adsorption into the iron coating.
- Only 4.5 % of sites are in equilibrium and represent fast-accessible sites.
- Optimal ICS filter operation contains recovery phases. Flow interruptions in the time scale of the slow adsorption process (weeks to months) can extend the filter operation time significantly.

5.7 Acknowledgments

This study was funded by P-TRAP (EU Grant No. 813438, Marie Skłodowska- Curie Actions). We like to thank Arcadis and Aquaminerals for the ICS. We like to acknowledge T.M. van Genuchten for his support with Stanmod, Karel As and Michael Thelen, and University Bayreuth for the BET analysis, Eric Hellebrand for SEM-EDX, and Erik van Vilsteren and Mingkai Ma for their support in building the column set-up.

5.8 Supplementary material

The supplementary material includes an image of the column set-up, a description of the analytical techniques, tracer test results of columns I, II, and III, sensitivity analysis of the parameters in Stanmod, more detailed BET-SSA results, and EDX spectra. The data set and model are available at https://github.com/victoriabarcala/ICS_adsorptionmodel.

5.9 References

- Ajmal, Z., Muhmood, A., Usman, M., Kizito, S., Lu, J., Dong, R., & Wu, S. (2018). Phosphate removal from aqueous solution using iron oxides : adsorption , desorption and regeneration characteristics. *Journal of Colloid And Interface Science*. <https://doi.org/10.1016/j.jcis.2018.05.084>
- Barcala, V., Rozemeijer, J., Osté, L., Van Der Grift, B., Gerner, L., & Behrends, T. (2020). Processes controlling the flux of legacy phosphorus to surface waters at the farm scale. *Environmental Research Letters*, 16(1). <https://doi.org/10.1088/1748-9326/abcdd4>
- Barcala, V., Stefan, J., Jan, G., Stefan, M., Andreas, V., & Thilo, B. (2022). Phosphorus adsorption on iron-coated sand under reducing conditions. *Journal of Environment Quality*. <https://doi.org/10.1002/jeq2.20432>
- Bierzoa, M., Bergström, L., Ulén, B., Djodjic, F., Tonderski, K., Heeb, A., Svensson, J., & Malgeryd, J. (2019). Hydrologic Extremes and Legacy Sources Can Override Efforts to Mitigate Nutrient and Sediment Losses at the Catchment Scale. *Journal of Environmental Quality*, 48(5), 1314–1324. <https://doi.org/10.2134/jeq2019.02.0063>
- Bol, R., Gruau, G., Mellander, P. E., Dupas, R., Bechmann, M., Skarbovik, E., Bierzoa, M., Djodjic, F., Glendell, M., Jordan, P., Van der Grift, B., Rode, M., Smolders, E., Verbeeck, M., Gu, S., Klumpp, E., Pohle, I., Fresne, M., & Gascuel-Oudou, C. (2018). Challenges of reducing phosphorus based water eutrophication in the agricultural landscapes of Northwest Europe. *Frontiers in Marine Science*, 5(AUG), 1–16. <https://doi.org/10.3389/fmars.2018.00276>
- Boujelben, N., Bouzid, J., Elouear, Z., Feki, M., Jamoussi, F., & Montiel, A. (2008). Phosphorus removal from aqueous solution using iron coated natural and engineered sorbents. *Journal of Hazardous Materials*, 151(1), 103–110. <https://doi.org/10.1016/j.jhazmat.2007.05.057>
- Bromly, M., Hinz, C., & Aylmore, L. A. G. (2007). Relation of dispersivity to properties of homogeneous saturated repacked soil columns. *European Journal of Soil Science*, February, 293–301. <https://doi.org/10.1111/j.1365-2389.2006.00839.x>
- Chardon, Groenenberg, J. E., Temminghoff, E. J. M., & Koopmans, G. F. (2012). Use of Reactive Materials to Bind Phosphorus. *Journal of Environmental Quality*, 41(3), 636–646. <https://doi.org/10.2134/jeq2011.0055>
- Chardon, W.J., Groenenberg, J. E., Vink, J. P. M., Voegelin, A., & Koopmans, G. F. (2021). Use of iron-coated sand for removing soluble phosphorus from drainage water. *Science of The Total Environment*, 815, 152738. <https://doi.org/10.1016/j.scitotenv.2021.152738>
- Das Gupta, M., Loganathan, P., & Vigneswaran, S. (2012). Adsorptive Removal of Nitrate and Phosphate from Water by a Purolite Ion Exchange Resin and Hydrous Ferric Oxide Columns in Series. *Separation Science and Technology (Philadelphia)*, 47(12), 1785–1792. <https://doi.org/10.1080/01496395.2012.658487>
- De Klein, J. J. M., & Koelmans, A. A. (2011). Quantifying seasonal export and retention of nutrients in

- West European lowland rivers at catchment scale. *Hydrological Processes*, 25(13), 2102–2111. <https://doi.org/10.1002/hyp.7964>
- Dupas, R., Tittel, J., Jordan, P., Musolff, A., & Rode, M. (2018). Non-domestic phosphorus release in rivers during low-flow: Mechanisms and implications for sources identification. *Journal of Hydrology*, 560, 141–149. <https://doi.org/10.1016/j.jhydrol.2018.03.023>
- Dzombak, D. A., & Morel, F. M. M. (1991). *Surface Complexation Modeling: Hydrous Ferric Oxide*. Wiley.
- Fiorellino, N., Kratochvil, R., & Coale, F. (2017). Long-Term Agronomic Drawdown of Soil Phosphorus in Mid-Atlantic Coastal Plain Soils. *Agronomy, Soils & Environmental Quality*. <https://doi.org/10.2134/agronj2016.07.0409>
- Fraters, B., Hooijboer, A., Vrijhoef, A., Plette, A., van Duijnhoven, N., Rozemeijer, J., Gosseling, M., Daatselaar, C., Roskam, J., & Begeman, H. (2021). *Agricultural practices and water quality in the Netherlands : status (2016-2019) and trends (1992-2019)*.
- Grafe, M., Eick, M. J., Grossl, P. R., & Saunders, A. M. (2002). Adsorption of Arsenate and Arsenite on Ferrihydrite in the Presence and Absence of Dissolved Organic Carbon. *Journal of Environmental Quality*, 1123(31), 1115–1123. <https://doi.org/doi:10.2134/jeq2002.1115>
- Groenenberg, J. E., Chardon, W. J., & Koopmans, G. F. (2013). Reducing Phosphorus Loading of Surface Water Using Iron-Coated Sand. *Journal of Environmental Quality*, 42(1), 250–259. <https://doi.org/10.2134/jeq2012.0344>
- Gu, S., Gruau, G., Dupas, R., Rumpel, C., Crème, A., Fovet, O., Gascuel-Oudou, C., Jeanneau, L., Humbert, G., & Petitjean, P. (2017). Release of dissolved phosphorus from riparian wetlands: Evidence for complex interactions among hydroclimate variability, topography and soil properties. *Science of the Total Environment*, 598(May), 421–431. <https://doi.org/10.1016/j.scitotenv.2017.04.028>
- Hiemstra, T. (2018). Ferrihydrite interaction with silicate and competing oxyanions : Geometry and Hydrogen bonding of surface species. *Geochimica et Cosmochimica Acta*, 238, 453–476. <https://doi.org/10.1016/j.gca.2018.07.017>
- Hong, S. U., Ouyang, L., & Bruening, M. L. (2009). Recovery of phosphate using multilayer polyelectrolyte nanofiltration membranes. *Journal of Membrane Science*, 327(1–2), 2–5. <https://doi.org/10.1016/j.memsci.2008.11.035>
- Ippolito, J. A., Barbarick, K. A., & Elliott, H. A. (2011). Drinking Water Treatment Residuals: A Review of Recent Uses. *Journal of Environment Quality*, 40(1), 1. <https://doi.org/10.2134/jeq2010.0242>
- Jentsch, T. L., & Penn, R. L. (2006). Influence of Aluminum Doping on Ferrihydrite Nanoparticle Reactivity. *Journal of Physical Chemistry*, 110, 11746–11750. <https://doi.org/10.1021/jp060957>
- Jerez, J., & Flury, M. (2006). Humic acid-, ferrihydrite-, and aluminosilicate-coated sands for column transport experiments. *Colloids and Surfaces A: Physicochemical and Engineering Aspects*, 273(1–3), 90–96. <https://doi.org/10.1016/j.colsurfa.2005.08.008>
- Koopmans, G. F., Hiemstra, T., Vaseur, C., Chardon, W. J., Voegelin, A., & Groenenberg, J. E. (2020). Use

- of iron oxide nanoparticles for immobilizing phosphorus in-situ: Increase in soil reactive surface area and effect on soluble phosphorus. *Science of the Total Environment*, 711, 135220. <https://doi.org/10.1016/j.scitotenv.2019.135220>
- Koopmans, Gerwin F., Chardon, W. J., de Willigen, P., & Van Riemsdijk, W. H. (2004). Phosphorus Desorption Dynamics in Soil and the Link to a Dynamic Concept of Bioavailability. *Journal of Environment Quality*, 33(33), 1393–1402.
- Kronvang, B., Vagstad, N., Behrendt, H., Bøgestrand, J., & Larsen, S. E. (2007). Phosphorus losses at the catchment scale within Europe: An overview. *Soil Use and Management*, 23(SUPPL. 1), 104–116. <https://doi.org/10.1111/j.1475-2743.2007.00113.x>
- Lambert, N., Van Aken, P., Van den Broeck, R., & Dewil, R. (2020). Adsorption of phosphate on iron-coated sand granules as a robust end-of-pipe purification strategy in the horticulture sector. *Chemosphere*, 267, 129276. <https://doi.org/10.1016/j.chemosphere.2020.129276>
- Lewis, J., & Sjöstrom, J. (2010). Optimizing the experimental design of soil columns in saturated and unsaturated transport experiments ☆. *Journal of Contaminant Hydrology*, 115(1–4), 1–13. <https://doi.org/10.1016/j.jconhyd.2010.04.001>
- Liu, A. R., Chi, L., Wang, X., & Sui, Y. (2018). Review of Metal (Hydr)oxide and Other Adsorptive Materials for Phosphate Removal from Water Ruiting. *Journal of Environmental Chemical Engineering*. <https://doi.org/10.1016/j.jece.2018.08.008>
- Lucas, E. R., Toor, G. S., & Mcgrath, J. M. (2021). Agronomic and environmental phosphorus decline in coastal plain soils after cessation of manure application. *Agriculture, Ecosystems and Environment*, 311(January), 107337. <https://doi.org/10.1016/j.agee.2021.107337>
- Maroto, J. A., de Dios, J., & de las Nieves, F. J. (2002). Use of a Mariotte bottle for the experimental study of the transition from laminar to turbulent flow. *American Journal of Physics*, 70(7), 698–701. <https://doi.org/10.1119/1.1469038>
- Mendez, J. C., & Hiemstra, T. (2019). Carbonate Adsorption to Ferrihydrite : Competitive Interaction with Phosphate for Use in Soil Systems. *ASC Earth Space Chemistry*, 3, 129–141. <https://doi.org/10.1021/acsearthspacechem.8b00160>
- Moelants, N., Smets, I. Y., & Van Impe, J. F. (2011). The potential of an iron rich substrate for phosphorus removal in decentralized wastewater treatment systems. *Separation and Purification Technology*, 77(1), 40–45. <https://doi.org/10.1016/j.seppur.2010.11.017>
- Morel, F. M., & Hering, J. G. (1993). *Principles and applications of aquatic chemistry*. John Wiley & Sons.
- Murphy, J., & Riley, J. P. (1962). A modified single solution method for the determination of phosphate in natural waters. *Analytica Chimica Acta*, 27(C), 31–36. [https://doi.org/10.1016/S0003-2670\(00\)88444-5](https://doi.org/10.1016/S0003-2670(00)88444-5)
- Mystrioti, C., Papassiopi, N., Xenidis, A., Dermatas, D., & Chrysochoou, M. (2015). Column study for the evaluation of the transport properties of polyphenol-coated nanoiron. *Journal of Hazardous*

- Materials*, 281, 64–69. <https://doi.org/10.1016/j.jhazmat.2014.05.050>
- Nur, T., Johir, M. A. H., Loganathan, P., Nguyen, T., Vigneswaran, S., & Kandasamy, J. (2014). Phosphate removal from water using an iron oxide impregnated strong base anion exchange resin. *Journal of Industrial and Engineering Chemistry*, 20(4), 1301–1307. <https://doi.org/10.1016/j.jiec.2013.07.009>
- Penn, C., Bryant, R. B., Callahan, M. P., & Mcgrath, J. M. (2011). Use of industrial by-products to sorb and retain phosphorus. *Communications in Soil Science and Plant Analysis*, 42(6), 633–644. <https://doi.org/10.1080/00103624.2011.550374>
- Penn, C., Chagas, I., Klimeski, A., & Lyngsie, G. (2017). A review of phosphorus removal structures: How to assess and compare their performance. *Water (Switzerland)*, 9(8), 1–22. <https://doi.org/10.3390/w9080583>
- Penn, C., Livingston, S., Shedekar, V., King, K., & Williams, M. (2020). Performance of field-scale phosphorus removal structures utilizing steel slag for treatment of subsurface drainage. *Water (Switzerland)*, 12(2). <https://doi.org/10.3390/w12020443>
- Pérez-López, R., Nieto, J. M., & de Almodóvar, G. R. (2007). Utilization of fly ash to improve the quality of the acid mine drainage generated by oxidation of a sulphide-rich mining waste: Column experiments. *Chemosphere*, 67(8), 1637–1646. <https://doi.org/10.1016/j.chemosphere.2006.10.009>
- Rittmann, B. E., Mayer, B., Westerhoff, P., & Edwards, M. (2011). Capturing the lost phosphorus. *Chemosphere*, 84(6), 846–853. <https://doi.org/10.1016/j.chemosphere.2011.02.001>
- Rozemeijer, J. C., Klein, J., Broers, H. P., Van Tol-Leenders, T. P., & Van der Grift, B. (2014). Water quality status and trends in agriculture-dominated headwaters; a national monitoring network for assessing the effectiveness of national and European manure legislation in The Netherlands. *Environmental Monitoring and Assessment*, 186(12), 8981–8995. <https://doi.org/10.1007/s10661-014-4059-0>
- Schoumans, O. F., Chardon, W. J., Bechmann, M. E., Gascuel-Oudou, C., Hofman, G., Kronvang, B., Rubæk, G. H., Ulén, B., & Dorioz, J. M. (2014). Mitigation options to reduce phosphorus losses from the agricultural sector and improve surface water quality: A review. *Science of the Total Environment*, 468–469, 1255–1266. <https://doi.org/10.1016/j.scitotenv.2013.08.061>
- Sharma, S., Petrusevski, B., & Schippers, J. C. (2002). Characterisation of coated sand from iron removal plant. *Water Science and Technology*, 2(2), 247–257. <https://doi.org/10.2166/ws.2002.0070>
- Sharpley, A., Jarvie, H. P., Buda, A., May, L., Spears, B., & Kleinman, P. (2013). Phosphorus Legacy: Overcoming the Effects of Past Management Practices to Mitigate Future Water Quality Impairment. *Journal of Environmental Quality*, 42(5), 1308–1326. <https://doi.org/10.2134/jeq2013.03.0098>
- Simunek, J., van Genuchten, M. T., Sejna, M., Toride, N., & Leij, F. J. (1999). The STANMOD Computer

- Software for Evaluating Solute Transport in Porous Media Using Analytical Solutions of Convection-Dispersion Equation. *Agriculture*, November, 20.
- Soetaert, K., & Herman, P. (2009). *A practical guide to ecological modelling Using R as a simulation platform*.
- Soetaert, K., & Meysman, F. (2012). Environmental Modelling & Software Reactive transport in aquatic ecosystems : Rapid model prototyping in the open source software R. *Environmental Modelling and Software*, 32, 49–60. <https://doi.org/10.1016/j.envsoft.2011.08.011>
- Soetaert, K., & Petzoldt, T. (2010). Solving Differential Equations in R : Package deSolve. *Journal of Statistical Software*, 33(9). <https://doi.org/10.18637/jss.v033.i09>
- Stoll, S., Frossard, E., Stamm, C., & Prasuhn, V. (2021). The time it takes to reduce soil legacy phosphorus to a tolerable level for surface waters : What we learn from a case study in the catchment of Lake. *Geoderma*, 403. <https://doi.org/10.1016/j.geoderma.2021.115257>
- Stoner, D., Penn, C., McGrath, J., & Warren, J. (2012). Phosphorus Removal with By-Products in a Flow-Through Setting. *Journal of Environmental Quality*, 41(3), 654–663. <https://doi.org/10.2134/jeq2011.0049>
- Toride, N., Leij, F. J., & Van Genuchten, M. T. (1995). The CXTFIT code for estimating transport parameters from laboratory or field tracer experiments. *Res Rep, Research R*(137), 1–138. http://www.researchgate.net/publication/247824027_The_CXTFIT_Ver_2.0_Code_for_estimating_transport_parameters_from_laboratory_or_field_tracer_experiments
- Van Beek, C. G. E. M., Dusseldorp, J., Joris, K., Huysman, K., Leijssen, H., Schoonenberg Kegel, F., De Vet, W. W. J. M., Van De Wetering, S., & Hofs, B. (2016). Contributions of homogeneous, heterogeneous and biological iron(II) oxidation in aeration and rapid sand filtration (RSF) in field sites. *Journal of Water Supply: Research and Technology - AQUA*, 65(3), 195–207. <https://doi.org/10.2166/aqua.2015.059>
- Van Beek, C. G. E. M., Hofman-Caris, C. H. M., & Zweere, G. J. (2020). Drinking water treatment and chemical well clogging by iron(II) oxidation and hydrous ferric oxide (HFO) precipitation. *Journal of Water Supply: Research and Technology - AQUA*, 69(5), 427–437. <https://doi.org/10.2166/aqua.2020.140>
- Van Genuchten, M. ., Simunek, J., Leij, F. J., & Toride, N. (2012). Stanmod: model use, calibration and validation. *American Society of Agricultural and Biological Engineers*, 55(4), 1353–1366.
- Vandermoere, S., Ralaizafisoloarivony, N. A., Van Ranst, E., & De Neve, S. (2018). Reducing phosphorus (P) losses from drained agricultural fields with iron coated sand (- glauconite) filters. *Water Research*, 141, 329–339. <https://doi.org/10.1016/j.watres.2018.05.022>
- Wang, Li, W., Harrington, R., Liu, F., Parise, J. B., Feng, X., & Sparks, D. L. (2013). Effect of ferrihydrite crystallite size on phosphate adsorption reactivity. *Environmental Science and Technology*, 47(18), 10322–10331. <https://doi.org/10.1021/es401301z>

- Willett, I. R., Chertres, C. J., & Nguyen, T. T. (1988). Migration of phosphate into aggregated particles of ferrihydrite. *Journal of Soil Science*, 39(2), 275–282. <https://doi.org/10.1111/j.1365-2389.1988.tb01214.x>
- Withers, P. J. A., Neal, C., Jarvie, H. P., & Doody, D. G. (2014). Agriculture and eutrophication: Where do we go from here? *Sustainability (Switzerland)*, 6(9), 5853–5875. <https://doi.org/10.3390/su6095853>
- Zhang, R., Wang, L., Hussain Lakho, F., Yang, X., Depuydt, V., Igodt, W., Quan Le, H., Rousseau, D. P. L., & Van Hulle, S. (2022). Iron oxide coated sand (IOS): Scale-up analysis and full-scale application for phosphorus removal from goat farm wastewater. *Separation and Purification Technology*, 284(November 2021), 120213. <https://doi.org/10.1016/j.seppur.2021.120213>
- Zhang, Y. (2008). *Geochemical kinetics*. Princeton University Press.

5.10 Supplementary material to Chapter 5: Transport limited kinetics of phosphate retention on iron-coated sand and practical implications

Victoria Barcala^{1,2}, Leonard Osté¹, Alraune Zech², and Thilo Behrends²

1 Inland Water Systems, Deltares, 600 Daltonlaan, 3584 BK Utrecht, The Netherlands

2 Department of Earth Sciences, Faculty of Geosciences, Utrecht University, 8 Princetonlaan, 3584 CB Utrecht, The Netherlands

The supplementary material includes an image of the column set-up, description of the analytical techniques, derivation of the model equations, tracer test results of columns I, II, and III, sensitivity analysis of the parameters in Stanmod, more detailed BET-SSA results, and EDX spectra. The data set and model are available at https://github.com/victoriabarcala/ICS_adsorptionmodel.

Column set-up

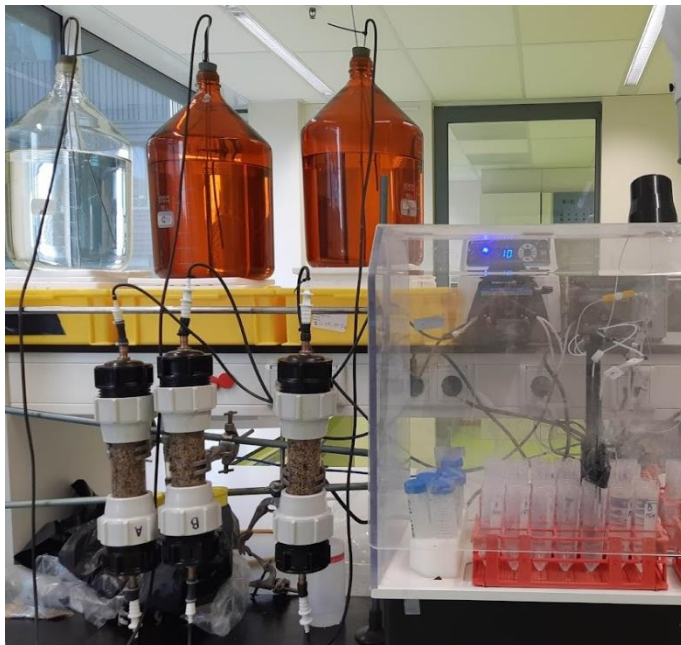


Figure S2 Columns I, II, and III with their feeding 10 L Mariotte bottles, tubing, Masterflex pump, SC-4DXS autosampler with pre-acidified tubes for sample collection. The bottles were covered with black plastic bags to prevent microbial growth.

ICS analytical techniques

For total extraction, ICS was ground in an agate mortar, 0.125 g sample was added to a 2.5 mL mix of HNO_3 (72%) and HClO_4 (65%) in a 1:3 volume ratio plus 2.5 mL HF (48%). The suspension was heated for 12 hours at 90 °C and 4 hours at 140 °C until the solution was evaporated. The precipitates were dissolved by adding 25 mL HNO_3 (72%) and heating overnight at 90 °C. The final solution was filtered (0.45 μm), and analyzed with ICP-OES (Avio 500, Perkin-Elmer). The extraction was done in duplicate.

A Brunauer-Emmet-Teller (BET) instrument (ASiQwin, Quantachrome Instruments) was used to determine the specific surface area and the porosity of the ICS grains. Prior to the

measurement, the physically adsorbed water was removed to prevent interferences with the gas adsorption by heating the sample at 150 °C for 24 hours. After evacuation of the sample, argon was incrementally added to 0.6911 g sample at 87.5 K. The adsorption isotherm was analyzed based on the BET theory providing information of specific surface area as well as intraparticle pore volume and pore size.

Derivation of model equations

Mass balance equations for the concentrations of dissolved P and P adsorbed onto sites with slow kinetics are given by:

$$\left(1 + \frac{\rho f K_p}{\theta}\right) \frac{\partial c}{\partial t} = D \frac{\partial^2 c}{\partial x^2} - v \frac{\partial c}{\partial x} - \frac{\rho \alpha}{\theta} (s_{eq} - s) \quad (\text{equation 1})$$

$$\frac{\partial s}{\partial t} = \alpha (s_{eq} - s) \quad (\text{equation 2})$$

Where c is the P concentration [mg/L] in the mobile phase, x is the longitudinal coordinate [cm], t is time [h], ρ is the dry bulk ICS density [g/L], f is the fraction of fast reacting sites, θ is the porosity, K_p is the equilibrium constant or partition coefficient [L/g], D is the dispersion coefficient [cm²/h], v is the pore-water velocity equal to the darcian flow velocity divided by porosity [cm/h]. α is the mass transfer coefficient [1/h] which can also be conceived as the rate constant for P desorption from the slowly reacting sites, and s is the P concentration in the solid phase for which adsorption is kinetically controlled [mg/g], i.e. the slowly reacting sites. $s_{eq} = K_p(1 - f)c$ is the equilibrium concentration of P adsorbed onto slow sites. The concentration of P bound to the fast-reacting sites is the product fcK_p .

The model equations are derived from the advection-dispersion equation that describes the solute transport through a porous medium with two reactive terms R1 and R2, The first term describes the fast equilibrium adsorption while R2 describes the slow mass transfer inside the iron-coating micro porosity:

$$\theta \frac{\partial c}{\partial t} = \theta D \frac{\partial^2 c}{\partial x^2} - \theta v \frac{\partial c}{\partial x} - R1 - R2$$

The starting point for both reactive terms is the assumption of reversible:



Here, S_{fast} and S_{slow} denote the unoccupied sites, while s_{fast} and s denote the occupied sites. The total concentration of sites in the solid phase S is the sum of all sites, available or occupied with P :

$$S = S_{fast} + s_{fast} + S_{slow} + s .$$

With f being the fraction of fast reacting sites, we get the mass balances for the sites: $S_{fast} + s_{fast} = f \cdot S$ and $S_{slow} + s = (1 - f)S$.

Both reactions are reversible leading to rate laws including a forward and inverse reaction rate constant $k_{fast_1}, k_{fast_{-1}}, k_{slow_1}, k_{slow_{-1}} = \alpha$. The rate constants can reflect the rates of the chemical reaction but also mass transfer in case of transport limited reactions. In the following consider identical ratios of both reactions rate constants, i.e. the same equilibrium constant: $\frac{k_{fast_1}}{k_{fast_{-1}}} = \frac{k_{slow_1}}{\alpha} = K'$. This is based on the assumption that both reactions behave similar at equilibrium conditions.

The rate law for the fast sites is given by:

$$\frac{\partial s_{fast}}{\partial t} = k_{fast_1} S_{fast} c - k_{fast_{-1}} s_{fast}$$

For the fast sites we assume equilibrium, i.e. $\frac{\partial s_{fast}}{\partial t} = 0$. Including the mass balance for surface sites, $S_{fast} = f \cdot S - s_{fast}$, gives :

$$\frac{s_{fast}}{c(fS - s_{fast})} = \frac{k_{fast_1}}{k_{fast_{-1}}} = K'$$

At low concentrations of dissolved P , the equation can be simplified by assuming that the vast majority of fast sites remains vacant in equilibrium. The concentration of s_{fast} is much smaller than the total number of fast sites $f \cdot S$. We can neglect s_{fast} in the denominator and obtain a linear adsorption equation with adsorption coefficient $K_p = K'_{fast} S$:

$$\frac{S_{fast}}{c} = SK'f = fK_p$$

Following the same approach of reaction kinetics for the slow sites, the rate law can be reformulated as:

$$\frac{\partial s}{\partial t} = k_{slow_1} S_{slow} c - \alpha s = \alpha(K' S_{slow} c - s) = \alpha(K'((1-f)S - s)c - s) \approx \alpha(K'((1-f)S)c - s) = \alpha(K_p \cdot (1-f)c - s) = \alpha(s_{eq} - s)$$

Here we assume again that $(1-f)S \ll s$ and make use of the equilibrium concentration of P adsorbed onto slow sites, $s_{eq} = K_p(1-f)c$. A similar mass balance is obtained when conceiving the pore volume inside the coating as a separate phase, in which adsorption equilibrium is reached. In this case, α represents the exchange coefficient between the stagnant, liquid phase inside the coating and the mobile phase (see for example Van Genuchten et al., 2012 or Schäfer et al. 1998).

In summary the mass balances obtained for the fast and slow reactions are:

$$\frac{\partial S_{fast}}{\partial t} = \frac{\partial K_p f c}{\partial t} = f K_p \frac{\partial c}{\partial t} \quad (R1)$$

$$\frac{\partial s}{\partial t} = \alpha(s_{eq} - s) \quad (R2)$$

Writing the advection-dispersion equations including expressions for R1 and R2, we obtain

$$\theta \frac{\partial c}{\partial t} = \theta D \frac{\partial^2 c}{\partial x^2} - \theta v \frac{\partial c}{\partial x} - \rho \frac{\partial S_{fast}}{\partial t} - \rho \frac{\partial s}{\partial t}$$

$$\theta \frac{\partial c}{\partial t} = \theta D \frac{\partial^2 c}{\partial x^2} - \theta v \frac{\partial c}{\partial x} - \rho f K_p \frac{\partial c}{\partial t} - \rho \alpha (s_{eq} - s)$$

$$\frac{\partial c}{\partial t} + \frac{\rho f K_p}{\theta} \frac{\partial c}{\partial t} = D \frac{\partial^2 c}{\partial x^2} - v \frac{\partial c}{\partial x} - \frac{\rho \alpha}{\theta} (s_{eq} - s)$$

$$\left(1 + \frac{\rho f K_p}{\theta}\right) \frac{\partial c}{\partial t} = D \frac{\partial^2 c}{\partial x^2} - v \frac{\partial c}{\partial x} - \frac{\rho \alpha}{\theta} (s_{eq} - s) \quad (\text{equation 1})$$

And equation 2 is the mass balance in the solid phase in the slow adsorption sites

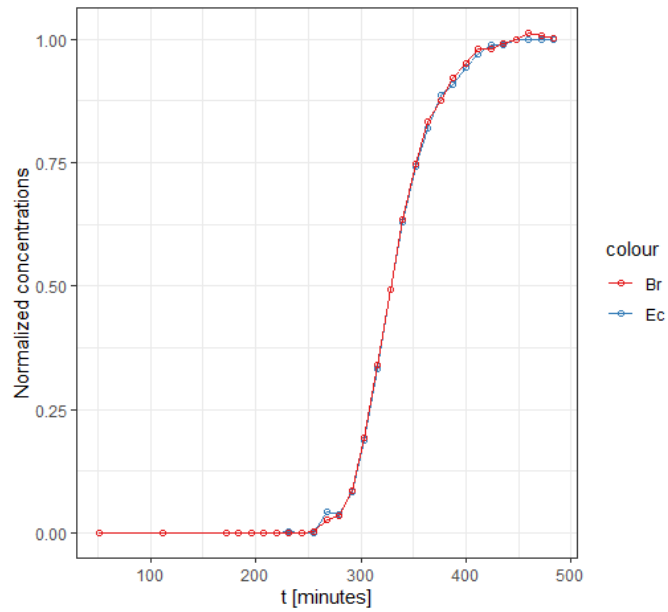
$$\frac{\partial s}{\partial t} = \alpha(s_{eq} - s).$$

(equation 2)

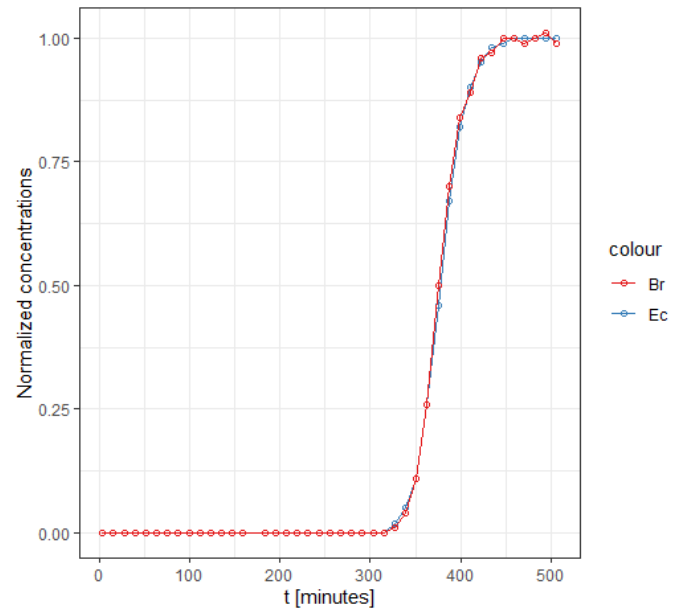
Experimental tracer test results

- Inflow tracer water: EC 2070 uS/cm, 809 mgBr/L.
- Previous background water: EC 1052 uS/cm, 0 mgBr/L.
- Darcy flow velocity 0.65 ml/min. The time in the tubing is already subtracted from the x-axis.

Tracer test column II



Tracer test column I



Tracer test column III

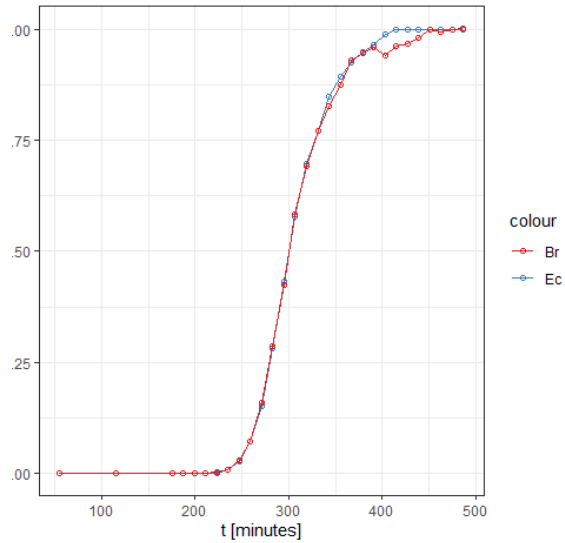


Figure S3 Normalized tracer test results of columns I, II, and III.

The “S” shape of the curves shows a good packing of the column material, in contrast to the asymmetrical shape of the adsorption experiments that denote kinetic adsorption.

Sensitivity analysis

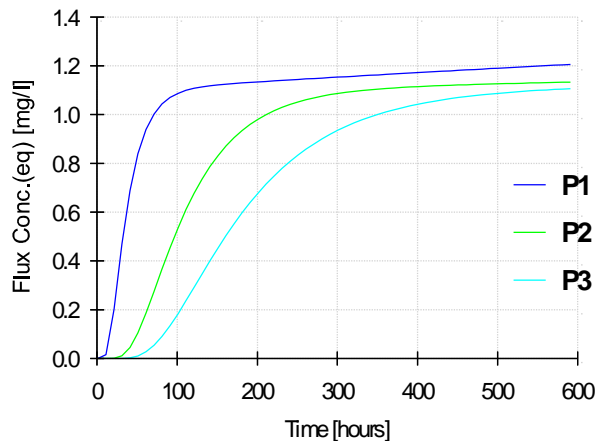
The sensitivity analysis is done with the Stanmod results with constant flow. Stanmod uses the same model equations but they are expressed with dimensionless parameters

$$\frac{\beta R \partial c_1}{\partial t} + \frac{(1-\beta)R \partial c_2}{\partial t} = \frac{D}{vL} \frac{\partial^2 c_1}{\partial x^2} - \frac{\partial c_1}{\partial x} \quad (\text{equation 1})$$

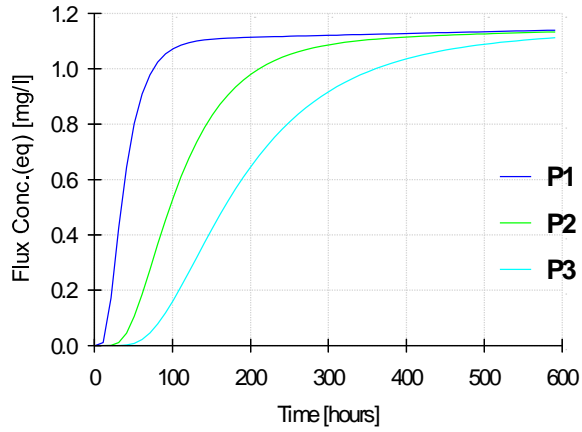
$$(1 - \beta)R \frac{\partial s}{\partial t} = \omega(c_1 - s) \quad (\text{equation 2})$$

Parameter	Definition/Value	Physical interpretation
R	$1 + \frac{\rho K}{\theta}$ (4)	Dimensionless retardation factor, R is 1 for non-reactive solutes as the tracer.
D	30 cm ² /h	Dispersion coefficient [L ² /T]. Represents local-scale flow around grains, differences in fluid velocity within single pores, and differences in adjacent velocity between adjacent pores. It needs to be fitted for each column.
β	$\frac{\theta + f \rho K}{\theta + \rho K}$ (5)	Dimensionless partitioning coefficient between fast and slow adsorption sites. $1 \leq \beta \leq 0$.
ω	$\frac{\alpha(1-\beta)RL}{v}$ (6)	Dimensionless mass transfer coefficient of the solute to the solid phase

a) R sensitivity 500 (P2) 95% CI [167, 834] (P1, P3). R represents K



b) β sensitivity 0.045 (P2) 95% CI [0.0159, 0.078] (P1, P3). β represents f



c) ω sensitivity 0.4677 (P2) 95% CI [0.441, 0.494] (P1, P3). ω represents α

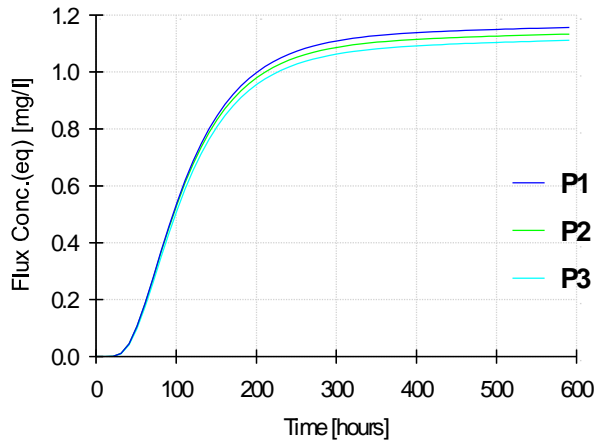


Table S2 Sensitivity analysis of the obtained parameters

The sensitivity was done for a D of $30 \text{ cm}^2/\text{h}$ and v of $4.92 \text{ cm}/\text{h}$, the same as in column I. The confidence in the first order mass transfer rate α is high, almost the same results were obtained with the upper and lower confidence intervals. The fraction of fast adoption sites is likely between 1.6 and 7.8 %, this does not affect the final quasi-equilibrium outflow.

However, higher f means the fast adsorption gains more importance which is relevant for the first stages of the breakthrough curve compared to and f of 4.5%. In R (and therefore K) is where the largest uncertainty lies, this is reflected in larger confidence intervals, variations in the breakthrough times and concentration at the quasi-steady state. Different K values are expected for different ICS from different origins, porosities, Fe content and impurities as Mn and could be adjusted with batch experiments if needed.

ICP-OES results first 40 days

In addition to using ICP-OES results to validate the phosphate measurements, the results could be used to control leaching of elements out of the column. The following were below the detection limit of the ICP-OES: As (detection limit 0.045 mg/L), Cd (detection limit 0.005 mg/L), Cr (detection limit 0.005 mg/L), Ni (detection limit 0.015 mg/L), Pb (detection limit 0.07 mg/L), Se (detection limit 0.15 mg/L). The fact that no toxic element leached is important as the ICS is placed in natural or agricultural areas. Color and particulate material were only detected in the “first flush” when the experiment started. When placing the filter in nature or in agricultural catchments it would be recommended either to wash the material previously or to flush it and collect the first flush as part of the installation procedure before leaving the filter ready to start working.

As for other elements leaching out the column in the first 40 days: Ca was 3.4 mg/L \pm 3.5 mg/L, Fe was 0.18 mg/L \pm 0.007 mg/L, S decreased from 0.881 mg/L to 0.142 m/g Si was 0.845 mg/L \pm 0.240 mg/L and Zn was 0.61 mg/L \pm 0.50 mg/L. S and Si leaching may be related to ion-exchange with phosphate.

BET-SSA results

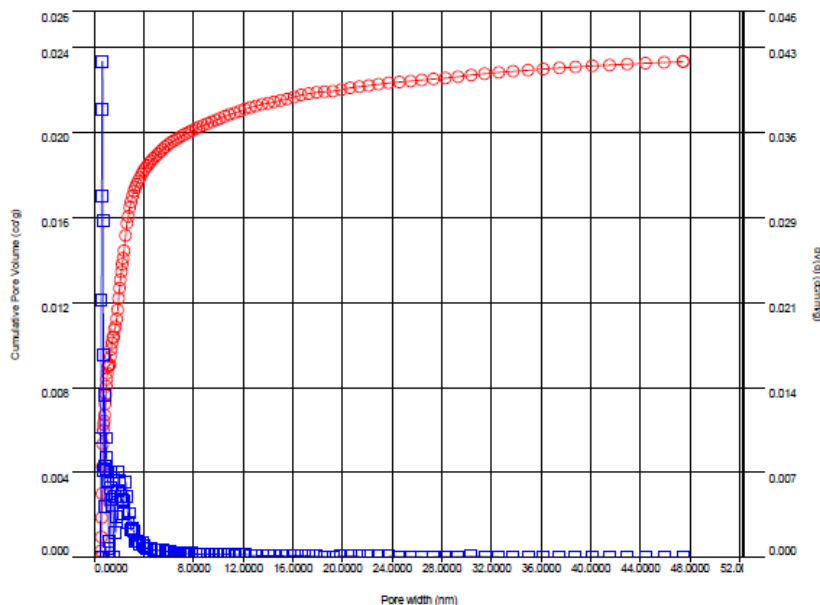
Quantachrome® ASiQwin™ - Automated Gas Sorption Data
Acquisition and Reduction
© 1994-2017, Quantachrome Instruments
version 5.2



Analysis		Report		
Operator:	AC1	Date:	8/10/2021	
Sample ID:	ICS1,18-2mm_Ar@87K_AutosorbFilename:	Operator:	ac1	
Sample Desc:	ICS1,18-2mm_Ar@87K_AutosorbComment:	ICS1,18-2mm_Ar@87K_Autosorb.QPS	Date:	2021/08/17
Outgas Time:	24.0 hrs	Outgas Temp:	150.0 °C	
Analysis gas:	Argon87	Molec. WT:	39.948 g	
Analysis Time:	2151.0 min	Instrument:	Autosorb 1	
		Sample Weight:	0.8911 g	
		Non-ideality:	3.94e-05 1/Torr	
		Bath temp.:	87.5 K	

DFT : dV(d)

Data Reduction Parameters		
DFT method	Thermal Transpiration: on	Eff. mol. diameter (D): 3.54 Å
	Calc. Model: Ar at 87 K_zeolites/silica (cylindr. pores, NLDFT ads.)	Eff. cell stem diam. (d): 4.0000 mm
Adsorbate model	Rel. press. range: 0.0000 - 1.0000	Moving pt. avg: off
	Argon87	Temperature: 87.450K
	Molec. Wt.: 39.948	Cross Section: 14.200 Å²
		Liquid Density: 1.400 g/cc



DFT method summary	
Pore volume =	0.023 cc/g
Surface area =	71.203 m ² /g
Lower confidence limit =	0.482 nm
Fitting error =	0.122 %
Pore width (Mode) =	0.642 nm
Moving point average :	off

Figure S3 Results of specific surface area (BET-SSA) of the ICS grains

The specific surface area (BET-SSA) of the ICS grains was $71.2 \text{ m}^2/\text{g}$, which is very similar to the value of $70 \text{ m}^2/\text{g}$ reported by Chardon et al. (2012). However, this value is not high for ferric iron (hydr)oxides. Zhang et al. (2022) reported a SSA of $249 \text{ m}^2/\text{g}$ for ICS from a drinking water treatment plant in Belgium and Wang et al. (2013) found values between 234 and $427 \text{ m}^2/\text{g}$ for laboratory synthesized ICS. With the measured specific surface area, the maximum adsorption at experimental conditions was $0.084 \text{ mg}/\text{m}^2$.

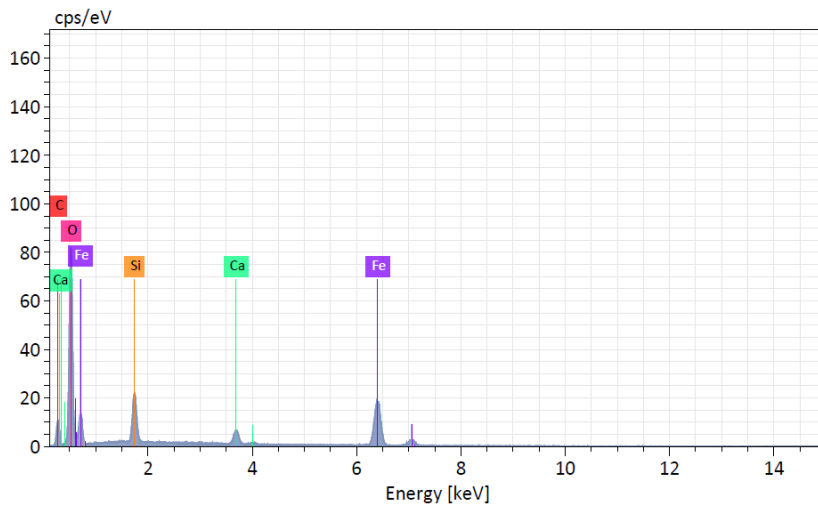
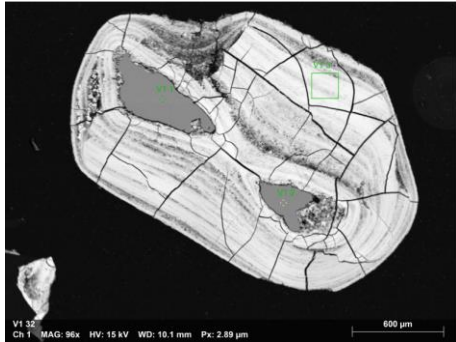
In the columns, the ICS had $71.2 \text{ m}^2/\text{g}$ of specific surface area and quartz sand typically has around $226 \text{ cm}^2/\text{g}$ ($0.02 \text{ m}^2/\text{g}$) (Pennell, 2018). In each column, there are 30 g of ICS and 660 g of quartz sand. Therefore, there are 2136 m^2 of specific surface area in the ICS and 13 m^2 in the quartz sand (only 0.6%). The quartz sand is assumed to be unreactive for this reason

. R model

The function that solves the ODE needs to be run (P_column_k.R) first. The solution for a constant velocity and variable velocity is included in Model_ICS_Script.R. The input files of column I, II, and III are available in the GitHub repository (https://github.com/victoriabarcala/ICS_adsorptionmodel) ready to import to the R script. The velocity, initial concentration, filter height, and porosity can be modified to model/predict different situations.

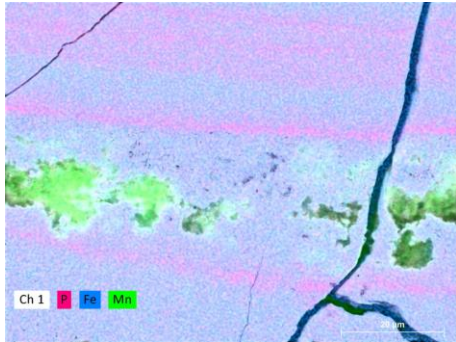
SEM-EDX results

Fe:O ratio 1:3 on light areas. (grain C) before adsorption



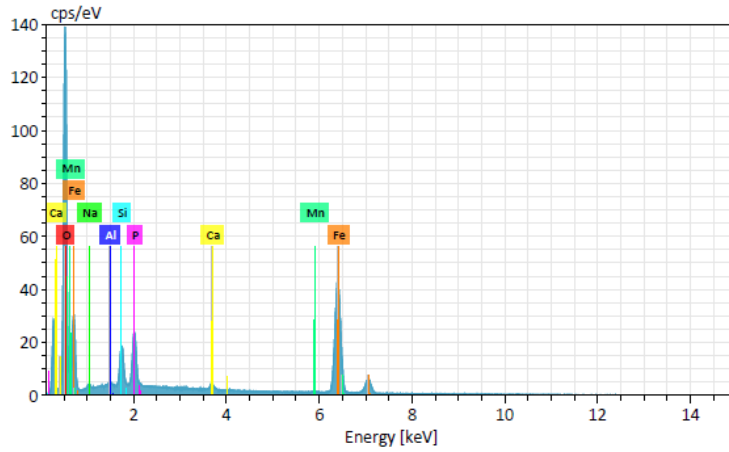
Atomic concentration [%]					
Spectrum	Carbon	Oxygen	Silicon	Calcium	Iron
V1 1	0.00	64.70	35.30		
V1 2	0.00	64.46	35.54		
V1 3	0.00	69.19	6.50	2.30	22.02
Mean	0.00	66.11	25.78	2.30	22.02
Sigma	0.00	2.66	16.70	0.00	0.00
SigmaMean	0.00	1.54	9.64	0.00	0.00

Mn-rich areas, P adsorption associated with iron rings (grain B)



Fe:O ratio on gray areas 1:2 (grain B)

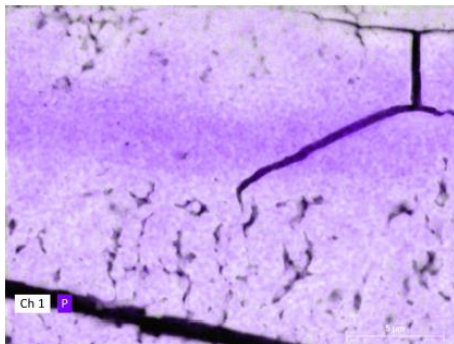




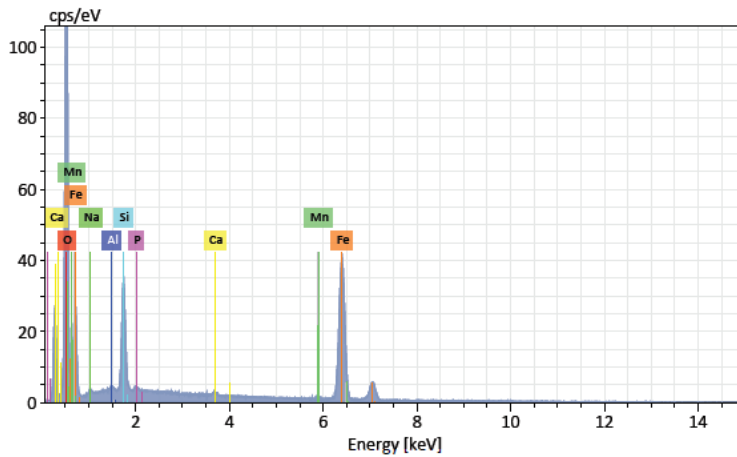
CC-gr1 670

Element	At. No.	Netto	Mass [%]	Mass Norm. [%]	Atom [%]	abs. error [% (1 sigma)]	rel. error [% (1 sigma)]
Oxygen	8	256319	27.50	36.29	65.76	3.00	10.90
Iron	26	199510	45.64	60.22	31.26	1.36	2.98
Phosphorus	15	34415	0.97	1.28	1.20	0.06	6.44
Calcium	20	8589	0.86	1.13	0.82	0.05	6.15
Silicon	14	20236	0.59	0.78	0.80	0.05	8.51
Manganese	25	1343	0.23	0.31	0.16	0.03	15.05
Sodium	11	0	0.00	0.00	0.00	0.00	4.18
Aluminium	13	0	0.00	0.00	0.00	0.00	2.62
		Sum	75.78	100.00	100.00		

P accumulation in areas with low porosity (grain B)

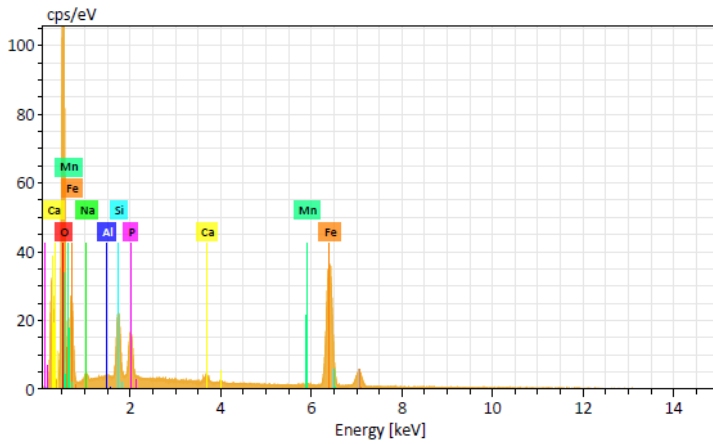


P:Fe ratio in low P area (grain A)



Element	At. No.	Netto	Mass [%]	Mass Norm. [%]	Atom [%]	abs. error [%] (1 sigma)	rel. error [%] (1 sigma)
Oxygen	8	249206	30.29	35.90	63.81	3.30	10.91
Iron	26	188124	47.98	56.86	28.96	1.43	2.98
Silicon	14	78709	4.86	5.76	5.84	0.23	4.69
Sodium	11	3436	0.48	0.57	0.70	0.06	12.05
Calcium	20	3424	0.32	0.38	0.27	0.04	11.30
Aluminium	13	2029	0.15	0.17	0.18	0.03	22.73
Phosphorus	15	1901	0.12	0.14	0.13	0.03	26.12
Manganese	25	973	0.19	0.22	0.11	0.03	18.08
		Sum	84.39	100.00	100.00		

P:Fe ratio in high-P area (grain A)



CC-gr4 678

Element	At. No.	Netto	Mass [%]	Mass Norm. [%]	Atom [%]	abs. error [%] (1 sigma)	rel. error [%] (1 sigma)
Oxygen	8	220555	26.19	36.21	65.31	2.87	10.97
Iron	26	169814	42.86	59.26	30.62	1.28	2.99
Silicon	14	35496	1.35	1.87	1.92	0.08	6.06
Phosphorus	15	22560	0.84	1.16	1.08	0.06	6.88
Calcium	20	7288	0.76	1.05	0.76	0.05	6.57
Manganese	25	1318	0.25	0.35	0.18	0.04	14.24
Sodium	11	914	0.08	0.11	0.14	0.03	39.37
Aluminium	13	0	0.00	0.00	0.00	0.00	2.62
		Sum	72.34	100.00	100.00		

References

- Chardon, Groenenberg, J. E., Temminghoff, E. J. M., & Koopmans, G. F. (2012). Use of Reactive Materials to Bind Phosphorus. *Journal of Environmental Quality*, 41(3), 636–646. <https://doi.org/10.2134/jeq2011.0055>
- Pennell, K. D. (2018). Specific Surface Area. *Methods of Soil Analysis, Part 4: Physical Methods*, 295–315. <https://doi.org/10.2136/sssabookser5.4.c13>
- Schäfer, D., Schäfer, W., & Kinzelbach, W. (1998). Simulation of reactive processes related to biodegradation in aquifers: 1. Structure of the three-dimensional reactive transport model. *Journal of contaminant Hydrology*, 31(1-2), 167-186.
- Wang, Li, W., Harrington, R., Liu, F., Parise, J. B., Feng, X., & Sparks, D. L. (2013). Effect of ferrihydrite crystallite size on phosphate adsorption reactivity. *Environmental Science and Technology*, 47(18), 10322–10331. <https://doi.org/10.1021/es401301z>
- Zhang, R., Wang, L., Hussain Lakho, F., Yang, X., Depuydt, V., Igodt, W., Quan Le, H., Rousseau, D. P. L., & Van Hulle, S. (2022). Iron oxide coated sand (IOS): Scale-up analysis and full-scale application for phosphorus removal from goat farm wastewater. *Separation and Purification Technology*, 284(November 2021), 120213. <https://doi.org/10.1016/j.seppur.2021.120213>



Chapter

6

6 Chapter 6: Synthesis

The research presented in this thesis was motivated by the impact that P leaching from agricultural catchments has on surface water quality and eutrophication. In many areas, eutrophication problems require measures to reduce the nutrients leaving the agricultural catchments. The objective of this thesis was to contribute to improving the management of drained agricultural areas and to optimize the retention of Fe-associated P. Different methodologies and a combination of laboratory experiments, field monitoring, and process- and data-based modeling were used. Monitoring of the nutrient transport is key to quantifying the nutrients export loads and determining the effectiveness of P retention measures. Chapters 2 and 3 investigated the transport of P at a dairy farm on the typical sandy iron-rich soils in the east of the Netherlands. In contrast, chapters 4 and 5 investigated the P retention onto filters made with an iron-by product (ICS) used in the west of the Netherlands, a region characterized for having iron-poor sandy soils and high P concentrations in the drainage water. This chapter synthesizes how the main findings of this thesis can help the monitoring and diagnosis of diffuse P pollution from agricultural areas and provide tools for designing and optimizing Fe-based P-retention measures. Finally, three case studies are used to illustrate the functioning of ICS filters in different settings.

6.1 New insights into the monitoring and diagnosis of diffuse P pollution in agricultural areas

To understand P transport processes, high frequency P measurements are needed to capture the large temporal variability in P concentrations, to quantify loads, and to evaluate the effectiveness of P-retention measures. However, high frequency monitoring equipment is vulnerable to technical failures resulting in data gaps. In chapter 3, six Machine Learning algorithms were evaluated for gap-filling of high-frequency water quality data. Random Forest showed the best performance with an R^2 higher than 0.92 for all test sets. Random Forest enabled the accurate reproduction of discharge-concentrations relations that are non-linear processes and was able to represent system changes that occurred within the training period. However, the prediction outside the training period showed large errors, because system modifications introduced by conservation measures caused changes in the nutrient

transport routes. Although the groundwater levels were used as input for the Random Forest predictive model, the model could no longer accurately predict the nutrient concentrations after water conservation was implemented. The higher groundwater levels induced top-soil P desorption and transport, which was not included in the training set. We concluded that Random Forest is a powerful tool for gap-filling but its use for forecasting and process interpretation should be done with care. Especially when the prediction involves scenarios with climate variability or climate change such as differences in rainfall and groundwater levels.

As a practical implication for monitoring, we advise incorporating additional sensors such as for turbidity, conductivity, and dissolved oxygen in high-frequency monitoring stations. Autoanalyzers such as for P and NH_4 continuous measurements are more sensitive and expensive than sensors. Autoanalyzers need reagents and are more likely to have gaps in the data series. In our dataset, the turbidity showed the largest information gain to fill the missing data. In addition, we advise keeping the Machine Learning models up to date with newly retrieved data to increase the reliability and robustness of the predictions. Furthermore, real-time Machine Learning models can be used in high-frequency monitoring stations for detection of anomalies and warn when maintenance is needed.

The groundwater quality was closely related to surface water quality. The interaction between groundwater and surface water is important in the nutrient transport. The groundwater quality showed heterogeneity in depth and in lateral distance to the drainage systems at the farms. Therefore, to study nutrient transport at the catchment scale we recommend putting some effort in shallow groundwater monitoring, together with tube drain effluent and ditch water monitoring. This can help identifying hot spots or nutrient sources. An alternative to measuring groundwater quality from permanent observation wells is the gas vapor probe (GVP) used for groundwater sampling in chapter 4. The GVP is a good tool to make shallow groundwater concentration-depth profiles (0 to 4 m depth). We recommend, if possible, to combine concentration-depth profiles with continuous groundwater level measurements and soil profiles to measure the dissolved Fe and P content together with other elements for which P has a strong affinity, such as Mn, Ca, and Al.

During this research, the nutrient input (manure and organic matter application in the field) was the information with the lowest level of detail. Precision farming can be a useful tool to incorporate and obtain high quality and detailed information on field-specific inputs. For future research we recommend looking into how to improve data collection on fertilizer application. It would be useful to collect data on the quantity of applied fertilizer, its form, and timing and incorporate this information into process- or data-based models.

6.2 Importance of understanding P-Fe interactions in P transport

It is important to understand P transport routes and the P-Fe interactions inside the farm to make a diagnosis and to select the best measures to reduce diffuse pollution. In this thesis we monitored farms with very different P-Fe dynamics. In both cases the soil was sandy, and the farms were drained with pipes and ditches, but the P transport dynamics from the soil to the surface water was different. The studied dairy farm in the east of the Netherlands had a low P/Fe ratio in the sub-soil and lower dissolved P concentrations in the drained water, while the two flower farms in the west had a high P/Fe ratio in the soil and high dissolved P concentrations in the drained water. To exemplify with values, the dairy farm in the east had a ammonium oxalate extractable P/(Fe+Al) molar ratio of 0.10-0.40 in the top soil and 0.04-0.10 in the subsoil with dissolved P concentrations in the drained water between 0.02 and 0.50 mg/L, while the flower farms in the west had a P/(Fe+Al) molar ratio of 0.40-0.60 in the top soil and 0.20-0.30 in the subsoil with dissolved P concentrations in the drained water between 2.50 and 10.00 mg/L.

In the case that Fe-related sorption capacity was not occupied to critical levels, P was retained when the water moved through the subsurface. Therefore, P was found predominately associated with Fe-rich particles in the ditch. Consequently, changes in the farm water management that modified the P transport paths through different soil layers affected the seasonal P loads. In contrast, in the flower fields most P was transported as dissolved P as there was not enough Fe present naturally in the soil to retain the high P loadings. This gave the opportunity to place Fe-based P retention measures. ICS filters around the drains were used to remove the dissolved P. In the next sections new insight on P retention are explored for the two different scenarios.

6.3 New insights into P transport in agricultural areas with Fe-rich subsoil

The P transport was investigated on a dairy farm with sandy Fe-rich subsoil in the east of the Netherlands in chapters 2 and 3. Results from soil analyses showed that the topsoil had accumulated high amounts of legacy P during the last decades leading to high P/Fe molar ratios and elevated dissolved P concentrations in the pore water, which implied a high risk of P leaching. However, the high Fe content in the subsoil (30-100 cm) and the water transport through this layer prevented high P concentrations in the groundwater and reduced the P losses to surface waters and deeper groundwaters. The transport through the iron-rich subsoil acted as a natural P-retention measure.

From the P fraction that was not retained by the Fe-rich subsoil and was exported to the ditch, most (78%) was associated with Fe-rich particles that were resuspended in the ditch during discharge peaks. The Fe-rich particles were formed on site as the Fe-rich groundwater exfiltrated into the ditch or tube drains and got in contact with oxygen (not by overland flow or erosion). The suggested P-retention measures such as the construction of sedimentation ponds, or wider and vegetated ditches, which should allow the groundwater flow to go through the Fe-rich sandy subsoil and reduce the transport of P-rich sediments in the ditch towards downstream surface waters. These measures should be combined with periodic removal of the sediment in the ditch and sedimentation ponds. The summer season, when the ditch is dry, offers an ideal time for sediment removal. The sediment is rich in P and organic matter and may be re-used in the farm to improve the soil properties.

We investigated whether water retention also enhances P retention. Water retention measures were implemented in the farm before the start of the 2020-2021 drainage season and resulted in a change of the nutrient transport routes. The water retention measures were designed to increase the groundwater levels and were thought as a climate-adaptation farming measure after the farm suffered from the effects of the drought in 2018. These water retention measures increased the lateral water transport through the P-rich topsoil which consequently increased significantly the P desorption from the top-soil and the P load transported downstream. This occurred despite the difference between the P input and uptake by the crop (P surplus) being negative in that year. Therefore, water retention involves

the risk of P-mobilization from the top-soil. We therefore advise to keep the groundwater levels below the topsoil and to combine water conservation with efforts to capture and reuse the ditch sediments.

6.4 New insights into the implementation of Fe-based P retention measures at the farm scale

Opposed to the dairy farm in the east of the Netherlands, the Fe-poor sandy soils of the tulip fields investigated in chapter 4 exhibited high P/Fe ratios in the soil and very high P concentrations in the groundwater. P was present in dissolved form and ICS filters were designed to retain it. Iron coated sand is a redox-sensitive material and when the ICS filters are placed below the groundwater level, the Fe could be reduced and, in turn, affect the P binding. The P (im)mobility at the onset of ICS reduction was investigated in two test fields and in the laboratory. In the two fields with three-year-old ICS filters, which were occasionally experiencing metal-reducing conditions, we observed that P was still efficiently removed by the ICS. Microcosm experiments were used to mimic the field conditions and investigate the P adsorption on ICS under reducing conditions further. For ICS with a molar P/Fe ratio of 0.013 and exposure times of 45 days, P was not released even after partial Fe and Mn reduction under weakly, moderately, and strongly reducing conditions. Almost no changes were observed in the P sorption capacity and in the ICS mineral structure after the treatments under moderately and weakly reducing conditions.

The main cause of the reducing conditions in the drainage water is the high organic matter content. When drains are below the groundwater level, the oxygen supply is limited. The absence of oxygen and the presence of dissolved organic matter can enable anaerobic respiration, in which microorganisms use nitrate (NO_3), manganese (Mn) and Fe (hydr)oxides, sulfate (SO_4), and/or CO_2 as terminal electron acceptors. If the conditions are moderately or strongly reducing, the Mn and Fe oxides present in the ICS were partially dissolved, therefore it is recommended to monitor the Mn and Fe concentrations coming out of ICS filters. As Mn reduction is usually initiated before Fe reduction, the increase in Mn concentrations can be taken as a good early warning indicator. We recommend monitoring the dissolved Fe and Mn losses as an early warning for reduced removal efficiency if the ICS filters are working under reducing conditions. In addition to Mn and Fe partial dissolution, mixed manganese-calcium

carbonate precipitates were formed in suspension under moderately and strongly reducing conditions, these particles could result in loss of hydraulic conductivity or clogging of filters.

P was not released from the ICS under reducing conditions during the experiment because there were enough adsorption sites available. Therefore, we recommend that if possible, the ICS filters placed below the groundwater level are dimensioned to maintain low P/Fe molar ratios. When the conditions are strongly reducing, the ICS grains may change color from orange-red to black. This happens when there is a transformation of the iron oxides to iron sulfides. This is not desirable as the iron sulfides have a lower phosphate retention capacity than iron oxides. According to our calculations, under the studied conditions, P release would not be expected to be relevant within the lifespan of the drain tubes, about 20 years. The formation of iron sulfides is reversible, if the material is exposed to (water with dissolved) oxygen, the reduced iron is oxidized again to iron oxides.

If the sulfide concentration is high in the drainage water or there are signs of sulfate reduction, using ICS may not be the best solution as the sulfide can reduce the Fe in the ICS. The redox sensitivity of Fe can be a limitation when applying ICS or iron sludge under strongly reducing conditions. Therefore, for future research, we recommend investigating other filter materials for such situations for example with elements that are not redox-sensitive and can bind P such as aluminum or calcium.

Another relevant issue is that water management decisions about, for example, pumping rates and the corresponding flow-through velocities should be taken in view of the kinetics of P retention in the ICS filters. In chapter 5, a two-site adsorption reactive transport model was calibrated and validated to describe the kinetics of P adsorption to ICS. The model's parametrization was based on long-term column experiments with two flow velocities and successfully represented adsorption and desorption processes, even under stop-flow conditions. Adsorption to the outer layers of the Fe-coating was conceived to be in equilibrium with the percolating water and follow a linear isotherm, but only represents a small fraction of the potential binding capacity. The lifespan of the filter is determined by the diffusion of P into the inner layers of the Fe coating, which is a slow process. For P concentrations below 20 mg-P/L, an equilibrium distribution coefficient of 28.1 L/g-Fe was obtained under the given conditions. This means that, for example, at a P concentration of

1.2 mg-P/L in the drainage water, ICS with 0.15 g-Fe/g-ICS and a can retain 5 mg-P/g-ICS (28.1x0.15x1.2) in equilibrium. The corresponding P/Fe molar ratio for this example is 0.06. However, it is important to notice that only about 5% of the adsorption capacity is found on the outer layers of the ICS grains and can retain P almost instantly. The other 95% of the retention capacity is inside the coating of the grains and is limited by the diffusion of the P to the inside. This is a slow process which has a characteristic time scale of 267 days.

Due to the slow P transport into the coating, optimal ICS filter operation includes resting periods, which can extend the filter operation time. To make use of the total P retention capacity, it is important to give time for the P to diffuse inside the ICS grains. We advise using ICS filters in slow-flow systems to optimize P adsorption, with flow velocities below 10 cm/h. Resting periods can be introduced to improve the performance of the ICS filters. For example, having two parallel filters and alternating their use every 2 weeks can improve P retention. This operation can be implemented for example in decentralized systems such as greenhouse effluents or in edge-of-field filters. In addition, the contribution of slow adsorption can be significant in ICS applications in natural systems, which are naturally exhibiting resting periods between rain events.

For future research we recommend performing a cost-benefit analysis and a life cycle assessment of different nutrient retention measures in agriculture including ICS filters. Moreover, it is interesting to evaluate the difference between ICS filters where the flow has stopped but the filter is still in contact with stagnant water versus filter, which dry out. The two scenarios might exert influence on P retention after the summer when water is percolating through the filter again. Currently, we do not know whether it is better to drain the ICS filter and keep it dry during the inactive summer period or to keep it wet. It would be interesting to do a pilot field study with ICS filters where the flow velocity is monitored to evaluate the reactive transport model under field conditions.

6.5 Case studies using ICS filters

The implementation of nutrient retention measures that sustain the growth of agriculture in a sustainable way are of great importance. With three case studies we want to show how the findings of this research contribute to the design and operation of P-retention measures that use ICS and offer new insights into the redox behavior and kinetic adsorption on ICS filters.

The first case study presented is about the ICS filters around drains presented in chapter 4. The second case study evaluates the performance of an ICS filter placed in surface waters. The third case study is on a protected natural area that had high particulate and dissolved P in the drainage water and a water retention basin was built to retain P particles combined with drains covered with ICS in the outflow to retain the dissolved P. For each case the principles of P retention, the main questions brought by the managers, and the advice offered are shortly described.

6.5.1 ICS around drains in the Bollenstreek

Phosphate adsorption on ICS was investigated under reducing conditions in two field sites. The ICS enveloped drains were constructed 3 years before and were during that time exposed to reducing conditions. The P concentrations in the drainage water are very high, between 2 and 10 mg/L. The region has nutrient-poor sandy soils and the farmers add a mix of compost and straw as fertilizer which are sources of P and organic matter. The drains transport rainwater and upwelling groundwater. The combination of these factors result in a high risk for dissolved P leaching. Furthermore, in the absence of oxygen and nitrate, it is likely that the abundant Fe and Mn oxides present in the ICS are used as terminal electron acceptors by dissimilatory metal-reducing organisms creating metal-reducing conditions.

In both fields, about 0.015 m³ of ICS were added per linear meter of drain (~ 26.5 kg ICS/m) without mechanical packing (figure 6-1). The drains were constructed every 10 m, placed 90 cm below the surface, and the groundwater level is kept at around 60 cm. In both fields, Rijnland waterboard, Delphy farmer association, and Deltares were involved in the design of the field experiment. The drains are connected to a main drain that discharges into a pumping station with a floater-activated pump that maintains the groundwater level constant by discharging into a ditch. In the summer, evapotranspiration is higher than precipitation and there is no need to continuously pump water out of the field, instead, the drains are used for irrigation, the level in the ditch is elevated and oxic water infiltrates from the ditch into the field via the tube drains.



Figure 6-1 ICS filter construction around drains in a flower growing farm in the west of the Netherlands

Although the ICS filters around the drains were only subject to moderate reducing conditions, we measured dissolved Fe and Mn in the outflow of the drains. The dissolved P was still efficiently removed with a removal efficiency between 50 and 80% in one field and 85 and 90% in the other. The differences in efficiency may be explained because the P concentrations measured in the shallow water may underestimate the real drainage water concentrations as the deeper groundwater had very high P concentrations at this location. Even though the removal efficiencies were high, they were lower than the 93% efficiency reported previously by a similar experiment in the Netherlands (Chardon et al., 2021). We believe that the difference in efficiency can be ascribed to different flow velocities. Active water pumping led to flow velocities around 180 cm/d in the ICS at the two fields investigated in this study, while the water flow in the ICS in the experiment described previously by Chardon et al. (2021) was only up to 60 cm/d and the water moved by gravity alone. Our results together with the ones presented in Chardon et al. (2021) provide evidence that ICS filters under weak and moderate reducing conditions retain P efficiently, up to 5 years after the construction tested so far.

6.5.2 Filter in De Put, Rijswijk, managed by Delfland

De Put is a recreation lake in the Rijswijk municipality in the Netherlands. The lake has an important recreational function in this dense urban area. There are a swimming club, fishing club, wedding resort, and tennis club around the lake. The lake was a sand extraction pit and is 12 m deep. Since 2015, the lake is having water quality issues resulting in algae blooms. Negative swimming advice was issued throughout the years 2016 to 2019 and the swimming club had to close its doors for these seasons. Another consequence of the poor water quality is that part of the fish population regularly dies in autumn. Due to fish mortality, the fishing club loses members, needs to buy new fish, and operates an aeration system, measures that are costly and not sustainable.

The water board (Delfland) studied the water quality of the lake and determined that the high nutrient contents were the cause for the algae blooms and that the source of nutrients was the sediment. Because the lake is deep and in a highly urbanized area, the waterboard decided it was better not to dredge or cover the sediment. Therefore, an innovative solution to reduce the P concentration in the lake was needed. Together with the support of Delfland and the province of South Holland, Arcadis designed a submerged pilot ICS filter to remove P from the water (figure 6-2). A video showing the construction is available here: https://youtu.be/YP_loWeLbKQ.

Two ICS filters were deployed, each consisting of 1 m³ of ICS inside a big bag with an electric pump in the center. The filter had a second function which was mixing the water in the lake. The pump was selected to work continuously at a 100 L/min flow rate. The water enters the filter from all the sides of the big bag and the outflow is a hose placed above the water level. The big bags were placed approximately 2 m below the surface. To avoid possible clogging, the ICS was sieved to sizes larger than 5 mm. The efficiency of the filter in the first four months of operation was very low (between 0 and 5%) despite being designed to remove 20% of the inflow P based on laboratory batch experiments. The managers posed the question why the filter was having lower performance than expected and if a solution could be identified.



Figure 6-2 ICS filter in a lake. The filters are two big-bags with 1m³ of ICS each and a pump in the center, the filters are 2 m below the surface. The water enters from all sides of the big-bag and the hose is the outflow of the filter.

We thought of possible reasons why the filters were having such low performance and later tested our hypothesis on a field experiment. The oxygen saturation average was 77%, therefore the conditions were oxic and issues related to reductive dissolution were discarded. Another possible explanation was the high flow and the short retention time of the water in the filter. The contact time was only 5 minutes. We proposed to increase the retention time to 60 minutes or more to make better use of the slow adsorption capacity of the ICS. However, the flow rate of the current pumps could not be adjusted, as the existing pump had to be replaced by a smaller pump which was not possible. As an alternative, we proposed to operate the filters in a stop-flow regime. This could be done simply by placing a timer in the pump's socket. The new flow regime was set for the filters to work 4 hours per day and rest during the rest 20 hours of the day.

Two weeks after the filters were working in the new regime, samples were taken during operation and the water flow was measured. One of the filters had constant flow and in the

other one the flow oscillated. The flow variations were linked to preferential flows. The preferential flows were likely caused by the reorganization of ICS grains during pumping, the height of the filters was about 30 cm lower than when deployed. In the filter with constant flow, the new flow regime had a positive effect on P removal. The starting removal efficiency was about 20% and it decreased after 2 hours to about 3%. This experiment proved the low efficiencies were explained by the high flow velocities and that higher removal rates could be achieved with longer retention times. Although the experiment successfully identified the problem, the measure was not considered suitable for the lake as too many filters would be needed to achieve the desired P removal in a short time frame.

6.5.3 Basin and filter in the inflow of the Grote Meer, managed by Brabantse Delta

The Grote Meer is a lake system in the Noord Brabant province of the Netherlands. The lake has several (rare) biological species and has had water quality problems in the last few years. High dissolved and particulate P concentrations are one of the reasons for the decrease in water quality. The lake is surrounded by farmlands and natural areas, it was agreed that the best option to preserve the lake's water quality was to reduce the P input towards the lake. A high winter removal efficiency was needed as in the summer very little water flows into the lake. For this reason, traditional solutions such as constructed wetlands were not suitable because they only have high removal efficiencies in summer.

The measure designed by Arcadis consists of a water retention basin of about 1 hectare and an ICS filter system in the outflow (figure 6-3). The retention basin was designed to retain particles that could clog the filter and buffer the peak flows as high flow velocities decrease the P retention efficiency. The system works by gravity. At the outflow of the basin, there are three drains covered with ICS inside a trench, 1100 m³ of ICS were used. The ICS filter construction was finished at the end of 2020 and treats approximately half of the water entering the Grote Meer lake system. A video of the ICS filter provided by the waterboard is available here: <https://youtu.be/ZmKvMsLqstI>. The ICS is obtained from AquaMinerals and is from the same batch that was used in chapters 4 and 5. The filter was designed to keep outflow concentrations below 0.08 mg/L. After one year, the monthly monitoring was analyzed. The monthly monitoring included one sample in the basin and one sample in the outflow of the filter. It measured total and dissolved P, total nitrogen, nitrate, and ammonia, dissolved oxygen, pH, and metals, including Fe (unfiltered). The ICS filter was having a positive

effect on the P concentrations in the lake. As a result of the measurements and monitoring, additional questions regarding the pH of the filter outflow, heavy metals, and P concentrations were formulated by the water board.

Water quality samples were taken inside the water retention basin and in the outflow of the ICS covered drains and measured total and dissolved P. Therefore, the efficiency considers the removal by the ICS filter but settling in the basin can also influence the results. The measurements show that the efficiency of the filter is high in the winter but decreased in the summer months. In the winter months from October to January, the dissolved P removal efficiency was between 95 and 99 %, and the dissolved P concentrations in the inflow between 0.25 and 0.80 mg/L. In the summer the efficiency decreased, moreover, the total P concentrations were very low in the inflow, below 0.08 mg/L, and the dissolved P was around 0.02 mg/L. The flow rate was not measured, but observations showed that in the summer almost no water flowed out of the filter. Therefore, the flow velocities were not expected to cause the decrease in efficiency. In the column adsorption experiments in chapter 5, the lowest P concentrations obtained were around 0.02 mg/L in the outflow when the experiment started. It is therefore possible that it is very hard to obtain lower effluent concentrations with this ICS which has a P/Fe molar ratio of 0.015. Adsorption is an equilibrium process; P retention is reduced at low P concentrations. After longer exposure periods when the P concentration in the solid increases, low P concentrations could even cause P desorption from the solid. If this were to happen in the future, the filter could be bypassed during the summer months. We advised measuring the amount of water flowing out of the filter together with the P concentrations to get a better impression of the P loads removed.

The pH increased about 1 unit after the filter but was always below 8 in the outflow. This effect was reported in the literature, Wang et al. (2013) measured OH⁻ ions release as they were exchanged for phosphate ions in the active sites of ICS. Moreover, nitrate and metals concentrations decreased when comparing the inflow and the outflow of the filter. This decrease implies there are other processes beyond P adsorption taking place in the filter, such as metal adsorption, sedimentation, and denitrification, which may influence the pH. Another explanation is that calcium concentrations in the effluent were consistently higher than in the influent. The dissolution of calcium containing minerals can lead to higher hydroxyl

concentrations and therefore to an increase of pH. If this was the reason for the increase in pH, we expect the effect to decrease in about 3.5 years (time expected for the excess calcium to be washed out and the outflow calcium concentrations to be similar to the inflow values). Only one measurement was done inside the lake during the operation of the filter where the pH was 6.3, therefore, it is not yet clear whether the pH change of the filter outflow water affects the pH in De Groote Meer. We advised continuing to monitor the filter outflow and adding a sampling point in the lake.



Figure 6-3 ICS filter and basin, three drains are covered by ICS which filters the water

The measurements showed that the filter also captures most of the trace metals. Nevertheless, nickel concentrations were higher in the outflow of the filter than in the inflow. Research shows that Fe (hydr)oxides can also adsorb trace metals (including nickel, zinc, cadmium, and copper), which may explain the decrease in the mentioned metals (Boujelben et al., 2009; Bruemmer et al., 1988; Cowan et al., 1991). A selection of metals (Cd, Cr, Li, Ni, Pb, and Zn) were measured with ICP-OES in the first 40 days of operation of the columns in chapter 5. No leaching of the mentioned metals was measured during the experiment; besides calcium, iron, and manganese, all metals were below the detection limit. For these reasons, it seems unlikely that the ICS is the cause of the additional increase in nickel. One possible explanation is the soil movement during the construction of the filter caused the additional nickel release. Pyrite is a mineral that is often associated with nickel. If this

explanation is correct, we expect a decrease in nickel over time. In the last month measured, the concentration of nickel decreased to be about the same as in the influent. We advised to continue monitoring these trace metals and if the nickel does not decrease to seal the bottom of the basin.

6.6 References

- Boujelben, N., Bouzid, J., & Elouear, Z. (2009). Adsorption of nickel and copper onto natural iron oxide-coated sand from aqueous solutions: Study in single and binary systems. *Journal of Hazardous Materials*, 163(1), 376–382. <https://doi.org/10.1016/j.jhazmat.2008.06.128>
- Bruemmer, G. W., Gerth, J., & TILLER, K. G. (1988). Reaction kinetics of the adsorption and desorption of nickel, zinc and cadmium by goethite. I. Adsorption and diffusion of metals. *Journal of Soil Science*, 39(1), 37–52. <https://doi.org/10.1111/j.1365-2389.1988.tb01192.x>
- Chardon, W., Groenenberg, J. E., Vink, J. P. M., Voegelin, A., & Koopmans, G. F. (2021). Use of iron-coated sand for removing soluble phosphorus from drainage water. *Science of The Total Environment*, 815, 152738. <https://doi.org/10.1016/j.scitotenv.2021.152738>
- Cowan, C. E., Zachara, J. M., & Resch, C. T. (1991). Cadmium Adsorption on Iron Oxides in the Presence of Alkaline-Earth Elements. *Environmental Science and Technology*, 25(3), 437–446. <https://doi.org/10.1021/es00015a009>
- Wang, Li, W., Harrington, R., Liu, F., Parise, J. B., Feng, X., & Sparks, D. L. (2013). Effect of ferrihydrite crystallite size on phosphate adsorption reactivity. *Environmental Science and Technology*, 47(18), 10322–10331. <https://doi.org/10.1021/es401301z>

7 Acknowledgments

First, I thank Leonard Osté and Thilo Behrends for being great supervisors and giving me the opportunity to work on this project, providing valuable guidance and feedback. Special thanks to my promotor Prof Jack Middelburg for guiding this doctoral thesis. I would also like to show gratitude to the committee formed for the evaluation of this thesis and to the anonymous reviewers who made valuable comments to improve the quality of each chapter.

I am also grateful to my colleagues from Deltares Joachim Rozemeijer, Stefan Jansen, Jan Gerritse, and Gerlinde Roskam, I am grateful for all I learned from you and enjoyed working together. Special thanks for all the great support from the laboratory team in Utrecht, Erik van Vilsteren, Rob van Galen, André Cinjee, and Fredericke Hannes. Thanks to Kevin Ouwerkerk, Bas van der Grift, and Laurens Gerner for their collaboration on chapters 2 and 3. I would like to thank Alraune Zech from Utrecht University for her support on chapter 5. Special thanks to Andreas Voegelin and Stefan Peiffer for their valuable input on this research. I would also like to extend my thanks to Arjon Buijert and Thijs Lieverse from Arcadis for the opportunity to do a secondment with them and for the fruitful discussions and brainstorming on ICS applications.

I enjoyed doing my Ph.D. in the European Union's Horizon 2020 Marie Skłodowska Curie Innovative Training Network. Very special thanks to all the P-TRAP ESRs: Xingyu Liu, Rochelle Saracanalao, Oleksandr Bolielyi, Lordina Eshun, Mingkai Ma, Ville Nenonen, Tolulope Ayeyemi, Karel As, Rouven Metz, and Melanie Münch. Special thanks to the "lake and catchment group", I always looked forward to our weekly discussions. Thanks to Sylvia Walter for her excellent project management and support in writing reports and blogs. Thanks to Menno Tiesma, I had a fun time doing fieldwork together in 2021. Thanks to the other Ph.D. students in Utrecht for help in the lab and nice lunch breaks. Thanks to all my old friends and to my new friends I made during these last three years.

I would like to thank my family: my mom, dad, Dani, and Ale for their lifelong love and support, also to my extended family Ingrid, Luis, and Pablo. Thanks to my grandparents Marú, Abú, and Cota for their unconditional love. Finally, I want to especially thank Manu, without your love and support I would have never started or finished this Ph.D.

8 List of Publications

Barcala, V., Rozemeijer, J., Osté, L., Van Der Grift, B., Gerner, L., & Behrends, T. (2020). Processes controlling the flux of legacy phosphorus to surface waters at the farm scale. *Environmental Research Letters*, *16*(1). <https://doi.org/10.1088/1748-9326/abcdd4>

Barcala, V., Jansen, S., Gerritse, J., Mangold, S., Voegelin, A., and Behrends, T. (2022) 'Phosphorus adsorption on iron-coated sand under reducing conditions', *Journal of Environmental Quality* <https://doi.org/10.1002/jeq2.20432>.

Barcala, V., Zech, A., Osté, L., and Behrends, T (2023) 'Transport limited kinetics of phosphate retention on iron-coated sand and practical implications', *Journal of Contaminant Hydrology*,. <https://doi.org/10.1016/j.jconhyd.2023.104160>

Barcala, V., Rozemeijer, J., Ouwerkerk, K., Gerner, L., Osté, L. (2022) 'Value and limitations of Machine Learning in high-frequency nutrient data for gap- filling, forecasting, and transport process interpretation', *Journal of Environmental Monitoring and Assessment, in Review*, <https://doi.org/10.21203/rs.3.rs-2201325/v1> (Preprint).

9 Summary

This research was motivated by the impact of the diffuse P sources coming from agriculture on surface water quality and eutrophication. The goal of this Ph.D. thesis was to contribute to improving the management of drained agricultural areas to optimize the retention of Fe-associated P. Because of the legacy P in the soil, P-retention measures are needed in agricultural catchments to improve the surface water quality in the short- to middle-term. The first part of this thesis focused on monitoring the P transport at the farm scale. The second part of this thesis focused on investigating the mechanisms of P-retention by iron-coated sand (ICS), a Fe-rich by-product from drinking water production.

At the monitored farm in the Fe-rich sandy soils in the east of the Netherlands, Fe had an important role in the P transport. After the first year of monitoring, it was observed that the topsoil (0-30 cm) had high soluble P contents and a high P/Fe molar ratio. This combination would result in a high risk of P leaching. However, the high Fe content in the subsoil prevented high P concentrations in the groundwater and reduced the P losses to surface waters and deeper groundwaters. Once in the ditch, most of the P was associated with Fe-rich particles. Particle transport to downstream areas mainly occurred when particles were resuspended during discharge peaks.

After four years of data were collected, we optimized the post-processing of high-frequency data using Machine Learning and investigated the effect of water retention measures on P transport loads. Random Forest enabled an accurate estimation of missing data but its use for forecasting should be done with care, especially in scenarios involving system changes, such as forecasting the effect of differences in rainfall and groundwater levels caused by climate change. In the last measured season, water retention measures were implemented and there was a negative P surplus. Despite these facts, even more P left the farm. When water retention measures were implemented on the farm, the nutrient transport routes changed. The transport through the P-rich topsoil increased the P desorption and increased the total P load transported downstream.

ICS filters are sometimes placed below the groundwater level and the oxygen supply is limited. Fe is a redox-sensitive material and the absence of oxygen and the presence of

dissolved organic matter can enable anaerobic metabolism which could affect the P retention. P adsorption on ICS was investigated under reducing conditions in two tulip field sites in the coastal dune sands and in the laboratory. Three-year-old ICS filters were subject to reducing conditions in the fields while P was still efficiently removed. Microcosm experiments were used to mimic the field conditions and P was also not released even after partial Fe and Mn reduction under weakly, moderately, and strongly reducing conditions. When the experiment ended, almost no changes were observed in the P sorption capacity and the ICS mineral structure. Only a small percentage of Fe transformed into iron sulfides in the outer layer of the Fe coatings under strongly reducing conditions which slightly reduced the P adsorption capacity. Nevertheless, these detrimental effects are expected to become relevant only after long operational periods (~20 years), i.e., similar to the lifespan of the drains.

The P retention on ICS is a kinetic process. A two-site adsorption reactive transport model was used to describe the kinetics of P adsorption on ICS. The model parametrization was based on long-term column experiments and supported by scanning electron microscopy (SEM-EDX). At the relatively low P concentrations found in agricultural catchments, the adsorption to the outer layers of the Fe-coating can be represented with linear equilibrium adsorption. Nevertheless, 95 % of the ICS adsorption capacity was determined by slow kinetics that described the intra-particle diffusion inside the Fe-coating. The model can be used to optimize the design and operation of ICS filters including resting periods to profit from the slow kinetics.

Take-home messages for managers include to have confidence in the use of ICS filters even if the filters are temporarily under moderately reducing conditions. We recommend monitoring the dissolved Fe and Mn losses as an early warning for ICS filters that are working under reducing conditions. Moreover, we recommend dimension the ICS filters to maintain low P/Fe ratios if they are constructed below the groundwater level. We support the incorporation of resting periods and low flow velocities in ICS filters and advice using the presented model (chapter 5) for their design and operation. We recommend the use of Machine Learning tools for the post-processing of monitoring data but warn against their use for forecasting, especially in scenarios involving climate change. Finally, we recommend the monitoring of system changes such as water retention measures or other farm practices and quantifying

the effect they have on nutrient transport to prevent water quality problems downstream. Hopefully, these results contribute to improving the management of Fe-associated P in agricultural areas.

10 Samenvatting

De aanleiding voor dit onderzoek is de impact van de diffuse P-bronnen afkomstig van de landbouw op de kwaliteit van het oppervlaktewater en de eutrofiëring. Het doel van dit proefschrift is een bijdrage te leveren aan de verbetering van het beheer van gedraineerde landbouwgebieden om de retentie van Fe-geassocieerd P te optimaliseren. Vanwege de historisch opgebouwde voorraad P in de bodem zijn P-retentiemaatregelen nodig in landbouwgebieden om de oppervlaktewaterkwaliteit op korte tot middellange termijn te verbeteren. Het eerste deel van dit proefschrift concentreert zich op het monitoren van het P-transport op bedrijfsschaal. Het tweede deel van dit proefschrift was gericht op het onderzoeken van de mechanismen van P-retentie door ICS (ijzerzand), een Fe-rijk bijproduct van drinkwaterproductie.

Op het onderzochte melkveebedrijf speelde Fe een belangrijke rol in het P-transport. Na het eerste monitoringsjaar werd vastgesteld dat de bovengrond (0-30 cm) hoge oplosbare P-gehalten en hoge P/Fe-molaire verhoudingen had. Deze combinatie leidt tot een hoog risico op P-uitspoeling. Omdat de meeste uitspoeling via de Fe-houdende onderlaag plaatsvindt, blijven de P-concentraties in het uitspoelingswater laag en de P-verliezen naar het oppervlaktewater en diepere grondwater beperkt. Eenmaal in de sloot bindt het meeste P aan Fe-rijke deeltjes, waardoor het transport naar benedenstroomse gebieden vooral plaatsvindt wanneer resuspensie optreedt tijdens afvoerpieken.

Nadat vier jaar lang gegevens werden verzameld, hebben we de nabewerking van hoogfrequente monitoringgegevens geoptimaliseerd met behulp van Machine Learning-technieken. Random Forest maakte een nauwkeurige schatting van de ontbrekende gegevens mogelijk, maar het gebruik van Machine Learning voor voorspellingen vraagt voorzichtigheid, vooral in scenario's met klimaatverandering, bijvoorbeeld bij het voorspellen van de effecten van verschillen in regenval en grondwaterstanden. In het laatste gemeten seizoen werden waterretentiemaatregelen uitgevoerd en was er een negatief fosfaatoverschot. Toch spoelde er meer P uit dan in andere jaren. Toen op het bedrijf waterretentiemaatregelen werden uitgevoerd, veranderden de transportroutes voor nutriënten. De extra grondwaterstroming door de P-rijke bovengrond verhoogde de P-desorptie uit de bodem en verhoogde de P-uitspoeling naar het oppervlaktewater.

ICS-filters worden soms onder het grondwaterniveau geplaatst en de zuurstoftoevoer is dan beperkt. Fe is een redoxgevoelig materiaal en de afwezigheid van zuurstof en de aanwezigheid van opgelost organisch materiaal kan anaeroob metabolisme mogelijk maken, en dit kan de P-retentie beïnvloeden. P-adsorptie aan ICS werd onderzocht onder reducerende omstandigheden op twee veldlocaties en in het laboratorium. In drie jaar oude ICS-filters in het veld ontwikkelden zich reducerende omstandigheden. Toch werd P nog steeds efficiënt verwijderd. Er werden microkosmos-experimenten gebruikt om de veldomstandigheden na te bootsen en ook na gedeeltelijke reductie van Fe en Mn onder zwak, matig en sterk reducerende omstandigheden kwam er geen P vrij. Aan het eind van het experiment werden vrijwel geen veranderingen waargenomen in de P-sorptiecapaciteit en de minerale structuur van ICS. Slechts onder sterk reducerende omstandigheden transformeerde een klein percentage Fe in ijzersulfiden in de buitenste laag van de ICS, waardoor de P-adsorptiecapaciteit enigszins afnam. Niettemin wordt verwacht dat deze nadelige effecten pas relevant zullen worden na lange operationele perioden vergelijkbaar met de levensduur van de drainagebuizen, circa 20 jaar.

De P-retentie op ICS is een kinetisch proces. Om de kinetiek van P-adsorptie op ICS te beschrijven werd een reactief transportmodel met twee typen bindingsplaatsen gebruikt: snel en langzaam. De parameterisering van het model was gebaseerd op lange termijn kolomexperimenten en werd ondersteund door een rasterelektronenmicroscop (SEM). Bij lage P-concentraties in landbouwgebieden kan de adsorptie aan de buitenste lagen van de Fe-coating worden gesimuleerd met lineaire evenwichtsadsorptie. Niettemin werd 95% van de adsorptiecapaciteit van ICS bepaald door een langzame bindingsplaatsen die pas na diffusie naar de binnenste lagen van de Fe-coating bereikbaar zijn. Het model kan worden gebruikt om het ontwerp en de werking van ICS-filters te optimaliseren, met inbegrip van rustperioden om optimaal gebruik te maken van de trage kinetiek.

Een van de conclusies voor beheerders is dat zij vertrouwen moeten hebben in het gebruik van ICS-filters, zelfs als de filters tijdelijk onder zuurstofloze omstandigheden werken. Wij bevelen aan de verliezen aan opgelost Fe en Mn te monitoren als indicatoren voor een mogelijke verminderde effectiviteit als de ICS-filters onder reducerende omstandigheden werken. Wij bevelen aan bij het ontwerp van de ICS-filters een hoge verhouding vaste stof/vloeistof te hanteren indien zij onder het grondwaterniveau worden aangelegd. Wij

raden rustperiodes en lage stroomsnelheden aan in ICS-filters en adviseren het gebruik van het gepresenteerde model (hoofdstuk 5) voor het ontwerp en beheer ervan. Wij raden het gebruik van Machine Learning aan voor de nabewerking van monitoringgegevens, maar waarschuwen voor het gebruik daarvan voor voorspellingen, vooral in scenario's waarin sprake is van klimaatverandering. Ten slotte adviseren wij systeemveranderingen zoals waterretentiemaatregelen of andere landbouwpraktijken te monitoren en het effect ervan op het transport van nutriënten te kwantificeren om waterkwaliteitsproblemen stroomafwaarts te voorkomen. Hopelijk dragen deze resultaten bij tot een beter beheer van Fe-geassocieerd P in landbouwgebieden.

11 Curriculum Vitae

Victoria (Vicky) Barcala was born on the 29th of July 1991 in Montevideo. In 2010 she started her studies in civil engineering in a five year's program specializing in hydraulic and environmental studies where she graduated first in the class at the Universidad de la República (Uruguay). After working for one year at the Ministry of Housing, Land Planning and Environment, Victoria obtained a Bill and Melinda Gates scholarship supported by the national research and innovation institute (ANII) to study a joint master's degree in urban water and sanitation at the Universidad del Valle (Colombia) and IHE Delft (the Netherlands). She graduated with distinction with a thesis related to phosphorous removal and recovery from point sources. After graduation she worked at the National Waterworks (OSE) and in environmental consultancy (EIA). In October 2019 she moved to the Netherlands and worked as early stage researcher at Deltares and was enrolled as a Ph.D. candidate at Utrecht University's School of Geosciences promoted by professor Jack Middelburg and under the supervision of Thilo Behrends and Leonard Osté. Her research on improving the management of drained agricultural areas to optimize the retention of iron-associated phosphorus was founded by the P-TRAP project a European Union's Horizon 2020 Marie Skłodowska Curie Innovative Training Network. While doing her Ph.D, she did a secondment at Arcadis and worked in projects related to full-scale iron-coated sand measures. She was awarded the 1st prize for young researchers at the 7th IAHR European congress in 2022. Since February 2023 Victoria works at the water technology department at TAUW. Victoria lives in Deventer with her husband Manuel, besides research they enjoy playing tennis and traveling.

